TRKC TARGETED PROBES FOR CANCER DIAGNOSIS AND THERAPEUTICS

A Dissertation

by

ANYANEE KAMKAEW

Submitted to the Office of Graduate and Professional Studies of
Texas A&M University
in partial fulfillment of the requirements for the degree of

DOCTOR OF PHILOSOPHY

Chair of Committee,	Kevin Burgess
Committee Members,	Karen L. Wooley
	Wenshe Liu
	Roula B. Mouneimne
Head of Department,	Francois P. Gabbai

August 2015

Major Subject: Chemistry

ABSTRACT

This dissertation features a small molecule, non-peptidic, ligand designed to bind a cell surface receptor called tropomyosin receptor kinase C (TrkC). TrkC is overexpressed on various types of tumors including breast cancer and melanoma. It would be advantageous in clinical applications to conjugate the novel ligand with imaging or therapeutic agents then treat TrkC-positive cancers.

For proof of concept, first, we used our ligand conjugated to a commercial cytotoxic drug, 6-mercaptopurine, then tested the agent in NIH-3T3 cells stably transfected with TrkC, and compared with wild type NIH-3T3 ($TrkC^-$). A targeting effect was observed but we could not obtain an IC_{50} value for the conjugate due to lack of solubility at the concentrations that would have been required. Therefore, we chose a cytotoxic rosamine dye to conjugate with the targeting ligand. Selective cytotoxicity of the conjugate was observed, but high levels of non-specific binding also occurred.

Conjugation of the TrkC-targeting ligand with a fluorescent dye may be useful for optical imaging *in vivo*, and they are also cytotoxic then these theranostics can be used to both image and treat the tumor. We hypothesized that BODIPY dye derivatives could be suitable candidates for this approach since they have excellent fluorescent characteristics and can be modified for photodynamic therapy (PDT). Results collected from cellular assays proved the selectivity of this probe and its fluorescence led us to where the conjugate functioned inside the living cells.

Some cancer cell lines that naturally overexpress TrkC include *metastatic* breast

cancer and *metastatic* melanoma. Consequently, this study was expanded from stable TrkC transfectants to include metastatic-breast and –melanoma. The results show the beneficial effects of TrkC targeting in histochemistry and cellular assays, including internalization and selective cell killing. In a mouse model, collaborators discovered our PDT probe at 10 mg/kg (one injection, intravenous tail vein) caused complete ablation of a tumor after 6 days post injection with no sign of metastasis to other organs.

PDT can be effective if near-IR absorbing photosensitizers (λ_{max} >700 nm) are used to excite organs located in the deeper tissue. For this reason, the cargo was modified to aza-BODIPY dyes, which can absorb light at a longer wavelength than BODIPYs. Simultaneously, the conjugate structure was changed because we hypothesized this might lead to decreased neurotoxicity. Histological studies showed the new probe selectively stained breast tissues leaving normal tissues unstained. *In vivo* optical imaging also proved that the new TrkC targeting probe was effective in a murine breast cancer model. Incidentally, the spinal cord of the mouse was nicely imaged by this same reagent, presumably because $TrkC^{+}$ cells are highly concentrated in the peripheral nervous system.

Finally, we hypothesized that the novel near-IR targeting probe could be applied to imaging and treatment of metastatic melanoma. A rare Sinclair Swine model, available at TAMU, was part of the plan for these studies. Histology results showed selective staining by the targeting probe on melanoma tissue, as compared with normal tissue obtained from the same pig. Similarly, our probe stained tissue from human patients with metastatic melanoma tissue, but it did not stain healthy skin.

DEDICATION

To

Mom

ACKNOWLEDGEMENTS

I would like to thank my research advisor, Dr. Kevin Burgess, for motivation and supervision throughout the course of my Ph.D. study. I appreciate all his support, patience and help with my projects. I also want to thank my committee members Dr. Karen L. Wooley, Dr. Wenshe Liu, and Dr. Roula B. Mouneimne, for their guidance and support during my research.

Thanks to Dr. Aurore Loudet for teaching me all about cell studies. Thanks to Dr. Cliferson Thivierge for all his valuable advice and help with my projects. Thanks to Dr. Arjun Raghuraman for his support and help during my Ph.D. study. Thanks to Dr. Eunhwa Ko for her friendship, collaborating and support on my targeting project. Thanks to Dr. Sakunchai Khumsubdee for his help and support throughout my study. Thanks to Dr. Darrel Pilling for teaching me how to perform immunohistochemistry and also useful advice for my projects. Thanks to Dr. Rung-Yi Lai for teaching me how to perform biological assays and all his supports. Thanks also go to all current Burgess group members for their friendships and supports.

Thanks also go to my collaborators, Dr. Robert C. Burghardt, Dr. Jean-Philippe Pellois, Dr. Hong Boon Lee, Dr. Lik Voon Kiew, Dr. Lip Yong Chung and Mr. Chin-Siang Kue.

I would like to also thank Jill Powers for assistance with all paper works as well as her warm and kindness support throughout my study.

Thanks also go to my friends and colleagues and the department faculty and staff for making my time at Texas A&M University a great experience.

Thanks to financial supports: Scholarship from Development and Promotion of Science and Technology Talents Project (DPST) Royal Thai Government, the National Institutes of Health (GM087981) and the Robert A. Welch Foundation (A-1121), the Texas A & M CONACYT program 2013-012(S), High Impact Research (HIR (UM.C/625/1/HIR/MOHE/MED/17 & UM.C/625/1/HIR/MOHE/MED/33) from the Ministry of Higher Education, Malaysia.

Finally, thanks to my parents for their encouragement and to my husband for his love and support.

TABLE OF CONTENTS

Page

Page

LIST OF FIGURES

Page

Page

Page

Page

Page

Page

CHAPTER I

INTRODUCTION AND LITERATURE REVIEW

Small Molecules for Active Targeting of Solid Tumors

Active targeting[1] involves use of an entity that selectively binds surface receptors of particular cell types, and can deliver cargos, preferably into the cells. In cancer research, active targeting can be used for histological staining, selective imaging, and to increase therapeutic indices for cytotoxic drugs. In other words, active targeting has enormous potential to improve diagnostics, imaging, and chemotherapy in cancer treatment.

Currently, the most prevalent active targeting systems are antibody–drug conjugates (ADCs).[2-6] Two ADCs are already on the market (trastuzumab emtansine[7] and brentuximab vedotin)[8] and many more are in clinical trials. Most active targeting strategies center on monoclonal antibodies (mAbs) because it is comparatively easy to produce ones that bind cell surface receptors. However, active targeting with mAbs has some serious limitations. First, mAbs are too big to penetrate and efficiently diffuse into tumors. Moreover, the ones that do diffuse into tissue tend to be trapped at the antigen barrier,[9-11] which is a concentration of antigen located on the perivascular tumor cells, preventing permeation into the tumor mass.[12] In addition, high normal tissue exposure[13-15] results from slow clearance of mAbs from the body. They tend to accumulate in the liver and some fragments in the kidneys and do *not* reach their targets.[16-17] MAbs can also cause immunogenicity which might change their pharmacokinetic properties.[17]

Moreover, issues associated with cost, and stability/shelf life of mAbs need to be considered.

Recently, many researchers have tried to develop lower molecular weight systems for active targeting (*e.g.* non-peptidic small molecule, aptamer and peptide targeted drugs).[18] *Small molecule* systems for actively targeted cancer agents are attractive because this technique is not constrained by the factors outlined above for mAbs. For instance, folate-rhodamine conjugates (EC 17) can saturate folate receptors on tumors within five minutes of intravenous injection and rapidly exit blood vessels.[19] Although, the antigen-barrier still affects folate-small molecule conjugates, there is almost no effect at saturating doses.[19] Generally, small molecules travel faster to their target *in vivo*, have no immunogenicity, can provide sites for conjugation to cargoes, they have superior stability/shelve lives relative to mAbs, and can be produced at lower cost.

There are a few small molecules for targeting agents, and we hypothesize this is because relatively few cell surface receptors are known to be useful for active targeting of cancer cells and cancer subtypes.[20-22] Small molecule ligands that are commonly used for active targeting include some vitamins (*e.g.* folic acid,[20-21,23-24] biotin,[25] and cobalamin[26-27]), RGD[28-32] and NGR[33] peptidomimetics, a few carbonic anhydrase ligands,[34-37] and mimics of the prostate specific membrane antigen (PSMA; Figure 1-1).[38-39] This is a limitation because not all tumor types overexpress high number of the corresponding receptors, and that some of these ligands have sub-optimal properties for targeting entities.[40]

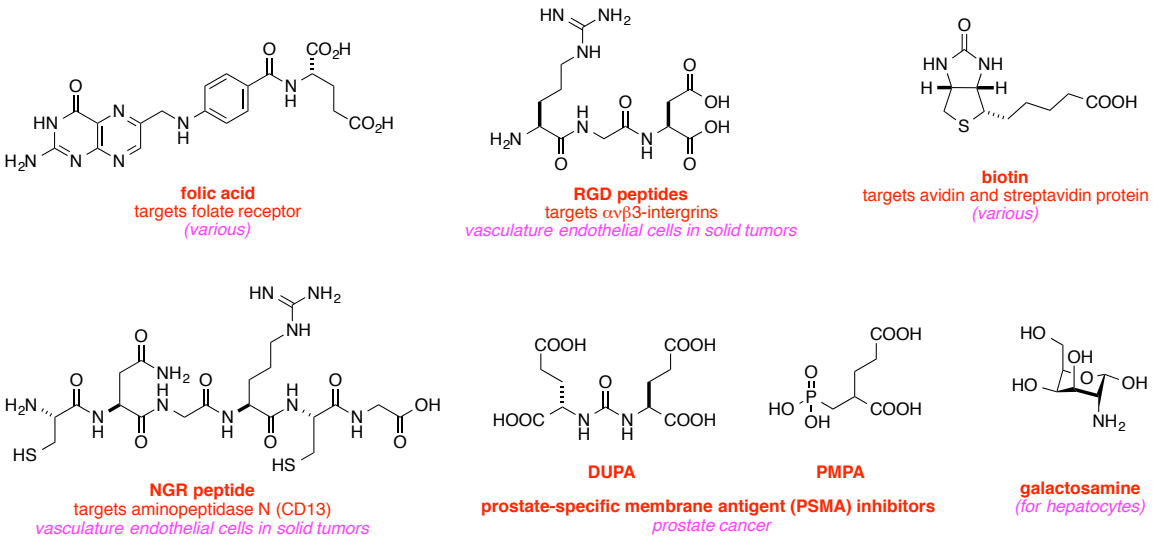

Figure 1-1. Small molecules that are most common in active targeting.

Design of agents for active targeting in cancer usually features selection of receptors that are overexpressed on certain tumors, identification of small molecule ligands for these, and design of suitable spacers to link these ligands to appropriate cargos.[41] For receptor selection, Phillip Low, a leader in the field, recommends at least appropriate levels of overexpression of the receptor must occur on tumor surface relative to normal cells.[42-43] Moreover, the ideal receptor should be expressed on the cell surface, and not only internally. The rate of internalization and receptor recycling is also crucial. Receptors that recycle frequently and/or are resynthesized or degraded quickly tend to be preferred.

Selection of suitable active targeting ligands in cancer is essential. Ligands with high binding affinity (*i.e.* sub-nanomolar dissociation constants, K_d) tend be preferable.

Additionally, the selectivity of a potential ligand is an issue. Targeting ligands should be easy to derivatize, and to conjugate with drugs of imaging agents without disrupting their binding abilities. Size of the conjugates also influences drug delivery mechanisms. Large conjugates, such as polymers or liposomes, usually accumulate in tumor tissues due to the enhanced permeability and retention (EPR) effect; however, large particles are often retained within blood vessels of healthy tissues, and that can cause unnecessary toxicities. Moreover, large particles usually have slow clearance from body.

Successful small molecule ligand conjugates in clinical treatments mostly involve removable linkers or spacers that facilitate penetration into tissue but do not interfere with receptor's binding and drug efficacy (Figure 1-2).

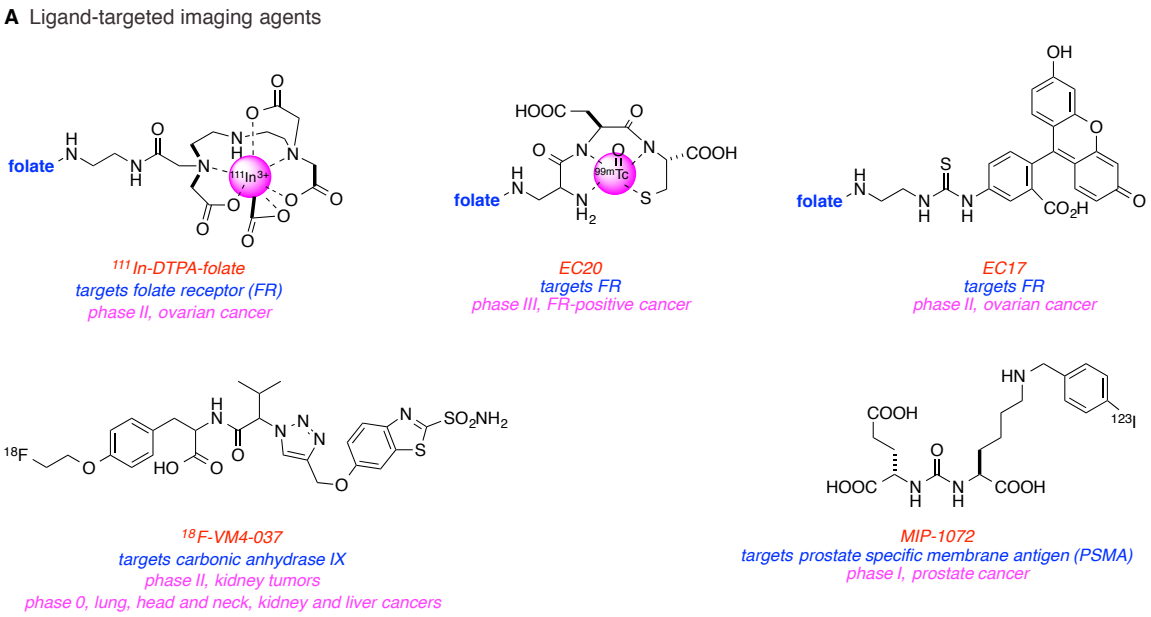

Figure 1-2. Examples of small molecule targeting ligands conjugated to imaging or therapeutic agents.

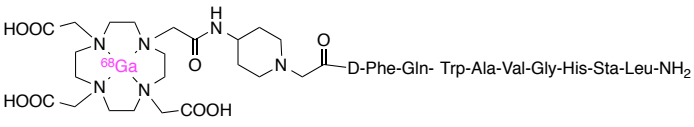

BAY86-7548 (bombesin-^{68}Ga)
targets bombesin receptor subtybe 2
phase I, prostate cancer

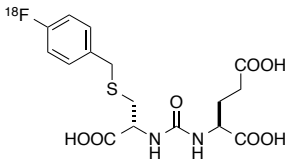

^{18}F-DCFBC
targets PSMA
phase II, metastatic prostate cancer

B Ligand-targeted therapeutic agents

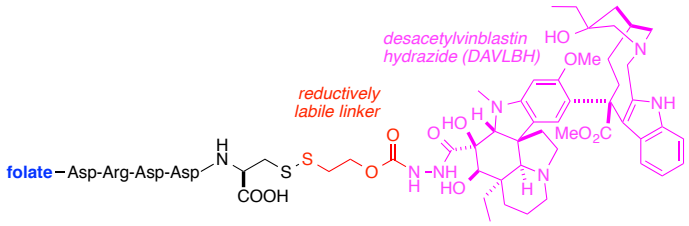

EC145 (Vintafolide)
targets FR
phase III, platinum resistant ovarian cancer (in combination with liposomal doxorubicin)
phase II, non-small cell lung, ovarian and endometrial cancers (in combination with docetaxel)

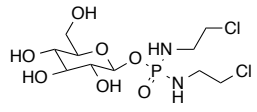

glufosfamide (glucose-iphosphoramide)
targets glucose transporter 1
phase III, metastatic pancreatic cacer

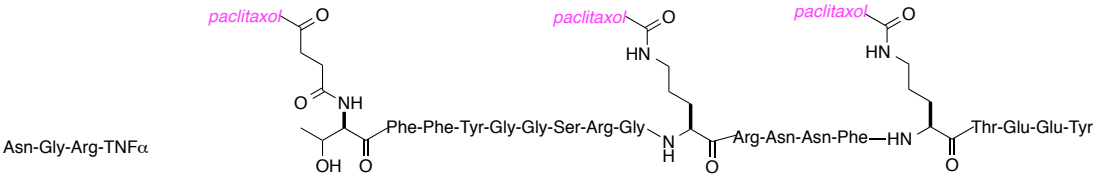

NGR-TNF
targets aminopeptidase N
phase II, soft tissue sarcomas, ovarian and kidney cancer
phase I, solid tumors
phase II and pilot, cancers of colorectal system

GRN1005 (AGN1005 or angiopep 2-paclitaxol)
targets low-density lipoprotein receptor-related protein 1
phase II, breast cancer with brain metastasis
phase II, non-small cell lung cancer (NSCLC) with brain metastasis (in combination with trastuzumab)

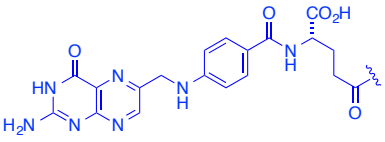

folate

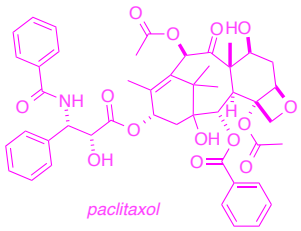

paclitaxol

Figure 1-2 Continued.

Small molecule ligands that target *neurotrophin receptors* are the main focus in this research. Two types of neurotrophin transmembrane receptors are known: (i) the p75 receptor, which binds all neurotrophins; and, (ii) a family of cell-surface neurotrophin receptor tyrosine kinases known as tropomyosin-receptor-kinase; TrkA, TrkB and TrkC which are more selective and tend to have higher binding affinities. For example, Nerve Growth Factor (NGF) selectively binds to TrkA, Brain-derived Neurotrophic Factor (BDNF) and neurotrophin-4/5 (NT-4/5) bind to TrkB, and neurotrophin-3 (NT-3) binds to TrkC. NT-3 can also bind to TrkA and TrkB receptors but with lower affinity. The binding of neurotrophin to Trk receptors may lead to activation of signal cascades resulting in the promotion of cell death, survival and differentiation.[44-49]

Up-regulation of Trk receptors is associated with several forms of cancer. For instance, overexpression of TrkC is found in some forms of neuroblastoma,[2,6-8,18,42-43,50-55] glioblastoma,[54,56-60] metastatic breast cancer[61-67] and metastatic melanoma.[68-76] Small molecule fragments that target TrkC are promising for use in several applications for treatment of these types of cancer.

Previous work in our group featured, bivalent peptide mimics designed to imitate β-turns of (NT-3).[77] These NT-3 mimics selectively bound TrkC, over TrkA and p75 receptors (*c.f.* NT-3 binds strongly to TrkC but has low affinity to TrkA, TrkB and p75). Our group discovered eight bivalent ligands that selectively bind to TrkC with small partial agonistic effects. Three of them regulated cell survival while the other five mimics induced neuron differentiation in the presence of NT-3. The use of these novel

ligands to conjugate with imaging or therapeutic agents would be useful in clinical applications.

Photodynamic Therapy

Photodynamic therapy (PDT: Figure 1-3) uses photochemical reactions for destruction of tissue.[60,78] A typical PDT clinical procedure is to inject an appropriate dose of photosensitizer into a patient's blood stream, where, ideally, the photosensitizer will accumulate in tumors. Light of a suitable wavelength, usually a red laser beam, will be directed to the tumors, where it excites the sensitizers, generating reactive oxygen species (ROS, e.g., $^1O_2$); ROSs cause cellular damage, resulting in vascular collapse, tissue destruction, and cell death.[79-80] Two important features of PDT are, first, the sensitizer only kills cells in the region that is irradiated ($^1O_2$ has a half-life of about 1 ns), and, second, targeting deep tissue requires agents that absorb light at longer wavelengths (ideally, >700 nm).[81-82]

PDT is a well-recognized modality for cancer treatment.[78-79,83] It destroys blood vessels that support tumor cells and activates immunological responses against them.[78] However, only a small number of PDT drugs have been approved; these include: (i) porfimer sodium (Photofrin) for the treatment of lung and digestive tract cancers and Barrett's esophagus; (ii) temoporfin (Foscan) for the treatment of head and neck cancers; and, (iii) aminolevulinic acid (ALA) for the treatment of actinic keratosis.[80]

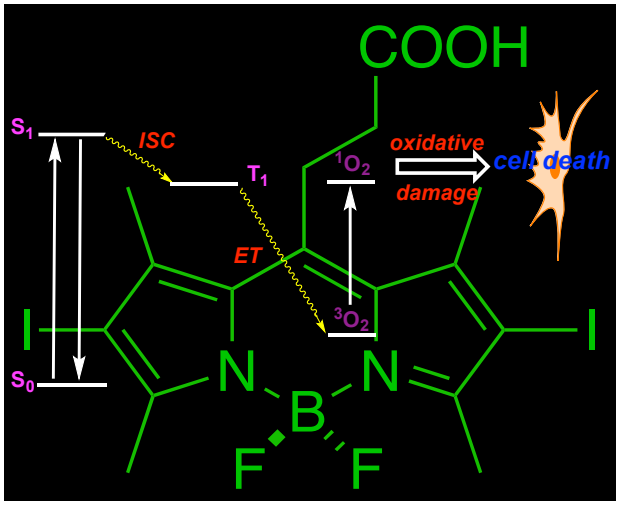

Figure 1-3. Illustrative photodynamic therapy (PDT). A photosensitizer (BODIPY shown in green) absorbs light at a specific wavelength, electrons from the ground state (S_0) will absorb energy and move to singlet-excited states (S_1). Some of the absorbed energy will be released via intersystem crossing (ISC) hence the promoted electron will move to a triplet-excited state (T_1). This triplet state has a relatively long half-life allowing energy to be transferred to oxygen molecules nearby, generating single oxygen that can damage the cells at that location.

Most clinically relevant PDT agents are cyclic tetrapyrroles (porphyrins, chlorins, and bacteriochlorins)[84-85] with modifications to modulate their photophysical and biological properties. However, there is growing interest in non-porphyrin photosensitizers that might be made more easily.[86-88] A well-known category of this type of PDT agent includes phenothiazinium-based structures; these are relatively easy to fabricate but have low light-to-dark toxicity ratios.[89]

A new class of PDT agents has emerged over the last decade and they are based on the 4,4-difluoro-4-bora-3a,4a-diaza-*s*-indacene (BODIPY) core. BODIPYs have many ideal photosensitizer characteristics including high extinction coefficients, environmental insensitivity, resistance to photobleaching,[90] and higher light-dark

toxicity ratios[91] than phenothiazinium[89] agents. Several reviews indicated the role of BODIPYs as fluorescence imaging probes,[92-96] but none of these focused on their PDT properties. Fluorescence occurs via relaxation from singlet excited states, hence high fluorescence quantum yields are *undesirable* for PDT sensitizers since the energy absorbed on excitation does *not* cross to triplet states if fluorescence occurs. Consequently, BODIPYs for PDT have to be modified to depress fluorescence and enhance singlet-to-triplet inter-systems crossing. Recent reviews in this area, one by us,[97] summarize characteristics of selected members in this emerging class of BODIPY-based PDT agents.[98]

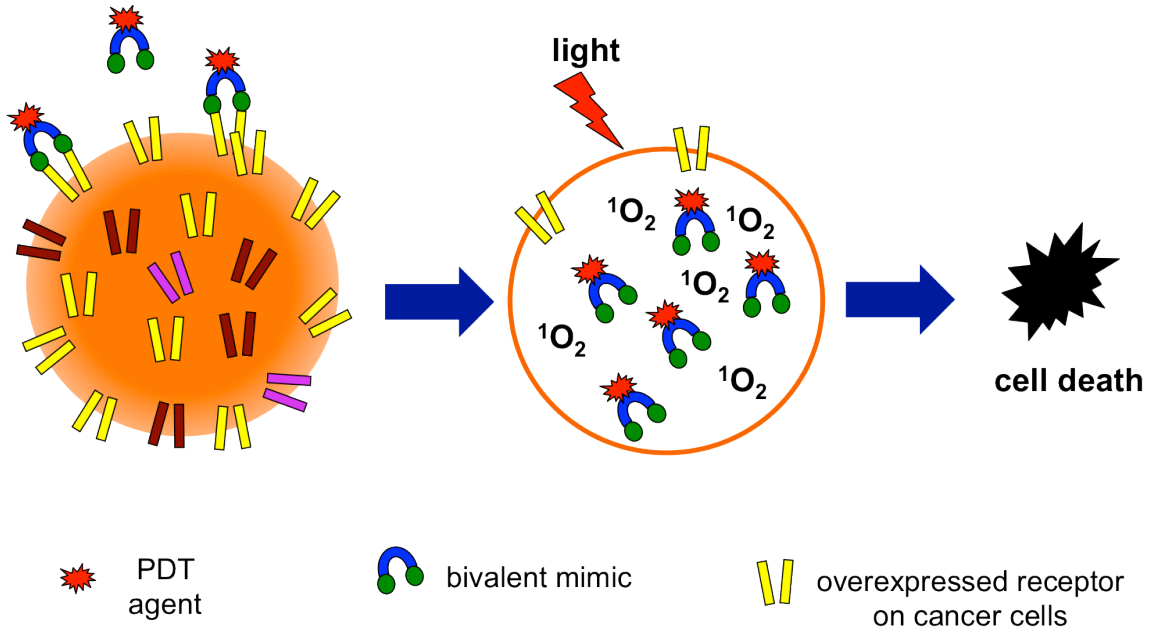

Figure 1-4. Concepts of active targeting via PDT. A PDT agent kill cells most effectively when it binds a cell surface receptor, induces receptor-mediated internalization, then light induces the generation of reactive oxygen species.

In this dissertation, novel BODIPY-based PDT agents have been synthesized. The use of *active targeting* to concentrate novel PDT sensitizer in tumors, and *spatial targeting* of light to ensure the PDT effect is confined to that region is one of the main focuses on my research (illustrate in Figure 1-4). There are several examples of actively targeted PDT agents in literature,[83,99-105] but this work gave the first agents for $TrkC^{+}$ tissue as applied to metastatic breast cancer and melanoma.

CHAPTER II

SMALL MOLECULE LIGANDS FOR ACTIVE TARGETING OF TRKC EXPRESSING TUMOR CELLS*

Introduction

Current US-approved small molecule pharmaceuticals for treatment of cancer tend to have low therapeutic indices, *i.e.* similarly toxic to cancerous and healthy tissue. Therapeutic indices of anti-cancer compounds can be increased by selective delivery; this is a form of "targeting". Unfortunately, the word "targeting" is ambiguous in biomedical research. For instance, compounds that inhibit enzymes over-expressed in tumor cells are sometimes described as "targeted", but they are not guided to the target via an extracellular chemical interaction.[106] Conversely, some physical or physiochemical properties (*e.g.* enhanced permeability and retention, and pH effects) favor accumulation of nanoparticles or acid-sensitive compounds in tumors; for the purposes of this work, we refer to this as *passive targeting*. Passive targeting can be useful, but the particles can still accumulate in healthy tissue surrounded by either relatively impermeable vasculature, or by abnormally acidic interstitial fluid. *Active targeting* occurs when proteins or small molecule ligands form chemical interactions with macromolecules selectively expressed on the surface of the targeted cells.[107]

---

* Reprinted with permission from "Small Molecule Ligands For Active Targeting Of TrkC-expressing Tumor Cells" by Eunhwa Ko, Anyanee Kamkaew, and Kevin Burgess, *ACS Med. Chem. Lett.* 2012, *3*, 10. Copyright 2012 American Chemical Society.

At least two possible factors can favor active targeting: (i) affinity of the ligand for that cell surface receptor; and, (ii) internalization of the ligand into the cells by the receptor. Actively targeted cytotoxicity occurs if one or both these effects are in play. One cells surface receptor that could be targeted is TrkC. We hypothesized this receptor is a good target because several tumor types over-express TrkC, including neuroblastoma,[50] medulloblastoma,[108] and breast cancer.[63] Moreover, this receptor internalizes the natural {neurotrophin} ligands that bind to it, fulfilling criterion (ii).[109]

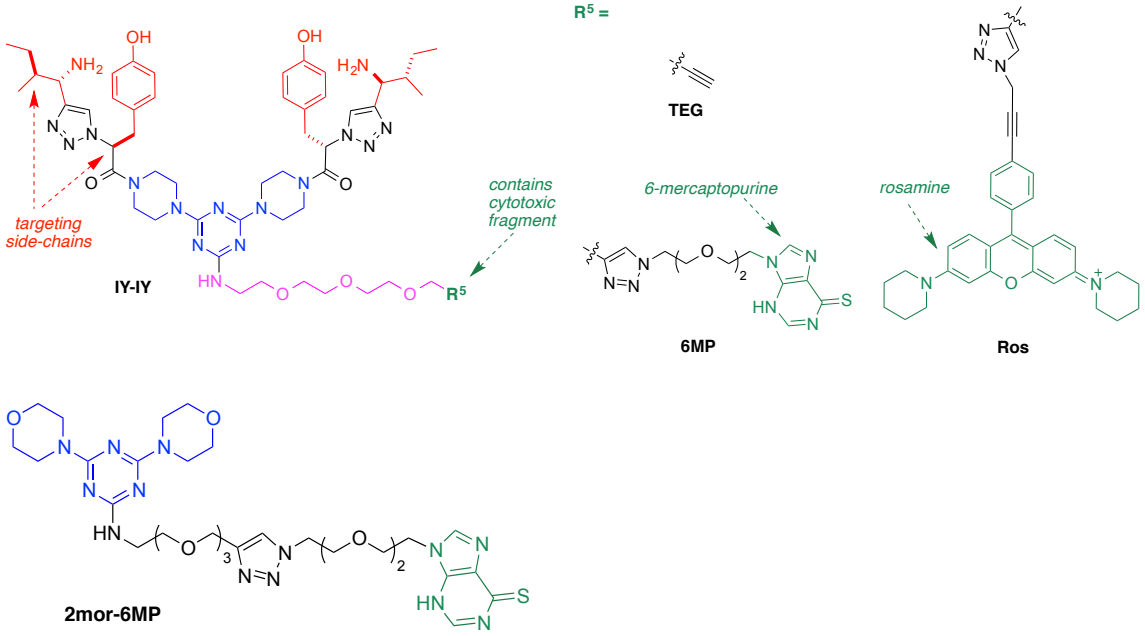

Figure 2-1. Targeting ligands used in this study, and the non-targeting control compound 2mor-6MP.

Research that is described in this *chapter* was undertaken to demonstrate active targeting of TrkC-expressing tumor cells could be affected using novel small molecule

targeting ligands. Specifically, a triazine-bridged compound **IY-IY-TEG** was used as a basis for this study (Figure 2-1). That compound was previously shown to bind TrkC-expressing cells and elicit agonistic effects, but only in synergy with the parent TrkC ligand, a protein growth factor called NT3.[77] Side-chain pharmacophores {shown in red} in **IY-IY-TEG** and related molecules were shown to be pivotal to binding.

Results and Discussion

The central hypothesis here is that the partial agonist activity of the **IY-IY** motif could be overwhelmed by incorporating a highly cytotoxic fragment in the same molecule, leading to selective binding and internalization for TrkC-expressing cells. 6-Mercaptopurine (**6MP**)[110] and a rosamine (**Ros**, a highly cytotoxic fluorescent probe)[111] were used for their cell-killing effects. We theorized permeation of **IY-IY-6MP** and **IY-IY-Ros** into cells would be disfavored because of size and polarity effects, *unless* active targeting was involved. To evaluate our hypothesis, cytotoxicities of **IY-IY-6MP** towards a cell line that does not express TrkC (wild type-NIH3T3 abbreviated to **WT**)[112-113] were compared with the same cell line stably transfected with TrkC (NIH3T3+TrkC abbreviated to **TrkC**; expression levels 10-20 x 10^3 receptors $cell^{-1}$).

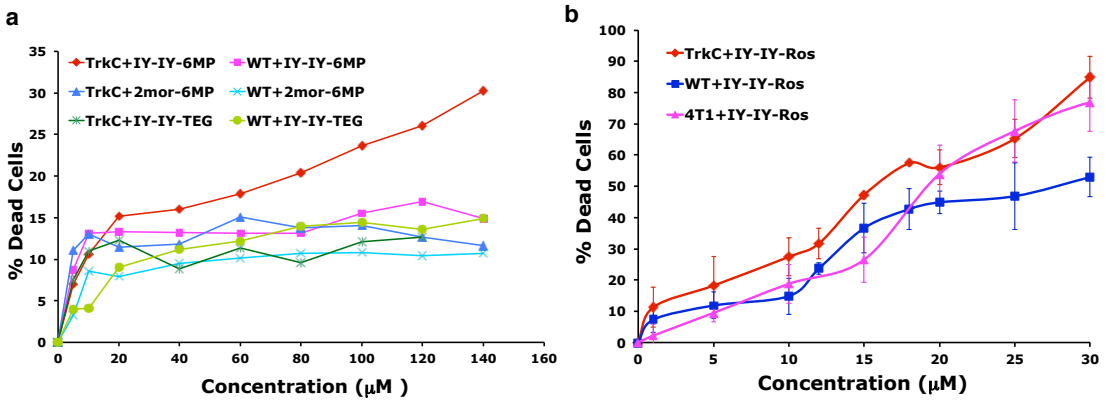

Figure 2-2. Anti-proliferative assays. **a IY-IY-6MP** selectively targets TrkC expressing cells (red) and not the parent line (**WT**, purple; data are shown with controls that demonstrate both the IY-IY amino acid side-chains and the **6MP** fragment were essential for cytotoxicity). **b IY-IY-Ros** shows more cytotoxicity for the TrkC expressing cells, **TrkC** (red) and **4T1** (purple), than non-TrkC expressing cells, **WT** (blue). Error bars were based on 3 runs, but are barely visible for the TrkC expressing cells (red) because they are so tight.

Figure 2-2a shows cytotoxicity data for **IY-IY-6MP**; the red line is for the TrkC-expressing cells (**TrkC**) and the purple one is for wild type (**WT**) NIH3T3 cells. *The conjugate is more cytotoxic towards cells that express TrkC*. All the other data in Figure 3-2a are for controls that, in the event, support this conclusion. Thus the non-targeted analog **2mor-6MP** (where the IY-IY motif is substituted by morpholine; Figure 3-2a) is not significantly cytotoxic to the **TrkC** or **WT** cells, and neither is the targeted but non-cytotoxic compound **IY-IY-TEG**.

It was impossible to determine an IC_{50} for **IY-IY-6MP** because the concentrations required exceeded the solubility of the compound. A relatively high amount was needed in solution because the cytotoxicities of N^9-alkylated derivatives of **6MP** are less than the parent system (ED_{50} = 50 μM for **6MP**, 400 μM for N^9-butyl and

600 μM for N^9-ethyl in Chinese hamster ovary cells).[114] For this reason the focus of the study shifted to **IY-IY-Ros**; the rosamine fragment of this molecule is significantly more cytotoxic (IC_{50} 0.39 ± 0.22 μM[111] for **Ros** *vs* 2.79 ± 0.69 μM[110] for **6MP**; both for MCF-7, human breast cancer cell line).

Figure 2-2b compares cytotoxicity data for **IY-IY-Ros** on the TrkC cells (**TrkC**; IC_{50} = 15.80 ± 0.18 μM), and on a murine breast cancer line that also expresses TrkC (**4T1**; IC_{50} = 19.88 ± 2.53 μM), with that for the non-TrkC expressing NIH3T3 cells (**WT**; IC_{50} = 27.58 ± 1.38 μM). More cell death occurred for the TrkC-expressing cells than for the non-TrkC expressing ones when ligand concentrations above about 18 μM were used. Cytotoxicity data for an analog with the *inverted* amino acid sequence **YI-YI-Ros** was used as a negative control (the **YI-YI** motif does not bind TrkC expressing cells).[77] The cytotoxicity of **YI-YI-Ros** with respect to the **TrkC** and **WT** cells was almost the same. Moreover, this data was also almost identical to that for **IY-IY-Ros** on the **WT** cells (IC_{50} = 25.80 ± 2.24 and 25.79 ± 1.79 μM); these data further support the targeting effect of the **IY-IY** motif.

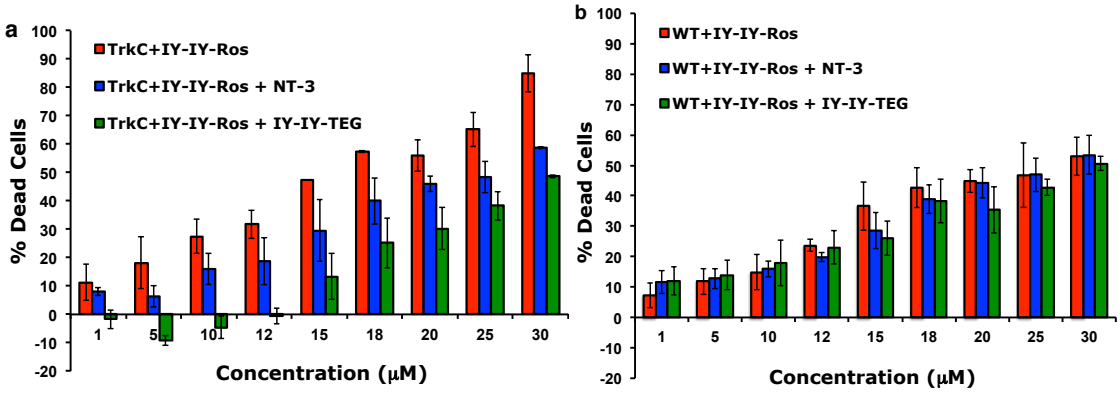

Figure 2-3. Dose-dependent reduction of **IY-IY-Ros** cytotoxicity (red) in competition with the TrkC ligands NT-3, 3.5 nM (blue) or **IY-IY-TEG**, 20 mM (green) occurs for **a TrkC** cells, but not for **b WT** cells. The concentration of NT-3 and **IY-IY-TEG** were kept constant throughout the experiments.

Further evidence for the targeting effect of the **IY-IY** motif was obtained from competition studies (Figure 2-3). The cytotoxicity of **IY-IY-Ros** was reduced in a dose dependent way by natural protein (NT3) and by synthetic (**IY-IY-TEG**) ligands, but only for the **TrkC** (Figure 2-3a), and not for the **WT** (Figure 2-3b), cells. Moreover, no competition was observed for the control with the inverted sequence **YI-YI-Ros** (see Appendix D).

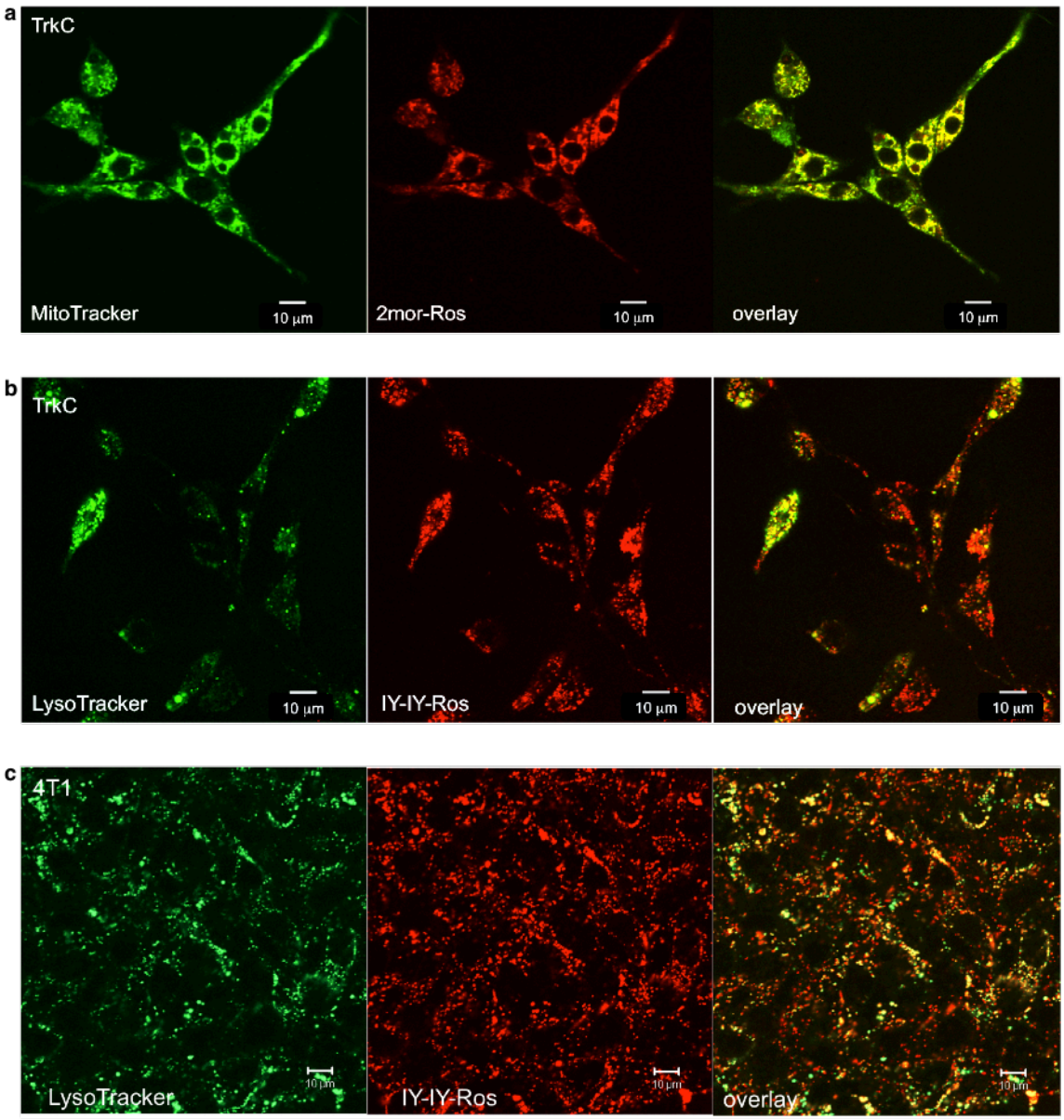

Figure 2-4. **a 2mor-Ros** and MitoTracker colocalize in TrkC cells; whereas, **b IY-IY-Ros** colocalizes with *LysoTracker* in the same cells, and **c** in murine 4T1 breast cancer cells that also express TrkC.

Complexes of NT3 with TrkC are internalized by cells and localize in the lysosome.[109] Conversely, the rosamine dye corresponding to **Ros** permeates into cells

and accumulates in the mitochondria.[111] Experiments were performed in the current study to probe if the rosamine fragment *with* the bridging triazine (**2mor-Ros**) was imported in the same way as the dye *without* that fragment (**Ros**). Figure 2-4a shows the distribution of the MitoTracker label in **TrkC** cells, distribution of **2mor-Ros** in the same cell, and the degree of overlay. These data indicate **2mor-Ros** localizes in the mitochondria, just as the parent dye does.

When the **Trk** cells were exposed to **IY-IY-Ros**, this *targeted* {cytotoxic} dye was internalized within 30 min. Fluorescence microscopy indicated the dye co-localized with LysoTracker (Figure 2-4b) and not with MitoTracker, *i.e. it accumulated in the same intracellular compartment as the TrkC-NT3 complex, and not in the same place as the rosamine dye.* When another TrkC-expressing line, murine 4T1 cells, was treated with **IY-IY-Ros** then this targeted {cytotoxic} dye also localized in the lysosome (Figure 2-4c). These data support the hypothesis that the **IY-IY** motif binds the TrkC receptor and is internalized.

Conclusions

A small molecule motif was used in "active targeting" to deliver cytotoxic substances into tumor cells that express the TrkC receptor. Underlying this study was the hypothesis that internalization of targeted conjugates into cells would be facile if mediated by receptor binding and receptor-ligand internalization. Initial experiments using 6-mercaptopurine gave encouraging data, but demonstrated the importance of maintaining solubility and high cytotoxicity. Conjugates of the targeting agent with a

cytotoxic rosamine (similar to a rhodamine) were more successful. Targeting of TrkC was observed, validated in a series of competition experiments featuring other TrkC ligands, and accumulation into lysosomes was observed, as expected for receptor-mediated internalization.

The featured targeted compounds **IY-IY-6MP** and **IY-IY-Ros** are *not* well suited for *in vivo* studies, for different reasons. The water-solubility and cytotoxicity of **IY-IY-6MP** is inadequate for *in vivo* work. For **IY-IY-Ros** the reasons are different; while these studies were in progress our collaborator Dr Hong Boon Lee tested the parent rosamine and found it caused severe weight loss in animals with inadequate concurrent reduction in tumor mass (personal communication). Consequently, studies to use the same targeting entities in conjunction with other cytotoxic compounds are underway.

Only a few small molecules are known for their active targeting effects; the important ones are as follows. Folic acid targets the folate receptor[23] expressed on many human cancers.[115] Mimics of the RGD peptide[116] target integrins,[117-118] and riboflavin-based compounds has been used to target its receptor expressed on some tumor types.[119-120] Bile acids target the vitamin D receptor in colon cancer and this has been exploited.[121] Lectin-based molecules[122] have been employed to direct therapeutic agents to the asialoglycoprotein receptor in the liver,[123] and cholestenoic acid, a ligand for the Liver X receptor,[124] also has value. γ-Amino-*n*-butyric acid (GABA) or the GABA-derivative baclofen targeting the $GABA_B$ receptor have been used in a novel approach for pancreatic cancer.[125] Overall, there is a great deal more interest in antibody-drug conjugates than in targeting-small-molecule-drug conjugates.

Given the exquisite affinities of antibodies (mAbs) for antigens, it is easy to understand why mAbs have attracted so much interest in targeting approaches. However, we postulated above that affinity *and* cell permeability are both important, and large proteins such as mAbs tend not to permeate into cells, where as small molecules can. Selective cytotoxicity studies of the kind performed here show the net effect of affinity *and* cell permeability.

Medicinal chemistry has been heavily biased towards the discovery and syntheses of cytotoxic compounds whereas development of small molecule ligands for active targeting has received much less attention. We suggest design and testing of small molecule ligands for active targeting of cancer cells, indeed for specific cell types in general, is both important and, so far, somewhat neglected.

CHAPTER III

DOUBLE-TARGETING USING A TRKC-LIGAND CONJUGATED TO BODIPY-BASED PDT AGENT[†]

Introduction

In oncology, the main problem with most FDA approved drugs is that they have poor therapeutic indices, *i.e.* they kill healthy tissue almost as effectively as tumors. In response there are many contemporary efforts to perturb biochemical pathways that are selectively upregulated in cancerous cells, *ie molecular* target-oriented approaches.[126] Kinase inhibitors are target-oriented in this way because they inhibit enzymes that are critical to the survival of cancer cells.[127-129] Another form of targeting features agents that selectively bind to certain types of *cells* and deliver imaging or cytotoxic agents inside. Most current research on *cellular* targeting involves antibodies; this strategy is useful but usually does not lead to intracellular delivery.[4,130] Conversely, some small molecules *can* be used for cell-based targeting and intracellular delivery;[20-22,118,131] the problem is how to design and validate substances that will do this. Yet another form of targeting is in photodynamic therapy (PDT). PDT is *physically* targeted insofar as only the tissue illuminated by the light source is vulnerable to production of reactive oxygen

---

[†] Reprinted with permission from "Double-Targeting Using a TrkC Ligand Conjugated to Dipyrromethene boron Difluoride (BODIPY) Based Photodynamic Therapy (PDT) Agent" by Anyanee Kamkaew and Kevin Burgess, *J. Med. Chem.* 2013, *56*, 7608. Copyright 2013 American Chemical Society.

species from a photosensitizer and triplet oxygen. One problem with PDT is how to localize the required photosensitizer in tumor tissue.

Any strategy that involves *two* of the approaches outlined above might be called "doubly-targeted". For instance, a PDT agent conjugated to a small molecule cell-targeting unit might preferentially localize in tumor cells, giving a first level of targeting. A second level of targeting could then be achieved by limiting the light excitation source and consequently generation of reactive oxygen species to that area. There is, in fact, very little in the literature about cell-targeted PDT agents,[83,99,132] and, to the best of our knowledge,[97] nothing on such agents featuring BODIPY-based photosensitizers.[98]

Chapter 2, we reported on a novel small molecule system for targeting cells that overexpress the TrkC receptor.[133] That study featured two conjugates with cytotoxic compounds (6-mercaptopurine and a rosamine derivative), neither of which are PDT active. We found the potency of the conjugates to be somewhat restricted by inadequate solubility or cytotoxicity of the cargo. This chapter reports conjugates of the same cell-targeting agent, based on Tyr and Ile side-chains (IY-IY), to a diiodo-BODIPY PDT sensitizer reported by Nagano *et al*.[90] and us.[91] Thus the featured conjugate called **IY-IY-PDT** (Figure 3-1) can target $TrkC^+$ cells and be physically-targeted by the regions exposed to light. We had believed this is the first example of double-targeting involving a BODIPY-based PDT agent, but we recently became aware of similar work by Ng *et al* in a paper that now accompanies this.[134]

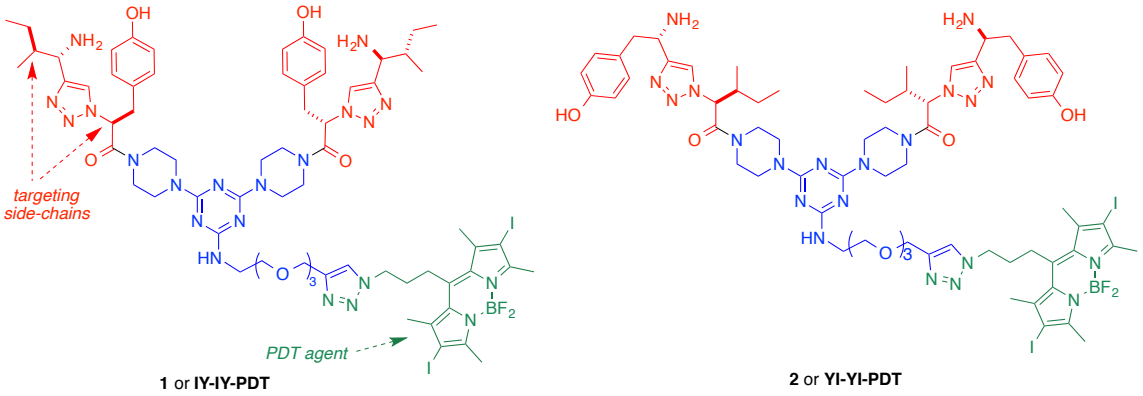

Figure 3-1. Structures of $TrkC^{+}$ targeting compound (**1** or **IY-IY-PDT**) and the scrambled control compound (**2** or **YI-YI-PDT**).

Results and Discussion

*Compound **1** and Cell Lines Used.* The targeting unit IY-IY has non-cytotoxic groups attached to the triazine entity; it weakly synergizes with the natural TrkC neurotrophin-ligand, NT3, enhancing cell survival but not differentiation.[77] Overexpression of TrkC receptors is associated with some forms of cancer (*e.g.* neuroblastoma,[50] medulloblastoma,[108] and breast cancer[63]), and with melanoma,[68,73,135-137] the latter being particularly interesting because lesions near the tissue surface can be most effectively radiated by UV light. Conversely, compounds with the inverted side-chain sequence, *ie* YI-YI, did not show this activity. Thus **IY-IY-PDT** is the featured cell-targeting agent, and **YI-YI-PDT** can be used as a negative control. Compound **2** or **YI-YI-PDT** is an excellent control being isomeric with **1** but unable to target the TrkC receptor (structures shown in Figure 3-1). Scheme 3-1 shows the synthetic route that was used to prepare **IY-IY-PDT** and **YI-YI-PDT**. Basically, this entails copper-

mediated 2+3 cycloaddition[138-139] of the azido-diiodoBODIPY **B**, which has apparently not been made before, with the alkyne **A** featured in our earlier studies.[77]

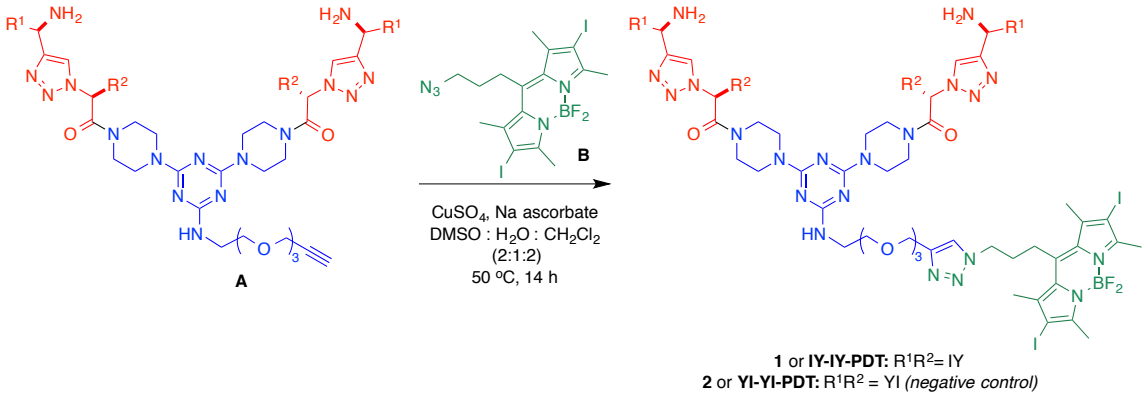

Scheme 3-1. Synthesis of **IY-IY-PDT** and **YI-YI-PDT**

Photophysical properties for the conjugates **1** and **2** were measured in DMSO and in DMEM medium; the data are presented in Figure 3-2 (and Appendix E). The absorption maximum of the BODIPY core for these molecules is in the region of 540 nm. We judged this to be perfectly fine for the planned *ex vivo* studies. As the project progresses after this paper, a more conjugated agent with a longer λ_{max} will be required for *in vivo* work since tissue is far more permeable to longer wavelength light.[140]

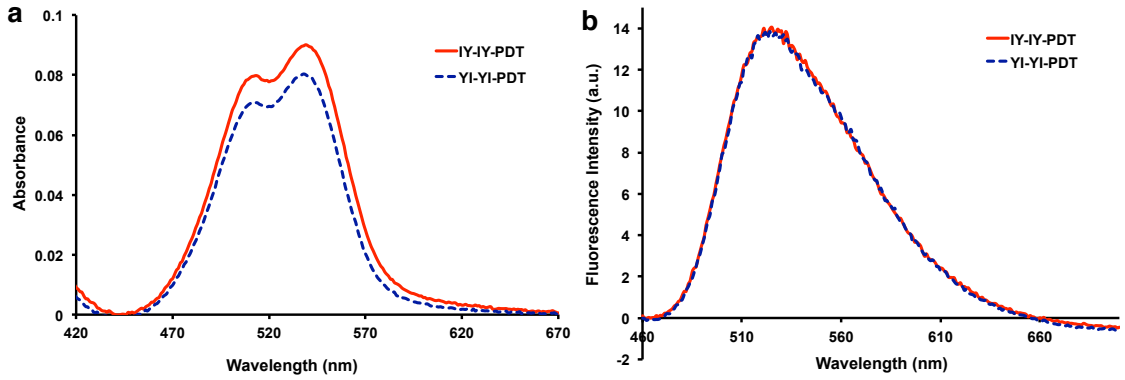

Figure 3-2. **a** UV-Vis and **b** fluorescence spectra (excited at 450 nm) of **1** and **2** (both at 5.5 μM) in DMEM medium.

Another strategy used to test for TrkC targeting in this work featured similar cell lines that do and do not express TrkC. Wild type NIH3T3 fibroblast cells (NIH3T3-WT) do not express TrkC,[141] and these could be compared with genetically modified forms of the same cell line stably transfected with TrkC at approximately 20,000 copies per cell (NIH3T3-TrkC, kindly supplied by Dr David Kaplan, The Hospital for Sick Children, Toronto). We also tested a human neuroblastoma cell line, SY5Y that is TrkC-positive.[52,108]

Light and Dark Cytotoxicities. Figure 3-3a shows data that demonstrates **IY-IY-PDT** is only cytotoxic to NIH3T3-TrkC cells when illuminated (>480 nm source with fluence rate 12.2 mW/cm^2 for 10 min), whereas this agent is not cytotoxic in the dark. The cells survive under the same conditions when a photosensitizer was not added (data not shown). A significant PDT effect was also observed for **IY-IY-PDT** on the NIH3T3-TrkC cells as compared with the non-targeted agent **YI-YI-PDT**, (IC_{50} 0.35

μM and >2 μM, respectively). These experiments were performed by treating the cells with **1** or **2**, washing them to remove the unbound agent, then illuminating. Observation of some PDT effect for the negative control **YI-YI-PDT** can be attributed to non-specific endocytosis; consistent with this light induced cell-death was also observed when the same experiment was performed using NIH3T3-WT cells (see Figure 3-6 below and Appendix E).

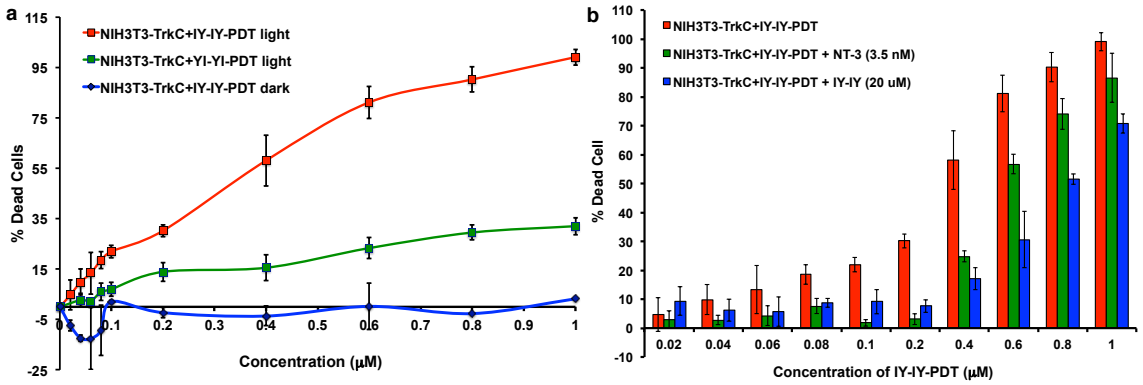

Figure 3-3. **a** Cytotoxicities induced by **IY-IY-PDT** under light (red) and dark (blue) and scrambled negative control **YI-YI-PDT** under light (green) conditions for a cell line stably transfected with TrkC receptors. Throughout this paper, in the light experiments the cells were illuminated with a broad spectrum source, filtered to only deliver photons of >480 nm wavelength, at a flux of approximately 12.2 mW/cm^2 for 10 mins. **b** Dose-dependent reduction of **IY-IY-PDT** photoinduced cytotoxicity (red) in competition with the TrkC ligands NT-3, 3.5 nM (green) or **IY-IY**, 20 μM (blue) on cells expressing TrkC. The concentration of NT-3 and **IY-IY** were kept constant throughout the experiments. Error bars were based on 3 runs.

The PDT effect of **1** on NIH3T3-TrkC cells was dose dependent (Figure 3-3b, red bars). In experiments also shown in Figure 3-3b the cells were simultaneously treated with a constant concentration of either the native ligand NT3 (green bars), or control compound **A** (or IY-IY; blue bars) comprised of the same targeting agent but

lacking the diiodo-BODIDY entity. Data for the two competition experiments shows a "breakpoint" at around 0.2 μM of **1**; below this, the two TrkC ligands that do not bear a PDT agent (*ie* 3.5 nM of NT3, and 20 μM of **A**) overwhelmed the affinity of **IY-IY-PDT** to the cells so the green and blue bars do not show much cell death, whereas there were significant cytotoxicities in the experiments without these competing agents (red bars). Above that breakpoint the effects of binding the targeted PDT agent are evident for the blue and green bars because the concentration of the PDT agent overwhelmed that of the innocuous competing controls.

Imaging of Internalization via Confocal Microscopy. NIH3T3 cells were treated with a supernatant containing 0.5 μM **IY-IY-PDT** for 2 h; the cells were washed (3 x PBS buffer), then imaged. Figure 3-4 shows that the weak I_2-BODIPY fluorescence becomes localized in punctates, but only for the cells that are transfected with TrkC. No intracellular fluorescence was observed under these conditions for the negative control **YI-YI-PDT** (second row), or for $TrkC^-$cells treated with the featured agent **IY-IY-PDT**.

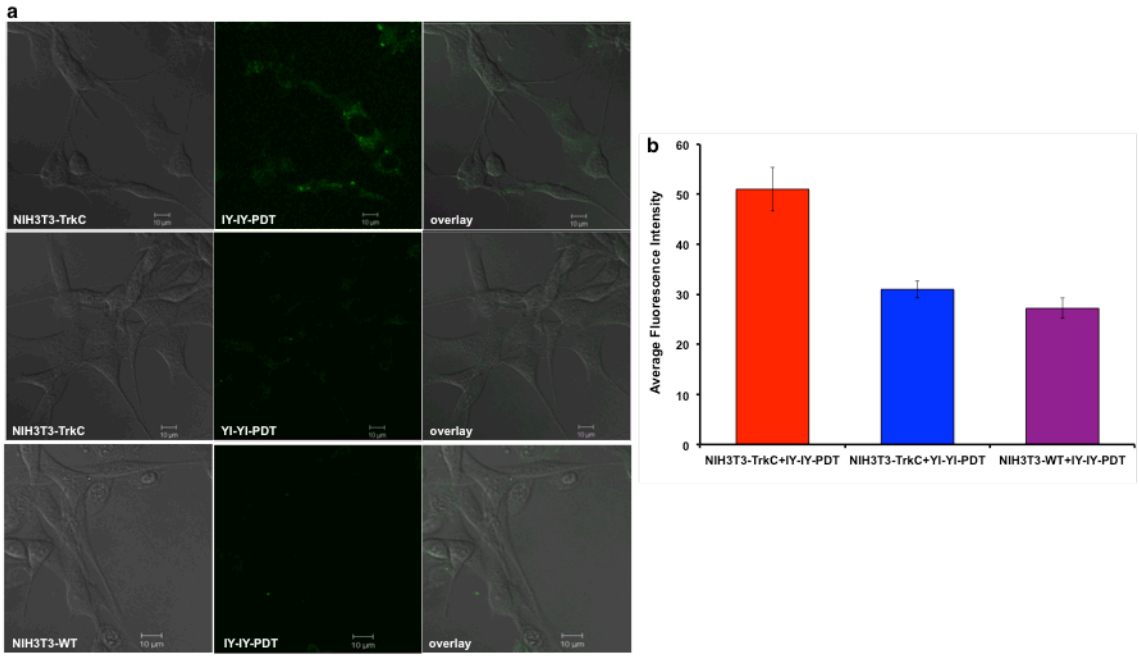

Figure 3-4. **a** Confocal imaging of: *first row*, the featured targeting ligand on $TrkC^{+}$ cells showing the compound is internalized; *second row*, the negative control **YI-YI-PDT** is not localized under the same conditions; *third row*, the featured agent is not observed in $TrkC^{-}$ cells under the same conditions. **b** Quantitative indications of the fluorescence intensity in each of the three experiments described above (error bars from 100 cells).

The images in Figure 3-4 do not show strong fluorescence because emission from IY-IY-PDT is intrinsically weak. However, bright images could be obtained by increasing the concentration and the incubation time from 2 h to 12 h, and these data are shown in Figure 3-5. The {higher magnification} images in Figure 3-5 include experiments with *LysoTracker Red* showing that IY-IY-PDT localizes in the lysosome, and not in the mitochondria and endoplasmic reticulum. It is known that when NT3 binds the TrkC receptor the complex is internalized and also localized in the

lysosome.[109] The fact that IY-IY-PDT is processed in the same way is therefore circumstantial evidence that it enters the cells via the same receptor, TrkC.

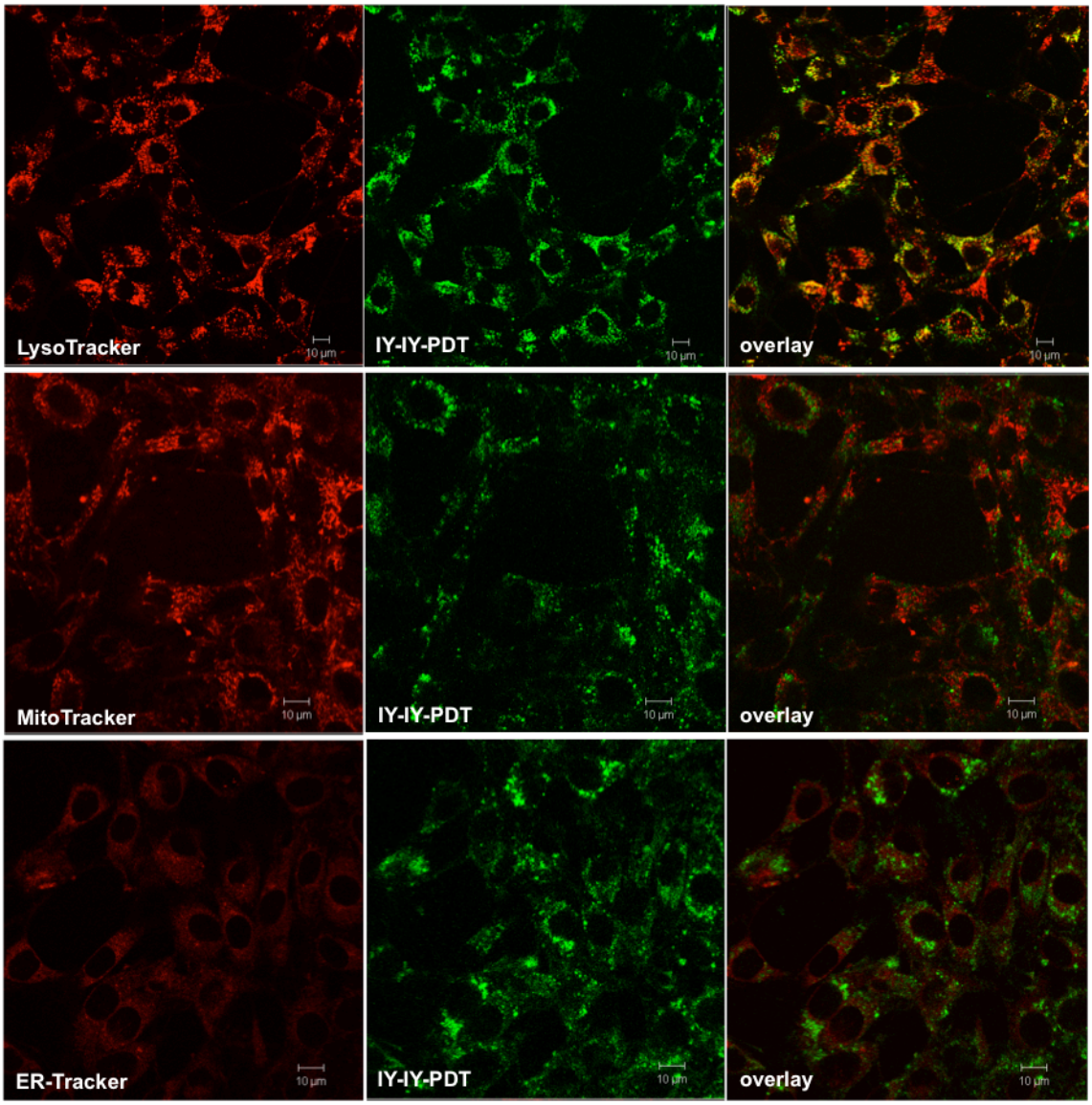

Figure 3-5. IY-IY-PDT colocalizes with *LysoTracker Red* in $TrkC^{+}$ cells. Throughout, the concentration of the agent used was 1 μM.

Photocytotoxicities on the SY5Y Neuroblastoma Cell Line. Figure 3-6 shows that **IY-IY-PDT** is photocytotoxic to the $TrkC^+$ neuroblastoma line SY5Y. We were unable to find a neuroblastoma line that does not express TrkC, so this plot also shows the photocytotoxicity of the same agent on NIH3T3-TrkC and NIH3T3-WT for comparison. The observed photocytotoxicity of **IY-IY-PDT** was significantly greater for the cells that express TrkC than that observed for the non-targeted **YI-YI-PDT** control on the SY5Y cells.

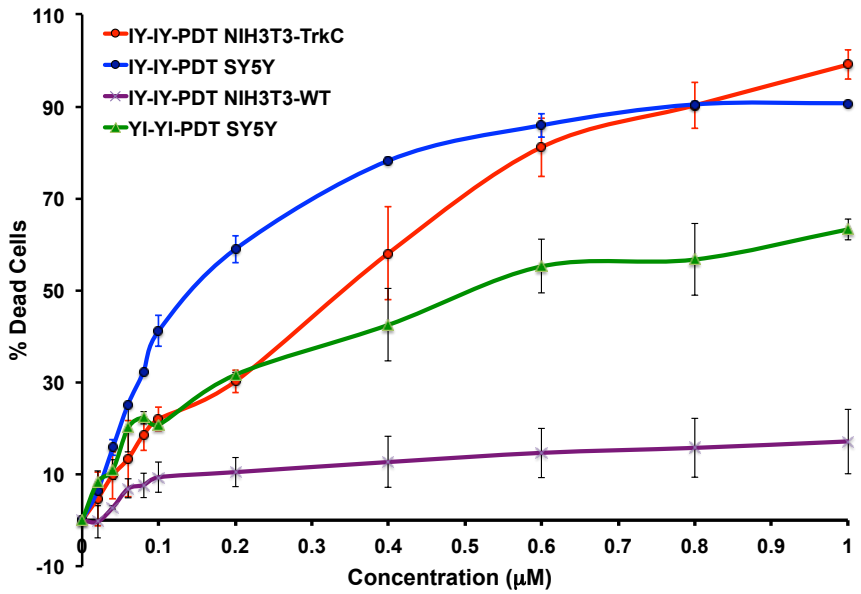

Figure 3-6. Photoinduced cytotoxicity assays. **IY-IY-PDT** shows high cytotoxicity for the TrkC expressing cells, NIH3T3-TrkC (red) and SY5Y (blue) compared to non-TrkC cells, NIH3T3-WT (purple). The non-targeting ligand, **YI-YI-PDT** (green) is significantly less photocytotoxic. Error bars were based on 3 runs.

Conclusions

The featured agent **IY-IY-PDT** showed significantly higher photocytotoxicities (IC_{50} = 0.35 ± 0.06 μM NIH3T3-TrkC; IC_{50} = 0.15 ± 0.02 μM SY5Y) than similar conjugates we prepared featuring 6-mercaptopurine and a rosamine in place of the PDT agent.[133] On the other hand, the non-targeted ligand **YI-YI-PDT** is considerably less cytotoxic.

In general, IC values can be used to calculate *ex vivo* therapeutic indices.[142] However, for **IY-IY-PDT** on $TrkC^+$ cells relative to $TrkC^-$ ones, this was impractical because the conjugate had such a low photocytotoxicity to the $TrkC^-$ cells, which made it difficult to determine even an IC_{10} value. These observations point to the considerable potential for selective killing of $TrkC^+$ tumor cells, and indicate further studies to monitor the effects of **IY-IY-PDT** on $TrkC^+$ tumors *in vivo*, and pharmacokinetic analyses of this agent, are justifiable.

Consideration of *The Human Protein Atlas*[143] reveals neuroblastoma tends to express high levels of TrkC, and several other tumor types (notably breast and melanoma) express lower, but significant TrkC levels. These tumors may therefore be suitable to test the targeting effects of IY-IY ligands.

Patients afflicted with the same type of cancer may have genetically different tumor cell types that express *different* levels of TrkC. Consequently, a goal for this type of research could be a form of personalized medicine of the following kind. More fluorescent cell-targeting conjugates similar to **IY-IY-PDT** would be used to identify and locate $TrkC^+$ cancers, cytotoxic materials like **IY-IY-PDT** are employed to reduce

the tumor mass, and the afflicted area is then re-imaged to gauge success. The next step towards reaching this goal will be to modify the PDT agents, for the reasons below.

Tissue is significantly more permeable to near-IR light than it is to radiation of shorter wavelengths.[140,144-146] Consequently, it will be important to use PDT agents that absorb at longer wavelengths when this work progresses to the *in vivo* stage because in that case tumors can be addressed in deeper tissue. The BODIPY fragment in **IY-IY-PDT** has a UV absorption maximum of around 540 nm in DMEM (one of the culture media used in this work). That absorption wavelength is suitable for *ex vivo* studies such as the ones described here. Alternatives to the diiodo-BODIPY fragments that could be used for *in vivo* studies include aza-BODIPYs,[147-151] and styryl-BODIPYs[152-154] as featured in the accompanying paper by Ng *et al*.[134]

CHAPTER IV

TARGETED PDT AGENT ERADICATES TRKC EXPRESSING TUMORS VIA PHOTODYNAMIC THERAPY (PDT)[‡]

Introduction

Agents that selectively associate with cell surface receptors over expressed on tumor cells can be used to deliver therapeutics. This strategy is referred to here as *active* to distinguish it from other forms of targeting (*e.g.* where the agent is intended to directly cause a therapeutic effect by binding cell surface receptor, or is designed to target intracellular pathways upregulated in cancer cells).[155-156]

The most widely investigated active targeting agents are humanized monoclonal antibodies (hmAbs), but mAbs in general have limitations.[40] First, only a few mAbs enter cells,[4] most do not,[12] and even cell-permeable mAbs may not reach the intracellular target.[5] Moreover, mAbs can have undesirable immunogenic effects, circulation times, and they are further restricted by cost and shelf-life issues.[16,157]

Active targeting via *small molecules* that selectively bind to receptors on tumor cells can have advantages relative to hmAbs with respect to cell-internalization and affordability; however, relatively few small molecule targeting entities are known. Folic acid[20-22,131] and Arg-Gly-Asp peptidomimetics[28-32] are probably the most widely

---

[‡] Reprinted with permission from "Targeted PDT Agent Eradicates TrkC Expressing Tumors Via Photodynamic Therapy (PDT)" by Chin-Siang Kue, Anyanee Kamkaew, Hong Boon Lee, Lik Voon Kiew, Lip Yong Chung, and Kevin Burgess, *Mol. Pharmaceutics* 2015, *12*, 212. Copyright 2015 American Chemical Society.

appreciated examples, but there are not many more besides these. There are no clinically approved small molecule active targeting agents for delivering therapeutics to breast cancer.[158]

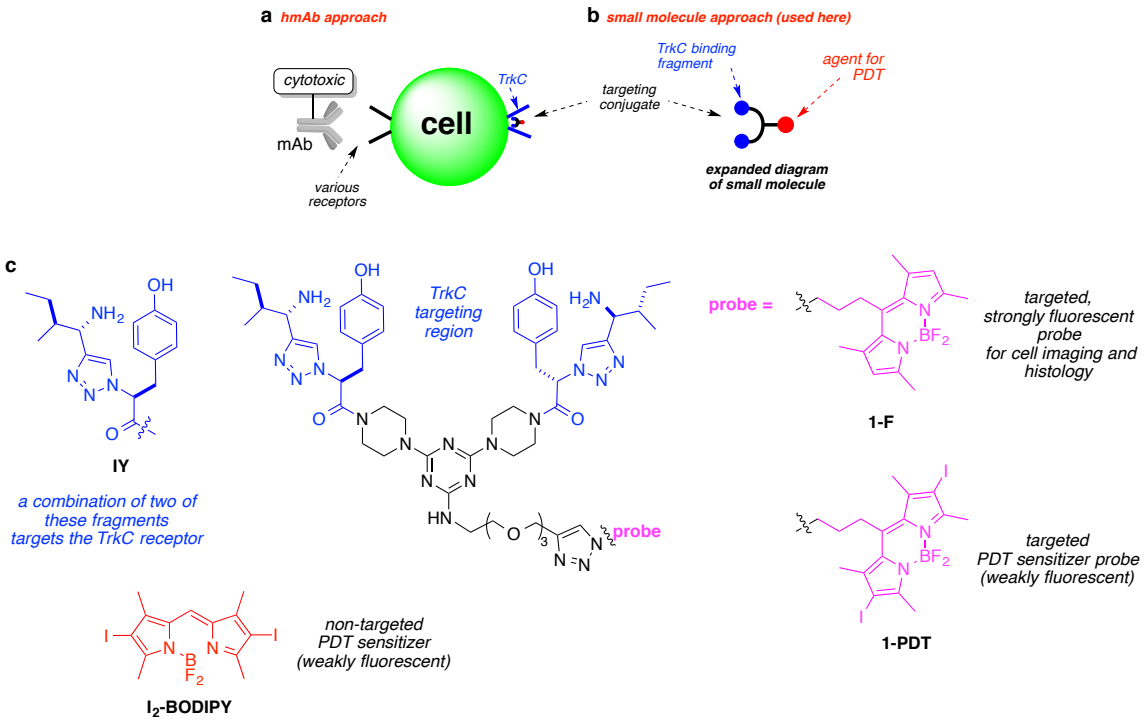

Figure 4-1. Fundamentals of active targeting. **a** mAb conjugates have limited cell permeabilities, but, **b** many small molecule conjugates can. **c** Structures of the targeted compounds featured in this work, **1-F** and **1-PDT**, and the parent iodinated BODIPY, **I_2-BODIPY**.

TrkC, is a cell surface receptor and its natural ligand neurotrophin-3 were reported to plays an essential role in breast cancer growth and metastasis;[61-62] suppression of TrkC expression in highly metastatic mammary carcinoma cells inhibited their growth *in vitro* and their ability to metastasize from the mammary gland to the lung

in vivo.[63] This paper features a novel molecular fragment **IY** (Figure 4-1) for active targeting of breast cancer types that overexpress TrkC.[77,159-160] TrkC-targeting molecules **1**, containing fragments **IY** (blue in Figure 4-1), elicit only weak functional effects.[77] One fragment **IY** is not enough to bind TrkC adequately, but two joined as shown give good affinity.[77] The scaffold part in molecules **1** (shown in black) supports the two TrkC-binding entities, and the BODIPY cargoes (colored purple and red here). The BODIPY dyes are similar, except that those without iodines are highly fluorescent, while ones with are only weakly fluorescent and act as sensitizers for singlet oxygen production. Thus, compound **1-F** (F = fluorescent) is designed for cell imaging and histology, while **1-PDT** is intended for use in PDT.[78,80]

Singlet oxygen is very reactive, half-life 1 ns to 1 ms, hence the effect of PDT agents illuminated in an aerobic environment is to generate $^1O_2$ that kill cells in a highly localized area. Some boron dipyrromethene (BODIPY) based-systems can have excellent attributes for PDT with high extinction coefficients, favorable light-to-dark toxicity ratios, high antitumor efficacies *in vivo*, and good body clearance[90-91,97-98,150] but they are not inherently inclined to localized in tumors; accumulation of the sensitizers in tumors is important for PDT. Experiments described in this paper were undertaken to explore the effects of coupling molecular fragments **IY** that can bind TrkC receptors expressed on breast cancer cells and deliver a BODIPY-based PDT agent to them. As far as we are aware, there are no other agents, in the clinic or in the literature on experimental modalities, that actively target $TrkC^+$ with a small molecular fragment that binds this receptor, conjugated to a therapeutic.

Results

Compound 1-F Selectively Stains TrkC-expressing Tissue, and Is Internalized by TrkC+ Cells. We hypothesized that agent **1-F** could be used to stain tissue that expresses $TrkC^+$ (*e.g.* from biopsies), and, $TrkC^+$ tumors and metastases during surgeries. In histochemistry on a commercial array of human breast cancer sections using **1-F**, all 36 malignant tissues showed evidence for expression of TrkC (23 % with unambiguous staining in the cytoplasm and cell membrane, 65 % same but not as clear, and in 12 % not all the tumor cells stained); conversely, none of the normal breast tissue showed significant staining in the cytoplasm and cell membrane just as fluorescent anti-TrkC mAb did (Figure 4-2a). We infer **1-F** has potential for histochemistry, and as a surgical marker for TrkC-expressing cancers.[63]

Intracellular imaging studies featuring **1-F** on murine 4T1 cells (Figure 4-2b) showed compound **1-F** is internalized and partially co-localizes with a lysosome tracker dye. Thus, **1-F** localizes into the lysosome, just as the natural TrkC ligand "neurotrophin-3" (NT3) does when it is internalized via the TrkC receptor,[109] implying **1-F** also enters the cell via TrkC. Similar experiments were performed using {the less fluorescent agent} **1-PDT**, and the outcome was much the same (Appendix F). Moreover, import of **1-PDT** at 2 h was more than **2-PDT** into 4T1 cells, and that uptake of **1-PDT** was suppressed by pre-treatment with the natural TrkC ligand, NT3.

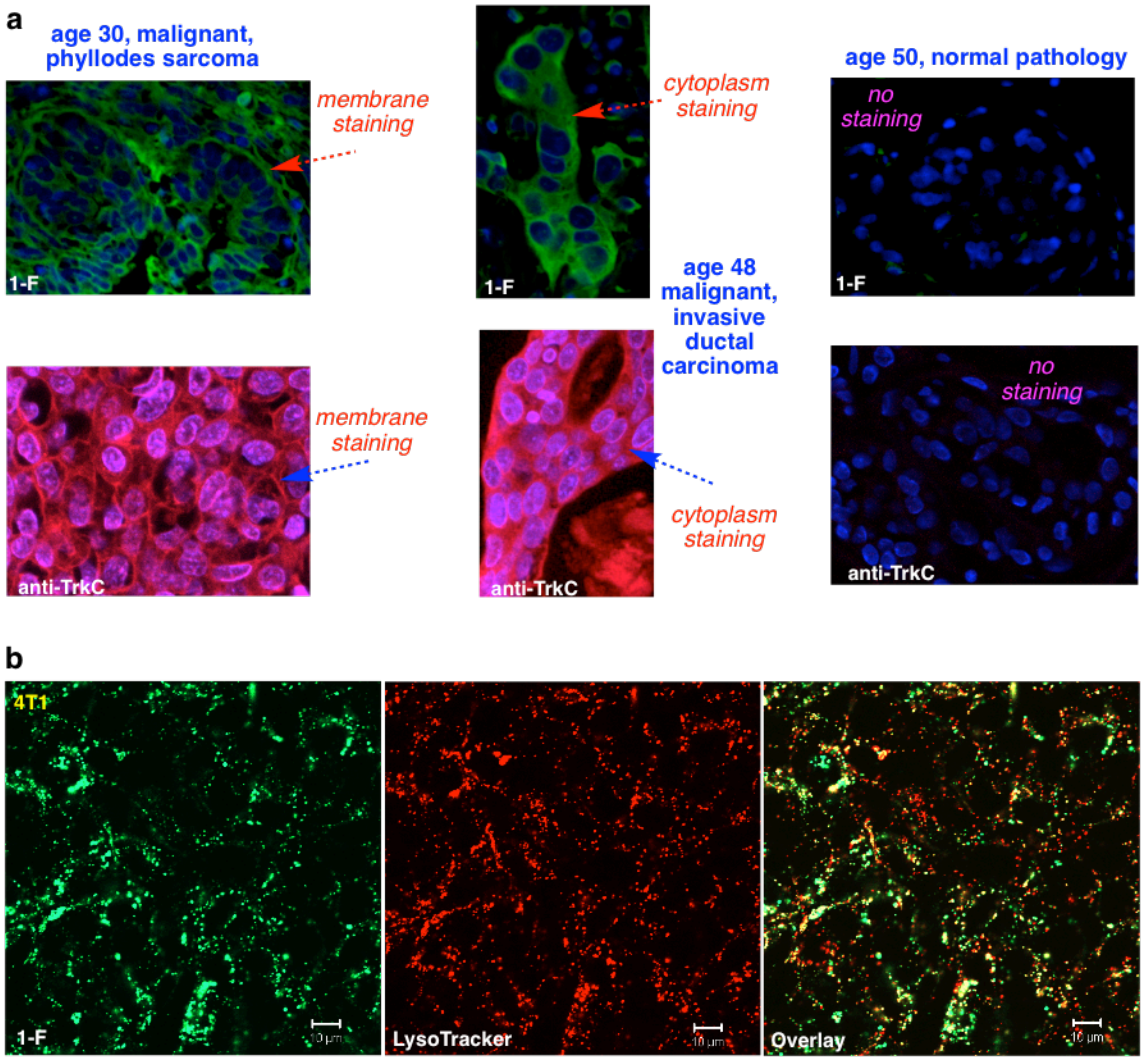

Figure 4-2. Compound **1-F** stains in TrkC^{+} tumor tissue and is internalized TrkC+ cells. **a** Histochemical stains for a library of 96 breast tissue slices were performed using **1-F** (top) and anti-TrkC antibody as control (bottom), and the three illustrative ones shown here illustrate staining of the malignant tumor, whereas normal tissue is not stained. No staining was observed in the tissues without the small molecule probe or mAb. **b** Cell imaging on 4T1 cells shows **1-F** was internalized into lysosomes just as the natural TrkC ligand NT3 is.

Compound 1-PDT Selectively Kills TrkC-expressing Cells in Tissue Culture.

Binding NT3 to TrkC on the surface of living cells causes growth and survival.[161-162]

Some common breast cell lines used for cancer research express TrkC (*eg* human Hs578t

and murine 4T1) [63,163] but not in others (*eg* SKBR3, 67NR and MCF-10A).[63,164] TrkC *is* expressed in the majority of metastatic breast tumors.[66]

Figure 4-3a shows photocytotoxicities of **1-PDT** are greater for the $TrkC^+$ breast cancer cell lines HS578t and 4T1 than the immortalized, $TrkC^-$, breast cell lines 67NR and MCF-10A. Comparison of photocytotoxicities for the targeted PDT agent **1-PDT** with the non-targeted form **2-PDT**, and **I2-BODIPY** on $TrkC^+$ expressing cells (Figures 4-3b and 4-3c) shows the targeted agent is more photocytotoxic (IC50 = 0.325 μM in 4T1; IC50 = 0.285 μM in HS578t) than the control ones, **2-PDT** and **I2-BODIPY** (undetermined IC50), which does not bind TrkC. These results suggest that **1-PDT** induces selective photocytotoxicity in TrkC-expressing cells via TrkC receptor targeting. Some photocytotoxicity was observed for **2-PDT** on the human HS578t but not on the murine 4T1 cells, indicating the scrambled control **2-PDT** might be binding to some other receptor on the human line.

Figure 4-3d shows the photocytotoxicities of **1-PDT** on $TrkC^+$ cells can be suppressed by the natural TrkC ligand (NT3) or the targeting agent without any BODIPY dye attached, "**IY-IY-TEG**" (structure in Appendix F). When interpreting this data it is important to note that the concentration of NT3 is constant throughout, so **1-PDT** only becomes noticeably competitive with the small molecule ligand at higher concentrations (*eg* > *ca* 0.1 μM for human cells, Figure 4-3d right side).

All the photocytotoxicity experiments described above involved adding the test compounds for 2 h incubation, washed off before illuminating the cells. Effects of prolonging the incubation on the cell viability in PDT revealed that more selective cell-

growth inhibition was achieved for TrkC$^+$ 4T1 compared to TrkC$^-$ 67NR at 2 h incubation (Appendix F), and the difference becomes less noticeable when 4 h and 6 h incubation was used; thus a shorter incubation time is optimal for selective photo-killing by the TrkC-seeking conjugate. For a full comparison, the same time course experiments for the untargeted **2-PDT** and the parent iodinated BODIPY, **I_2-BODIPY**, were also performed (Appendix F). As expected, both compounds caused increased photocytotoxicity with increasing incubation time. However, the cell viability observed between 4T1 and 67NR cells were similar across the different time points for incubation implying no selective binding to cell surface receptors (Appendix F).

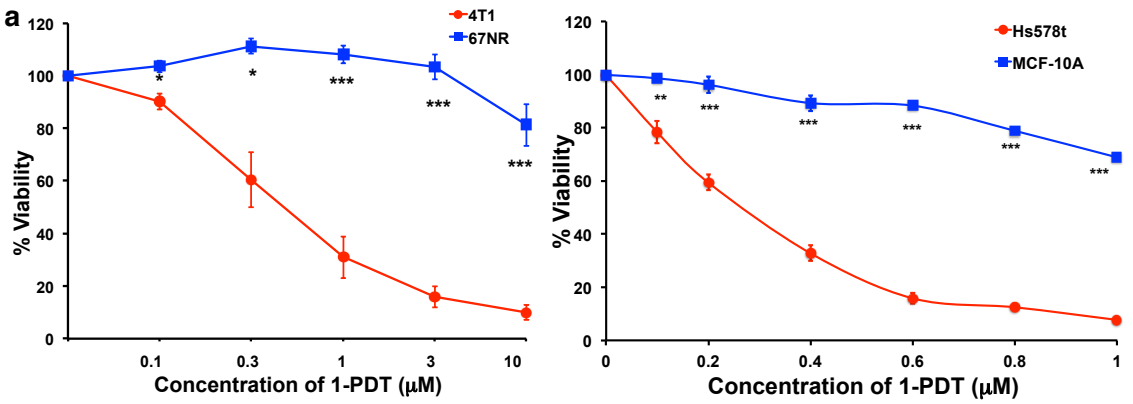

Figure 4-3. 1-PDT is photocytotoxic in TrkC+ cell lines. **a** Photocytotoxicities for **1-PDT** are more for the following breast cells: murine metastatic 4T1 and human metastatic, Hs578t; compared with the following breast cell lines: murine non-metastatic, 67NR; human immortalized MCF-10A. **b** Photocytotoxicities on the 4T1 and Hs578t cells were enhanced for **1-PDT** compared to the scramble control **2-PDT** featuring an isomer of the targeting fragment that does not adhere to TrkC$^+$ cells and control **I2-BODIPY**. **c** Structure of **2-PDT**. **d** Photocytotoxicities for **1-PDT** on 4T1 and HS578t cells are dose dependent (red bars), and suppressed by fixed concentrations of competing: (i) natural ligand NT3 (blue); and, (ii) targeting ligand without a PDT group "IY-IY-TEG". Data shown are mean ± SEM of three independent experiments. *, $p < 0.05$; **, $p \leq 0.01$; ***, $p \leq 0.001$ *vs* control using One-way ANOVA (A. TrkC$^-$ cell line; B. I2-BODIPY; D. red bars)

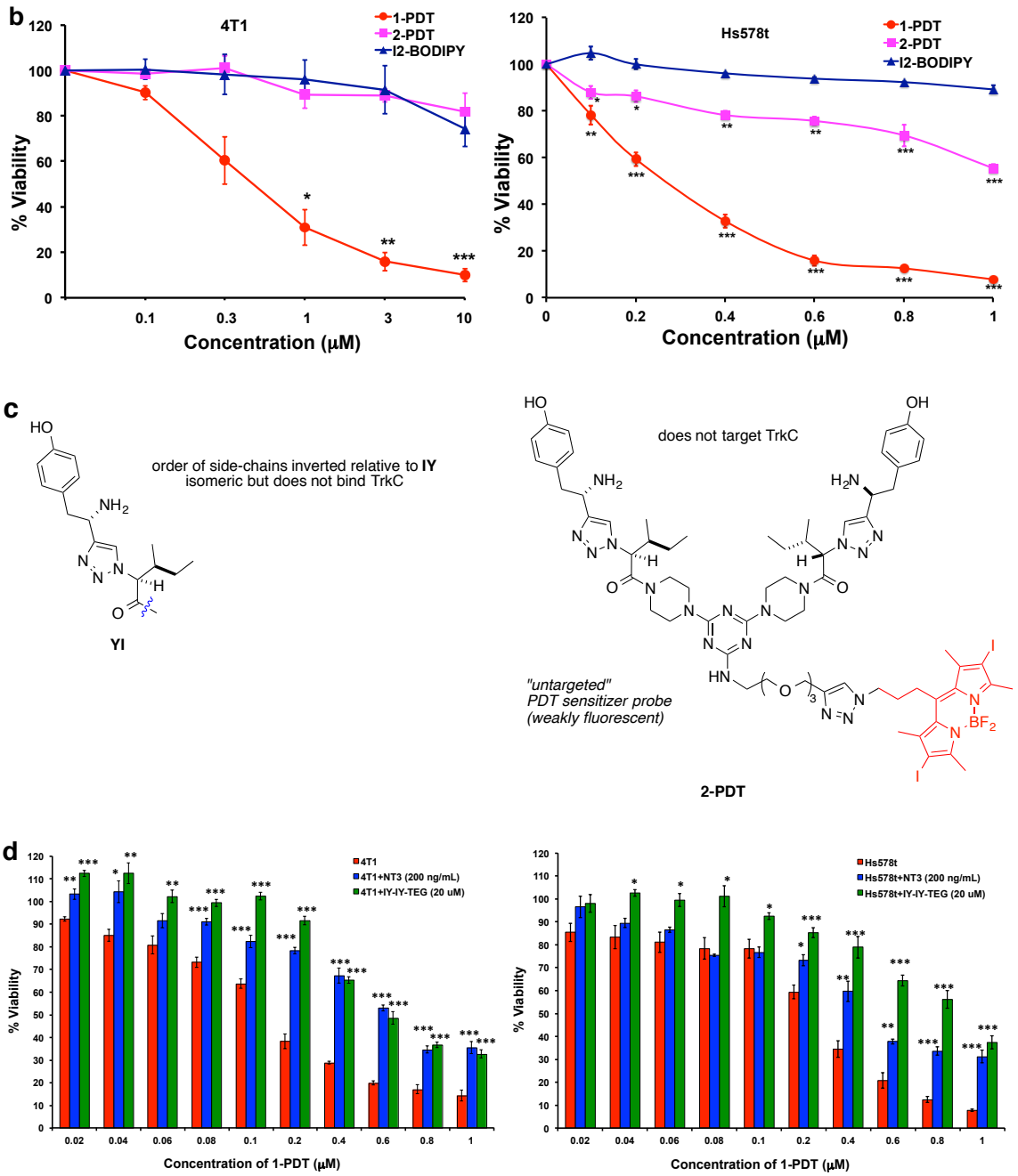

Figure 4-3 Continued.

Maximal Tolerated Dose (MTD) of 1-PDT is 20 mg/kg in a Murine Model. **1-PDT** at 20, 30 and 100 mg/kg was administered to mice intravenously via the tail vein, and toxicity was evaluated based on typical symptoms (apathy, horrent fur, diarrhea, behavior changes, and loss of body weight). All mice receiving doses of 30 mg/kg or more experienced motility and balancing difficulties, and died 1-3 h post drug administration. However, 20 mg/kg **1-PDT** was well tolerated, and gave no signs of toxicity and death up to 17 days of post-treatment (Figure 4-4), and no sign of gross organ toxicity was found in autopsies performed at the end of study.

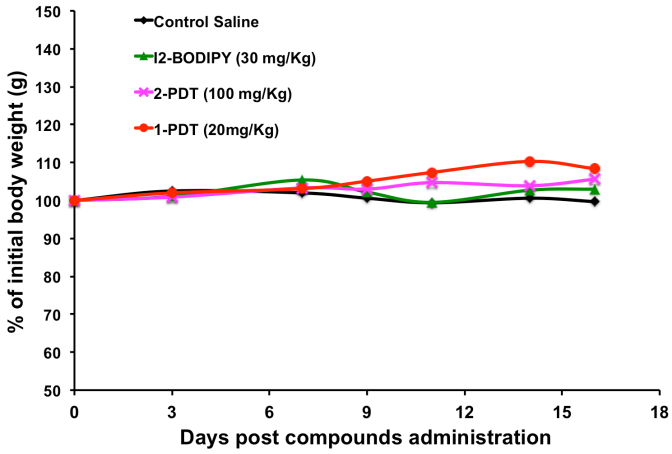

Figure 4-4. **1-PDT** was not toxic to mice at 20 mg/kg. Healthy 7-8 weeks old Balb/c female mice were administered intravenously via tail vein respectively with **1-PDT** and **2-PDT** at 20, 30, and 100 mg/kg (**I_2-BODIPY** content equivalent to 6.25, 10, and 30 mg/kg respectively, *ie* corrected for MW), and the parent **I_2-BODIPY** (30 mg/kg). The mice were then kept in the dark and observed for 16 days. Data represent the average body weight (grams) of 2 mice/treatment group.

No death or signs of toxicity was observed in mice receiving equivalent doses of **2-PDT** and BODIPY. These results suggest 20 mg/kg is the maximum tolerated dose

(MTD) for **1-PDT**. If after further studies, these compounds were to be used therapeutically, then the dose should be significantly less than this; however, modifications to the dye structures are required first (*see below*).

Agent 1-PDT Accumulated Maximally in Tumor Tissues 1 h after Administration and Cleared from the Body 72 h Post-treatment. The biodistribution of **1-PDT** and the isomeric non-TrkC targeting control **2-PDT** were monitored in 4T1 tumor bearing mice (n=3) up to 72 h. Significant and prolonged accumulation of **1-PDT** was observed in tumor (Figure 4-5). At 1 h post administration, the fluorescence intensity of tumors in mice treated with **1-PDT** was 2.1x higher (897,000 ± 135,800) than the corresponding intensities for tumors treated with the non-targeted control 2-PDT (416,000 ± 43,000) ($p<0.05$, Student's t test). The **1-PDT** dye intensity in tumor tissue remained significantly higher compared with **2-PDT** for up to 6 h, but there were no significant differences at 24 h onwards. Trends in the **1-PDT** tumor distribution were significantly different to that of **2-PDT**, indicating selective accumulation of **1-PDT** in the tumor. Maximum accumulation of **1-PDT** at 1 h post administration led us to adopt a drug-to-light interval of 1 h in determining **1-PDT**'s *in vivo* antitumor efficacies in the subsequent studies.

A large amount of **1-PDT** accumulated in the liver (*ca.* 20 fold more than in the tumor), then in the kidney and lung within the first 3 h post administration (Figure 4-5), but these accumulations dissipated swiftly in the subsequent monitoring period. A similar pattern of accumulation was found for **2-PDT**. Swift clearance of both compounds in this organs is typical of small molecular weight compounds,[150] and

indicates that the accumulation in these organs was random and not due to TrkC receptor binding.

Non-selective accumulation of **1-PDT** and **2-PDT** was also observed in lymphoid organs such as spleen and lymph node at a much lower level (Figure 4-5); others have observed no significant TrkC expression for these organs.[165] Interestingly, **2-PDT** but not **1-PDT** was found to accumulate significantly in the lymph node for a prolonged period of time. The eye has relatively impermeable blood capillaries and low TrkC receptor expression,[166] whereas murine eyes express relatively few TrkC receptors, concentrated mainly at nerve bundle portions.[167]

1-PDT at 10 mg/kg Gave Effective Eradication of 4T1 Tumor with 96% Average Tumor Regression. Compound targeting efficacies and effects on $TrkC^+$ tumors were assessed in the following experiments. Aggressive $TrkC^+$ murine breast carcinoma (4T1) cancer cells were subcutaneously injected to the murine mammary fat pad and then treated with **1-PDT**, **2-PDT**, and **I_2-BODIPY** when the tumor sizes reached 80 mm^3. In a control, mice inoculated with $TrkC^-$ murine breast carcinoma 67NR cancer cells were also treated using these compounds.

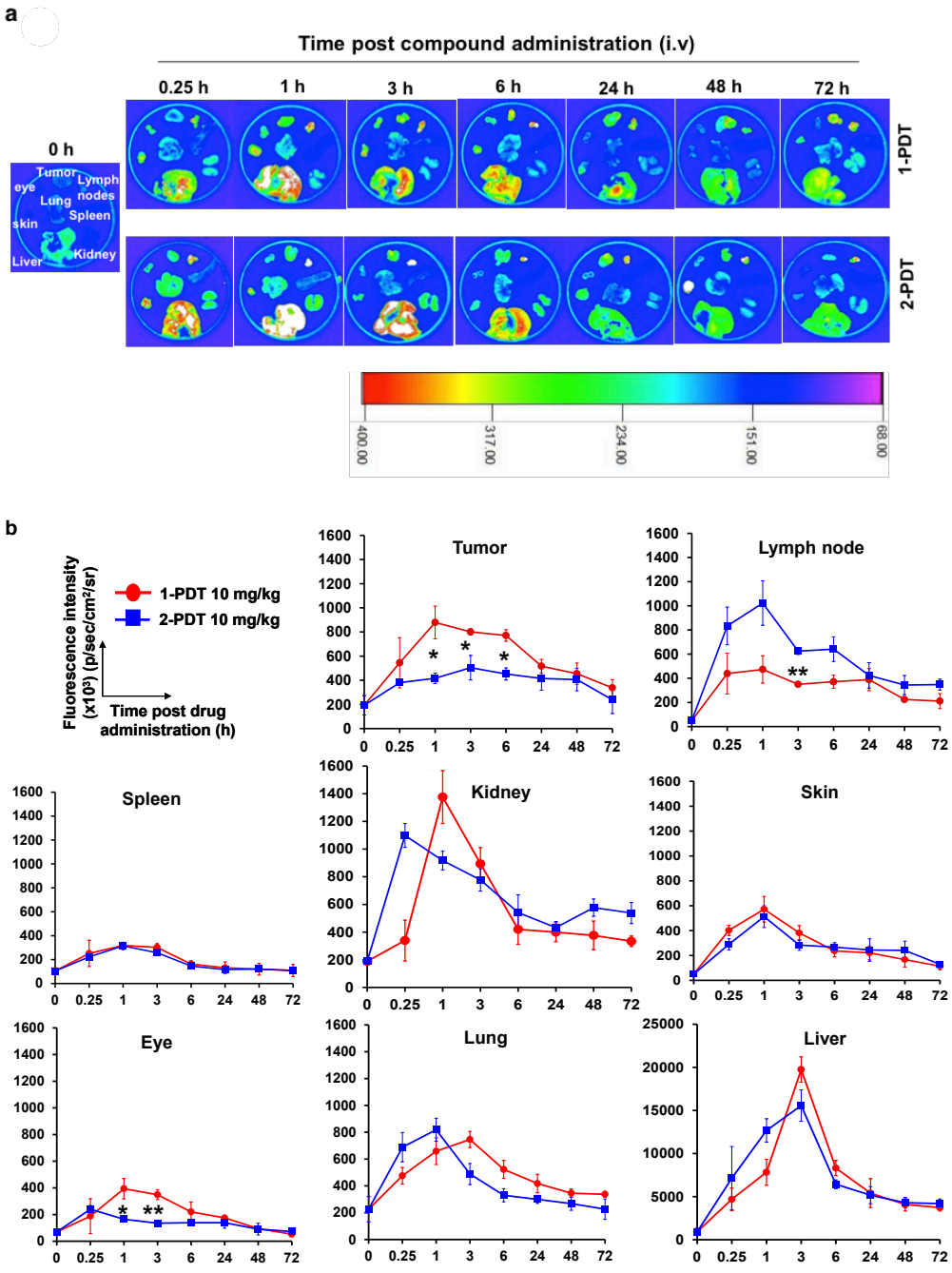

Figure 4-5. 1-PDT demonstrated significant and prolonged accumulation in tumor tissue for up to 6 h and cleared from the body 72 h post-administration. 4T1-tumor bearing female Balb/c mice were treated at 10 mg/kg via the tail vein. Mice (n=3) were sacrificed at 0, 0.25, 1, 3, 6, 24, 48, 72 h. **a** Organs and tissues (tumor, draining lymph nodes, spleen, kidney, liver, lung, skin and eye) were harvested; and, **b** fluorescence intensities in each organ were imaged using an *in vivo* imager (data represent mean ± SEM of three mice at each time point). * $p< 0.05$; ** $p< 0.01$ Student's t test; for **1-PDT** *vs* **2-PDT**.

Agent **1-PDT** significantly reduced tumor growth after illumination when treated at 2 and 10 mg/kg (equivalent to 0.6 and 3.0 mg/kg of **I_2-BODIPY**, respectively). Inflammation and erythema surrounded the irradiated tumor region was observed in the **1-PDT** treated groups at 4-6 days post PDT, but was less pronounced or not observed in the control groups (Figure 4-6a). Subsequently, tumor sizes were drastically reduced in the **1-PDT** treated groups 4-6 d post-illumination (61 % and 96 % maximum tumor reduction in mice treated with 2 and 10 mg/kg of compound compared to pre-treatment tumor size, Figure 4-6b). In contrast, **2-PDT** and **I_2-BODIPY** treatment induced only moderate tumor size reduction within the first 6 d after illumination (20 % reduction for mice treated with 10 mg/kg of **2-PDT**, and 11% reduction for mice treated with 10 mg/kg of **I_2-BODIPY,** Figure 4-6b). At day 13, both **2-PDT** and **I_2-BODIPY** treated mice showed rapid tumor re-growth at the necrotic tumor tissue periphery while tumor regrowth in **1-PDT** treated mice was minimal and delayed (Figure 4-6a & 4-6b). More importantly, 1 out of 7 mice (14%) treated with 2 mg/kg, and 5 out of 7 mice (71%) treated with 10 mg/kg of **1-PDT** healed from eschar by day 13-15 after illumination, and showed no palpable tumor for up to 90 d post-treatment. Such total tumor remission was not found in both the **2-PDT** and **I_2-BODIPY** treated groups.

To confirm the targeting ability of **1-PDT** on $TrkC^+$ cells *in vivo*, the compound efficacy in the non-TrkC expressing 67NR tumor cell line in mice was examined and compared to that in the 4T1 model; as expected, neither **1-PDT** nor **2-PDT** at 10 mg/kg fully eradicated the 67NR tumors in mice (Figure 4-6c); the tumor volumes were reduced at day 4 - 6 days post-illumination but re-grew at day 9.

*Mice Surviving Treatment with **1-PDT** Showed Complete Remission up to 90 Days Post-illumination, with No Metastasis Development.* All **1-PDT** treated mice that showed complete tumor regression remained disease free with no palpable tumor at the primary site up to 90 d. Tumors from 4T1 cancer cells are known to be aggressive and typically metastasize to lymph nodes, liver and lung, even in the early stages of the disease[168]. Thus, at 90 d post-illumination, the surviving mice that were physically active were sacrificed for major organ/tissue histopathology by a certified veterinary pathologist. H&E staining showed no 4T1 tumor metastases in all the examined organs (liver, lung, draining lymph node, spleen, kidney and heart) of the 10 mg/kg **1-PDT** treated survivor mice and tumor free control mouse (Figure 4-6d). However, in 4T1 tumor bearing control mice, tumor metastases were found in liver, lung, lymph nodes and spleen with extramedullary hematopoiesis observed in this animal (Figure 4-6d). These results show effective eradication of TrkC expressing 4T1 tumor by **1-PDT** post PDT treatment in the survivor mice.

Discussion

The assertion that agent **1-PDT** targets $TrkC^+$ breast cancer cells is supported by the observation that it has a more profound effect on these tumors than the isomeric compound, **2-PDT**, and the PDT agent without any appendage, *ie* **I_2-BODIPY**. This is consistent with the significant *in vivo* selective accumulation of **1-PDT** in $TrkC^+$ tumors 1 h after administration, as calibrated relative to levels of **2-PDT** at the same time.

Moreover, **1-PDT**, **2-PDT**, and **I_2-BODIPY** have comparable effects on tumors from TrkC$^-$ cell lines.

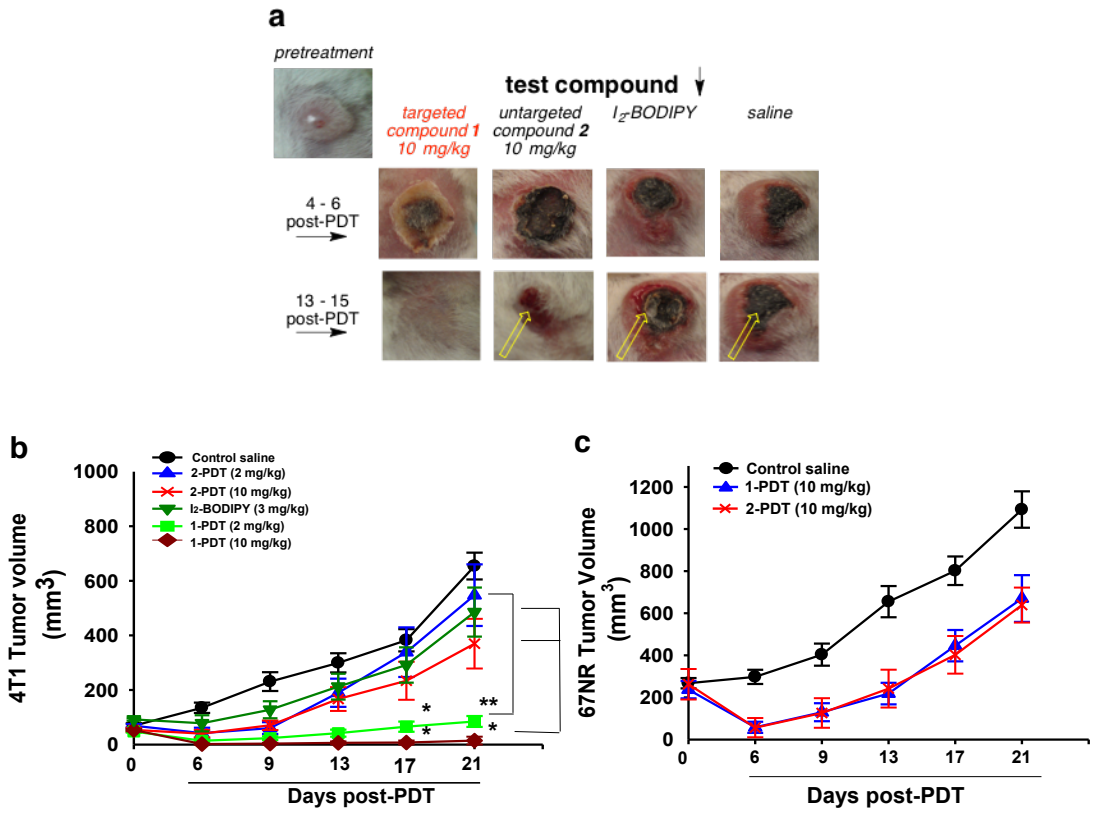

Figure 4-6. **1-PDT** effectively suppressed the growth of TrkC$^+$ (4T1) tumor, but not in TrkC$^-$ (67NR). **a** Regrowth of TrkC$^+$ 4T1 tumor (yellow arrow) in female Balb/C mice receiving **2-PDT** (10 mg/kg), **I_2-BODIPY** (3.0 mg/kg) and saline controls, but not in mice receiving **1-PDT** (10 mg/kg). **b** Significant dose dependent mean tumor volume reduction and delayed tumor regrowth in TrkC$^+$ 4T1 tumor bearing mice receiving 2 and 10 mg/kg **1-PDT**, as compared to rapid tumor growth in mice receiving the control substances. **c** **1-PDT** gave impermanent and non-selective antitumor effect (resembled that with **2-PDT**) in mice bearing TrkC$^-$ 67NR tumor. Photo-activation was conducted at 100 J/cm^2 with a fluence rate of 0.16 W/cm^2 1 h after intravenous injection of the compounds. All graph showed mean tumor volume ± SEM (n=7). * $p< 0.05$; ** $p< 0.005$; for **I2-BODIPY** *vs* **1-PDT** and **2-PDT** group using One-way ANOVA. **d** There were no tumor metastases in **1-PDT** treated survivor mice post 90 d. Mice treated with 10 mg/kg **1-PDT** that survived up to 90 d with no palpable primary tumor found were metastases free in all the major organs assessed (liver, lung, draining lymph node, and spleen, representative histological images). Control (tumor free healthy and 4T1 tumor burden mice) results were included for comparison (yellow arrow = 4T1 tumor metastases). Scale bar: 100 mm. The current results had been verified by certified veterinary pathologist.

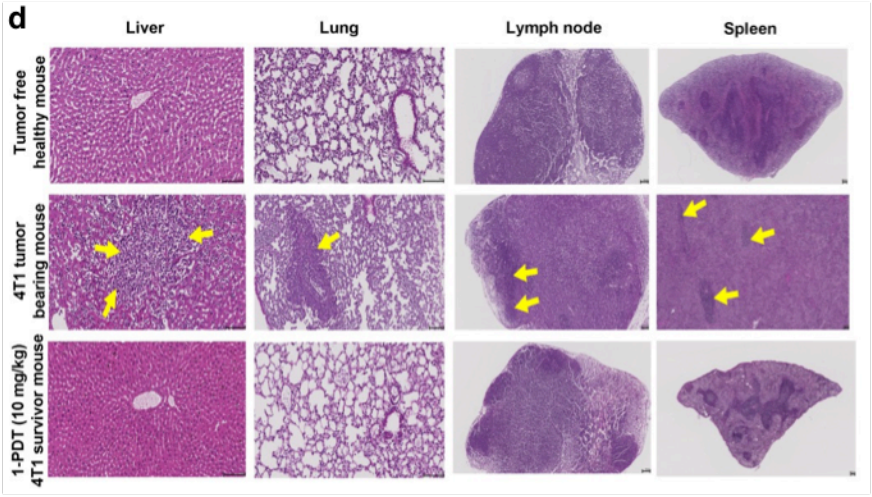

Figure 4.6 Continued.

The data outlined above are consistent with *ex vivo* studies on cells stably transfected with TrkC,[169] but those experiments did *not* involve breast cancer cells. In this manuscript we report selective photocytotoxicity of **1-PDT** *ex vivo* correlates with natural levels of $TrkC^+$ expression *in breast cell lines*. The cell studies established that a 4 – 6 h interval between treatment and illumination *decreased* the selectivity for TrkC-expressing cells relative to a 2 h interval; perhaps due to relatively slower, and non-selective, interaction with cells, something that could be anticipated from the literature.[107,170] Consequently, we used a 1 h interval between injection and light treatment for the *in vivo* work.

It is remarkable that **1-PDT** at 10 mg/kg *in vivo* caused, on average, 96% tumor volume reduction in the mice bearing $TrkC^+$ tumor at day 6 post-PDT. Among these

mice, 71 % showed full remission and were tumor- free for 90 days after therapy, and histology indicated no metastasis development in these animals. The fact that **1-PDT** was ineffective for suppressing $TrkC^-$ (67NR) tumors in mice supports the overall assertion that this compound targets $TrkC^+$ expressing tissue *in vivo*.

Long- and short-term toxicities of agents like **1-PDT** must be considered in the context of experimental therapeutics. In the dark, the TrkC-targeting fragments featured are capable of transducing signals similar to NT3 upon binding to TrkC,[77] so it is conceivable that in the long term **1-PDT** might induce tumorigenesis just as NT3 does.[62-63,171] However, this was *not* the case in the extended time course of these experiments since, *in the dark* mice receiving saline control or **2-PDT** (no TrkC binding) have comparable tumor volumes, with no significant differences, to the **1-PDT** group (Appendix F).

Another relevant long-term toxicity issue relates to photosensitivity. Intravenous administration of photosensitizers can result in accumulation in different tissues and undesirable photosensitivities.[172] Adverse photosensitivity is common in PDT,[173-174] but targeting PDT agents to tumors that express TrkC should alleviate some of these effects. Short-term toxicities for agents that bind TrkC could be anticipated since NT3 promotes neuronal cell survival, differentiation and synapse transmission, antagonism at the TrkC receptor might have undesirable effects.

Short-term toxicities of agent **1-PDT** are a concern because, while doses of 20 mg/kg were tolerated, 30 mg/kg was not. A claim that high doses of neurotrophins (including NT3) promote relatively rapid excitotoxic necrosis of neurons [175] might be

pertinent. In any event, **1-PDT** requires further structural modifications because the light wavelength to excite this is optimally around 520 nm whereas PDT agents should absorb above 700 nm if they are to be addressed at more than 1 cm tissue penetration.[140,144-146] Consequently, **1-PDT** is a prototype for other compounds, currently under development in our laboratories, that involve the same targeting fragments differently disposed around other PDT active dyes. It is anticipated that the short-term toxicities of the second-generation systems will be structure-dependent.

Conclusions

Overall, the data presented here demonstrate the potential of targeting $TrkC^+$ tumors with PDT agents. Excellent therapeutic indices can be achieved because PDT is spatially restricted to the illumination area, and active targeting accumulates the agents in the tumors. This study features dosing with a targeted-PDT agent alone, but there is also the intriguing possibility of combination therapies featuring Trk inhibitors currently in trials as chemotherapeutic agents (*eg* Lestauritinib[176] and PLX7486 (http://clinicaltrials.gov/show/NCT01804530).

CHAPTER V

AN AGENT FOR OPTICAL AND PET TARGETING OF THE TRKC RECEPTOR

Introduction

Tropomyosin receptor kinases (Trk's) are a family of cell-surface receptors that bind the neurotrophin growth hormones.[177] For instance, docking neurotrophin-3 (NT3) with TrkC triggers intracellular phosphorylation, then a network of cell signaling processes that lead to cell growth and differentiation.[161,178] Mis-regulation of Trk receptors is associated with several forms of cancer. Thus TrkC receptors are over-expressed in some forms of neuroblastoma,[2,6-8,18,42-43,50-55] glioblastoma,[54,57-60,179] metastatic breast cancer[61-67] and metastatic melanoma.[68-76]

Correlation of Trk receptor expression with cancer[67,135,180-181] means that these receptors are possible targets for imaging agents. Consequently, synthetic TrkB-[182] and pan-Trk-binding agents[55] functionalized with radionuclei have been explored for imaging with positron emission tomography (PET). However, to the best of our knowledge, no synthetic imaging agents have been reported for selective PET- or optical-imaging of TrkC *in vivo*.

Research described here was undertaken to establish a TrkC-selective optical imaging agent that could also be used for PET studies. Prior studies from our laboratories featured the TrkC-homing ligand shown in **1** and a control, isomer **2**, that does not bind TrkC (see Chapter 3 and 4 for details). System **1** equipped with the BODIPY dye fragment shown was internalized by TrkC-expressing cells and it could

also be used as a staining agent for breast cancer and melanoma tissue, both of which are associated with TrkC overexpression. There are methods for ^{19}F-to-^{18}F substitution in BODIPY dyes,[183-186] and in unpublished studies we tested these for **1** and obtained a derivative that selectively radiolabeled TrkC-expressing cells. Based on these observations it seemed likely that a PET/optical imaging theranostic could be obtained from system **1**, but the structure of the dye required optimization first, for the following reasons.

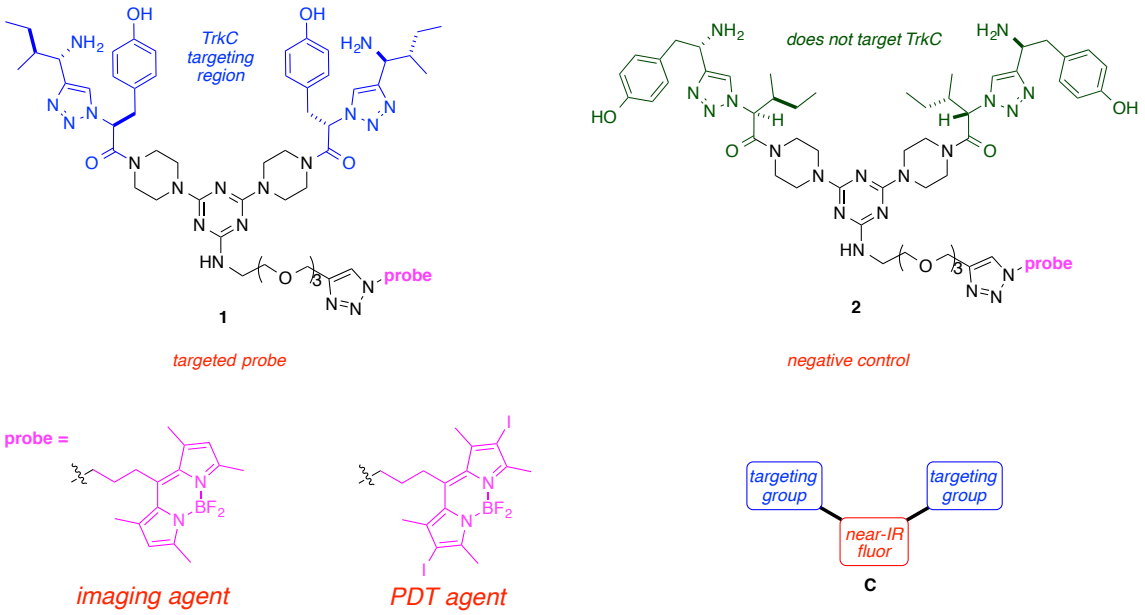

Figure 5-1. First generation TrkC targeting ligand-conjugate (**1**) and its control (**2**). Second generation TrkC targeting proposed system **C**.

Light of wavelength 520 nm, as used to excite the BODIPY in **1**, is too short for efficient penetration of more a few mm in tissue.[97-98] To overcome this challenge, the

most obvious solution is to prepare an almost identical structure with a near-IR-absorbing probe directly replacing the BODIPY. However, modifications to fluors to make them near-IR absorbing invariably increase their molecular size because more extended conjugation is necessary. This requirement runs counter to a desire to keep the molecular mass of the targeted probe to a minimum thereby avoiding undesirable absorption, metabolism, and excretion effects. We hypothesized one way to reconcile these opposing parameters was to replace the black part of structure **1**, which serves no purpose other than as a scaffold-spacer, with a near-IR fluor giving the conceptual structures **C** (Figure 5-1). Syntheses of these molecules would facilitate answering the key issue, *ie* what impact this structural modification has on the targeting efficiency.

We speculated that type-**C** molecules might also help alleviate another issue with the design **A**: toxicity at elevated doses. In a photodynamic therapy experiment,[83,97-98] 10 mg/Kg of **A** (where the probe is an iodinated BODIPY dye) caused complete ablation of a tumor. That amount of compound (10 mg/Kg) is well below the maximum tolerated dose (*ca* 20 mg/Kg) but above 30 mg/Kg that compound caused lethal neurotoxic effects in mice.[187] Moreover, neurotoxicity was also observed when a much smaller dose (*eg ca* 1mg/kg) was used *in anesthesia mouse model*. There was no way to test the hypothesis that adjusting the spacing of the targeting groups as in **C** might modulate the neurotoxicity, other than synthesis and testing. Consequently, we set out to prepare type-**C** molecules and assay their targeting properties *in vivo*, while observing for evidence of neurotoxicity.

Design considerations noted above led to embodiments of systems **C** wherein the fluor is an aza-BODIPY (Figure 5-2). Aza-BODIPY dyes tend to have significantly longer absorption and emission wavelength maxima than their BODIPY analogs.[94,188-189] Moreover, in our experience, aza-BODPY dyes tend to be more stable than alternatives like cyanines, and have the added advantage that the BF_2 fragment can be tagged with ^{18}F. Thus we decided to prepare the targeted aza-BODPY dyes **3a** and **b**. Probe **3a** was appealing because the sulfonic acid groups would enhance the hydrophilicity of the molecule and their negative charge might reduce non-specific binding to cells. Conversely, **3b** has the advantages of smaller size, and more facile synthetic access. The objective of this study was to come to an early decision about the probe design, **3a** or **3b**, with the most suitable properties for targeting, by considering the physical properties of the dyes. The lead candidate probe would then be tested for: (i) binding and internalization by TrkC-expressing cells; (ii) staining TrkC-expressing fixed tissue (histochemistry); and, (iii) comparative distribution in healthy mice and ones bearing TrkC-expressing breast cancer.

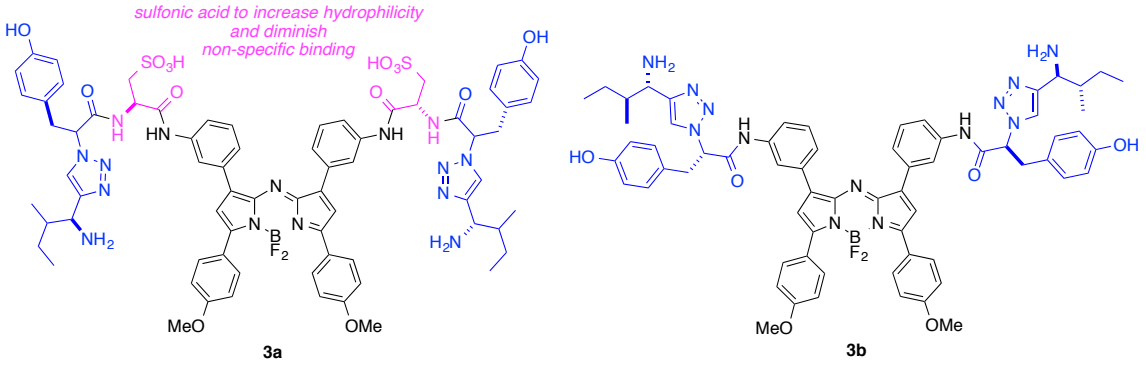

Figure 5-2. Second generation TrkC targeting ligands featured in this work.

Results and Discussion

Coupling of the azido acid derived from L-tyrosine[190] with the disulfonated aza-BODIPY 5-2, prepared as described in Appendix C,[191] gave the diazide 5-3. A copper-mediated cycloaddition[138,192] of 5-3 with the alkyne derived from L-leucine[190] gave the desired product 1a. Probe 1b was prepared via an analogous route, but beginning with a diamine aza-BODIPY precursor to 5-2; a Scheme and full details of that synthesis are given in Appendix G.

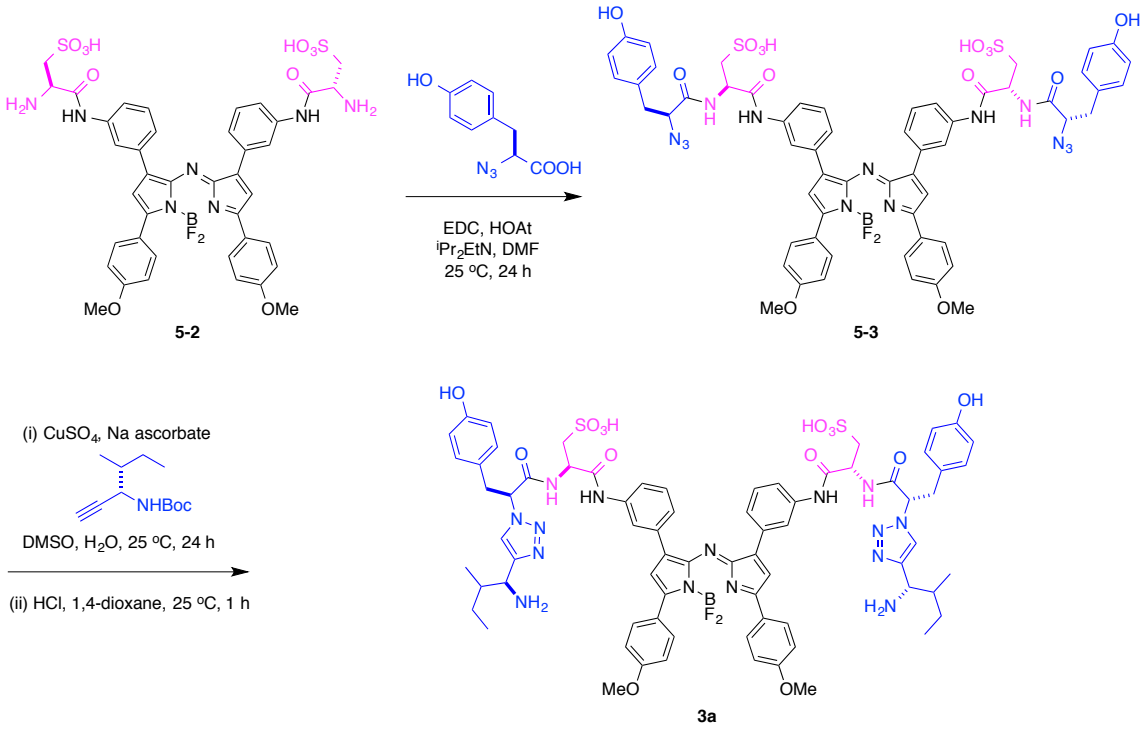

Scheme 5-1. Preparation of TrkC-targeted near IR probe **3a**.

*Distribution of Probes **3a** and **b** in TrkC+ Murine Breast Cancer Cells.* TrkC-expressing, murine breast cancer cells (4T1 line) were treated with probes **3a** and **b**. Observation of the cells using confocal microscopy (Figure 5-3a) showed the sulfonated system **3a** was efficiently internalized whereas the more lipophilic system **3b** gave significantly more cell-surface binding (Fig 5-3b). For both probes, the material that was internalized overlaid with a lysosome tracker, indicating it accumulated in that organelle.

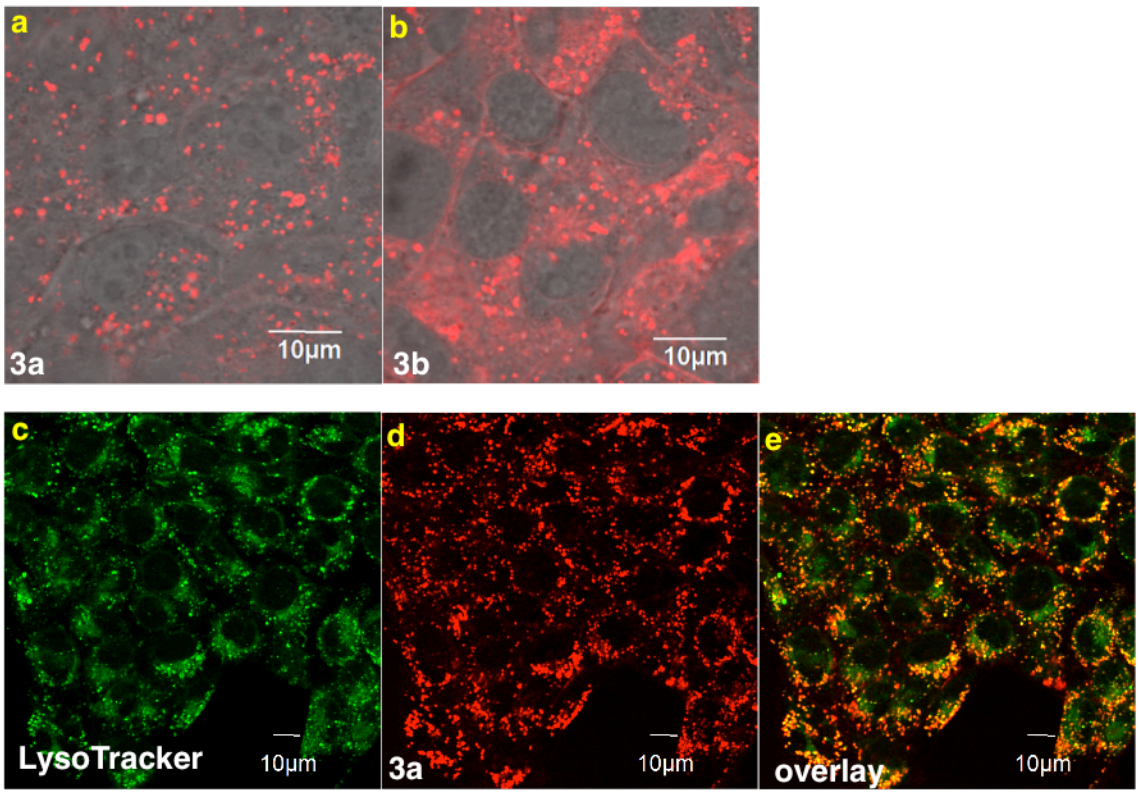

Figure 5-3. Imaging with 4T1 cells. **a** Probe **3a** was internalized; whereas, **b** much more of **3b** accumulated in the cell walls. **c** LysoTracker and probe **3a** (**d**) colocalized; the fraction of **3b** that internalized also accumulated in the lysosomes (not shown, see Appendix G).

Data shown in Figure 5-3 support the assertion that the sulfonic acid groups of **3a** reduce non-specific binding to $TrkC^+$ cells relative to the neutral probe **3b**. This is somewhat expected because of repulsion between the negatively charged sulfonic acids and polar head groups at the cell surface.[193] Consequently, all the subsequent work in this research was focused on **3a**, and studies of **3b** were discontinued.

Probe **3a** showed no signed of toxicity to 4T1 cells at concentrations up to and including 25 μM. The intrinsic fluorescence of **3a** was used to determine a dissociation constant for its binding to TrkC on the cell surface.

Commercial samples of fixed human tissue from patients with stage 1, 2, and 3 malignant breast cancer were purchased (US Biomax). Probe **3a** was used to treat these samples and the staining was compared to that observed for normal breast tissue proximal to the tumor, obtained from the same patient in each case; illustrative data are shown in Figure 5-4. In all cases the tumor tissue stained strongly whereas the healthy samples showed much less fluorescence. We were encouraged by the selectivity, but slightly surprised that the healthy tissue showed faint staining. It appears that this is genuine binding to the TrkC receptor in the healthy tissue (rather than non-specific binding or fluorescence leakage into the red channel) because fluorescently labeled TrkC mAb also stained the normal tissue (see Appendix G). This may mean the tumor environment is causing the surrounding normal tissue to upregulate TrkC expression.

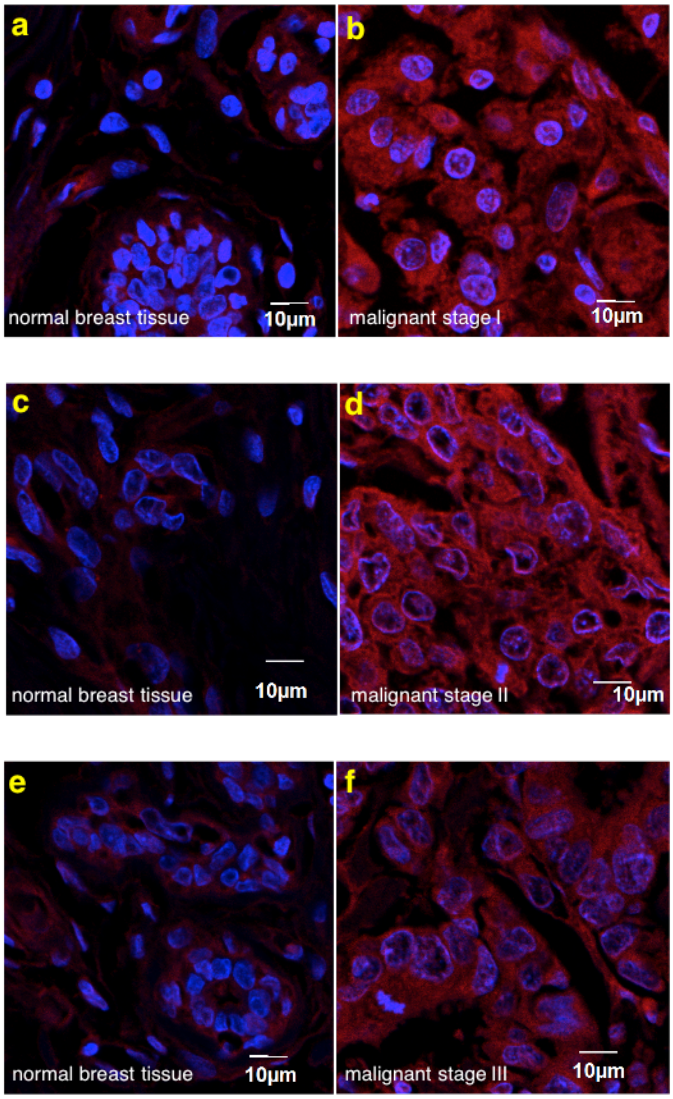

Figure 5-4. Histochemistry on human breast tissue array. Probe **3a** stained on breast cancer tissue (**b**) much brighter than matched adjacent breast tissue control (**a**), (example from 3 cases).

In vivo studies of **3a** were done by our collaborator in Houston Methodist Research Institute, Dr. Zheng Li. Probes **3a** and its control (isomer of **3a**, structure in Appendix G) were injected into a murine breast cancer model via tail vein. The optical imaging showed **3a** rapidly accumulated in the tumor but was completely cleared after

24 h while most of the control compound accumulates in kidney, no tumor accumulation is observed (Figure 5-5). Moreover, neurotoxicity was *not* observed at 100 nM and during the time course of the experiments.

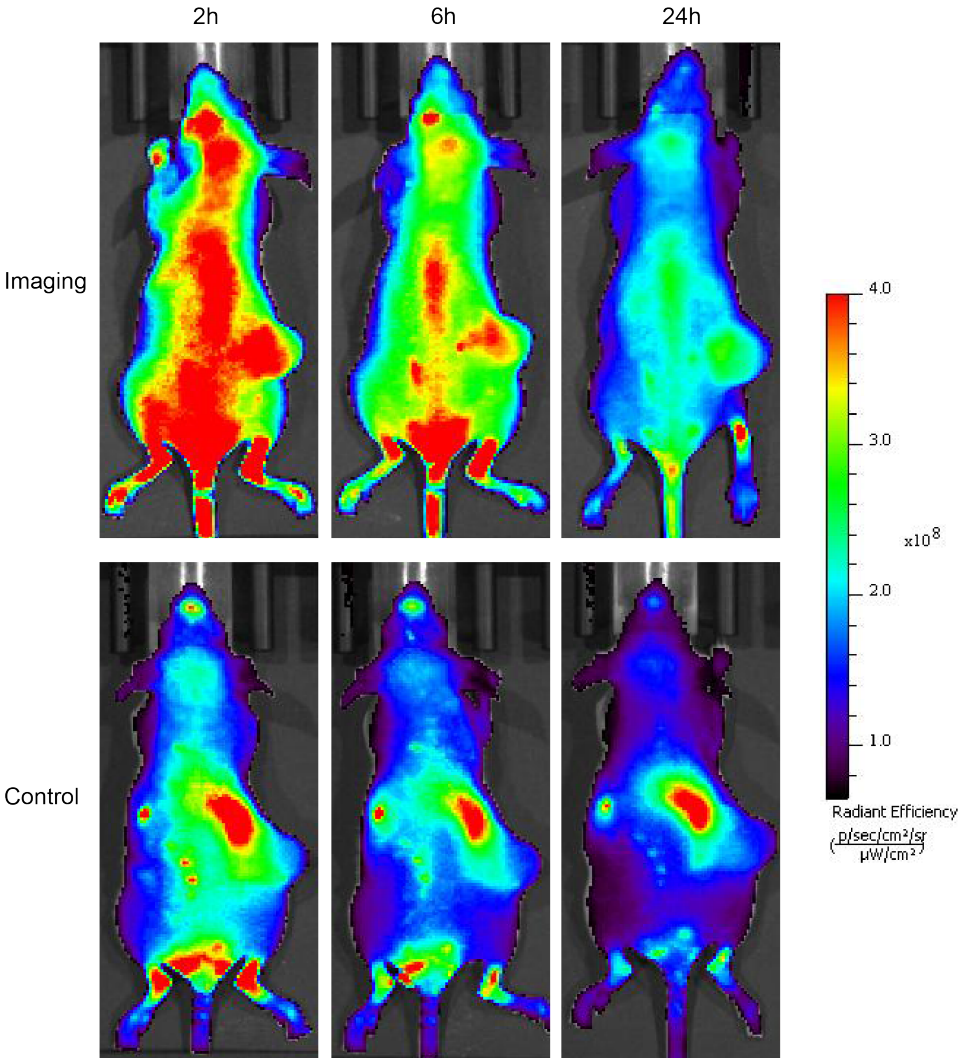

Figure 5-5. *In vivo* imaging of **3a** in mice bearing 4T1 breast tumor model. *Top panel*, compound **3a** accumulates in tumor and clearance from the body after 24 h. In the *control panel*, most of the control compound (structure in Appendix G) accumulates in kidney, no tumor accumulation is observed.

Incidentally, the spinal cord of the mouse was nicely imaged by **3a**, presumably because $TrkC^+$ cells are highly concentrated in the peripheral nervous system. This is interesting because a weak agonist of TrkC, that causes cells expressing that receptor to grow and divide have the potential to stimulate nerve cell regrowth; this can be useful for regeneration of spinal cord injury. Thus, agonistic effect of **3a** is under investigation. Our hypothesis is that the neat property of our agonist is that it is also a near-IR dye that would facilitate: (i) visualization of the spinal cord in animal model; and, (ii) may induce some spinal cord repair if administered repeatedly over time, and be self-indicating to observe that.

Conclusions

Our second generation targeting probe is more suitable for *in vivo* studies because of its near-IR absorption. Agent **3a** is more practical than **3b** because it has two sulfonic acid groups to enhance hydrophilicity and reduce non-specific binding. Histology and live cell imaging showed **3a** selectively bound to $TrkC^+$ tumor cells. Furthermore, *in vivo* imaging using a murine breast cancer model showed **3a** accumulated rapidly in the tumor but was completely cleared after 24 h; moreover, neurotoxicity was *not* observed. Probe **3a** also has potential as a positron emission tomography (PET) agent via ^{19}F to ^{18}F exchange; use of this probe for PET is under investigation by collaborators.

CHAPTER VI

ACTIVELY-TARGETED, NEAR-IR, PET-IMAGING AND PDT AGENTS FOR TREATMENT OF MELANOMA

Introduction

About a third of all cancers in the United States are associated with the skin, mostly basal- and squamous-cell carcinomas (*ie* surface and sub-surface). Only 4% of these are malignant melanomas, but they are responsible for more than 75% of all skin cancer deaths.[194] An estimated 114,900 new cases of melanoma were diagnosed in the United States in 2010 with nearly 8,700 resulting in death, and these were responsible for the third most common type of brain metastasis after lung and breast cancer. Melanoma is particularly resistant to conventional therapies.[82]

Imaging Of Melanoma. Each of the methods for imaging melanoma has attributes and limitations, so it is unclear which one is preferred. Computed tomography (CT), magnetic resonance imaging (MRI), and ultrasound are anatomical imaging techniques. CT and MRI detect structural changes, while tissue-density fluctuations at secondary tumor sites are exposed by ultrasound; however, tissue-density fluctuations are not characteristic of all forms of melanoma. Ultrasound contrast agents have improved the accuracy of sentinel lymph node metastasis detection, but only if near the primary tumor. Finally, fluorescence imaging is also valuable; surgical procedures can be improved by using fluorescent probes that bind to cancer cells, making them more conspicuous.[195]

2-^{18}Fluor-deoxy-D-glucose (^{18}FDG) labeling is the most common PET technique for detection of metastatic lesions and staging of melanoma.[196-198] This method is sensitive and specific, but it tends to fail to detect lesions smaller than 3 – 4 mm, and tumors having insignificantly increased FDG metabolism.[199] Moreover, FDG ^{18}F can accumulate in inflammatory tissue and this may cause false positives which give the erroneous impression that certain patients are not responding to treatment.[200] Thus imaging of cancer using PET would be advanced by development of targeting agents that overcome these problems, particularly for micrometastases.

Syntheses of all new agents for ^{18}F-PET imaging must overcome several challenges. The only practical source of ^{18}F, 18-fluoride, is generated by proton irradiation of $H_2{}^{18}O$ in a cyclotron.[201-204] The half-life of ^{18}F is short (110 min) so its use requires fast, high-yielding, incorporation into the imaging agent immediately before administration. However, fluoride ions are relatively unreactive to most electrophiles even at high concentrations in anhydrous media, and this inertness is accentuated for low concentrations of aqueous $^{18}F^-$ by dilution and *H*-bonding effects. Consequently, syntheses must accommodate late-stage incorporation of ^{18}F atoms into the imaging agents via reactions that can be performed in an hour or so, preferably with dilute aqueous $^{18}F^-$, and which do not require extensive purification. Many desirable potential ^{18}F PET agents simply cannot be made via procedures that fit this description.

There have been some attempts featuring radiolabeled peptides to increase the sensitivity and specificity of PET for imaging small peripheral metastases.[205] These studies include peptides targeting somatostatin receptors, metalloproteases,[206-207]

vasointestinal peptides, oligosaccharides targeting sentinel lymph nodes,[208] gastrin-releasing peptide,[209] or the fibronectins[210-211].[212-213] None of these targeted PET-imaging strategies are particularly suitable for melanoma.

Photodynamic Therapy (PDT) Of Melanoma. Photodynamic therapies feature photosensitizers that generate reactive oxygen species from triplet oxygen, thus inhibiting cell proliferation and survival, upregulating apoptosis, and inducing autophagy. This strategy is minimally invasive, and inherently targeted (though not *actively targeted*) because tissue damage can be constrained to the illuminated area.[194]

Preclinical studies of PDT for melanoma therapy[194] have shown that methylene blue, verteporfin, and several other photosensitizers are effective.[214] These data contradict a dogma, widely held until about 2005, that PDT is ineffective for treatment of melanoma because the dark-colored melanocytes interfere with absorption of light by the PDT agent.[214] In fact, PDT can be effective if near-IR absorbing photosensitizers (λ_{max} >700 nm) are used.[81-82] Photosensitizers of this kind can be excited at relatively deep tissue penetrations, and at wavelengths above the absorption maxima of melanins.[81-82,215] For instance, a human clinical trial using chlorin e_6 as a PDT agent resulted in complete regression of skin melanoma metastases with no recurrence during the 2 year study.[216]

The Sinclair Swine Melanoma Model. The Sinclair swine cutaneous malignant melanoma model is highly heritable, highly penetrant, and histopathologically well-characterized.[217] This condition can develop *in utero* or after birth, and is lethal to about

one quarter of the animals. All the congenital lesions in this model arise from epidermal melanocytes.

Sinclair pigs are excellent for preclinical studies because their melanoma occurs naturally without the need for suppression of the immune system or surgical procedures. This is important because tumor development and inflammation tend to be intimately related. Pig models are more relevant to humans than many frequently used alternatives. The Sinclair model has similar pathology to human melanoma,[218] and gives rise to a pattern of metastatic spread that is analogous to metastases in humans; in both cases the primary tumors can spontaneously metastasize to numerous organs including the brain. Consequently, Sinclair pigs are especially useful in studies to enhance PET and MRI imaging of small solid tumor metastases. The Sinclair pig model is not widely available, but it is established at TAMU (Prof. Duane Kraemer at TAMU).

Experience gained applying this model at TAMU has shown that piglets as young as 6 wks old (3 – 5 Kg bw) can tolerate PET and MRI under anesthesia, and that the wash out times for labeling agents are comparable with those in humans.

Figure 6-1. Tumor on right leg of Sinclair piglet; subject died 4 weeks post-partum due to lung and liver metastases.

Photosensitizers coupled to targeting agents can be used to confine the PDT effect to tumor regions that are illuminated; this *doubly* targeted approach could greatly reduce collateral damage to healthy tissues. Humanized mAbs have been used to achieve this,[101] but these large proteins generally prevent PDT agents attached to them entering cells, lowering their effectiveness. Moreover, application of mAbs in the clinic is restricted by the cost and difficulties of large-scale, GMP mAb preparations. For these reasons, small molecule targeting may be preferable but, to the best of our knowledge, no small molecule ligands have been used to actively target PDT agents to melanoma.

A small molecule that can be used to localize imaging agents in tumors must be a candidate to similarly direct conjugated PDT agents for therapy. Consequently, simultaneous development of imaging and PDT agents based on the same small molecule targeting groups are highly synergistic.

Results and Discussion

Two fragments of the targeting, "IY" novel dipeptide mimics containing isoleucine and tyrosine side-chains are joined in molecule **1** (Figure 6-2). This probe binds cells which overexpress TrkC,[133,169] but it has only mild agonistic effects on the cells at high concentrations (20 μM).[77] When that targeting motif is attached to an agent for fluorescence we refer to it as **1-F**, or for photodynamic therapy (PDT) then the compound may be called **1-PDT**. Compound **2**, an isomer of **1** with a scrambled of

dipeptide fragment; it is a useful control because it has the same molecular mass, and therefore very similar polarity, solubility *etc*, but it does *not* target TrkC.

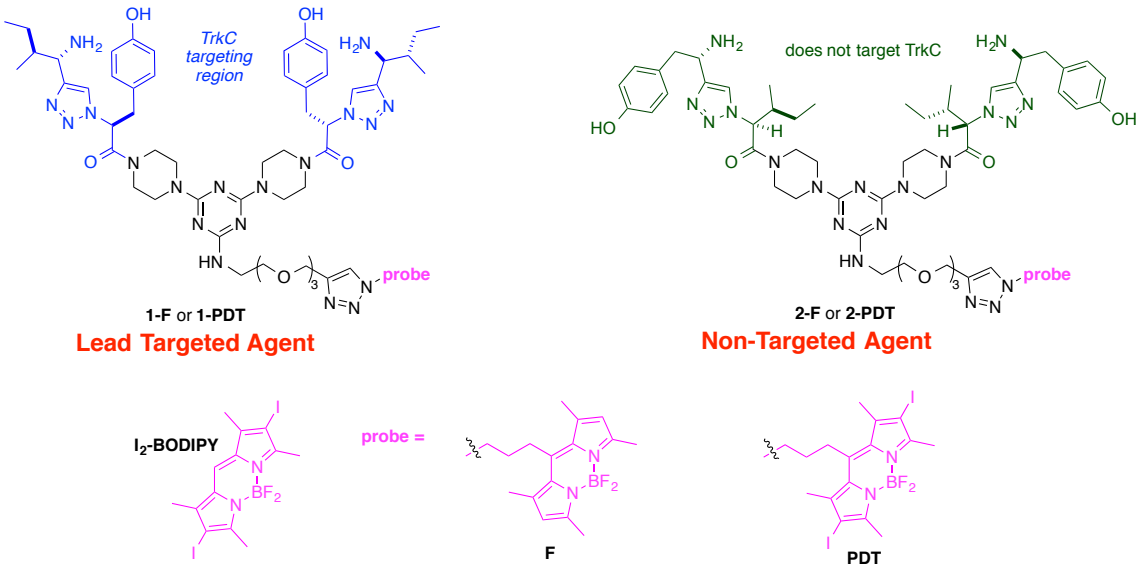

Figure 6-2. a Structures of first-generation agent **1**, and an important control, **2**. **I_2-BODIPY** is another control; it is the PDT photosensitizer without any targeting group.

In healthy *Balb/c* mice, 20 mg/kg **1-PDT** was well tolerated, and gave no signs of toxicity or death up to 17 d of post-treatment or indication of gross organ toxicity in autopsies at the end of study (see Chapter 4 for details; collaborative study with workers at University of Malaysia). Agent **1-F** is used in histological stains and intracellular imaging via confocal microscopy. Tumor and healthy skin tissues were obtained from the same melanoma-afflicted pig (Figure 6-3b and c).

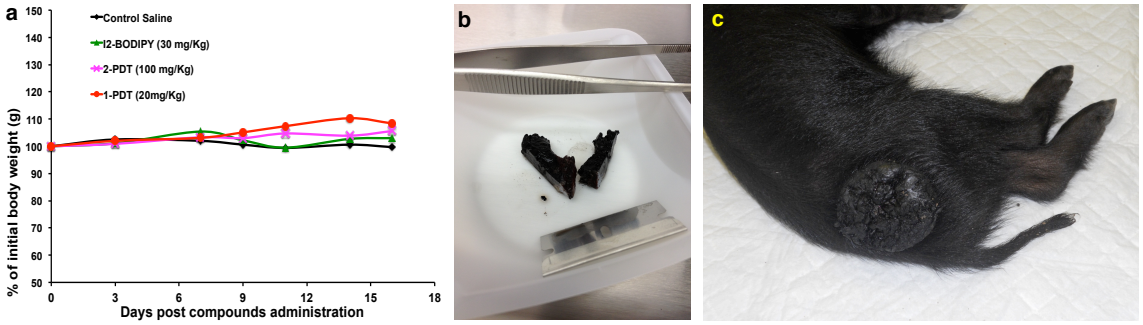

Figure 6-3. **a** Under ambient light, **1-PDT** shows no evidence of toxicity in mice (data obtained by collaborators, Dr's L. Y. Chung and L. Kiew, University of Malaysia). **b** Melanoma tissue from a melanoma afflicted pig (**c**).

Figure 6-4 shows immunohistology that confirms the pig melanoma tissue, but not healthy skin from the same pig, expresses TrkC (binds anti-TrkC mAb). Similarly, histochemistry confirms **1-F** binds to cell surface receptors in melanoma tissue, but not to the healthy keratinocytes, from the same pig, implying the anti-TrkC mAb and agent **1-F** have similar binding profiles. However, agent **2-F**, the control probe, does not show significant fluorescence in melanoma or healthy skin tissue, implying that **2-F** does not bind a receptor overexpressed on the skin surface (*i.e.* TrkC).

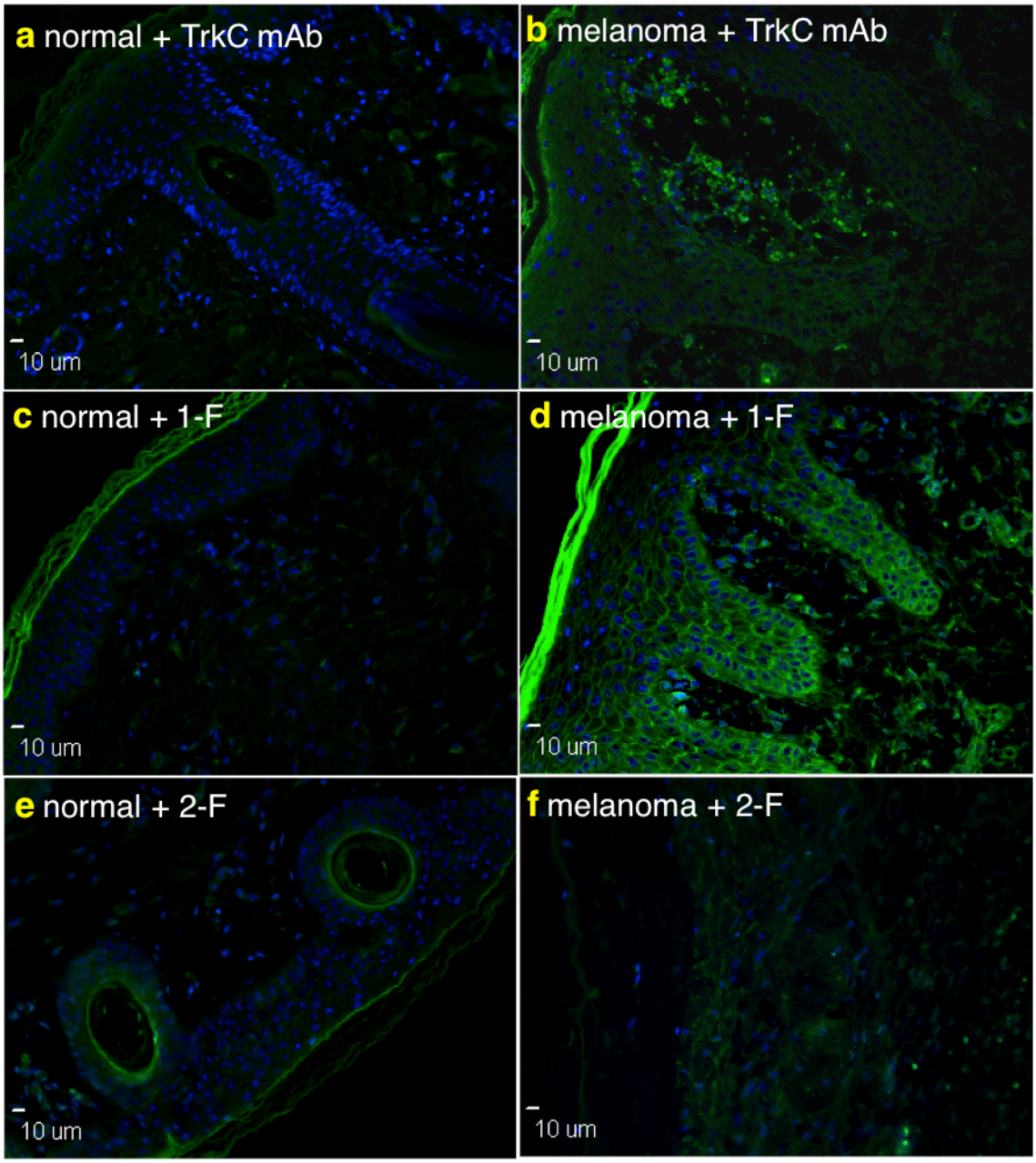

Figure 6-4. Staining with a fluorescently labeled TrkC mAb shows **a** healthy skin tissue does not, but **b** melanoma tissue does, express significant amounts of the TrkC receptor. **c** When treated with **1-F**, healthy skin do not stain, but melanoma tissue from the same pig does (**d**), similar to anti-TrkC-F* mAb. No significant fluorescence was observed from agent **2-F** in both normal tissue (**e**) and melanoma (**f**). Throughout the blue stains in cell nuclei, and the green coloration is due to the fluorescent mAb or **1-F**.

The experiments in Figure 6-4 support the assertion that melanoma in the Sinclair swine overexpresses TrkC relative to healthy keratinocytes. Human tissue samples were also tested to see if this observation holds for melanoma patients. Thus, 48 human tissue samples (US Biomax) were obtained, 40 from melanoma patients, and 8 from healthy tissue. There was some variance in the staining data from different tissue samples, but Figure 6-5 is representative of the overall trend. All tissue samples from the melanoma patients stained in the cytoplasm and/or on the membrane when treated with **1-F** (or anti-TrkC mAb), whereas the healthy tissues gave no similar staining

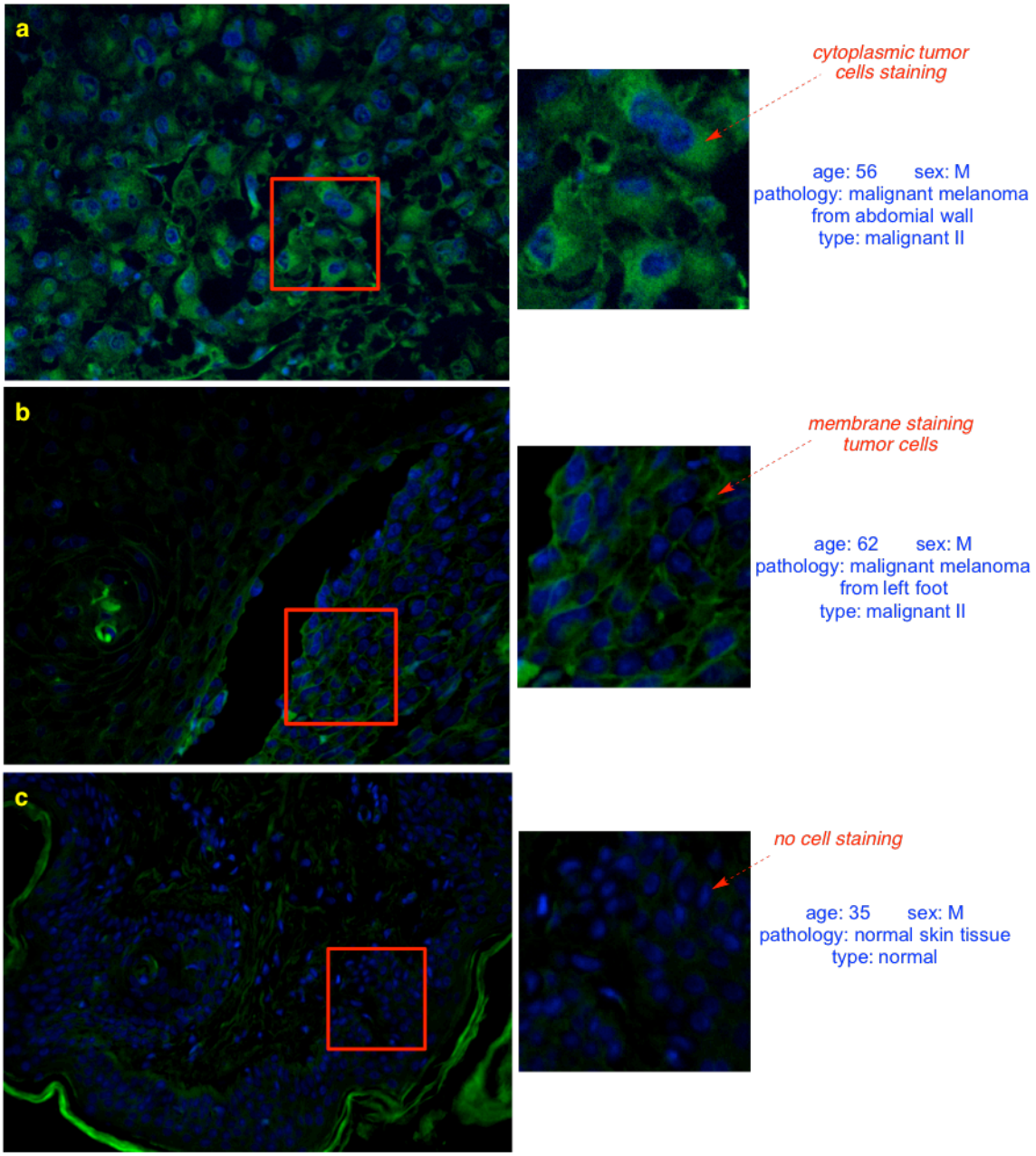

Figure 6-5. Human melanoma tissues stained with **1-F** in the cytoplasm (**a**), or on the membrane (**b**), whereas normal tissue does not.

We have cultured melanoma and healthy skin from the same pig, overcoming the problems that prevent healthy cells being cultivated through several passes. The tissue cultures shown in Figure 6-6a on the left are from melanoma cells; these were relatively easy to grow. However, the cultured healthy skin cells shown on the right would ordinarily be difficult to culture, but we were able to do this via "The Georgetown Method" (ROCK inhibitor and irradiated fibroblast feeder cells).[219-220]

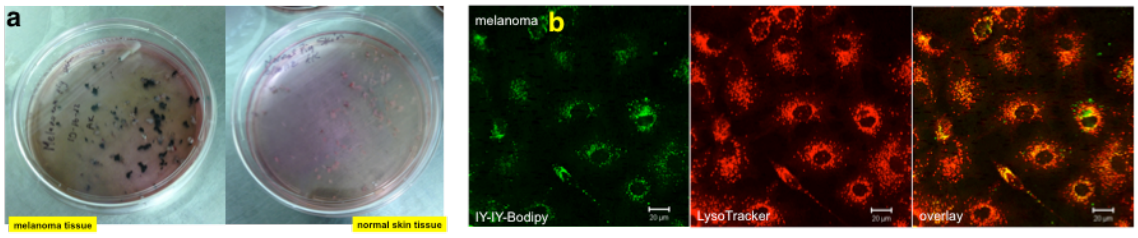

Figure 6-6. **a** Cultured melanoma and normal skin from the same pig. Healthy skin cells were cultured using "The Georgetown Method" that features irradiated feeder cells and a ROCK kinase inhibitor to ensure that multiple passages could be obtained.[219-220] **b** **1-F** is internalized into the lysosome of melanoma cells, (fluorescence overlays well with LysoTracker dye).

Figure 6-7 shows the differential light induced toxicity of **1-PDT** on melanoma cells relative to healthy skin cells. The targeted PDT agent shows more photocytotoxicity to the pig melanoma cells, which overexpress TrkC, than to healthy pig keratinocytes that have insignificant TrkC expression. Moreover, the targeted probe is more phototoxic than the control one (Figure 6-7a). Parallel experiments featuring B16 murine melanoma cells, have been performed, and the outcome was similar (data not shown). Figure 6-7b shows how the dose dependent effects of the targeted PDT agent can be competed using the natural TrkC ligand NT3, or the targeting fragment

with no appendage for PDT. The background phototoxicity might be due to non-specific binding of PDT probes or the effect of PDT from the I_2-BODIPY fragment.

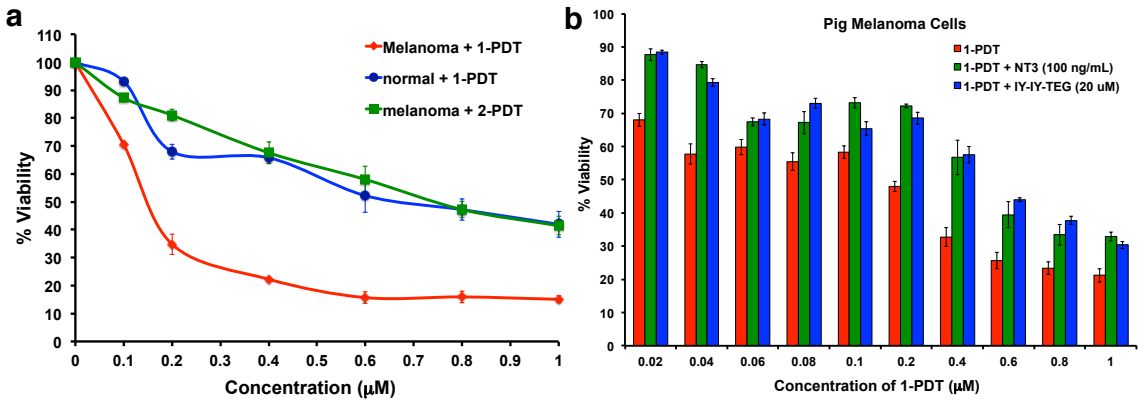

Figure 6-7. **a** **1-PDT** is more toxic to melanoma than to healthy keratinocytes ("normal") from the same pig. The targeted PDT is more toxic than the control one. **b** Targeted photocytotoxicity of **1-PDT** for melanoma cells can be suppressed by the natural protein ligand for TrkC (NT3), or by the targeting fragment without a PDT label on it (**IY-IY-TEG**, TEG = triethylene glycol) in a dose dependent manner.

For *in vivo* optical imaging, the fluor in **1b**, which absorbs around 520 nm, is *unsuitable* because observation of non-superficial tissue requires agents that absorb at longer wavelengths (ideally, >700 nm). Therefore the near-IR probe that is used to target TrkC in the breast cancer model (Chapter 5) must be able to target TrkC in melanoma. To prove this, probe **3a** was used to stain tissues obtained from the Sinclair Swine. Figure 6-8 shows bright fluorescence of **3a** can be observed from melanoma tissue but significantly less is seen for the normal tissue.

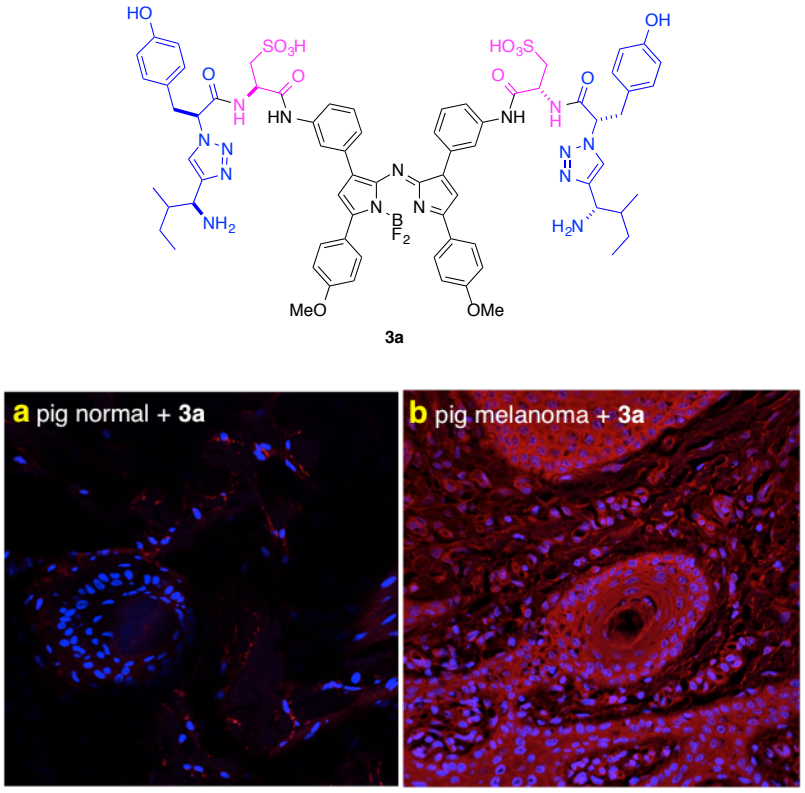

Figure 6-8. Melanoma pig tissues staining with **3a** shows **a** healthy skin tissue does not, but **b** melanoma tissue does, imply significant amounts of the TrkC receptor expressed on melanoma.

Data from one particular Sinclair swine is not reliably indicative of a trend in human melanoma. Thus a panel of commercially available human melanoma tissue samples was stained to estimate the fraction of cases that would bind agent **3a** (Figure 6-9). Duplicate tissue samples from 22 metastatic-melanoma patients were tested, and *every one of them stained with agent **3a***. Conversely, no significant staining was observed when the two duplicate samples of normal skin available were treated with the same probe.

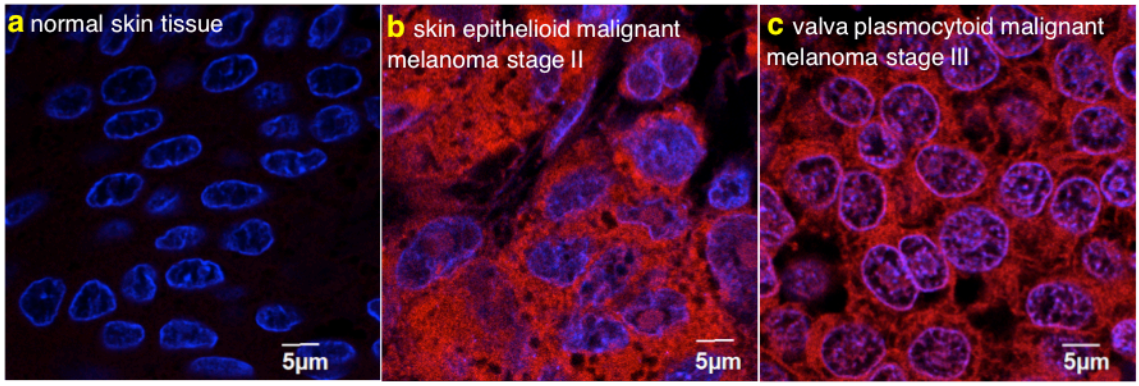

Figure 6-9. Example of human tissues stained with agent **3a**. **a** Normal skin tissue does not show significant staining while the other malignant tissues do (**b** and **c**).

The "aza-BODIPY"[221-222] system **3a** is suitable for observation of non-superficial tissue because it can absorb light at a longer wavelength (around 700 nm) than probe **1-F**.[97-98] Moreover, the probe is also amenable to $^{19}F/^{18}F$ metathesis (Gabbai, personal communication) which can be used for PET imaging.

It is possible to modify compound **3a** to be a PDT agent. Substitution of halogen atoms (*i.e.* Br or I) at the 2,6-positions of the aza-BODIPY core results in an increased population of triplet states upon excitation, giving of PDT activity.[97-98] Thus, the structure shown in Figure 6-10 was conceived, synthesized and tested for active targeting of TrkC in melanoma.

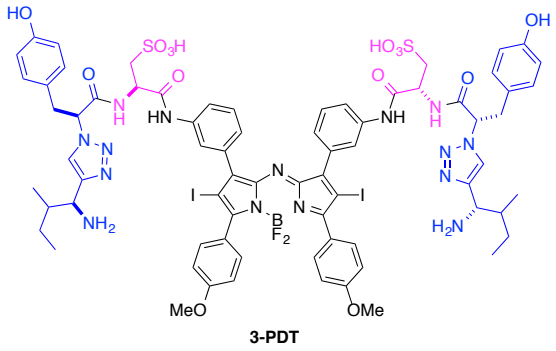

Figure 6-10. Proposed structure of near-IR targeted PDT probe for TrkC cells.

Conclusions

An active targeting probe for TrkC receptors on melanoma, possibly the first of its kind, has been successfully made and tested in histology and cell expreiments. The first generation probe proved targeting efficacy in cells, and we hypothesize this can be used for diagnostic (fluorescence imaging or possibly PET imaging) and therapeutic (PDT) applications in melanoma-afflicted pigs. Our second generation targeting probe is more suitable for *in vivo* studies because of its near-IR absorption; this probe showed its stained melanoma tissue from pigs and human patients. PDT studies of this modified structure in mice and pigs is planned (samples have been submitted for the mouse studies, are in hand for the pig studies, and will be used if the murine model is successful). From the preliminary results, we believe the new agent will be successful for treatment of melanoma.

CHAPTER VII

CONCLUSIONS

This dissertation featured design and development of novel active-targeting probes for treatment of TrkC overexpressing tumors, specifically metastatic forms of breast cancer and melanoma. The first generation targeting probe (**1-PDT**) showed encouraging, positive results from *in vivo* studies testing its role as a therapeutic. Thus at day 6 post-illumination, **1-PDT** at 10 mg/kg (single injection) caused 96 % volume reduction in murine $TrkC^+$ (4T1 murine breast cancer cells) tumors. Among these mice, 71 % showed full diminution and were tumor-free for 90 days after therapy. Moreover, histopathology indicated no metastasis development in these animals. However, **1-PDT** required further structural modifications for several reasons. The first of these was that it triggered neurotoxicity at high doses (> 30 mg/kg) in mice. Secondly, the light wavelength to excite **1-PDT** is optimally ~520 nm whereas PDT agents should absorb above 700 nm to be effective in deeper tissue. Our second-generation targeting probes were designed to use the aza-BODIPY (λ_{max} around 700 nm) for more effective imaging in tissue, and as a spacer between two targeting **IY** fragments to make the system more compact. Agent **3a** of this type was more difficult to produce than **3b** but it has two sulfonic acid groups to enhance hydrophilicity and reduce non-specific binding. Histology and live cell imaging showed **3a** selectively bound to $TrkC^+$ tumor cells. Furthermore, *in vivo* imaging using an orthotopic breast cancer model showed **3a** accumulated rapidly in the tumor but was completely cleared after 24 h; moreover,

neurotoxicity was *not* observed. Probe **3a** also has potential as a positron emission tomography (PET) agent via ^{19}F to ^{18}F exchange; use of this probe for PET is under investigation by collaborators using material made in this thesis work. In the last chapter, a Sinclair Swine model was used in melanoma research. Our first- and second-generation probes were shown to successfully bind and treat melanoma tissue *ex vivo*. The near-IR absorbing probe **3-PDT** was prepared and sent to collaborators to investigate as a therapeutic agent in the pig model.

REFERENCES

(1) Torchilin Vladimir, P. *Handb. Exp. Pharmacol.* **2010**, *197*, 3.

(2) Sassoon, I.; Blanc, V. In *Antibody-Drug Conjugates*; Ducry, L., Ed.; Humana Press, 2013; Vol. 1045.

(3) Zolot, R. S.; Basu, S.; Million, R. P. *Nat Rev Drug Discov* **2013**, *12*, 259.

(4) Sievers Eric, L.; Senter Peter, D. *Annu. Rev. Med.* **2013**, *64*, 15.

(5) Alley, S. C.; Okeley, N. M.; Senter, P. D. *Curr. Opin. Chem. Biol.* **2010**, *14*, 529.

(6) Bander, N. In *Antibody-Drug Conjugates*; Ducry, L., Ed.; Humana Press, 2013; Vol. 1045.

(7) Krop, I.; Winer, E. P. *Clin. Cancer Res.* **2014**, *20*, 15.

(8) Perini, G.; Pro, B. *Biologics in Therapy* **2013**, *3*, 15.

(9) Saga, T.; Neumann, R. D.; Heya, T.; Sato, J.; Kinuya, S.; Le, N.; Paik, C. H.; Weinstein, J. N. *Proc. Natl. Acad. Sci. U. S. A.* **1995**, *92*, 8999.

(10) Adams, G. P.; Schier, R.; McCall, A. M.; Simmons, H. H.; Horak, E. M.; Alpaugh, R. K.; Marks, J. D.; Weiner, L. M. *Cancer Res.* **2001**, *61*, 4750.

(11) Rudnick, S. I.; Lou, J.; Shaller, C. C.; Tang, Y.; Klein-Szanto, A. J. P.; Weiner, L. M.; Marks, J. D.; Adams, G. P. *Cancer Res.* **2011**, *71*, 2250.

(12) Dennis, M. S.; Jin, H.; Dugger, D.; Yang, R.; McFarland, L.; Ogasawara, A.; Williams, S.; Cole, M. J.; Ross, S.; Schwall, R. *Cancer Res.* **2007**, *67*, 254.

(13) Baluk, P.; Morikawa, S.; Haskell, A.; Mancuso, M.; McDonald Donald, M. *Am. J. Pathol.* **2003**, *163*, 1801.

(14) di Tomaso, E.; Capen, D.; Haskell, A.; Hart, J.; Logie, J. J.; Jain, R. K.; McDonald, D. M.; Jones, R.; Munn, L. L. *Cancer Res.* **2005**, *65*, 5740.

(15) O'Connor, R. *Anticancer Res.* **2007**, *27*, 1267.

(16) Borsi, L.; Balza, E.; Bestagno, M.; Castellani, P.; Carnemolla, B.; Biro, A.; Leprini, A.; Sepulveda, J.; Burrone, O.; Neri, D.; Zardi, L. *Int. J. Cancer* **2002**, *102*, 75.

(17) Carrasco-Triguero, M.; Yi, J.-H.; Dere, R.; Qiu, Z. J.; Lei, C.; Li, Y.; Mahood, C.; Wang, B.; Leipold, D.; Poon, K. A.; Kaur, S. *Bioanalysis* **2013**, *5*, 1007.

(18) Trapani, G.; Denora, N.; Trapani, A.; Laquintana, V. *J. Drug Targeting* **2012**, *20*, 1.

(19) Vlashi, E.; Sturgis, J. E.; Thomas, M.; Low, P. S. *Mol. Pharmaceutics* **2009**, *6*, 1868.

(20) Lu, Y.; Low Philip, S. *Adv. Drug Deliv. Rev.* **2012**, *64*, 342.

(21) Xia, W.; Low, P. S. *J. Med. Chem.* **2010**, *53*, 6811.

(22) Hilgenbrink, A. R.; Low, P. S. *J. Pharm. Sci.* **2005**, *94*, 2135.

(23) Low, P. S.; Henne, W. A.; Doorneweerd, D. D. *Acc. Chem. Res.* **2008**, *41*, 120.

(24) Vlahov, I. R.; Leamon, C. P. *Bioconjug. Chem.* **2012**, *23*, 1357.

(25) Ojima, I. *Acc. Chem. Res.* **2008**, *41*, 108.

(26) Gupta, Y.; Kohli, D. V.; Jain, S. K. *Crit. Rev. Ther. Drug Carrier Systems* **2008**, *25*, 347.

(27) Waibel, R.; Treichler, H.; Schaefer, N. G.; van Staveren, D. R.; Mundwiler, S.; Kunze, S.; Kuenzi, M.; Alberto, R.; Nuesch, J.; Knuth, A.; Moch, H.; Schibli, R.; Schubiger, P. A. *Cancer Res.* **2008**, *68*, 2904.

(28) Lee, S.; Xie, J.; Chen, X. *Chem. Rev.* **2010**, ACS ASAP.

(29) Martin, M. E.; Rice, K. G. *AAPS Journal* **2007**, *9*, E18.

(30) Garanger, E.; Boturyn, D.; Dumy, P. *Anti-Cancer Agents Med. Chem.* **2007**, *7*, 552.

(31) Dunehoo, A. L.; Anderson, M.; Majumdar, S.; Kobayashi, N.; Berkland, C.; Siahaan, T. J. *J. Pharm. Sci.* **2006**, *95*, 1856.

(32) Li, F.; Liu, J.; Jas, G. S.; Zhang, J.; Qin, G.; Xing, J.; Cotes, C.; Zhao, H.; Wang, X.; Diaz, L. A.; Shi, Z.-Z.; Lee, D. Y.; Li, K. C. P.; Li, Z. *Bioconjugate Chem.* **2010**, *21*, 270.

(33) Liu, F.; Li, M.; Liu, C.; Liu, Y.; Liang, Y.; Wang, F.; Zhang, N. *Pharm. Res.* **2014**, *31*, 475.

(34) Krall, N.; Pretto, F.; Neri, D. *Chem. Sci.* **2014**, in the press.

(35) Krall, N.; Pretto, F.; Decurtins, W.; Bernardes, G. J. L.; Supuran, C. T.; Neri, D. *Angew. Chem., Int. Ed.* **2014**, *53*, 4231.

(36) Klier, M.; Andes, F. T.; Deitmer, J. W.; Becker, H. M. *J. Biol. Chem.* **2014**, *289*, 2765.

(37) Takacova, M.; Bartosova, M.; Skvarkova, L.; Zatovicova, M.; Vidlickova, I.; Csaderova, L.; Barathova, M.; Breza, J., Jr.; Bujdak, P.; Pastorek, J.; Breza, J., Sr.; Pastorekova, S. *Oncol. Lett.* **2013**, *5*, 191.

(38) Henne, W. A.; Kularatne, S. A.; Ayala-Lopez, W.; Doorneweerd, D. D.; Stinnette, T. W.; Lu, Y.; Low, P. S. *Bioorg. Med. Chem. Lett.* **2012**, *22*, 709.

(39) Jayaprakash, S.; Wang, X.; Heston, W. D.; Kozikowski, A. P. *ChemMedChem* **2006**, *1*, 299.

(40) Krall, N.; Scheuermann, J.; Neri, D. *Angew. Chem., Int. Ed.* **2013**, *52*, 1384.

(41) Srinivasarao, M.; Galliford, C. V.; Low, P. S. *Nat Rev Drug Discov* **2015**, *14*, 203.

(42) Gwangsik, S.; Tae-Wook, K.; Sungjin, Y.; Su-Jin, B.; Yong-Su, J.; Seon-Young, K. *Cancer Informatics* **2011**, 149.

(43) Rhodes, D. R.; Yu, J.; Shanker, K.; Deshpande, N.; Varambally, R.; Ghosh, D.; Barrette, T.; Pander, A.; Chinnaiyan, A. M. *Neoplasia* **2004**, *6*, 1.

(44) Skaper, S. D. *CNS Neurol. Disord.: Drug Targets* **2008**, *7*, 46.

(45) Volosin, M.; Song, W.; Almeida, R. D.; Kaplan, D. R.; Hempstead, B. L.; Friedman, W. J. *J. Neurosci.* **2006**, *26*, 7756.

(46) Ivanisevic, L.; Saragovi, H. U. *Handb. Biol. Act. Pept.* **2006**, 1407.

(47) Mocchetti, I. *Neurobiology of the Neurotrophins*; FP Graham Publishing Co.: Johnson City, TN, 2001.

(48) Miller, F. D.; Kaplan, D. R. *Cell Mol Life Sci.* **2001**, *58*, 1045.

(49) Lee, F. S.; Chao, M. V. *Proc Natl Acad Sci U S A* **2001**, *98*, 3555.

(50) Yamashiro, D. J.; Nakagawara, A.; Ikegaki, N.; Liu, X. G.; Brodeur, G. M. *Oncogene* **1996**, *12*, 37.

(51) Brodeur, G. M.; Nakagawara, A.; Yamashiro, D. J.; Ikegaki, N.; Liu, X. G.; Azar, C. G.; Lee, C. P.; Evans, A. E. *J. Neuro-Oncology* **1997**, *31*, 49.

(52) Encinas, M.; Iglesias, M.; Llecha, N.; Comella, J. X. *J. Neurochem.* **1999**, *73*, 1409.

(53) Brodeur, G. M.; Minturn, J. E.; Ho, R.; Simpson, A. M.; Iyer, R.; Varela, C. R.; Light, J. E.; Kolla, V.; Evans, A. E. *Clin. Cancer Res.* **2009**, *15*, 3244.

(54) Bassili, M.; Birman, E.; Schor, N. F.; Saragovi, H. U. *Cancer Chemother. Pharmacol.* **2010**, *65*, 1047.

(55) Bernard-Gauthier, V.; Aliaga, A.; Aliaga, A.; Boudjemeline, M.; Hopewell, R.; Kostikov, A.; Rosa-Neto, P.; Thiel, A.; Schirrmacher, R. *ACS Chem. Neurosci.* **2014**, in press.

(56) Dutta, A. K.; Kamada, K.; Ohta, K. *Photochem. Photobiol.* **1996**, *93*, 57.

(57) Wang, Y.; Hagel, C.; Hamel, W.; Muller, S.; Kluwe, L.; Westphal, M. *Acta Neuropathol. (Berl)* **1998**, *96*, 357.

(58) Calatozzolo, C.; Salmaggi, A.; Pollo, B.; Sciacca, F. L.; Lorenzetti, M.; Franzini, A.; Boiardi, A.; Broggi, G.; Marras, C. *Neurol. Sci.* **2007**, *28*, 304.

(59) Assimakopoulou, M.; Kondyli, M.; Gatzounis, G.; Maraziotis, T.; Varakis, J. *BMC Cancer* **2007**, *7*, 202.

(60) Velema, W. A.; Szymanski, W.; Feringa, B. L. *J. Am. Chem. Soc.* **2014**, *136*, 2178.

(61) Stephens, P.; Edkins, S.; Davies, H.; Greenman, C.; Cox, C.; Hunter, C.; Bignell, G.; Teague, J.; Smith, R.; Stevens, C.; O'Meara, S.; Parker, A.; Tarpey, P.; Avis,

T.; Barthorpe, A.; Brackenbury, L.; Buck, G.; Butler, A.; Clements, J.; Cole, J.; Dicks, E.; Edwards, K.; Forbes, S.; Gorton, M.; Gray, K.; Halliday, K.; Harrison, R.; Hills, K.; Hinton, J.; Jones, D.; Kosmidou, V.; Laman, R.; Lugg, R.; Menzies, A.; Perry, J.; Petty, R.; Raine, K.; Shepherd, R.; Small, A.; Solomon, H.; Stephens, Y.; Tofts, C.; Varian, J.; Webb, A.; West, S.; Widaa, S.; Yates, A.; Brasseur, F.; Cooper, C. S.; Flanagan, A. M.; Green, A.; Knowles, M.; Leung, S. Y.; Looijenga, L. H. J.; Malkowicz, B.; Pierotti, M. A.; Teh, B.; Yuen, S. T.; Nicholson, A. G.; Lakhani, S.; Easton, D. F.; Weber, B. L.; Stratton, M. R.; Futreal, P. A.; Wooster, R. *Nat. Genet.* **2005**, *37*, 590.

(62) Ivanov, S. V.; Panaccione, A.; Brown, B.; Guo, Y.; Moskaluk, C. A.; Wick, M. J.; Brown, J. L.; Ivanova, A. V.; Issaeva, N.; El-Naggar, A. K.; Yarbrough, W. G. *Oncogene* **2013**, *32*, 3698.

(63) Jin, W.; Kim, G.-M.; Kim, M.-S.; Lim, M.-H.; Yun, C.-H.; Jeong, J.; Nam, J.-S.; Kim, S.-J. *Carcinogenesis* **2010**, *31*, 1939.

(64) Jin, W.; Yun, C.; Kwak, M. K.; Kim, T. A.; Kim, S. J. *Oncogene* **2007**, *26*, 7684.

(65) Jin, W.; Yun, C.; Jeong, J.; Park, Y.; Lee, H.-D.; Kim, S.-J. *J. Biol. Chem.* **2008**, *283*, 1391.

(66) Blasco-Gutierrez, M. J.; San Jose-Crespo, I. J.; Zozaya-Alvarez, E.; Ramos-Sanchez, R.; Garcia-Atares, N. *Cancer Invest.* **2007**, *25*, 405.

(67) Hondermarck, H. *Cytokine Growth Factor Rev.* **2012**, *23*, 357.

(68) Xu, X.; Tahan, S. R.; Pasha, T. L.; Zhang, P. J. *J. Cutan. Pathol.* **2003**, *30*, 318.

(69) Marconi, A.; Terracina, M.; Fila, C.; Franchi, J.; Bonte, F.; Romagnoli, G.; Maurelli, R.; Failla, C. M.; Dumas, M.; Pincelli, C. *J. Invest. Dermatol.* **2003**, *121*, 1515.

(70) Marchetti, D.; Murry, B.; Galjour, J.; Wilke-Greiter, A. *J. Cell. Biochem.* **2003**, *88*, 865.

(71) Hendrix, M. J. C.; Seftor, E. A.; Kirschmann, D. A.; Quaranta, V.; Seftor, R. E. B. *Ann. N. Y. Acad. Sci.* **2003**, *995*, 151.

(72) Marconi, A.; Panza, M. C.; Bonnet-Duquennoy, M.; Lazou, K.; Kurfurst, R.; Truzzi, F.; Lotti, R.; De Santis, G.; Dumas, M.; Bonte, F.; Pincelli, C. *Int. J. Cosmet. Sci.* **2006**, *28*, 255.

(73) Truzzi, F.; Marconi, A.; Lotti, R.; Dallaglio, K.; French, L. E.; Hempstead, B. L.; Pincelli, C. *J. Invest. Dermatol.* **2008**, *128*, 2031.

(74) Botchkarev, V. A.; Yaar, M.; Peters, E. M. J.; Raychaudhuri, S. P.; Botchkareva, N. V.; Marconi, A.; Raychaudhuri, S. K.; Paus, R.; Pincelli, C. *J. Invest. Dermatol.* **2006**, *126*, 1719.

(75) Marchetti, D.; Denkins, Y.; Reiland, J.; Greiter-Wilke, A.; Galjour, J.; Murry, B.; Blust, J.; Roy, M. *Pathol. Oncol. Res.* **2003**, *9*, 147.

(76) Denkins, Y.; Reiland, J.; Roy, M.; Sinnappah-Kang, N. D.; Galjour, J.; Murry, B. P.; Blust, J.; Aucoin, R.; Marchetti, D. *Neuro-Oncology* **2004**, *6*, 154.

(77) Chen, D.; Brahimi, F.; Angell, Y.; Li, Y.-C.; Moscowicz, J.; Saragovi, H. U.; Burgess, K. *ACS Chem. Biol.* **2009**, *4*, 769.

(78) Juarranz, A.; Jaen, P.; Sanz-Rodriguez, F.; Cuevas, J.; Gonzalez, S. *Clin. Transl. Oncol.* **2008**, *10*, 148.

(79) Agostinis, P.; Berg, K.; Cengel Keith, A.; Foster Thomas, H.; Girotti Albert, W.; Gollnick Sandra, O.; Hahn Stephen, M.; Hamblin Michael, R.; Juzeniene, A.; Kessel, D.; Korbelik, M.; Moan, J.; Mroz, P.; Nowis, D.; Piette, J.; Wilson Brian, C.; Golab, J. *CA Cancer J Clin* **2011**, *61*, 250.

(80) Allison, R. R.; Sibata, C. H. *Photodiag. Photodyn. Ther.* **2010**, *7*, 61.

(81) Baldea, I.; Filip, A. G. *J. Physiol. Pharmacol.* **2012**, *63*, 109.

(82) Huang, Y.-Y.; Vecchio, D.; Avci, P.; Yin, R.; Garcia-Diaz, M.; Hamblin Michael, R. *Biol. Chem.* **2013**, *394*, 239.

(83) Schmitt, F.; Juillerat-Jeanneret, L. *Anti-Cancer Agents Med. Chem.* **2012**, *12*, 500.

(84) Sternberg, E. D.; Dolphin, D.; Brückner, C. *Tetrahedron* **1998**, *54*, 4151.

(85) Nyman, E. S.; Hynninen, P. H. *J. Photochem. Photobiol., B* **2004**, *73*, 1.

(86) Wainwright, M.; Giddens, R. M. *Dyes and Pigments* **2003**, *57*, 245.

(87) Day, C. L.; Chen, L.; Richardson, S. J.; Harrison, P. J.; Huang, D. C. S.; Hinds, M. G. *J. Biol. Chem.* **2005**, *280*, 4738.

(88) Wainwright, M. *Photodiag. Photodyn. Ther.* **2005**, *2*, 263.

(89) Wainwright, M.; Phoenix, D. A.; Rice, L.; Burrow, S. M.; Waring, J. *J. Photochem. Photobiol. B* **1997**, *40*, 233.

(90) Yogo, T.; Urano, Y.; Ishitsuka, Y.; Maniwa, F.; Nagano, T. *J. Am. Chem. Soc.* **2005**, *127*, 12162.

(91) Lim, S. H.; Thivierge, C.; Nowak-Sliwinska, P.; Han, J.; Van den Bergh, H.; Wagnieres, G.; Burgess, K.; Lee, H. B. *J. Med. Chem.* **2010**, *53*, 2865.

(92) Loudet, A.; Burgess, K. *Chem. Rev.* **2007**, *107*, 4891.

(93) Boens, N.; Leen, V.; Dehaen, W. *Chem. Soc. Rev.* **2012**, *41*, 1130.

(94) Loudet, A.; Burgess, K. In *Handbook of Porphyrin Science: With Applications to Chemistry, Physics, Materials Science, Engineering, Biology and Medicine*; Kadish, K., Smith, K., Guilard, R., Eds.; World Scientific, 2010.

(95) Ulrich, G.; Ziessel, R.; Harriman, A. *Angew. Chem. Int. Ed.* **2008**, *47*, 1184.

(96) Ziessel, R.; Ulrich, G.; Harriman, A. *New J. Chem* **2007**, *31*, 496.

(97) Kamkaew, A.; Lim Siang, H.; Lee Hong, B.; Kiew Lik, V.; Chung Lip, Y.; Burgess, K. *Chem. Soc. Rev.* **2012**, *42*, 77.

(98) Awuah, S. G.; You, Y. *RSC Adv.* **2012**, *2*, 11169.

(99) Sharman, W. M.; van Lier, J. E.; Allen, C. M. *Adv. Drug Delivery Rev.* **2004**, *56*, 53.

(100) Juillerat-Jeanneret, L. *Trends Cancer Res.* **2006**, *2*, 71.

(101) Bullous, A. J.; Alonso, C. M. A.; Boyle, R. W. *Photochem. Photobiol. Sci.* **2011**, *10*, 721.

(102) He, H.; Lo, P.-C.; Yeung, S.-L.; Fong, W.-P.; Ng, D. K. P. *J. Med. Chem.* **2011**, *54*, 3097.

(103) Liu, T.; Wu, L. Y.; Berkman, C. E. *Cancer Lett.* **2010**, *296*, 106.

(104) Morosini, V.; Bastogne, T.; Frochot, C.; Schneider, R.; Francois, A.; Guillemin, F.; Barberi-Heyob, M. *Photochem. Photobiol. Sci.* **2011**, *10*, 842.

(105) De Angelo, D.; Erba, H. P.; Maris, M. B.; Swords, R. T.; Anwer, F.; Arlman, J.; Hua, Z.; Blakemore, S.; Faessel, H.; Dezube, B. J.; Medeiros, B. C. *Blood* **2013**, *122*, 1443.

(106) Brannon-Peppas, L.; Blanchette, J. O. *Adv. Drug Delivery Rev.* **2004**, *56*, 1649.

(107) Peer, D.; Karp, J. M.; Hong, S.; Farokhzad, O. C.; Margalit, R.; Langer, R. *Nat. Nanotechnol.* **2007**, *2*, 751.

(108) Segal, R. A.; Goumnerova, L. C.; Kwon, Y. K.; Stiles, C. D.; Pomeroy, S. L. *Proc. Nat'l Acad. Sci. USA* **1994**, *91*, 12867.

(109) Butowt, R.; von Bartheld, C. S. *J. Neurosci.* **2001**, *21*, 8915.

(110) Saczewski, F.; Maruszak, M.; Bednarski, P. J. *Arch. Pharm. Chem. Life Sci.* **2008**, *341*, 121.

(111) Lim, S. H.; Wu, L.; Burgess, K.; Lee, H. B. *Anti-Cancer Drugs* **2009**, *20*, 461.

(112) Eibl, J. K.; Chapelsky, S. A.; Ross, G. M. *J. Pharmacol. Exp. Ther.* **2010**, *332*, 446.

(113) Rabin, S. J.; Bachis, A.; Mocchetti, I. *J. Biol. Chem.* **2002**, *277*, 49466.

(114) Nelson, J. A.; Vidale, E. *Cancer Res.* **1986**, *46*, 137.

(115) Antony, A. C. *Annu. Rev. Nutr.* **1996**, *16*, 501.

(116) Plow, E. F.; Haas, T. A.; Zhang, L.; Loftus, J.; Smith, J. W. *J. Biol. Chem.* **2000**, *275*, 21785.

(117) Hynes, R. O. *Cell* **1987**, *48*, 549.

(118) Desgrosellier, J. S.; Cheresh, D. A. *Nat. Rev. Cancer* **2010**, *10*, 9.

(119) Plantinga, A.; Witte, A.; Li, M.-H.; Harmon, A.; Choi, S. K.; Banaszak Holl, M. M.; Orr, B. G.; Baker, J. R.; Sinniah, K. *ACS Med. Chem. Lett.* **2011**, *2*, 363.

(120) White, H. B., III; Merrill, A. H., Jr. *Annu. Rev. Nutr.* **1988**, *8*, 279.

(121) Makishima, M.; Lu, T. T.; Xie, W.; Whitfield, G. K.; Domoto, H.; Evans, R. M.; Haussler, M. R.; Mangelsdorf, D. J. *Science* **2002**, *296*, 1313.

(122) Andre, S.; Frisch, B.; Kaltner, H.; Desouza, D. L.; Schuber, F.; Gabius, H.-J. *Pharm. Res.* **2000**, *17*, 985.

(123) Ashwell, G.; Harford, J. *Annu. Rev. Biochem.* **1982**, *51*, 531.

(124) Song, C.; Liao, S. *Endocrinology* **2000**, *141*, 4180.

(125) Schuller, H. M.; Al-Wadei, H. A. N.; Majidi, M. *Cancer* **2008**, *112*, 767.

(126) Chabner, B. A.; Roberts, T. G. *Nat. Rev. Cancer* **2005**, *5*, 65.

(127) Zhang, J.; Yang, P. L.; Gray, N. S. *Nat. Rev. Cancer* **2009**, *9*, 28.

(128) Prien, O. *ChemBioChem* **2005**, *6*, 500.

(129) Barnett, S. F.; Bilodeau, M. T.; Lindsley, C. W. *Curr. Top. Med. Chem.* **2005**, *5*, 109.

(130) Schrama, D.; Reisfeld, R. A.; Becker, J. C. *Nat. Rev. Drug Discovery* **2006**, *5*, 147.

(131) Low, P. S.; Kularatne, S. A. *Curr. Opin. Chem. Biol.* **2009**, *13*, 256.

(132) Verma, S.; Watt, G. M.; Mai, Z.; Hasan, T. *Photochem. Photobiol.* **2007**, *83*, 996.

(133) Ko, E.; Kamkaew, A.; Burgess, K. *ACS Med. Chem. Lett.* **2012**, *3*, 1008.

(134) Ke, M.-R.; Yeung, S.-L.; Ng, D. K. P.; Fong, W.-P.; Lo, P.-C. *J. Med. Chem.* **2013**, *56*, 8475.

(135) Truzzi, F.; Marconi, A.; Pincelli, C. *Derm.-Endocrinol.* **2011**, *3*, 32.

(136) Pincelli, C. D., K. ; Truzzi F *Breakthroughs in Melanoma Research* **2011**.

(137) Innominato, P. F.; Libbrecht, L.; van den Oord, J. J. *J. Pathol.* **2001**, *194*, 95.

(138) Meldal, M.; Tornoe, C. W. *Chem. Rev.* **2008**, *108*, 2952.

(139) Kolb, H. C.; Finn, M. G.; Sharpless, K. B. *Angew. Chem. Int. Ed.* **2001**, *40*, 2004.

(140) Ballou, B.; Ernst, L. A.; Waggoner, A. S. *Curr. Med. Chem.* **2005**, *12*, 795.

(141) Guillemard, V.; Ivanisevic, L.; Garcia, A. G.; Scholten, V.; Lazo, O. M.; Bronfman, F. C.; Saragovi, H. U. *Dev. Neurobiol.* **2010**, *70*, 150.

(142) Bosanquet, A. G.; Bell, P. B. *J. Exp. Ther. Oncol.* **2004**, *4*, 145.

(143) Uhlen, M.; Oksvold, P.; Fagerberg, L.; Lundberg, E.; Jonasson, K.; Forsberg, M.; Zwahlen, M.; Kampf, C.; Wester, K.; Hober, S.; Wernerus, H.; Bjoerling, L.; Ponten, F. *Nat. Biotechnol.* **2010**, *28*, 1248.

(144) Rao, J.; Dragulescu-Andrasi, A.; Yao, H. *Curr. Opin. Biotechnol.* **2007**, *18*, 17.

(145) Frangioni, J. V. *Curr. Opin. Chem. Biol.* **2003**, *7*, 626.

(146) Sevick-Muraca, E. M.; Houston, J. P.; Gurfinkel, M. *Curr. Opin. Chem. Biol.* **2002**, *6*, 642.

(147) Gallagher, W. M.; Allen, L. T.; O'Shea, C.; Kenna, T.; Hall, M.; Gorman, A.; Killoran, J.; O'Shea, D. F. *Br. J. Cancer* **2005**, *92*, 1702.

(148) McDonnell, S. O.; Hall, M. J.; Allen, L. T.; Byrne, A.; Gallagher, W. M.; O'Shea, D. F. *J. Am. Chem. Soc.* **2005**, *127*, 16360.

(149) Quartarolo, A. D.; Russo, N.; Sicilia, E. *Chem.--Eur. J.* **2006**, *12*, 6797.

(150) Byrne, A. T.; O'Connor, A. E.; Hall, M.; Murtagh, J.; O'Neill, K.; Curran, K. M.; Mongrain, K.; Rousseau, J. A.; Lecomte, R.; McGee, S.; Callanan, J. J.; O'Shea, D. F.; Gallagher, W. M. *Br. J. Cancer* **2009**, *101*, 1565.

(151) Batat, P.; Cantuel, M.; Jonusauskas, G.; Scarpantonio, L.; Palma, A.; O'Shea, D. F.; McClenaghan, N. D. *J. Phys. Chem. A* **2011**, *115*, 14034.

(152) Erbas, S.; Gorgulu, A.; Kocakusakogullari, M.; Akkaya, E. U. *Chem. Commun.* **2009**, 4956.

(153) Cakmak, Y.; Kolemen, S.; Duman, S.; Dede, Y.; Dolen, Y.; Kilic, B.; Kostereli, Z.; Yildirim, L. T.; Dogan, A. L.; Guc, D.; Akkaya, E. U. *Angew. Chem., Int. Ed.* **2011**, *50*, 11937.

(154) He, H.; Lo, P.-C.; Yeung, S.-L.; Fong, W.-P.; Ng, D. K. P. *Chem. Commun.* **2011**, *47*, 4748.

(155) Agarwal, A.; Saraf, S.; Asthana, A.; Gupta, U.; Gajbhiye, V.; Jain, N. K. *Int. J. Pharm.* **2008**, *350*, 3.

(156) Minko, T.; Dharap, S. S.; Pakunlu, R. I.; Wang, Y. *Curr. Drug Targets* **2004**, *5*, 389.

(157) Kaur, S. *Bioanalysis* **2013**, *5*, 981.

(158) Meng, Q.; Li, Z. *Int. J. Biomed. Imaging* **2013**, 1.

(159) Liu, J.; Brahimi, F.; Saragovi, H. U.; Burgess, K. *J. Med. Chem.* **2010**, *53*, 5044.

(160) Brahimi, F.; Malakhov, A.; Lee, H. B.; Pattarawarapan, M.; Ivanisevic, L.; Burgess, K.; Saragovi, H. U. *Peptides* **2009**, *30*, 1833.

(161) Chao, M. V. *Nat. Rev. Neurosci.* **2003**, *4*, 299.

(162) Pattarawarapan, M.; Burgess, K. *J. Med. Chem.* **2003**, *46*, 5277.

(163) Louie, E.; Chen, X. F.; Coomes, A.; Ji, K.; Tsirka, S.; Chen, E. I. *Oncogene* **2012**, *32*, 4064.

(164) Vanhecke, E.; Adriaenssens, E.; Verbeke, S.; Meignan, S.; Germain, E.; Berteaux, N.; Nurcombe, V.; Le Bourhis, X.; Hondermarck, H. *Clin. Cancer Res.* **2011**, *17*, 1741.

(165) Levanti, M. B.; Germana, A.; Catania, S.; Germana, G. P.; Gauna-Anasco, L.; Vega, J. A.; Ciriaco, E. *Anat. Histol. Embryol.* **2001**, *30*, 193.

(166) Cui, Q.; Tang Louisa, S.; Hu, B.; So, K.-F.; Yip Henry, K. *Invest. Ophthalmol. Vis. Sci.* **2002**, *43*, 1954.

(167) Botchkarev, V. A.; Metz, M.; Botchkareva, N. V.; Welker, P.; Lommatzsch, M.; Renz, H.; Paus, R. *Lab. Invest.* **1999**, *79*, 557.

(168) Aslakson, C. J.; Miller, F. R. *Cancer Res* **1992**, *52*, 1399.

(169) Kamkaew, A.; Burgess, K. *J. Med. Chem.* **2013**, *56*, 7608.

(170) Veenhuizen, R.; Oppelaar, H.; Ruevekamp, M.; Schellens, J.; Dalesio, O.; Stewart, F. *Int. J. Cancer* **1997**, *73*, 236.

(171) Sasahira, T.; Ueda, N.; Kurihara, M.; Matsushima, S.; Ohmori, H.; Fujii, K.; Bhawal, U. K.; Yamamoto, K.; Kirita, T.; Kuniyasu, H. *Hum. Pathol.* **2013**, *44*, 1098.

(172) Solban, N.; Rizvi, I.; Hasan, T. *Lasers Surg Med* **2006**, *38*, 522.

(173) Gomer, C. J.; Ferrario, A. *Cancer Res.* **1990**, *50*, 3985.

(174) Boch, R.; Canaan, A. J.; Cho, A.; Dolphin, D. D.; Hong, L.; Jain, A. K.; North, J. R.; Richter, A. M.; Smits, C.; Sternberg, E. D. *Photochem. Photobiol.* **2006**, *82*, 219.

(175) Koh, J.-Y.; Gwag, B. J.; Lobner, D.; Choi, D. W. *Science* **1995**, *268*, 573.

(176) Chan, E.; Mulkerin, D.; Rothenberg, M.; Holen, K. D.; Lockhart, A. C.; Thomas, J.; Berlin, J. *Invest. New Drugs* **2008**, *26*, 241.

(177) Patapoutian, A.; Reichardt, L. F. *Cur. Opin. Neurobio.* **2001**, *11*, 272.

(178) Huang, E. J.; Reichardt, L. F. *Annu. Rev. Biochem.* **2003**, *72*, 609.

(179) Kumar, S.; de Vellis, J. *J. Neurosci. Res.* **1996**, *44*, 490.

(180) Vaishnavi, A.; Le Anh, T.; Doebele Robert, C. *Cancer Discov.* **2015**, in press.

(181) Dolle, L.; Adriaenssens, E.; Yazidi-Belkoura, I. E.; Bourhis, X. l.; Nurcombe, V.; Hondermarck, H. *Current Cancer Drug Targets* **2004**, *4*, 463.

(182) Bernard-Gauthier, V.; Boudjemeline, M.; Rosa-Neto, P.; Thiel, A.; Schirrmacher, R. *Bioorg. Med. Chem.* **2013**, *21*, 7816.

(183) Liu, S.; Lin, T.-P.; Li, D.; Leamer, L.; Shan, H.; Li, Z.; Gabbai, F. P.; Conti, P. S. *Theranostics* **2013**, *3*, 181.

(184) Li, Z.; Lin, T.-P.; Liu, S.; Huang, C.-W.; Hudnall, T. W.; Gabbai, F. P.; Conti, P. S. *Chem. Commun.* **2011**, *47*, 9324.

(185) Li, Z. C., Kantapat; Liu, Shuanglong; Eade, R. Casey; Conti, S. Peter; Gabbai, P. Francois **2012**, 1.

(186) Lin, T.-P.; Gabbai, F. P.; Li, Z. *Abstracts of Papers, 243rd ACS National Meeting & Exposition, San Diego, CA, United States, March 25-29, 2012* **2012**, INOR.

(187) Kue, S. C., Anyanee Kamkaew, Hong Boon Lee, Lip Long Chung, Lik Voon Kiew, and Kevin Burgess *Mol. Pharmacetics* **2014**, in the press.

(188) Ziessel, R.; Goze, C.; Ulrich, G. *Synthesis* **2007**, *6*, 936.

(189) Lu, H.; Mack, J.; Yang, Y.; Shen, Z. *Chem Soc Rev* **2014**.

(190) Angell, Y.; Chen, D.; Brahimi, F.; Saragovi, H. U.; Burgess, K. *J. Am. Chem. Soc.* **2008**, *130*, 556.

(191) Kamkaew, A.; Burgess, K. *Chem. Comm.* **2015**, submitted.

(192) Wu, P.; Fokin, V. V. *Aldrichimica Acta* **2007**, *40*, 7.

(193) Johnson, G. A.; Muthukrishnan, N.; Pellois, J.-P. *Bioconjugate Chem.* **2013**, *24*, 114.

(194) Davids, L. M.; Kleemann, B. *Cancer Treat. Rev.* **2011**, *37*, 465.

(195) Nguyen, Q. T.; Olson, E. S.; Aguilera, T. A.; Jiang, T.; Scadeng, M.; Ellies, L. G.; Tsien, R. Y. *Proc. Natl. Acad. Sci. U. S. A.* **2010**, *107*, 4317.

(196) Gambhir, S. S. *Nat. Rev. Cancer* **2002**, *2*, 683.

(197) Chen, Z.; Li, X.; Li, F.; Ouyang, Q.; Yu, T. *Eur J Radiol* **2010**, *75*, 329.

(198) Hooker, J. M. *Curr. Opin. Chem. Biol.* **2010**, *14*, 105.

(199) Podoloff, D. A.; Ball, D. W.; Ben-Josef, E.; Benson, A. B., III; Cohen, S. J.; Coleman, R. E.; Delbeke, D.; Ho, M.; Ilson, D. H.; Kalemkerian, G. R.; Lee, R.

J.; Loeffler, J. S.; Macapinlac, H. A.; Morgan, R. J., Jr.; Siegel, B. A.; Singhal, S.; Tyler, D. S.; Wong, R. J. *J. Natl. Compr. Cancer Network* **2009**, *7*, S/1.

(200) van Waarde, A.; Elsinga, P. H. *Curr. Pharm. Des.* **2008**, *14*, 3326.

(201) Dolle, F.; Roeda, D.; Kuhnast, B.; Lasne, M.-C. *Fluorine Health* **2008**, 3.

(202) Cai, L.; Lu, S.; Pike, V. W. *Eur. J. Org. Chem.* **2008**, 2853.

(203) Li, Z.; Conti, P. S. *Adv. Drug Delivery Rev.* **2010**, *62*, 1031.

(204) Gu, Y.; Huang, D.; Liu, Z.; Huang, J.; Zeng, W. *Med. Chem.* **2011**, *7*, 334.

(205) Miao, Z.; Levi, J.; Cheng, Z. *Amino Acids* **2011**, *41*, 1037.

(206) Li, Y.; Ting, R.; Harwig, C. W.; auf dem Keller, U.; Bellac, C. L.; Lange, P. F.; Inkster, J. A. H.; Schaffer, P.; Adam, M. J.; Ruth, T. J.; Overall, C. M.; Perrin, D. M. *MedChemComm* **2011**, *2*, 942.

(207) auf dem Keller, U.; Bellac, C. L.; Li, Y.; Lou, Y.; Lange, P. F.; Ting, R.; Harwig, C.; Kappelhoff, R.; Dedhar, S.; Adam, M. J.; Ruth, T. J.; Benard, F.; Perrin, D. M.; Overall, C. M. *Cancer Res.* **2010**, *70*, 7562.

(208) Ting, R.; Aguilera, T. A.; Crisp, J. L.; Hall, D. J.; Eckelman, W. C.; Vera, D. R.; Tsien, R. Y. *Bioconjugate Chem.* **2010**, *21*, 1811.

(209) Dijkgraaf, I.; Franssen, G. M.; McBride, W. J.; D'Souza, C. A.; Laverman, P.; Smith, C. J.; Goldenberg, D. M.; Oyen, W. J. G.; Boerman, O. C. *J. Nucl. Med.* **2012**, *53*, 947.

(210) Amigues, E.; Schulz, J.; Szlosek-Pinaud, M.; Fernandez, P.; Silvente-Poirot, S.; Brillouet, S.; Courbon, F.; Fouquet, E. *ChemPlusChem* **2012**, *77*, 345.

(211) Laverman, P.; D'Souza, C. A.; Eek, A.; McBride, W. J.; Sharkey, R. M.; Oyen, W. J. G.; Goldenberg, D. M.; Boerman, O. C. *Tumor Biol.* **2012**, *33*, 427.

(212) Ambrosini, V.; Campana, D.; Tomassetti, P.; Grassetto, G.; Rubello, D.; Fanti, S. *Eur. J. Radiol.* **2011**, *80*, e116.

(213) Baum Richard, P.; Kulkarni Harshad, R.; Carreras, C. *Semin. Nucl. Med.* **2012**, *42*, 190.

(214) Choromanska, A.; Kulbacka, J.; Chwilkowska, A.; Skolucka, N.; Gamian, A.; Saczko, J. In *Treatment of Metastatic Melanoma*; Morton, R., Ed.; InTech: Europe, 2011.

(215) Kolarova, H.; Nevrelova, P.; Bajgar, R.; Jirova, D.; Kejlova, K.; Strnad, M. *Toxicol. in Vitro* **2007**, *21*, 249.

(216) Sheleg, S. V.; Zhavrid, E. A.; Khodina, T. V.; Kochubeev, G. A.; Istomin, Y. P.; Chalov, V. N.; Zhuravkin, I. N. *Photodermatol., Photoimmunol. Photomed.* **2004**, *20*, 21.

(217) Tissot, R. G.; Beattie, C. W.; Amoss, M. S., Jr. *Cancer Res.* **1987**, *47*, 5542.

(218) Das Gupta, T. K.; Ronan, S. G.; Beattie, C. W.; Shilkaitis, A.; Amoss, M. S., Jr. *Pediatr. Dermatol.* **1989**, *6*, 289.

(219) Chapman, S.; Liu, X.; Meyers, C.; Schlegel, R.; McBride, A. A. *J. Clin. Invest.* **2010**, *120*, 2619.

(220) Liu, X.; Ory, V.; Chapman, S.; Yuan, H.; Albanese, C.; Kallakury, B.; Timofeeva, O. A.; Nealon, C.; Dakic, A.; Simic, V.; Haddad, B. R.; Rhim, J. S.;

Dritschilo, A.; Riegel, A.; McBride, A.; Schlegel, R. *Am. J. Pathol.* **2012**, *180*, 599.

(221) Gorman, A.; Killoran, J.; O'Shea, C.; Kenna, T.; Gallagher, W. M.; O'Shea, D. F. *J. Am. Chem. Soc.* **2004**, *126*, 10619.

(222) Rogers, M. A. T. *J. Chem. Soc.* **1943**, 590.

(223) Walsh, G. *Nat Biotech* **2006**, *24*, 769.

(224) Morris, M. C.; Depollier, J.; Mery, J.; Heitz, F.; Divita, G. *Nature Biotech.* **2001**, *19*, 1173.

(225) Deshayes, S.; Morris, M. C.; Divita, G.; Heitz, F. *Biochim. Biophys. Acta, Biomembr.* **2006**, *1758*, 328.

(226) Gros, E.; Deshayes, S.; Morris, M. C.; Aldrian-Herrada, G.; Depollier, J.; Heitz, F.; Divita, G. *Biochim. Biophys. Acta, Biomembr.* **2006**, *1758*, 384.

(227) Morris, M. C.; Robert-Hebmann, V.; Chaloin, L.; Mery, J.; Heitz, F.; Devaux, C.; Goody, R. S.; Divita, G. *J. Biol. Chem.* **1999**, *274*, 24941.

(228) Mahlum, E.; Mandal, D.; Halder, C.; Maran, A.; Yaszemski, M. J.; Jenkins, R. B.; Bolander, M. E.; Sarkar, G. *Anal. Biochem.* **2007**, *365*, 215.

(229) Sarkar, G.; Curran, G. L.; Mahlum, E.; Decklever, T.; Wengenack, T. M.; Blahnik, A.; Hoesley, B.; Lowe, V. J.; Poduslo, J. F.; Jenkins, R. B. *PLoS One* **2011**, *6*, e28881.

(230) Sarkar, G.; Curran, G. L.; Sarkaria, J. N.; Lowe, V. J.; Jenkins, R. B. *PLoS One* **2014**, *9*, e97655.

(231) Boussif, O.; Lezoualc'h, F.; Zanta, M. A.; Mergny, M. D.; Scherman, D.; Demeneix, B.; Behr, J.-P. *Proc. Natl. Acad. Sci.* **1995**, *92*, 7297.

(232) Breunig, M.; Lungwitz, U.; Liebl, R.; Fontanari, C.; Klar, J.; Kurtz, A.; Blunk, T.; Goepferich, A. *J. Gene Med.* **2005**, *7*, 1287.

(233) Didenko, V. V.; Ngo, H.; Baskin, D. S. *Anal. Biochem.* **2005**, *344*, 168.

(234) Loudet, A.; Han, J.; Barhoumi, R.; Pellois, J.-P.; Burghardt, R. C.; Burgess, K. *Org. Biomol. Chem.* **2008**, *6*, 4516.

(235) McRae, R. L.; Phillips, R. L.; Kim, I.-B.; Bunz, U. H. F.; Fahrni, C. J. *J. Am. Chem. Soc.* **2008**, *130*, 7851.

(236) Feng, X.; Liu, L.; Wang, S.; Zhu, D. *Chem. Soc. Rev.* **2010**.

(237) Pu, K.-Y.; Li, K.; Shi, J.; Liu, B. *Chem. Mater.* **2009**, *21*, 3816.

(238) Feng, X.; Tang, Y.; Duan, X.; Liu, L.; Wang, S. *J. Mater. Chem.* **2010**, *20*, 1312.

(239) Xu, H.; Gao, S.-L.; Yang, Q.; Pan, D.; Wang, L.-H.; Fan, C.-H. *ACS Appl. Mater. Interfaces* **2010**, *2*, 3211.

(240) Wang, B.; Yang, Q.; Liu, L.; Wang, S. *Colloids Surf., B* **2011**, *85*, 8.

(241) Feng, X.; Lv, F.; Liu, L.; Tang, H.; Xing, C.; Yang, Q.; Wang, S. *ACS Appl. Mater. Interfaces* **2010**, *2*, 2429.

(242) Magzoub, M.; Graeslund, A. *Quarterly Reviews of Biophysics* **2004**, *37*, 147.

(243) Brooks, H.; Lebleu, B.; Vives, E. *Adv. Drug Delivery Rev.* **2005**, *57*, 559.

(244) http://www.Synvoluxproducts.com.

(245) http://www.sigmaaldrich.com.

(246) Lee, A. L. Z.; Wang, Y.; Ye, W.-H.; Yoon, H. S.; Chan, S. Y.; Yang, Y.-Y. *Biomaterials* **2008**, *29*, 1224.

(247) Vinogradov, S. V.; Batrakova, E. V.; Li, S.; Kabanov, A. V. *J. Drug Targeting* **2004**, *12*, 517.

(248) Futaki, S. *Adv. Drug Delivery Rev.* **2005**, *57*, 547.

(249) Kosuge, M.; Takeuchi, T.; Nakase, I.; Jones, A. T.; Futaki, S. *Bioconjugate Chem.* **2008**, *19*, 656.

(250) Lee, Y.-J.; Erazo-Oliveras, A.; Pellois, J.-P. *ChemBioChem* **2010**, *11*, 325.

(251) Wender, P. A.; Jessop, T. C.; Pattabiraman, K.; Pelkey, E. T.; VanDeusen, C. L. *Org. Lett.* **2001**, *3*, 3229.

(252) Guterstam, P.; Madani, F.; Hirose, H.; Takeuchi, T.; Futaki, S.; El Andaloussi, S.; Graeslund, A.; Langel, U. *Biochim. Biophys. Acta, Biomembr.* **2009**, *1788*, 2509.

(253) Takeuchi, T.; Kosuge, M.; Tadokoro, A.; Sugiura, Y.; Nishi, M.; Kawata, M.; Sakai, N.; Matile, S.; Futaki, S. *ACS Chem. Biol* **2006**, *1*, 299.

(254) Mosmann, T. *J. Immunol. Meth.* **1983**, *65*, 55.

(255) Guo, Z.-S.; Pei, J.; Zhou, Z.-L.; Zhao, L.; Gibson, G.; Lam, S.; Brug, J. *Polymer* **2009**, *50*, 4794.

(256) Wang, H.; Lu, P.; Wang, B.; Qiu, S.; Liu, M.; Hanif, M.; Cheng, G.; Liu, S.; Ma, Y. *Macromol. Rapid Commun.* **2007**, *28*, 1645.

(257) Sun, B.; Sun, M.-J.; Gu, Z.; Shen, Q.-D.; Jiang, S.-J.; Xu, Y.; Wang, Y. *Macromolecules* **2010**, *43*, 10348.

(258) Perret, F.; Nishihara, M.; Takeuchi, T.; Futaki, S.; Lazar, A. N.; Coleman, A. W.; Sakai, N.; Matile, S. *J. Am. Chem. Soc.* **2005**, *127*, 1114.

(259) Shi, Q.; Nguyen, A. T.; Angell, Y.; Deng, D.; Na, C.-R.; Burgess, K.; Roberts, D. D.; Brunicardi, F. C.; Templeton, N. S. *Gene Ther.* **2010**, *17*, 1085.

(260) Ko, E.; Liu, J.; Burgess, K. *Chem. Soc. Rev.* **2011**, *40*, 4411.

(261) Ko, E.; Liu, J.; Perez, L. M.; Lu, G.; Schaefer, A.; Burgess, K. *J. Am. Chem. Soc.* **2011**, *133*, 462.

(262) Conte, L. L.; Chothia, C.; Janin, J. *J. Mol. Biol.* **1999**, *285*, 2177.

(263) Reyes, S. J.; Burgess, K. *Chem. Soc. Rev.* **2006**, *35*, 416.

(264) Okomo-Adhiambo, M.; Rink, A.; Rauw, W. M.; Gomez-Raya, L. *Animal* **2012**, *6*, 179.

(265) Kurosawa, H. *J. Biosci. Bioeng.* **2012**, *114*, 577.

(266) Alper, P. B.; Hung, S.-C.; Wong, C.-H. *Tetrahedron Lett.* **1996**, *37*, 6029.

(267) Hall, M. J.; McDonnell, S. O.; Killoran, J.; O'Shea, D. F. *J. Org. Chem.* **2005**, *70*, 5571.

(268) Fan, G.; Yang, L.; Chen, Z. *Front. Chem. Sci. Eng.* **2014**, *8*, 405.

(269) Tasior, M.; Murtagh, J.; Frimannsson, D. O.; McDonnell, S. O.; O'Shea, D. F. *Org. Biomol. Chem.* **2010**.

(270) Collado, D.; Vida, Y.; Najera, F.; Perez-Inestrosa, E. *RSC Adv.* **2014**, *4*, 2306.

(271) Murtagh, J.; Frimannsson, D. O.; O'Shea, D. F. *Org. Lett.* **2009**.

(272) Li, L.; Han, J.; Nguyen, B.; Burgess, K. *J. Org. Chem.* **2008**, *73*, 1963.

(273) Shah, M.; Thangaraj, K.; Soong, M. L.; Wolford, L.; Boyer, J. H.; Politzer, I. R.; Pavlopoulos, T. G. *Heteroat. Chem.* **1990**, *1*, 389.

(274) Wories, H. J.; Koek, J. H.; Lodder, G.; Lugtenburg, J.; Fokkens, R.; Driessen, O.; Mohn, G. R. *Recl. Trav. Chim. Pays-Bas* **1985**, *104*, 288.

(275) Bharate, S. S.; Vishwakarma, R. A. *Bioorg. Med. Chem. Lett.* **2015**, *25*, 1561.

(276) Jiao, L.; Yu, C.; Li, J.; Wang, Z.; Wu, M.; Hao, E. *J. Org. Chem.* **2009**, *74*, 7525.

(277) McMurry, J. *Organic Chemistry, 7th Edition*; Brooks/Cole, 2008.

(278) Carroll, F. I.; Philip, A. *J. Org. Chem.* **1968**, *33*, 3776.

(279) Wu, L.; Burgess, K. *J. Org. Chem.* **2008**, *73*, 8711.

(280) Ueno, Y.; Jose, J.; Loudet, A.; Perez-Bolivar, C.; Anzenbacher Jr., P.; Burgess, K. *J. Am. Chem. Soc.* **2011**, *133*, 51.

APPENDIX A

CATIONIC POLYFLUORENES FOR INTRACELLULAR DELIVERY OF PROTEINS[§]

A.1 Introduction

Delivering native and active proteins into cells is essential to many therapeutic applications.[223] Protein-based therapeutic methods are safer in comparison to gene therapy because only transient actions of proteins are required and no random, permanent genetic changes are involved. In general, most native proteins are unable to cross the plasma membrane and usually suffer from loss of biological function due to proteolysis or aggregation in serum; consequently, a general intracellular protein delivery system is highly desirable. One approach to achieve intracellular protein delivery is via *non-covalent* delivery agents.

Our hypothesis for the mode of action for non-covalent carrier agents is that they tend to contain hydrophobic parts that can bind similarly lipophilic regions of protein cargos, then somehow facilitate passage through cell membranes. Stoichiometries of carrier-to-protein in such delivery systems are often set to ensure that the complexes have a net positive charge, which creates an attractive electrostatic interaction with cell membranes. Hydrophobic parts of carriers tend to embed into the membranes and

---

[§] "Cationic Polyfluorenes For Intracellular Delivery Of Proteins" by Anyanee Kamkaew, Roula Barhoumi, Robert C. Burghardt, and Kevin Burgess, *Org. Biomol. Chem.* 2011, *9*, 6513. Reproduced by permission of The Royal Society of Chemistry. Copyright 2011 The Royal Society of Chemistry.

initiate the translocation event. After passage through the membrane some of the cargoes imported into cells are encapsulated in endosomes while others escape from the endosomes to provide functional responses. In summary, we surmised that ideal carrier systems might have: (i) hydrophobic regions to bind protein and to associate with the inner cell membrane; (ii) positive-charged complexes to facilitate attraction to cell membranes: and, (iii) properties conducive to endosomal release.

Some non-covalent carriers including a few commercial products have been reported. Pep-1, a commercial peptide from Active Motif (Figure A-1), complexes with proteins or peptides and facilitates their transport into cells.[224-226] It has been shown that Pep-1 can transport large fluorescent proteins (>119 kDa, and mAb's of *ca.* 250 kDa) at a high transport efficiency (65 - 95%).[224,227] The fluorescent protein-Pep-1 complex rapidly dissociates upon cellular internalization. Inventors of Pep-1 claimed that this deliverly system allows the fluorescently-tagged protein cargos to proceed to their intracellular targets while Pep-1 is degraded. Subsequent studies, however, have shown that the cargo is often entrapped in endosomes after Pep-1-mediated import.

An alternative to the Pep-1 delivery system is the K16SP peptide linked with the signal peptide sequence of Kaposi's fibroblast growth factor (AAVALLPAVLLALLAP).[228] This system was reported to be 3 – 4 times more effective than Pep-1 for non-covalent transport of proteins into cells (four different human cell lines were tested), but endosomal release was not addressed. Later, the same research group synthesized K16 peptide linked with 20-amino acid segment corresponding to the low-density lipoprotein receptor (LDLR)-binding domain of

apolipoprotein E (LRVR LASH LRKL RKRL LRDA), called K16ApoE.[229] This carrier peptide can successfully transport various proteins, immunoglobulins and some therapeutic agents across the blood brain barrier (BBB) in a non-covalent manner.[229-230]

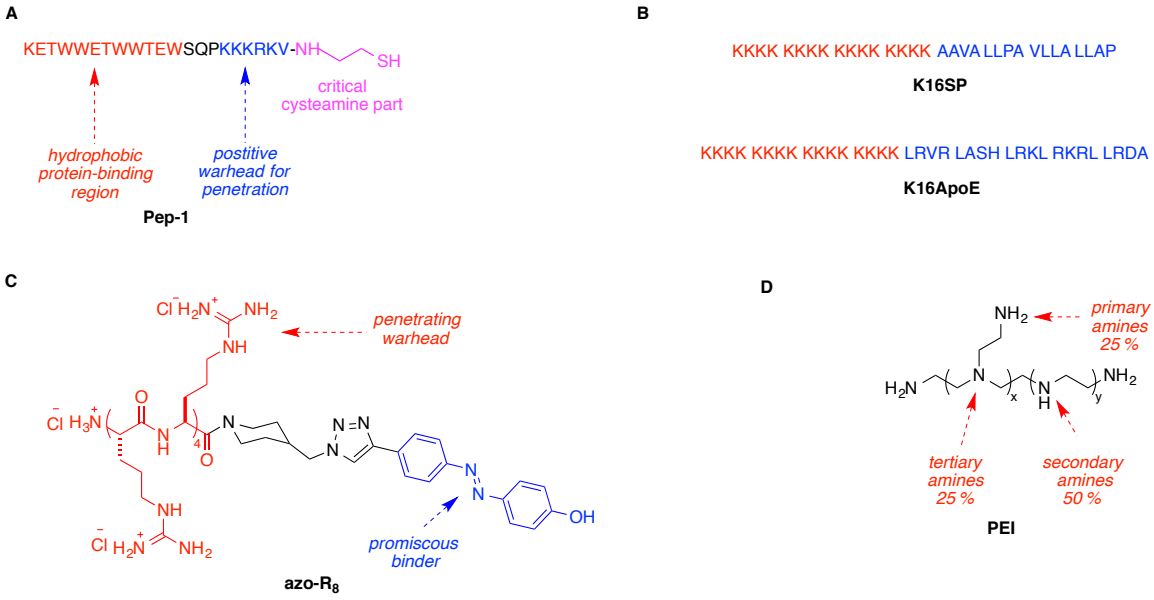

Figure A-1. Structures of some non-covalent carriers.

A well known DNA transfection agent[231], polyethyleneimine (PEI),[232] is also a non-covalent carrier for proteins.[233] In one example, PEI transported avidin-Alexa Fluor 488 and the antibody, *anti*-lamin, into human fibroblast cells without degrading protein's structure.

Arginine-rich peptides, R_8 and azo-R_8, have been reported to import four differently labeled (Alexa Fluor® 488) proteins {avidin, recombinant streptavidin, bovine serum albumin (BSA), and beta-galactosidase} via non-covalent delivery.[234] R_8

and azo-R_8 (*ie* a conjugate of R_8 with an azo-compound that binds proteins non-specifically) showed similar temperature dependence of carrier-mediated protein delivery to Pep-1. At 37 ºC, labeled-avidin was imported but the fluorescence primarily accumulated in vesicles that co-localized with the endosomal marker FM 4–64. Surprisingly, however, diffuse fluorescence was observed within the cytoplasm with little evidence of punctate vesicle formation at 4 ºC.

Interactions of polymers with cells depend on a complex interplay of chemical and physical properties. For instance, the cationic poly(p-phenyleneethynylene) material **A** (Figure A-2) is imported into punctate endosomal structures within NIH 3T3 fibroblast cells, whereas the corresponding anionic polymer binds to fibronectin fibrils on the surface of those cells.[235]

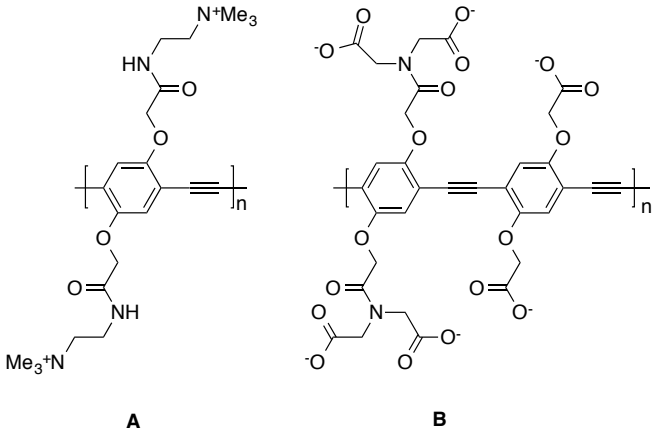

Figure A-2. Structures of cationic (**A**) and anionic (**B**) polymers.

There is much to be learned about polyfluorene derivatives interacting with cells, and there is considerable potential for exploiting this knowledge. Fluorene monomers can be easily derivatized to incorporate charges, impart water solubilities, and be conjugated to biomolecules.[236] Moreover, polyfluorenes are brilliant and conspicuous under fluorescence microscopes due to their high extinction coefficients and fluorescence quantum yields. Consequently, polyfluorene (or dendric fluorene) derivatives have been tested for cell permeation and staining of organelles,[237] transfection of DNA plasmids,[238-240] and import then release of cytotoxic materials.[241]

We are particularly interested in non-covalent import of proteins into cells for imaging intracellular biochemical events. *Covalently* bound carriers based on HIV-1 Tat and *Drosophila* Antennapedia homeodomain proteins[242-243] are common, but agents that can simply be added to protein cargoes to bring about import are much rarer. Some of the first *non-covalent* protein import systems include Chariot®,[224] the cationic pyridinium amphiphile and a helper lipid, SAINT-PhD,[244] BPQ24 BioPORTER® QuikEase™ (a protein delivery kit of unspecified composition),[245] the peptide K16SP,[228] a cationic polymer containing cholesterol,[246] and the somewhat cytotoxic polyethyleneimine (PEI),[233,247] None of these systems are perfect, and many import proteins into living cells but deposit them in endosomes or lysosomes where they are degraded. Consequently, there is considerable interest in finding simpler systems that release protein cargoes into the cytoplasm of living cells. For instance, the oligomers of arginine, R8 and R16 have been reported to facilitate significant cellular uptake, while R_4 gave relatively little internalization.[248-249] However, we showed that these systems

tend to result in endosome-trapped proteins, unless the import was carried out at reduced temperatures (4 ^{o}C).[234,250] In any case, oligomers of arginine are not particularly easy to make.[251] Meanwhile others have observed that delivery of proteins into cells can be influenced by lipophilic counter-ions like pyrenebutyrate.[252-253]

In the research described here, we investigated how the simple, and readily accessible, cationic polyfluorenes might function with respect to import of proteins into living cells. Proteins of different sizes and pI values were used, and they were either labeled with small molecule fluors (FITC, Texas Red®, Alexa Fluor®488) or chosen because they are intrinsically fluorescent (green fluorescent protein, GFP). The objectives of this study were to establish where the protein and polymer are delivered to inside cells, if indeed they were imported at all.

A.2 Materials and methods

See the section A.6 for protocols and characterization information for polymers **1** and **2**. Avidin-FITC and streptavidin-Texas Red® conjugates were purchased from Invitrogen by Life Technologies. b-Galactosidase was purchased from Calbiochem and labeled with Alexa Fluor® 488. GFP was kindly provided by Dr Wenshe Liu at Texas A&M University.

Cell culture

Clone 9 cells were cultured on 75 cm^2 culture flasks in Ham's Nutrient Mixture F-12 with 10% fetal bovine serum (FBS) in a humidified incubator at 37 ^{o}C with 5% CO2. Cells grown to subconfluence were plated in Lab-Tek two-well chambered

coverglass slides (Nunc) 2–3 d prior to the experiments. CHO K1 cells were cultured on 75 cm^2 culture flasks in DMEM supplemented with 10% FBS in a humidified incubator at 37 ^oC with 5% CO_2. Again, cells grown to subconfluence were plated in Lab-Tek two-well chambered coverglass slides 2-3 d prior to the experiments.

Fluorescence microscopy

Subcellular protein localization was measured on living Clone 9 and CHO K1 cells using a Zeiss 510 META NLO Multiphoton Microscope System consisting of an Axiovert 200 MOT microscope. Throughout, digital images were captured with a 40x /1.3 oil objective with the following filter sets: for polymer **1** and **2**: excitation 740 nm; emission BP 435–485; for FITC, Alexa Fluor® 488 and LysoTracker ® Green DND- 26 (abbreviated to "LysoTracker® Green" above): excitation 488 nm; emission BP 500–530; for the Texas Red® protein conjugates: excitation 543 nm; emission BP 565–615 Sequential optical sections (Z-stacks) from the basal-to-apical surfaces of the cell were acquired. Digital image acquisition was initiated approximately 1 mm below the basal surface of the cells and optical slices were collected at 0.5 mm steps through their apical surface using a high numerical objective lens (C-APO 63X/1.2W CORR D = 0.28M27). These wide-field images were subjected to deconvolution using Intelligent Imaging Innovations (3I) software.

The protein : carrier complexes were pre-formed at room temperature for 1 h by mixing (mol : mol ratios throughout) the protein and the carrier in Ham's Nutrient Mixture F-12 supplemented with 10% FBS for Clone 9 cells. The CHO K1 cells were supplemented with DMEM containing 10% FBS. Protein : carrier at 1 : 1 was used for

avidin-FITC and streptavidin-Texas Red®, while 3 : 1 GFP, and 1.0 : 25 b-gal-Alexa Fluor® were used. To study the cellular uptake of the proteins, the culture medium was removed, the preformed protein : carrier complexes were added, and the cells were incubated for 12 h at 37 ^{o}C. After the incubation period, the cells were washed with phosphate-buffered saline (PBS, pH 7.4) and heparin solution several times before imaging.

Lysosomal colocalization

Clone 9 cells were incubated with streptavidin : polymer complex for 12 h at 37 ^{o}C. After the cells were washed with PBS and heparin, LysoTracker® Green was added and the cells were incubated for 30 min at 37 ^{o}C. The cells were washed again with PBS before imaging.

Cell viability assays

Clone 9 cells (3.5 K cells/well, 50 mL, in Ham's medium) were plated on 96-well plates and allowed to adhere at 37 ^{o}C in 5% CO2 and 95% air for 3 h. The cells were then treated with 50 mL of each test compounds in PHFM-II (protein free medium) at 0 to 200 mM concentrations. The cells were then incubated for 72 h at 37 ^{o}C, then their viabilities were assessed through an MTT conversion assay.[254] Briefly, 25 mL of 3-(4,5-dimethylthiazol-2-yl)-2,5-diphenyltetrazolium bromide MTT (5 mg mL^{-1}, in Hank's balanced salt solution) were added and the cells were incubated for an additional 2 h. They were then lysed and the dark blue crystals solubilized with 100 mL of an aqueous solution containing 35% (v/v) *N*,*N*-dimethylformamide, 15% (v/v) glacial acetic acid, 15% (w/v) SDS with an adjusted pH of 3.8. The optical density of each well (at

570 nm) was measured with a BioTek Synergy 4 Microplate Reader. The viability of each cell line in response to the treatment with tested compounds was calculated as: % dead cells = 100 - (OD treated/OD control) × 100.

A.3 Results and discussion

Design and synthesis of potential polyfluorene carriers

Amino functionalized polyfluorenes have been made before[255] but never exploited as protein delivery systems. Our early studies showed that only the quaternary ammonium system **1** was water soluble; corresponding primary amine, secondary *N*-methylamine, and tertiary *N*,*N*-dimethyl amines polymers were all surprisingly *insoluble* in aqueous media, even at reduced pHs. However, the quaternary salt **1**, very similar to a known material,[256] gave a clear solution in water even at neutral pH. Consequently we made a batch of this material *via* a modification of the literature procedure[256] that involved similar steps but in a different order.

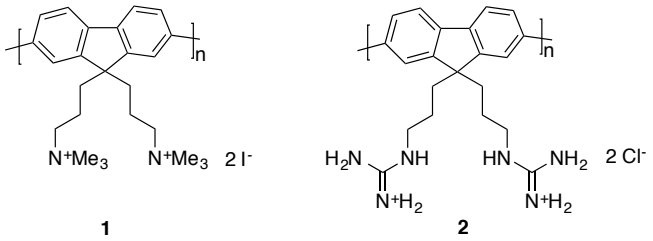

Figure A-3. Polymers **1** and **2** that feature in this study.

Material **1** (Figure A-3) is a polyamine derivative whereas the oligoarginines in HIV-TAT mimics contain multiple guanidine functionalities. Consequently, we

also prepared the guanidine-functionalized polyfluorene **2**. Synthesis of one monomer for the preparation of polymer **2** was achieved *via* modification of the protected diamine **3** into the masked guanidine **4** (Scheme A-1). The complementary diboronate **7** was prepared *via* the azide intermediates **5** and **6**. Finally, Suzuki coupling of monomers **4** and **7**, then deprotection afforded the target material **2**.

Polymers **1** and **2** had the weight average molecular weight (Mw) of 8200 (Poly Dispersity Index, PDI, 1.21) and 9400 (1.25), respectively, from gel permeation chromatography (GPC). Dynamic light scattering experiments (DLS) indicated polymer **1** in water aggregated to form particles that had average diameters of 140 nm. Polymer **2** was insoluble in water, but it appeared to dissolve in methanol while DLS indicated it had in fact aggregated to form particles with an average diameter of 45 nm. Both polymers exhibited a strong UV absorbance centered on 380 nm, and they fluoresced around 415 nm in water with quantum yields of 0.58 (**1**) and 0.42 (**2**).

We were particularly interested in the cytotoxicities of these nanoparticles, so they were tested using Clone 9 rat liver cells in an MTT assay. No significant cytotoxicity was observed for either polymer (IC_{50} 100 mM for both; polymer **2** was delivered as a suspension in buffer). Based on these data it appeared that **1** and **2** were suitable for testing with regards to their abilities to act as carriers for protein import.

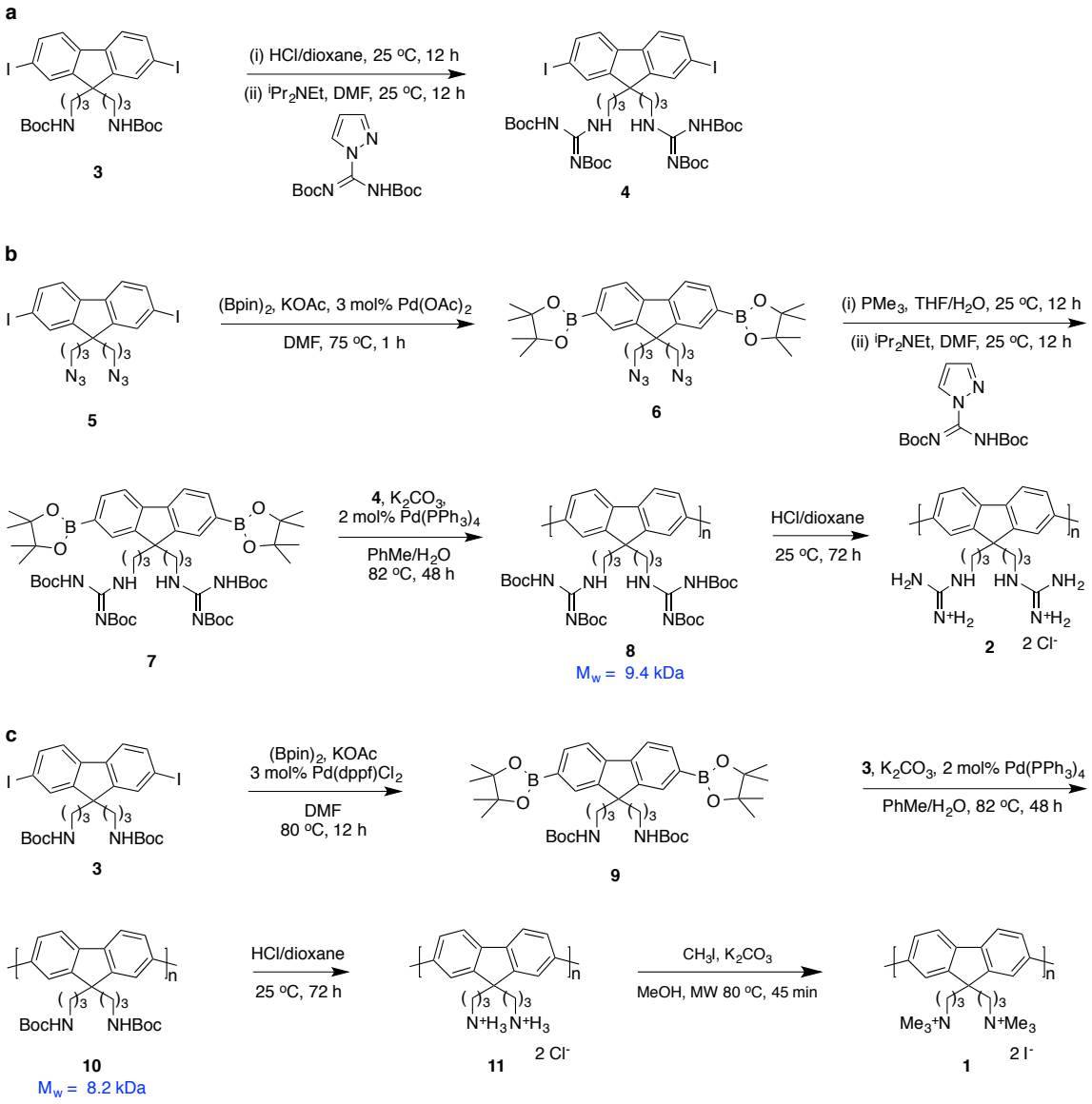

Scheme A-1. Syntheses of polymer **1** and **2**.

Delivery at 37 °C: uptake into punctate vesicular structures

Four proteins were selected for uptake experiments (Table 2.1). These were cationic (avidin) or anionic (GFP, b-galactosidase, streptavidin), with molecular masses

between 26.9 and 540 kDa, and labeled with anionic dye (FITC, Alexa Fluor®488), cationic dye (Texas Red®), or no dye at all (GFP). Two cell lines, Clone 9 and Chinese hamster ovary (CHO), were used in the import studies.

Polymeric carrier-to-protein cargo ratios were optimized so that the signals observed in the cells were visible yet not saturated. A 1 : 1 ratio (mol:mol throughout) was thus found to be optimal for the two proteins of intermediate size. Conversely, less carrier was used for the smallest protein (GFP; 1 : 3 carrier : cargo), and more was necessary for the largest (b-galactosidase; 25 : 1.0 carrier : cargo). In each case, images for the uptake were recorded after 12 h of incubation, then checked after another 24 h. However, the signal for GFP was almost completely lost after 24 h indicating degradation, but the polymer fluorescence was still observed.

Table A-1 Proteins For Cellular Uptake Studies

Protein	Molecular Weight (kDa)	Amino Acids	pI (unlabelled protein)
Avidin-FITC	66-68	512	10 – 10.5
GFP	26.9	238	5.3
Streptavidin-Texas Red	52.8	4 x 159	4.5
β-Galactosidase-Alexa Fluor 488	540	1171	4.8

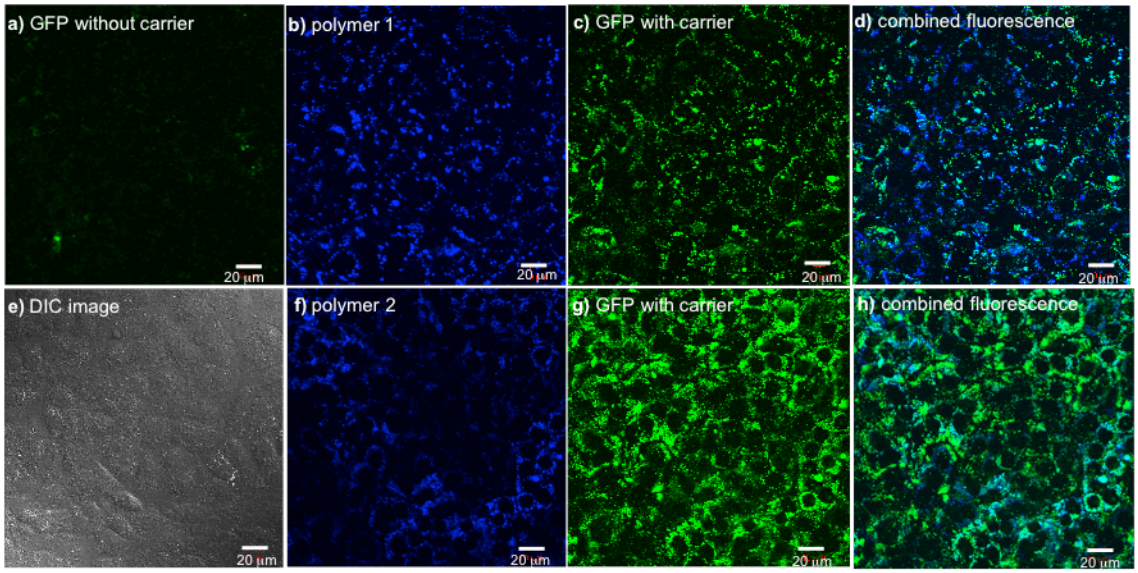

Figure A-4. Delivery of GFP into Clone 9 cells at 37 °C mediated by polymers 1 and 2; a represents no carrier used, and e is a differential interference contrast (DIC) image. Data for polymer 1: b channel showing fluorescence by polymer 1; c channel showing GFP import mediated by 1; d combined fluorescence for GFP and 1 inside the cells. Data for polymer 2: f channel showing fluorescence by polymer 2; g channel showing GFP import mediated by 2; h combined fluorescence for GFP and 2 inside the cells. Throughout, the Clone 9 cells were incubated with the carrier (1.0 mM) and GFP (3.0 mM) at 37 °C for 12 h; the cells were then washed 3x with PBS buffer and 3x with heparin and analyzed by fluorescence microscopy. Scale bar is 20 mm.

Figure A-4 gives illustrative data for the cellular uptake experiments. This graphic features GFP, but similar images were obtained for all the proteins in both cell lines (see supplement materials below). Without carrier, little or no visible GFP was imported into the cells (Figure A-1a).

A polyfluorene-based polymer similar to **1** (different alkyl groups, and another monomer included) has been reported to be imported into cells.[257] Consequently, we were not surprised that polymer **1** alone permeated into the cells (data not shown). Polymer **1** and GFP incubated with the cells for 12 h resulted in import of *both*

fluorescent molecules (b and c). Figure A-4d shows the extent of fluorescence overlap from the polymer and protein; this may be expressed in terms of a "colocalization coefficient" deduced using laser scanning microscopy (LSM) software, with larger coefficients corresponding to greater overlap. In this particular case, *i.e*. for GFP and polymer **1**, the coefficient was 0.48. After a further 24 h the signals were weaker, but no diffuse fluorescence was observed.

Polymer **2** under the same conditions gave noticeably more uptake of GFP in experiments for which the *polymer* signal inside the cells was qualitatively similar to those with GFP/polymer **1**. However, more of the GFP colocalized with **2** (colocalization coefficient 0.68) than with polymer **1**. Images for import of the other proteins are shown in the supplement materials below and Figure A-5 summarizes the colocalization coefficients. Overall, more protein was released from the quaternary amine polymer **1** than it was from the guanidine **2**.

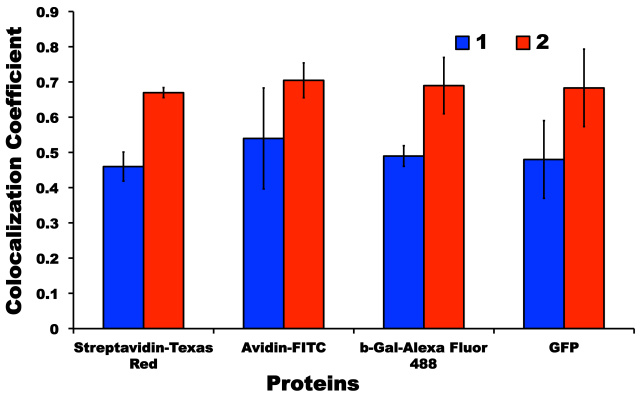

Figure A-5. Colocalization coefficients for polymers **1** (blue) and **2** (red) for the four featured proteins in Clone 9 cells.

Attempts to establish the location of the protein and polymer were made for each of the proteins imported. Figure A-6 shows the data obtained to track the quaternary amine coated polymer **1**, streptavidin-TexasRed®, and LysoTracker® Green. Three dyes are involved in these experiments and all of them show up distinctly (**a** shows channel to detect polyfluorene; **b** streptavidin-Texas Red®; **c** LysoTracker® Green). *Three* colocalization coefficients are significant in these experiments: LysoTracker® Green/polymer **1**, LysoTracker® Green/streptavidin-Texas Red®, and polymer **1**/streptavidin-Texas Red®. These coefficients were 0.35, 0.56, and 0.46, respectively. This data indicates most of the polymer has escaped from the lysosomes, and less than half of the fluorescent protein escaped. Correlations between the polymer **1** and streptavidin-Texas Red® do not distinguish if they are together in the lysosomes, elsewhere, or both. However, Figure A-6d and A-6h show areas where all three fluorescent entities are colocalized in *white*. Quantitative analysis of this situation is difficult and somewhat unnecessary because it is evident that for the quaternary amine polymer **1** regions with distinct blue, red, and green signals predominate; conversely, white areas indicating colocalization of all three labels are prevalent for the guanidine-sheathed polymer **2**.

Colocalization experiments that parallel those above were attempted with markers for other organelles. Specifically, streptavidin-Texas Red® was tested with compounds that are thought to localize in endosomes, and in the endoplasmic reticulum (ER). However, no significant colocalization was observed.

Similar series of experiments were attempted for the three other proteins. However, the labels involved (GFP, FITC, and Alexa Fluor®) are all green, so LysoTracker® Green could not be used. LysoTracker® Red was tested, but crosstalk between the red and green channels precluded accurate analyses. Other labels could have been tested, but the chances of success were only moderate, and we made the decision that the scientific gains made by determining the degree of colocalization for these three proteins were not worth the costs and effort involved.

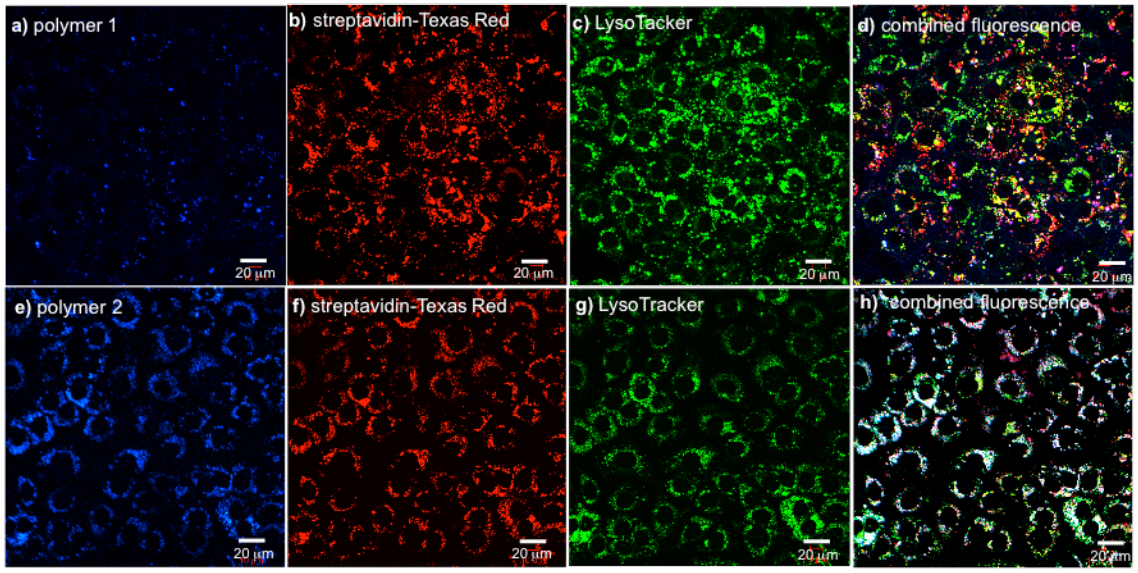

Figure A-6. Delivery of streptavidin-Texas Red® into Clone 9 cells at 37 °C mediated by 1 and 2. Data for transport using polymer 1: (a) polymer 1 channel; (b) streptavidin-TexasRed® channel; (c) LysoTracker® Green; (d) colocalization shows mostly distinct blue, red, and green areas. Data for transport using polymer 2: (e) polymer 2 channel; (f) streptavidin-Texas Red® channel; (g) LysoTracker® Green; (h) colocalization shows mainly white areas where all three labels coexist. Throughout, the carrier (1.0 mM), streptavidin-Texas Red® (1.0 mM), and the Clone 9 cells were incubated at 37 °C for 15 h; the cells were then washed 3X with PBS buffer and 3X with heparin and analyzed *via* fluorescence microscopy. Scale bar is 20 mm.

In previous studies, we had found that $(Arg)_8$ mediated import of some of the same protein cargoes into lysosomes at 37 ^{o}C, but *into the cytosol* at 4 ^{o}C.[234] Experiments to test import with polymers **1** and **2** *at 4 ^{o}C* showed both polymers impregnated into the cell wall membrane, and none of the four proteins were imported. Futaki and co-workers have studied the influence of the lipophilic, fluorescent counter ion, pyrenebutyrate, in import mediated by oligoarginine-based cell penetrating peptides.[252-253,258] Here import of bovine serum albumin-Texas Red® (BSA, MW = 66 kDa, 538 amino acids, pI = 4.7) mediated by polymer **1** was briefly tested in the presence of pyrenebutyrate. This counter ion dramatically increased the *rate* of transport into the cells at 37 ^{o}C so that the protein was conspicuous after only 5 min incubation. However, most of the protein colocalized with LysoTracker® Green and it was not liberated into the cytosol even after extended incubation. The same experiment but run at 4 ^{o}C showed only impregnation of the polymer into the membrane as in the absence of pyrenebutyrate (see supporting materials below).

A.4 Conclusion

These studies were undertaken to determine if the cationic polymers **1** and **2** would import large and small, negative and positively charged, proteins into cells. If protein import was observed, then it was also important to determine if the polymer would "let go" of the protein once inside the cell. The data described shows that both the quaternary amine- and the guanidine-containing polymers **1** and **2** mediated import into the cells at 37 ^{o}C (but not at 4 ^{o}C). Once inside the cells, the quaternary amine polymer

1 releases more of the protein cargoes than its guanidine relative **2**, irrespective of the charge and size of the proteins involved.

It was conveniently possible to determine the degree of endosomal release for streptavidin Texas Red®. In this regard, it was again the quaternary amine polymer **1** that gave superior release (*cf*. less white regions indicating colocalization of all three labels in Figure A-6d as compared with Figure A-6h). Preliminary experiments indicate that the rate of import of proteins by these polymers is increased by pyrenebutyrate, just as Futaki *et al.* have observed in other systems.

Intracellular localization of the proteins featured in this study (GFP, b-galactosidase, and avidin) is of little interest. However, others focused on the delivery of more significant proteins might now consider import using these fluorescent polymers, and the quaternary amine **1** system in particular.

A.5 Acknowledgements

We thank The National Institutes of Health (GM087981), and The Robert A. Welch Foundation (A-1121) for financial support. We also thank Drs Aurore Loudet and Cliferson Thivierge for helpful discussions.

A.6 Supporting Materials

General Procedures

Dry DMF, (<50 ppm water) was purchased from Acros. THF was dried with molecular sieves and Et_3N was distilled from CaH_2. Other solvents and reagents were

used as received. All reactions were carried out under an atmosphere of dry nitrogen. Unless otherwise indicated, common reagents or materials were obtained from commercial source and used without further purification.

NMR spectra were recorded on a VXP-300 MHz and Inova-500 MHz spectrometers (^{1}H at 300 MHz or 500 MHz, and ^{13}C at 75 or 125 MHz) at room temperature unless other mentioned. Chemical shifts of ^{1}H NMR spectra were recorded and chemical shifts are reported in ppm from the solvent resonance ($CDCl_3$ 7.26 ppm, CD_3OD 3.30 ppm, CD_3SOCD_3 2.50 ppm). Data are reported as follows: chemical shift, multiplicity (s = singlet, br = broad, d = doublet, t = triplet, q = quartet, m = multiplet), coupling constants, and number of protons. Proton decoupled ^{13}C NMR spectra were also recorded in ppm from tetramethylsilane resonance ($CDCl_3$ 77.0, CD_3OD 49.1, DMSO-d_6 39.5 ppm). Analytical thin layer chromatography (TLC) was performed on EM Reagents 0.25 mm silica-gel 60-F plates, and visualized with UV light. Flash chromatography was performed using silica gel 60 (230–400 mesh). MS were measured under ESI or MALDI conditions.

Experimental Procedures and Characterization Of Compounds 1 - 11

9,9-*bis*(3-Azidopropyl)-2,7-diiodo-9*H*-fluorene (5). 9,9-*bis*(3-Bromopropyl)-2,7-diiodo-9*H*-fluorene (1.5 g, 2.3 mmol), prepared by alkylation of 2,7-diiodo-9*H*-fluorene and 1,3-dibromopropane (Liu, H. *et al*. *Chem. Eur. J.* 2009, **15**, 2289-2295), NaN_3 (533 mg, 8.20 mmol) and 40 mL DMSO were added into a 250 mL round bottom flask. The mixture was stirred at 70 ^{o}C for 12 h. The reaction mixture was extracted with Et_2O (100

mL) then water (50 mL). Aqueous layer was re-extracted with Et_2O (50 mL x 2). The combined organics were washed with water (50 mL x 3), brine (50 mL x 2), then dried over $MgSO_4$. The product was obtained without further purification (1.3 g, 98%) as yellow solid. ^{1}H NMR (300 MHz, $CDCl_3$), d 7.71-7.67 (m, 4H), 7.42 (d, J = 8.1 Hz, 2H), 3.03 (t, J = 6.6 Hz, 4H), 2.06-2.01 (m, 4H), 0.90-0.84 (m, 4H); ^{13}C NMR (75 MHz, $CDCl_3$), d 150.6, 139.7, 136.8, 131.9, 121.8, 93.6, 54.6, 51.3, 37.0, 23.3. FT-IR (NaCl): N_3 band at 2101.72 cm^{-1}.

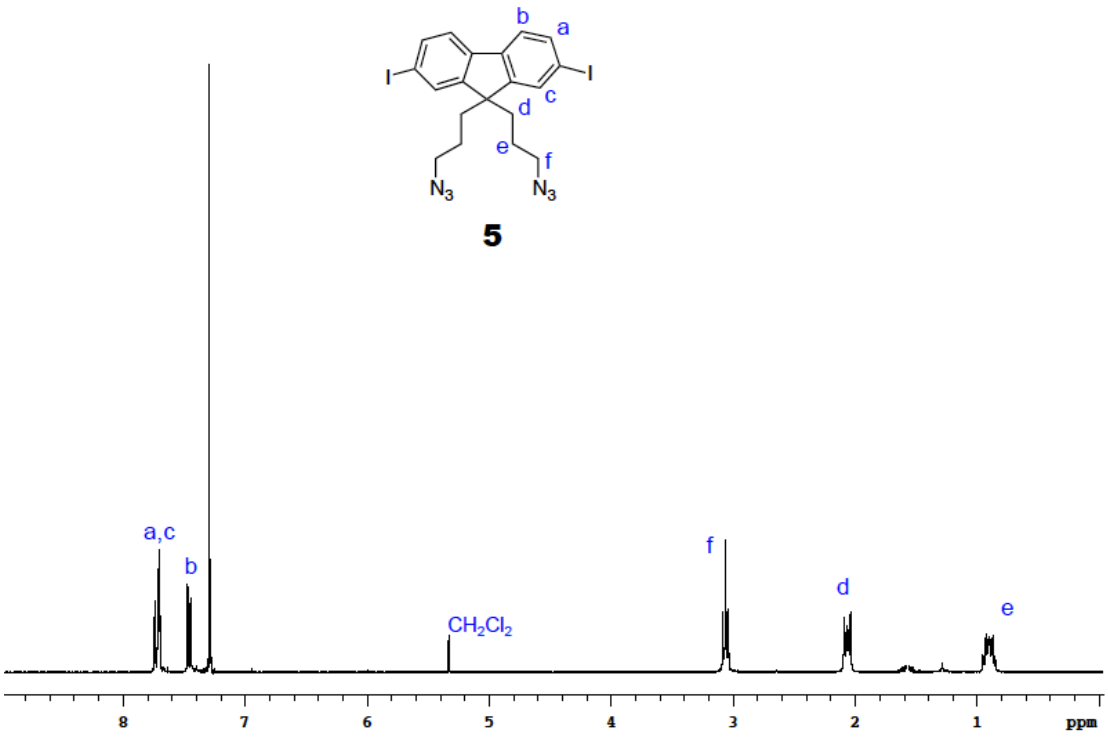

^{1}H-NMR of **5**

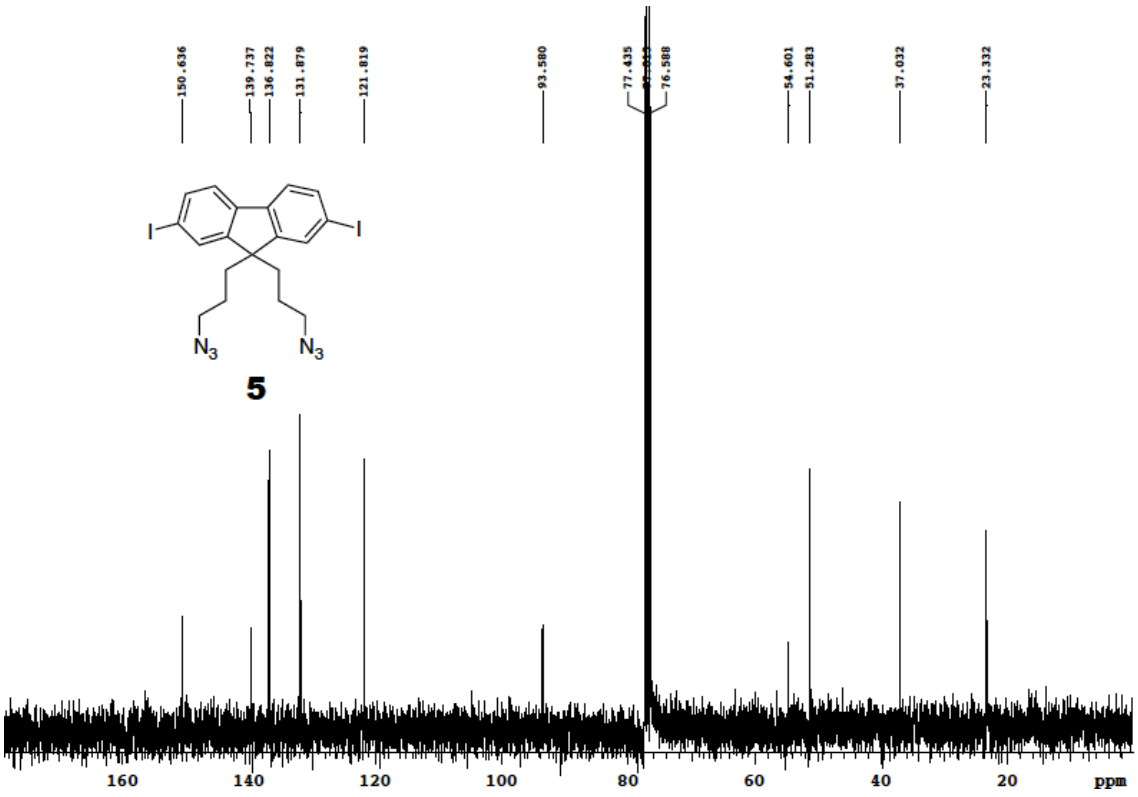

^{13}C-NMR of **5**

Di-*tert*-butyl ((2,7-diiodo-9*H*-fluorene-9,9-diyl)bis(propane-3,1-diyl))dicarbamate (3). Compound **5** (1.3 g, 2.2 mmol) was dissolved in THF (40 mL) and H_2O (5 mL) in a 250 mL flask. Triphenyl phosphine (1.56 g, 5.94 mmol) was added to the solution and the mixture was stirred at 25 ^{o}C for 12 h. The solvents were removed under reduced pressure. The residue and di-*tert*-butyl dicarbonate (1.07g, 4.90 mmol) were dissolved in THF (45 mL). The mixture was stirred at 25 ^{o}C for 12 h. The solvent was removed under reduced pressure. The residue was purified by flash chromatography eluting with CH_2Cl_2 and MeOH (98:2) to give desired product (1.5 g, 92%) as white solid. ^{1}H NMR (300 MHz, $CDCl_3$), d 7.67-7.62 (m, 4H), 7.39 (d, J = 7.8 Hz, 2H), 4.30-4.18 (br, 2H),

2.89-2.85 (m, 4H), 2.02-1.85 (m, 4H), 1.39 (s, 18H), 0.78-0.67 (m, 4H); ^{13}C NMR (75 MHz, $CDCl_3$), d 155.8, 151.2, 139.7, 136.5, 131.8, 121.7, 93.4, 54.7, 40.4, 37.1, 28.4, 24.5 MS (MALDI) calcd for $C_{29}H_{38}I_2N_2NaO_4$ $(M+Na)^+$ 755.08, found 755.30.

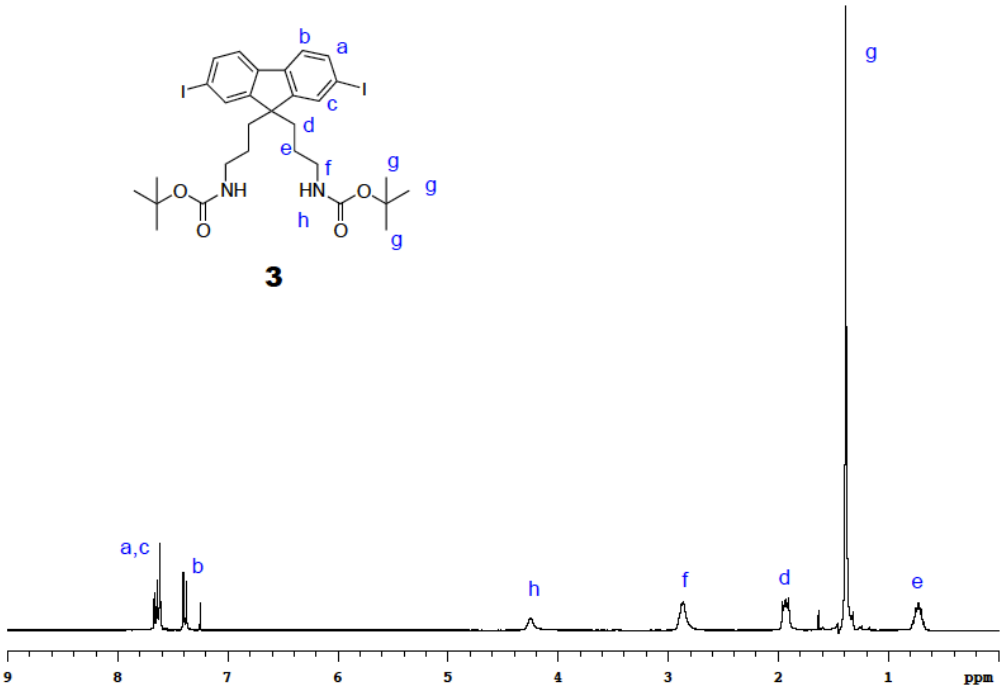

^{1}H-NMR of **3**

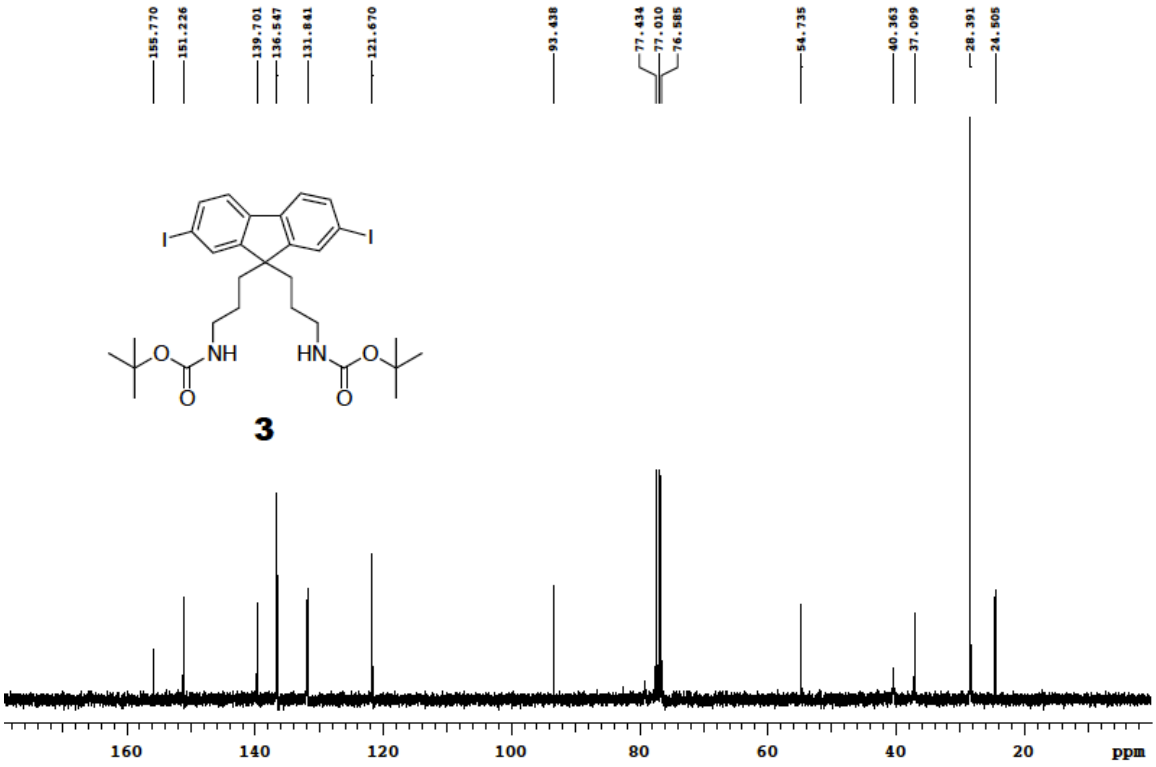

^{13}C-NMR of **3**

Di-*tert*-butyl ((2,7-*bis*(4,4,5,5-tetramethyl-1,3,2-dioxaborolan-2-yl)-9*H*-fluorene-9,9-diyl)*bis*(propane-3,1-diyl))dicarbamate (9). In a 100 mL flask, compound **3** (500 mg, 0.680 mmol), KOAc (400 mg, 4.08 mmol), bis(pinacolato)diborane (433 mg, 1.70 mmol) in degassed DMF (30 mL) were stirred at 25 ^{o}C. The catalyst, Pd(dppf)Cl_2 was added in one portion. The mixture was deoxygenated for 3 min. The reaction mixture was stirred at 80 ^{o}C under N_2 for 12 h. Water (50 mL) was added to the reaction mixture, and the product was extracted from water with CH_2Cl_2 (50 mL x 3). The combined organics were washed with water (50 mL x 3) and brine (50 mL x 2), then dried over $MgSO_4$. After removing the organic solvent under reduced pressure, the

crude product was purified by flash chromatography eluting with CH_2Cl_2 and MeOH (99:1) to give desired product (400 mg, 80 %) as brown solid. ^{1}H NMR (300 MHz, $CDCl_3$), d 7.84 (d, *J* = 7.5 Hz, 2H), 7.74 (d, *J* = 7.5 Hz, 4H), 4.21-4.18 (br, 2H), 2.90-2.80 (m, 4H), 2.10-2.05 (m, 4H), 1.40 (s, 18H), 1.31 (s, 24H), 0.80-0.65 (m, 4H). ^{13}C NMR (75 MHz, $CDCl_3$), d 155.8,149.2, 143.9, 134.2, 128.8, 119.7, 83.9, 83.6, 54.4, 40.6, 28.4, 25.1, 25.0, 24.5. MS (MALDI) calcd for $C_{41}H_{62}B_2N_2NaO_8^+$ $(M+Na)^+$, 755.46, found, 755.66.

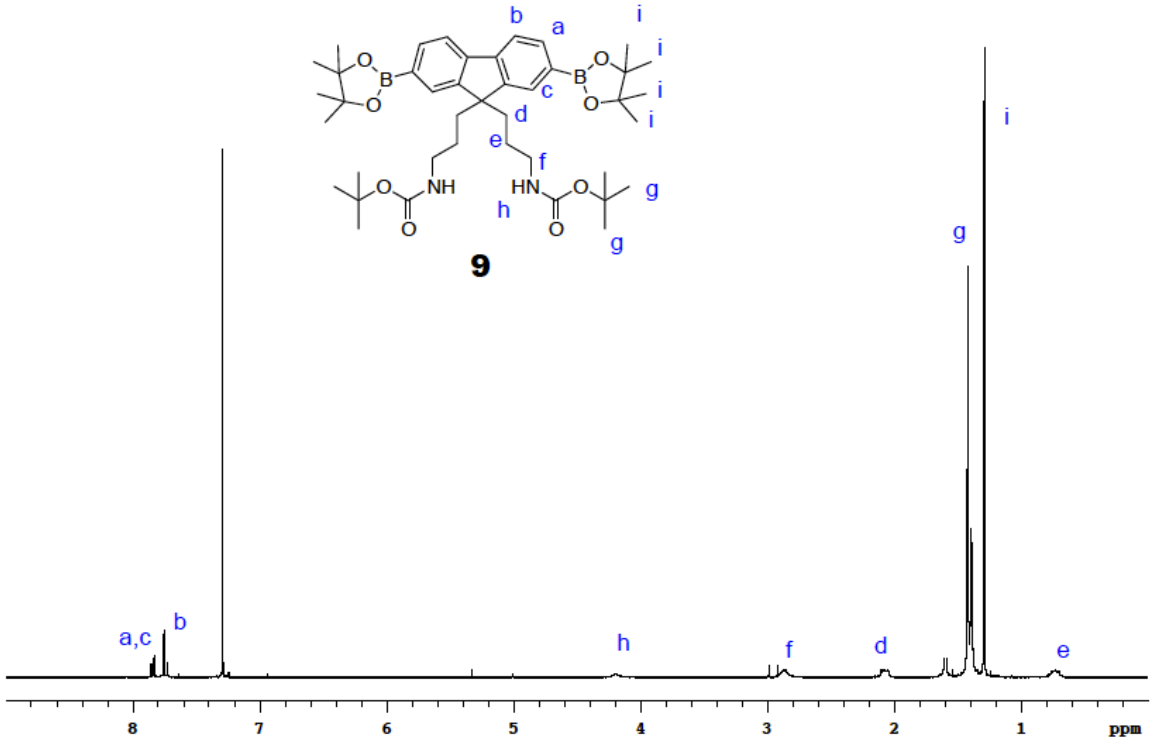

^{1}H-NMR of **9**

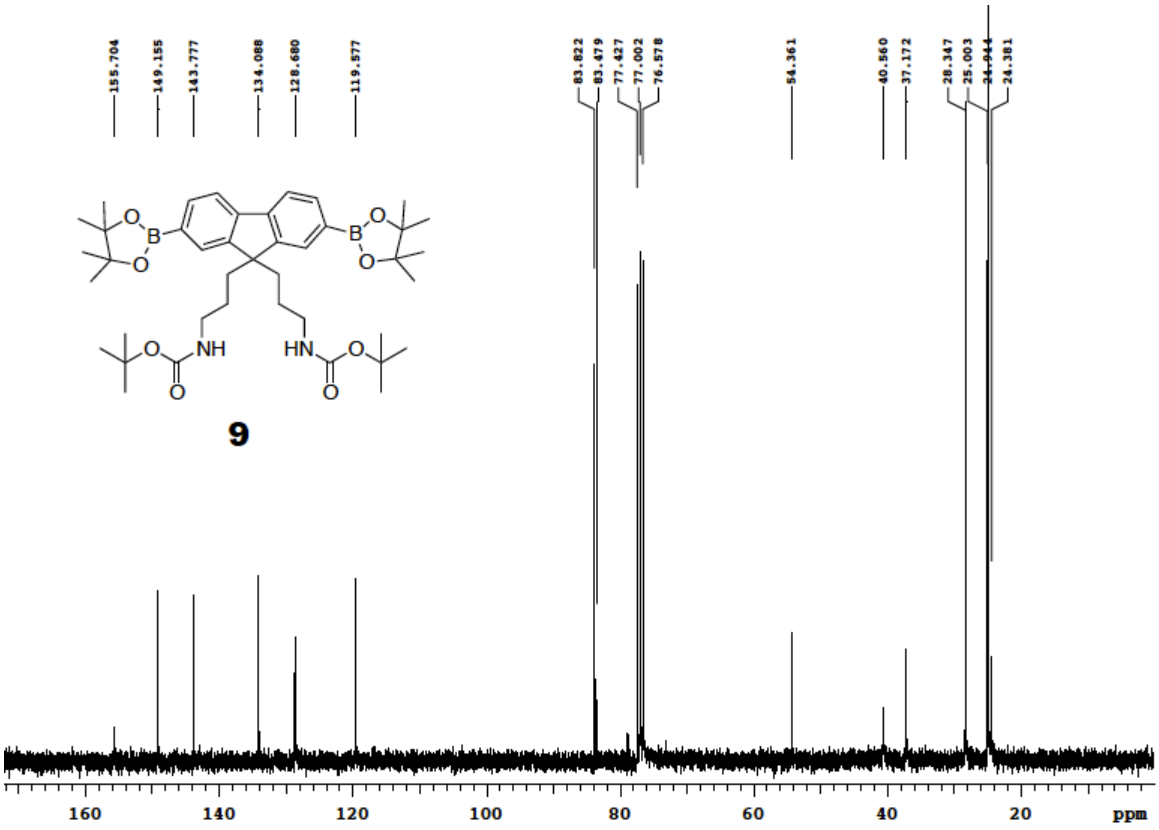

^{13}C-NMR of **9**

Polymer 10. In a 5 mL flask, compounds **3** (50 mg, 0.068 mmol), **9** (50 mg, 0.068 mmol), K_2CO_3 (116 mg, 0.840 mmol), and *tetra*-*N*-butylammonium bromide (0.45 mg, 0.0014 mmol) in degassed 4:1 toluene/H_2O (3 mL) were stirred at 25 ^{o}C. The catalyst $Pd(PPh_3)_4$ (2.0 mg, 0.0014 mmol) was added. The mixture was deoxygenated for 5 min. The reaction was then heated to 82 ºC with stirring under N_2. After 48 h, 2 drops of iodobenzene were added and the reaction was stirred for an additional 12 h at 82 ºC. After cooling to 25 ^{o}C, water (10 mL) was added to the reaction mixture, and the product was extracted with $CHCl_3$ (10 mL x 3). The combined organics were washed with water

(10 mL x 3), brine (10 mL x 2), then dried over $MgSO_4$. After removal of the solvent under reduced pressure, the residue was added to petroleum ether to give a precipitate. The precipitate was transferred to a vial equipped with a stir bar and was stirred in 5mL of acetone at 25 ºC. After 24 h, the acetone was decanted off and the solid was stirred into an additional 5 mL of acetone. This was repeated for a total of 3 times (72 h). Polymer **10** was obtained as a yellow powder (37 mg). ^{1}H NMR (300 MHz, $CDCl_3$): d 7.93-7.82 (br, 4H), 7.82–7.60 (br, 2H), 3.16-2.85 (br, 4H), 2.93-1.50 (br, 4H), 1.41(s, 18H), 1.03-0.78 (br, 4H). GPC (THF): M_n = 6762, M_w = 8187, PDI = 1.21 based on GPC analysis. FT-IR (NaCl): NH band at 3345.77 and 1506.48 cm^{-1}; C=O band at 1700.23 cm^{-1}.

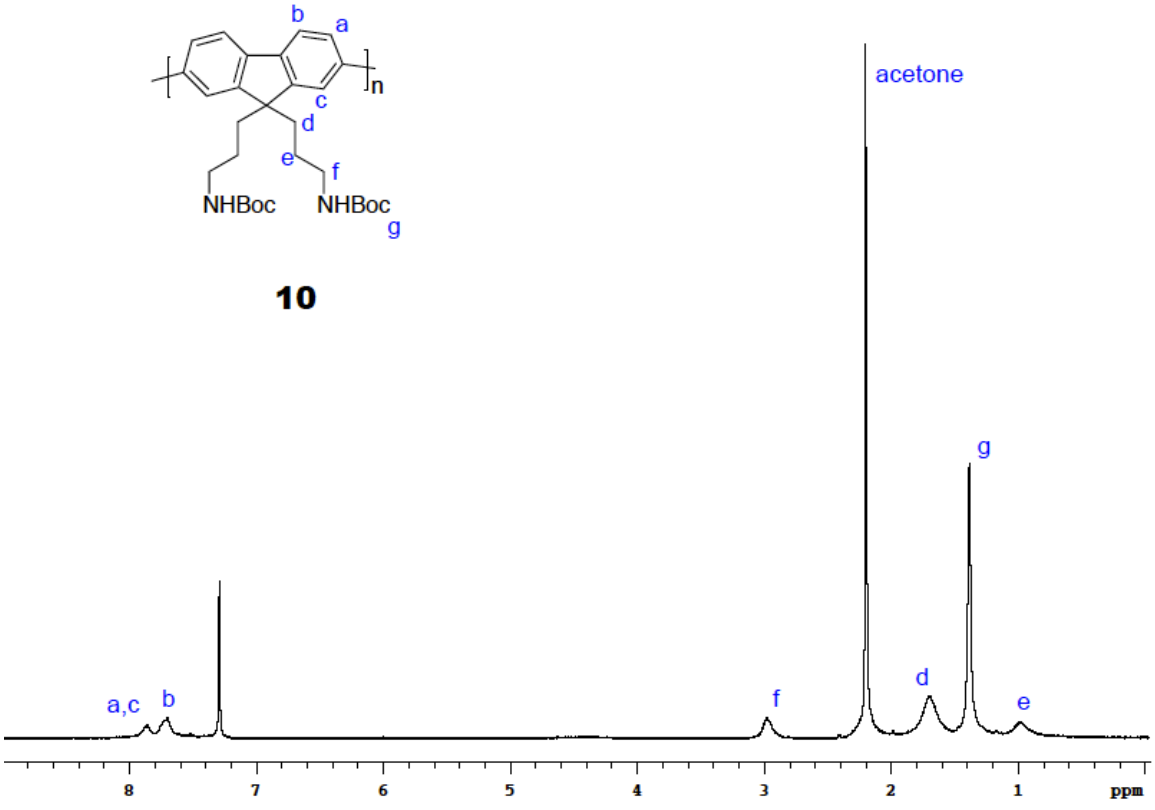

10

^{1}H-NMR of **10**

Polymer 11. Polymer **10** (30 mg) was dissolved in 1,4-dioxane (10 mL) in a 25 mL flask, then HCl in dioxane (4 M, 2 mL) was added in one portion and the solution mixture was stirred at 25 ºC for 72 h. After removal of the solvent under reduced pressure, 5 mL of acetone was added to give a precipitate; this was filtered and washed with chloroform to give polymer **11** as a yellow powder (18 mg). ^{1}H NMR (300 MHz, CD_3OD): d 8.20–7.70 (m, 6H), 2.91–2.69 (m, 4H), 2.59-2.40 (m, 4H), 1.23-0.97 (m, 4H). FT-IR (NaCl): NH ($NH_3^+Cl^-$) band at 3448.16 and 1656.36 cm^{-1}; C=O band at 1700.23 cm^{-1}.

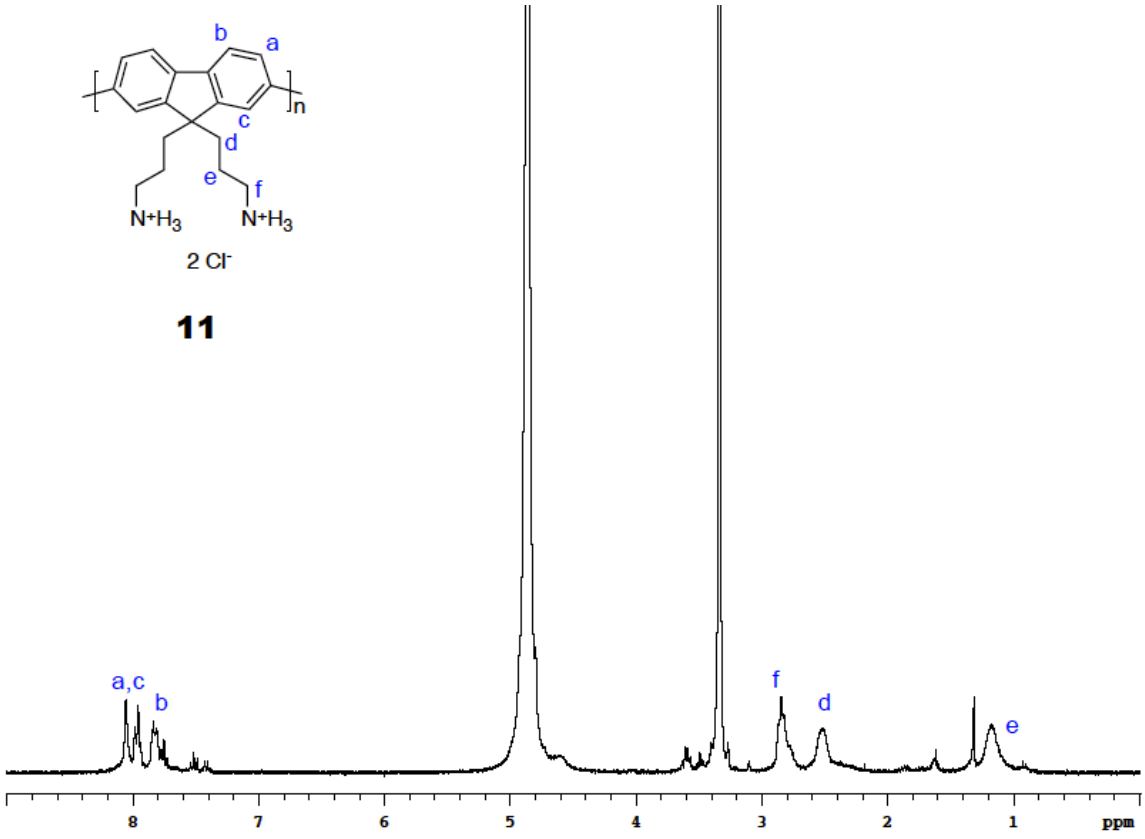

^{1}H-NMR of **11**

Polymer 1. In a sealed tube, polymer **11** (8 mg), MeI (0.20 mL, 3.2 mmol), and K_2CO_3 (442 mg, 3.20 mmol) were added in MeOH (2 mL). The mixture was heated to 80 ^oC in a CEM Discover microwave for 45 min. Polymer **1** was obtained as a brown powder (10 mg). ^1H NMR (300 MHz, DMSO-d_6): d 8.39-7.70 (br), 3.20-2.80 (br), 2.60-2.40 (br), 1.10-0.78 (br). FT-IR (NaCl) shows the absence of a N-H stretch in the region 3300-3000 cm^{-1}.

BOC-Protected Guanidine 4. In a 250 mL flask, compound **3** (800 mg, 1.09 mmol) was dissolved in dioxane (50 mL), then HCl in dioxane (4M, 8 mL) was added and the solution mixture was stirred at 50 ^oC for 12 h. After cooling to 25 ^oC, the solvent was removed and the residue was dissolved in MeOH (10 mL). An aqueous solution of KOH (10 % wt, 10 mL) was added. The mixture was stirred for 15 min and the solvents were removed. The residue was extracted with CH_2Cl_2. The organic layer was washed with H_2O and brine, and then dried over $MgSO_4$. The solvent was removed and the yellow oil product was dissolved in DMF (12 mL). *N,N'*-bis(*tert*-Butoxycarbonyl)1*H*-pyrrazole-1-carboxamidine (744 mg, 2.40 mmol), diisopropylethylamine (12 mL) were added to the solution. The reaction mixture was stirred at 25 ^oC for 12 h. The solvent was removed under reduced pressure. The residue was purified by flash chromatography eluting with CH_2Cl_2 and MeOH (99:1) to give desired product (930 mg, 85%) as yellow solid. ^1H NMR (300 MHz, $CDCl_3$): d 11.43 (s, 1H), 8.32 (s, 1H), 7.62-7.69 (m, 4H), 7.41 (d, J = 8.1 Hz, 2H), 6.42 (s, 1 H), 3.16 (q, J = 5.4 Hz, 4H), 1.98 (m, 4H), 1.45 (s,

36H), 0.83-0.75 (m, 4H). ^{13}C NMR (75 MHz, $CDCl_3$): d 163.4, 155.9, 153.2, 150.7, 142.7, 139.7, 139.1, 136.7, 131.7, 128.9, 121.8, 109.8, 93.6, 83.1, 79.2, 54.6, 40.6, 37.2, 29.7, 28.3, 28.1, 28.0, 23.2. MS (ESI) calcd for $C_{41}H_{59}I_2N_6O_8^+$ $(M+H)^+$ 1017.25, found 1017.27.

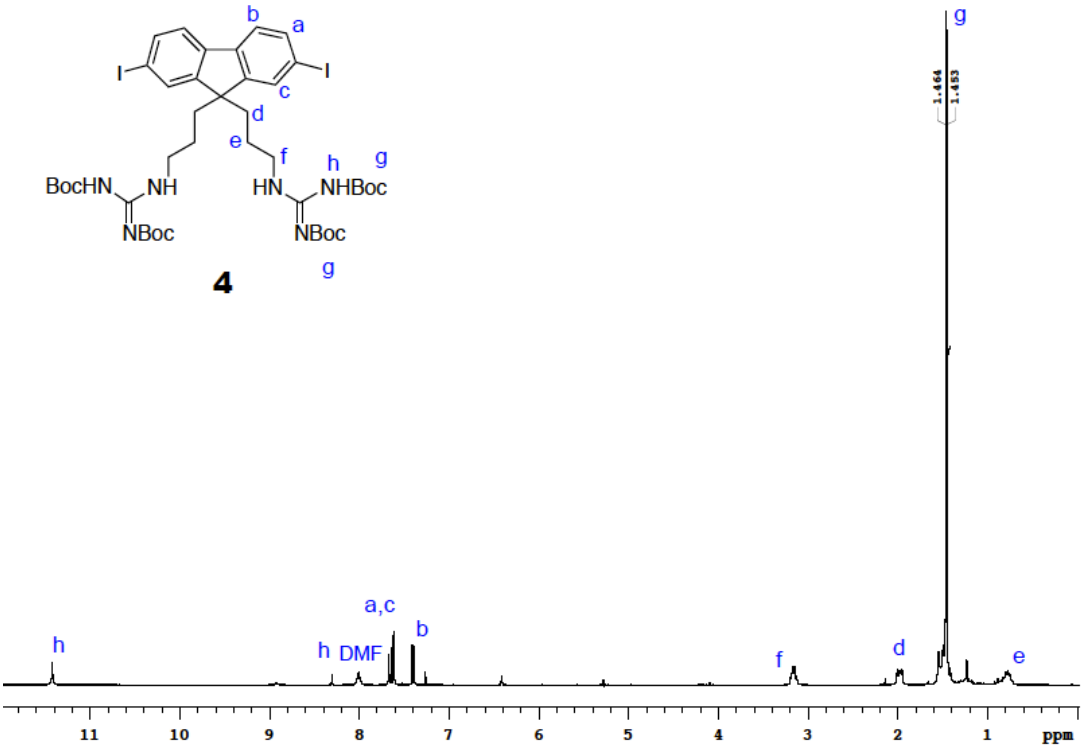

^{1}H-NMR of **4**

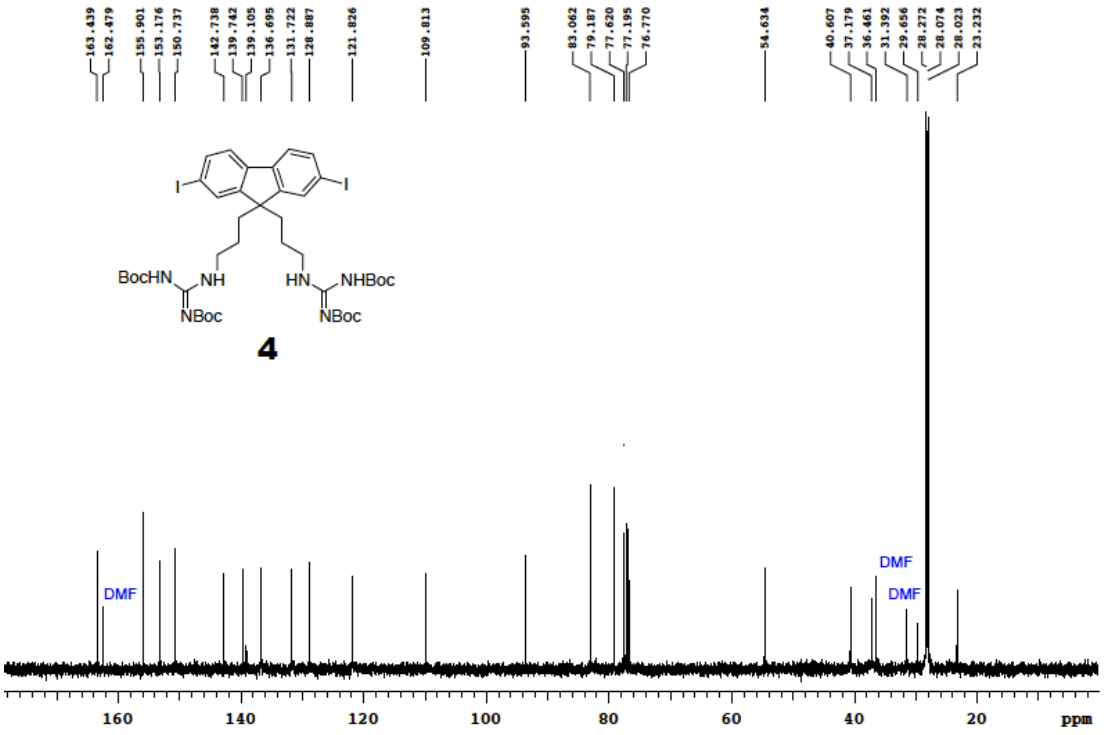

^{13}C-NMR of **4**

Diborate Ester 6. In a 250 mL flask, compound **5** (500 mg, 0.860 mmol), KOAc (500 mg, 5.16 mmol), bis(pinacolato)diborane (524 mg, 2.06 mmol) in degassed DMF (50 mL) were stirred at 25 ^{o}C. The $Pd(OAc)_2$ catalyst (2 mg, 0.01 mmol) was added in one portion, and the mixture was deoxygenated for 3 min. The reaction mixture was stirred at 75 ^{o}C under N_2 for 1 h. The solution was filtered through celite and the solvent was removed under reduced pressure. The product was obtained without further purification (500 mg, quantitative) as brown solid. ^{1}H NMR (300 MHz, $CDCl_3$), d 7.83-7.59 (m, 6H), 3.05-2.83 (m, 4H), 2.22-2.07 (m, 4H), 1.21 (s, 24H) 1.01-0.78 (m, 4H). ^{13}C NMR (125 MHz, CD_3Cl_3), d 148.6, 143.8, 134.6, 128.7, 119.8, 83.9, 83.5, 83.1, 83.0, 54.4,

54.3, 51.5, 51.4, 37.0, 29.7, 25.0, 24.9, 24.8, 24.5, 24.1, 23.4. MS (ESI) calcd for $C_{31}H_{43}B_2N_6O_4^{3+}$ $(M+H)^+$ 585.35, found 585.35.

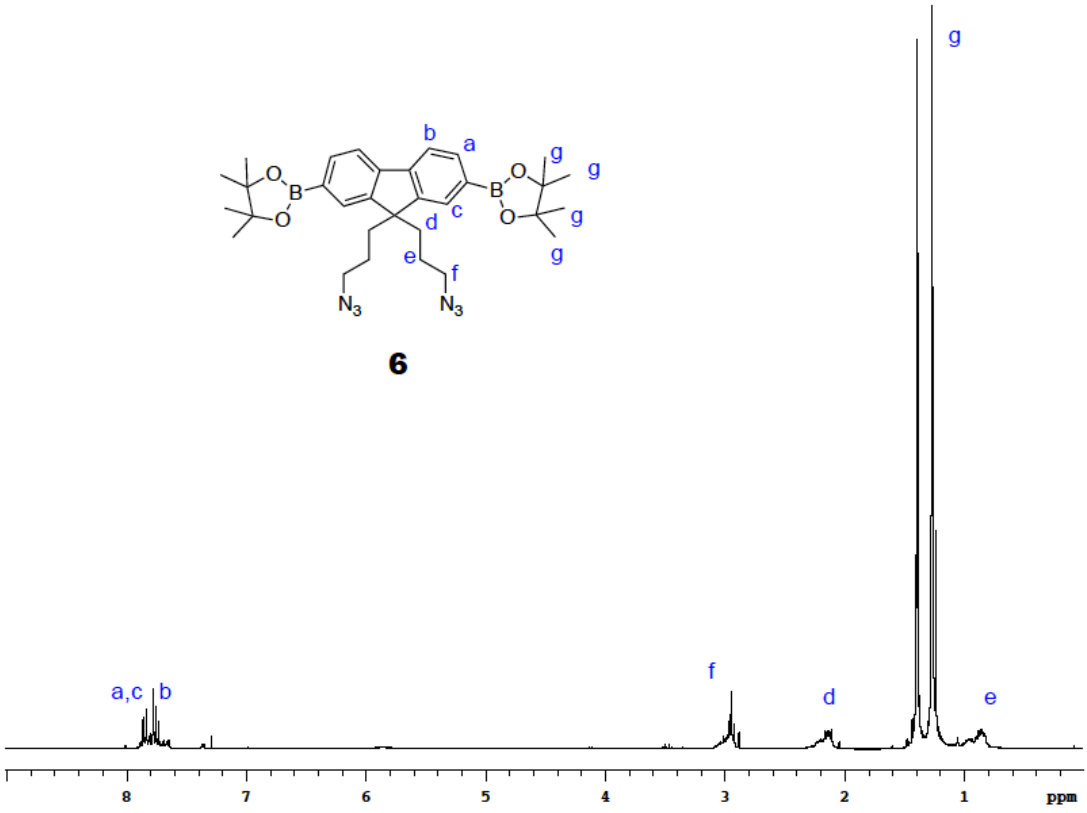

^{1}H-NMR of **6**

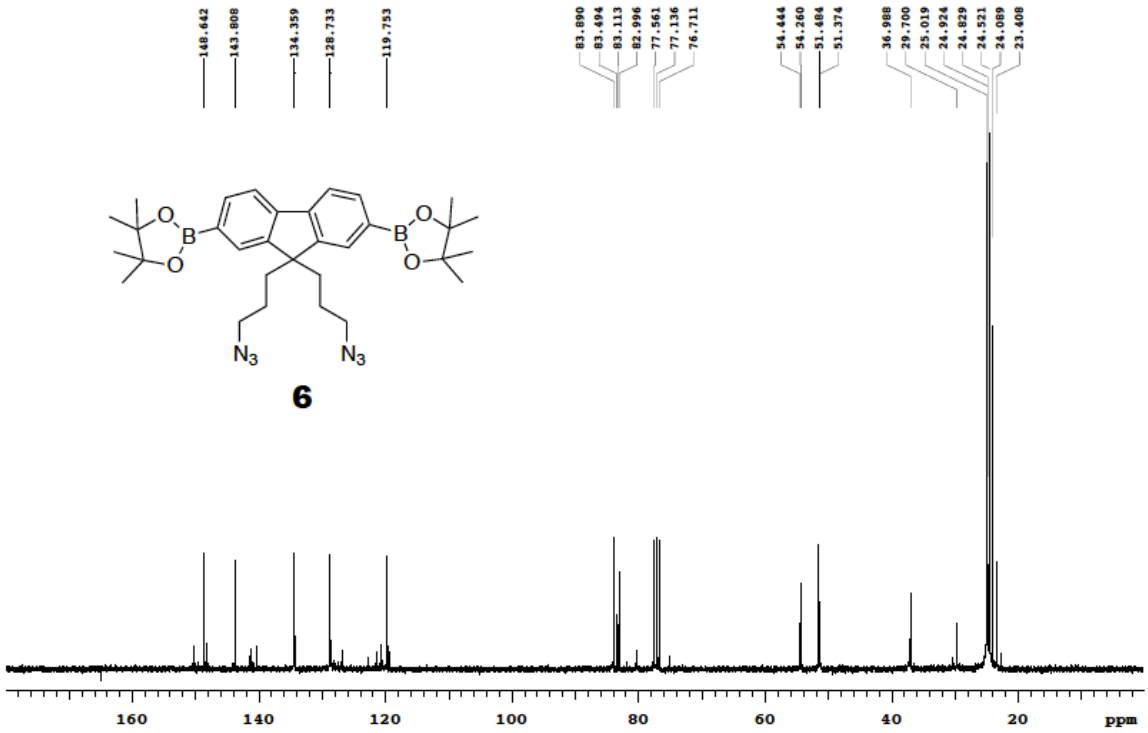

^{13}C-NMR of **6**

Boc-Protected Diguanidine 7. Compound **6** (300 mg, 0.51 mmol) was dissolved in THF (22 mL) and H_2O (3 mL) in a 100 mL flask. Then PMe_3 (1M in THF; 1.28 mL, 1.28 mmol) was added to the solution and the mixture was stirred at 25 ^oC for 12 h. The solvents were removed under reduced pressure, then the residue was dissolved in DMF (6 mL) and *N,N'*-bis(*tert*-butoxycarbonyl)1*H*-pyrrazole-1-carboxamidine (348 mg, 1.12 mmol), and diisopropylethylamine (6 mL) were added. The reaction mixture was stirred at 25 ^oC for 12 h. The solvent was removed under reduced pressure. The residue was purified by flash chromatography eluting with CH_2Cl_2 and MeOH (99:1) to give desired product (360 mg, 69%) as yellow solid. ^{1}H NMR (300 MHz, $CDCl_3$): d 11.40-11.35 (br, 2H), 7.92-7.35 (m, 6H), 3.18-2.98 (m, 4H), 2.18-1.87 (m, 4H), 1.41-1.35 (m, 36H), 1.19

(s, 24H), 0.85-0.58 (m, 4H). ^{13}C NMR (75 MHz, $CDCl_3$, ppm): d 155.7, 153.0, 150.9, 132.2, 132.0, 131.9, 128.6, 128.6, 128.4, 83.8, 82.9, 79.1, 41.1, 37.3, 31.9, 29.7, 29.3, 28.3, 28.0, 25.0, 22.7. MS (ESI) calcd for $C_{41}H_{59}I_2N_6O_8^+$ $(M+H)^+$ 1017.25, found 1017.27.

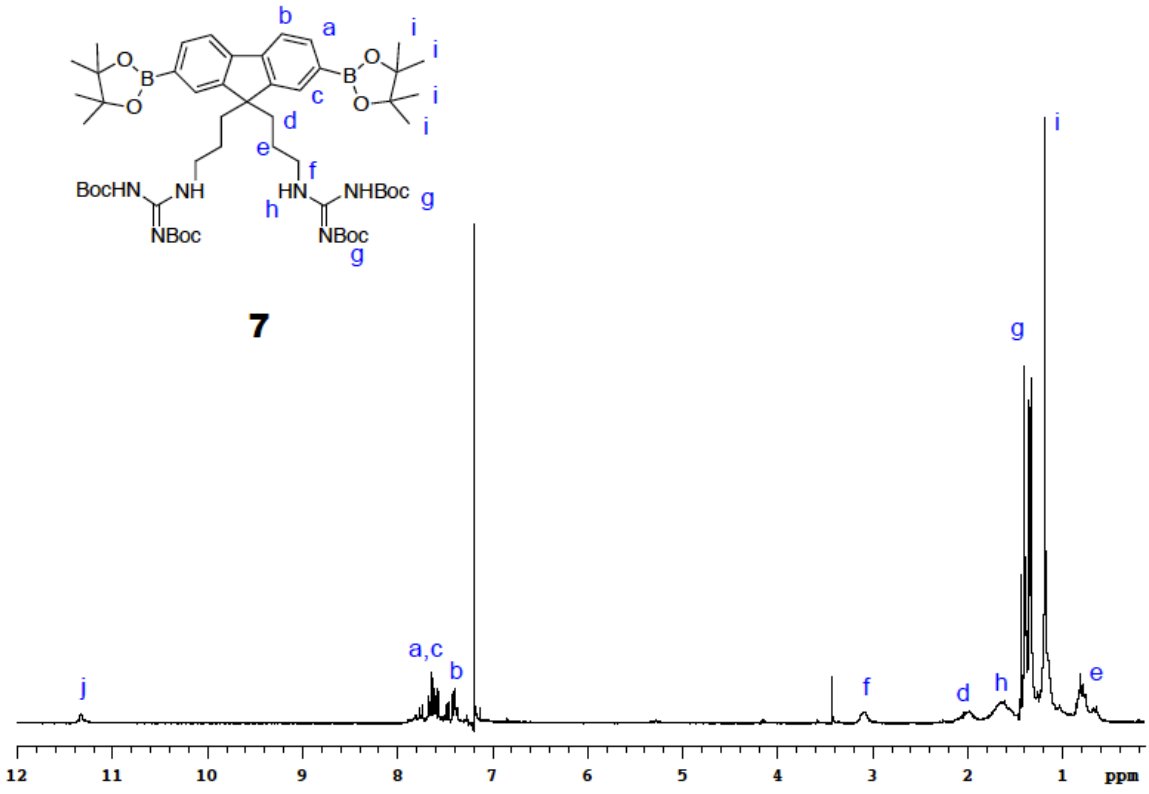

^{1}H-NMR of **7**

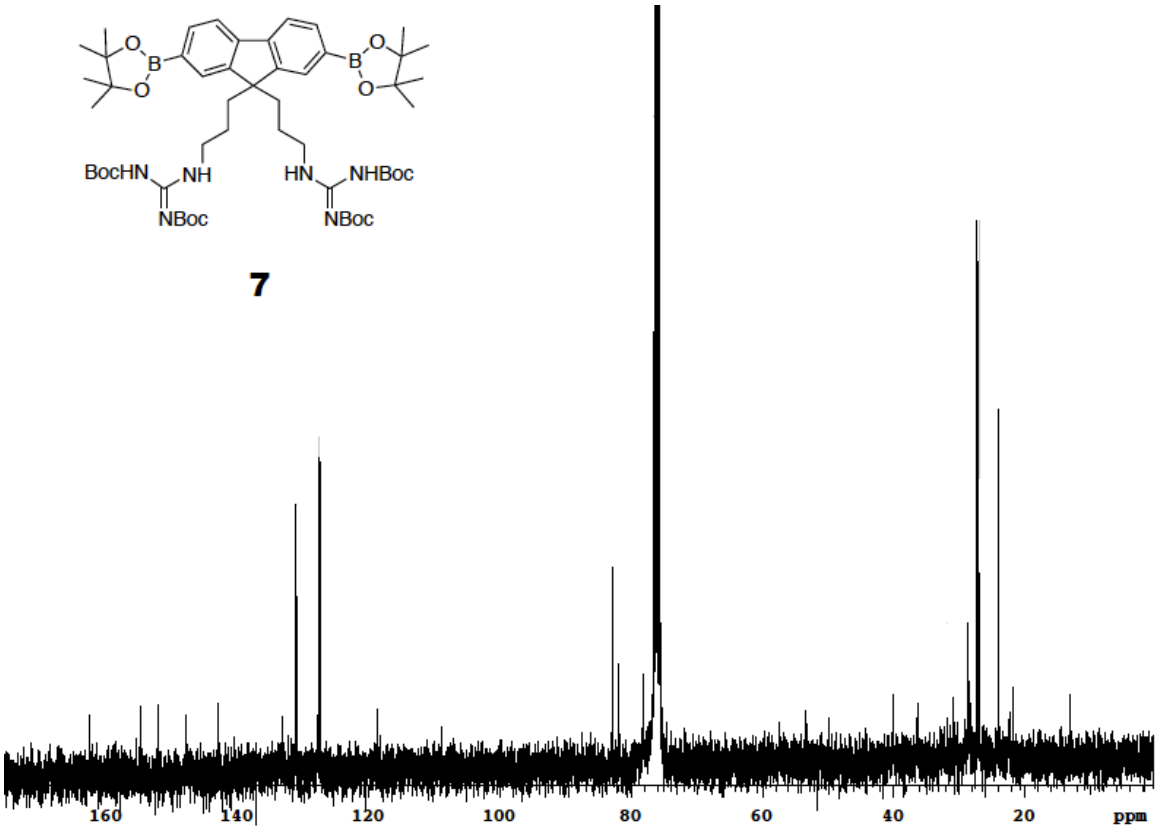

^{13}C-NMR of **7**

Boc-Protected Oligoguanidine 8. In a 5 mL flask, compound **7** (50 mg, 0.05 mmol), compound **4** (50 mg, 0.05 mmol), K_2CO_3 (83 mg, 0.6 mmol), and tetrabutylammonium bromide (0.3 mg, 0.001 mmol) in degassed 4:1 toluene/H_2O (3 mL) were stirred at 25 ^{o}C. Catalytic $Pd(PPh_3)_4$ (1.2 mg, 0.001 mmol) was added, and the mixture was deoxygenated for 5 min. The reaction was heated to 80 ºC with stirring under N_2. After 48 h, 2 drops of iodobenzene were added and the reaction was stirred for an additional 1 h at 80 ºC. The mixture was then precipitated by addition of MeOH, filtered, and thoroughly washed with MeOH. The precipitate was transferred to a vial equipped with

a stir bar and was stirred in 5 mL of acetone at 25 ºC under N_2. After 24 h, the acetone was decanted off and the solid was stirred into an additional 5 mL of acetone. This was repeated for a total of 3 times (72 h). Polymer **8** was obtained as a yellow powder (15 mg). ^{1}H NMR (300 MHz, CD_3OD): d 7.98–7.56 (m, 6H), 3.11-2.65 (br, 4H), 2.23-1.78 (br, 4H), 1.37(br, 36H), 0.93-0.54 (br, 4H). GPC (THF): M_n = 7558, M_w = 9446, PDI = 1.25 based on GPC analysis. FT-IR (NaCl): NH band at 3393.31 cm^{-1}; C=N band at 1623.46 cm^{-1}; C=O band at 1700.23 cm^{-1}.

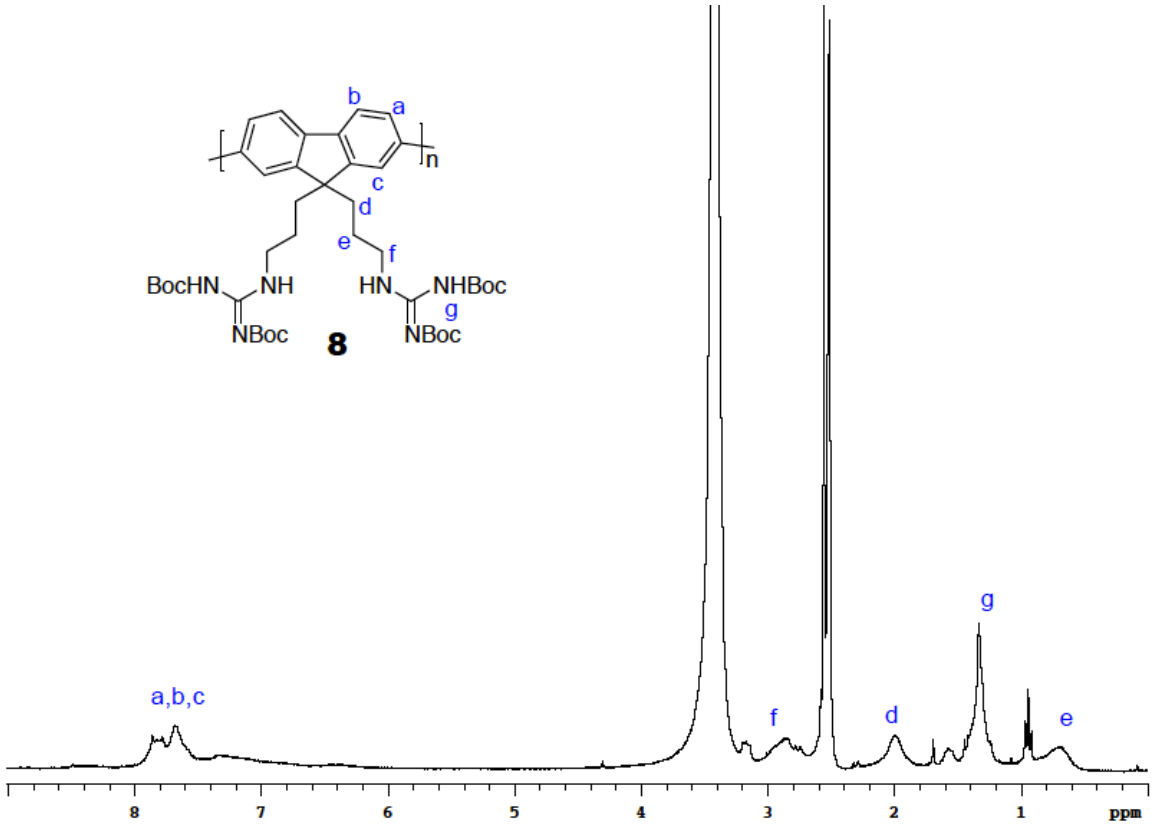

^{1}H-NMR of **8**

Oligoguanidine 2. In a 25 mL flask, polymer **8** (10 mg) was dissolved in dioxane (10 mL). HCl in dioxane (4 M, 2 mL) was added and the solution mixture was stirred at 25 ºC for 72 h. Polymer **2** was obtained as a yellow powder (5 mg). ^{1}H NMR (500 MHz, CD_3OD): d 9.35-9.25 (br), 8.10–7.30 (br), 3.25-2.85 (br), 2.23-1.98 (br), 1.03-0.58 (br). FT-IR (NaCl): NH (amine) band at 3329.74 cm^{-1}; NH (imine) band at 3161.91 cm^{-1}; C=N band at 1651.51 cm^{-1}.

*Delivery Of Avidin-FITC and b-Galactosidase-Alexa Fluor® 488 (at 37 °C mediated by polymer **1** and **2** into Clone 9 cells)*

A.

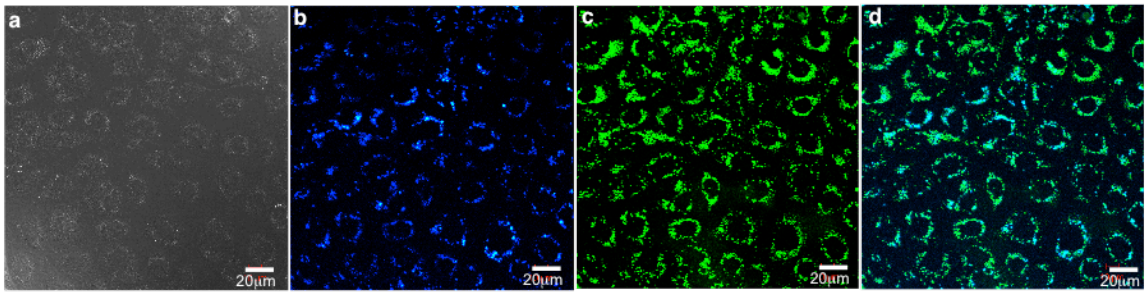

(1-avidin-FITC**)**

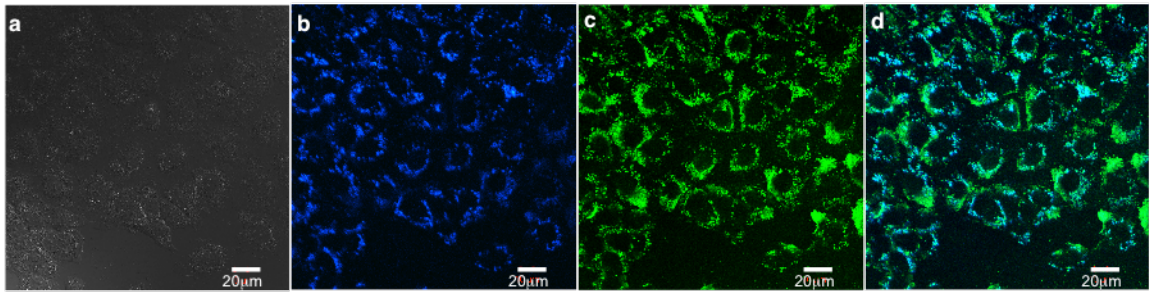

(2-avidin-FITC**)**

B.

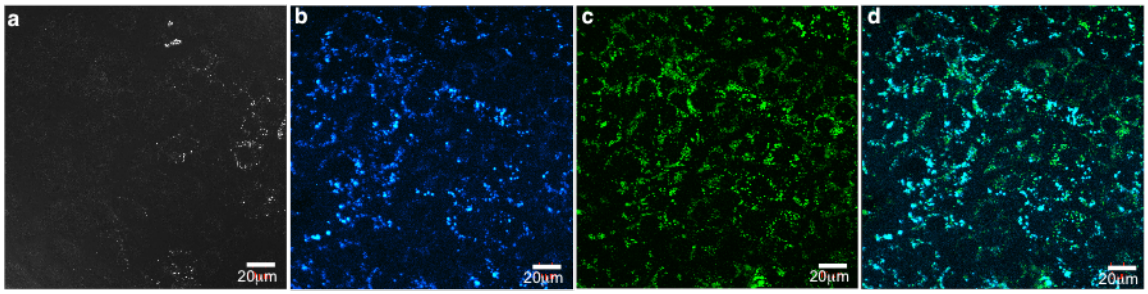

(1-*b*-galactosidase-Alexa Fluor® 488**)**

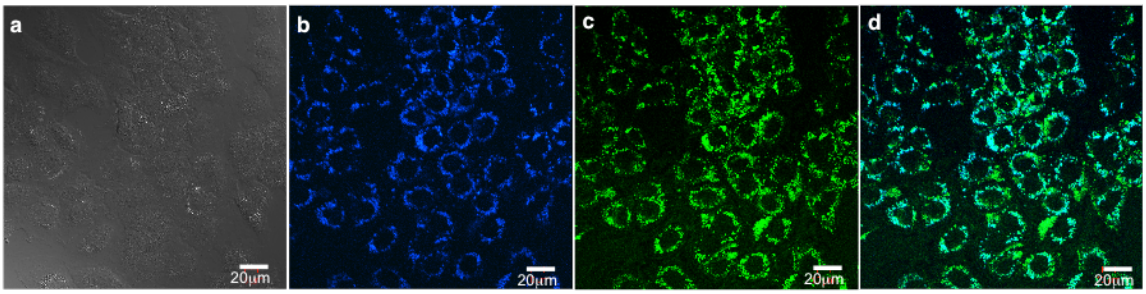

(2-*b*-galactosidase-Alexa Fluor® 488**)**

Figure A-S1. Delivery of avidin-FITC (**A**) and *b*-galactosidase-Alexa Fluor® 488 (**B**) into Clone 9 cells at 37 ºC mediated by polymers **1** and **2**; **a** channels represent differential interference contrast (DIC) images, **b** channels showing fluorescence by polymer; **c** channel showing avidin-FITC import (**A**) and *b*-galactosidase-Alexa Fluor® 488 (**B**) mediated by **1** or **2**; **d** combined fluorescence for protein and polymer inside the cells. The Clone 9 cells were incubated at 37 ºC for 12 h; the cells were then washed 3x with PBS buffer and 3x heparin and analyzed by fluorescence microscopy. *Note;* the polymer **2** was added in 1 % MeOH, and a blank (no nanoparticles) was performed in parallel to check for the effects of MeOH.

*Delivery Of Streptavidin-Texas Red, Avidin-FITC, b-Galactosidase-Alexa Fluor® 488, and GFP (at 37 °C mediated by **1** and by **2** in CHO-K1 cells)*

Figure A-S2. Delivery of streptavidin-Texas Red® (**A**), avidin-FITC (**B**), *b*-galactosidase-Alexa Fluor® 488 (**C**), and GFP (**D**) into CHO K1. Data for streptavidin-Texas Red® transport: (**a**) polymer channel; (**b**) streptavidin-Texas Red® channel; (**c**) LysoTracker® Green; (**d**) colocalization shows mostly distinct blue, red, and green areas for polymer **1** system while colocalization shows mainly white areas where all three labels coexist for polymer **2** system. Data for other proteins transport: **a** channels represent differential interference contrast (DIC) images, **b** channels showing fluorescence by polymer; **c** channel showing avidin-FITC import (**B**), *b*-galactosidase-Alexa Fluor® 488 (**C**) and GFP (**D**) mediated by **1** or **2**; **d** combined fluorescence for protein and polymer inside the cells. The CHO K1 cells were incubated at 37 ºC for 12 h; the cells were then washed 3x with PBS buffer and 3x heparin and analyzed by fluorescence spectroscopy. *Note;* the polymer **2** was added in 1 % MeOH, and a blank (no nanoparticles) was performed in parallel to check for the effects of MeOH.

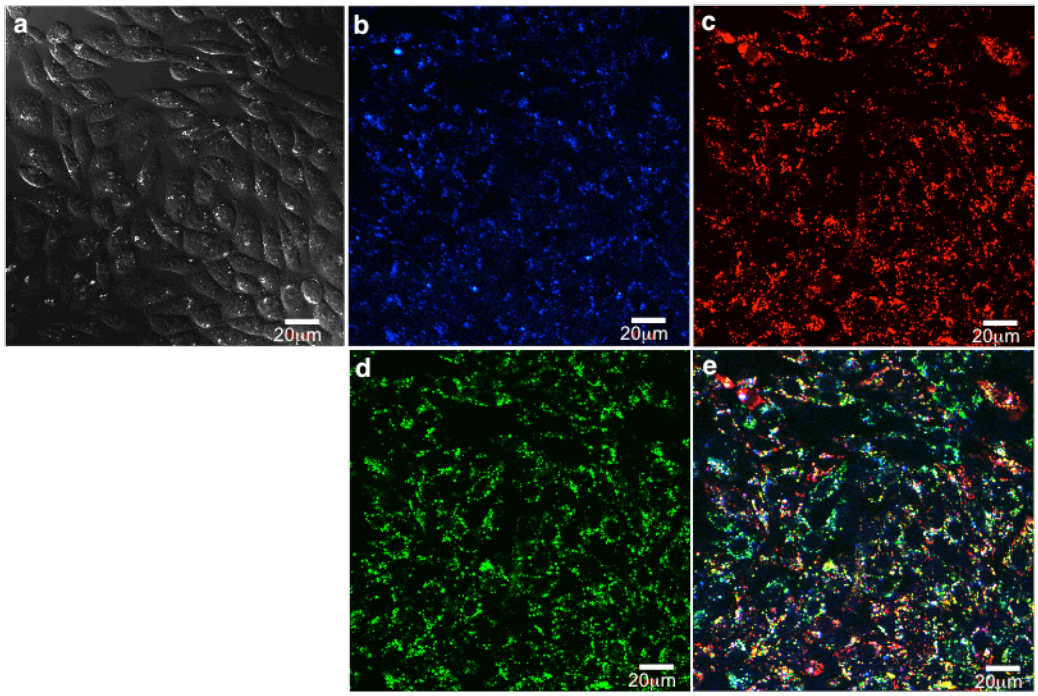

A. (**1**- streptavidin-Texas Red®)

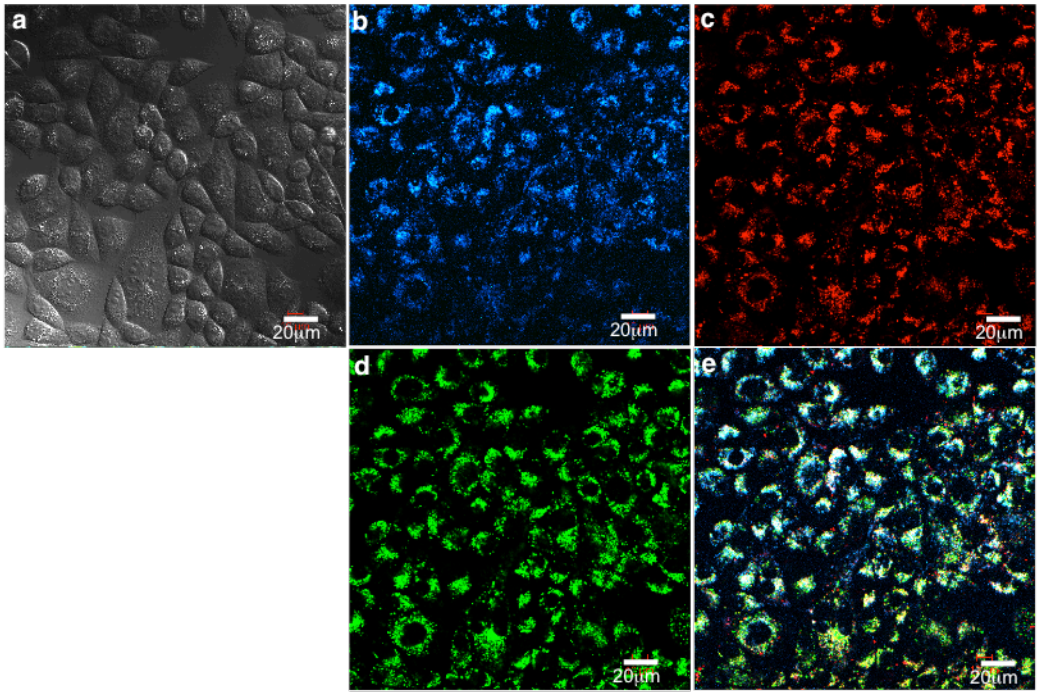

A. (**2**-streptavidin-Texas Red®)

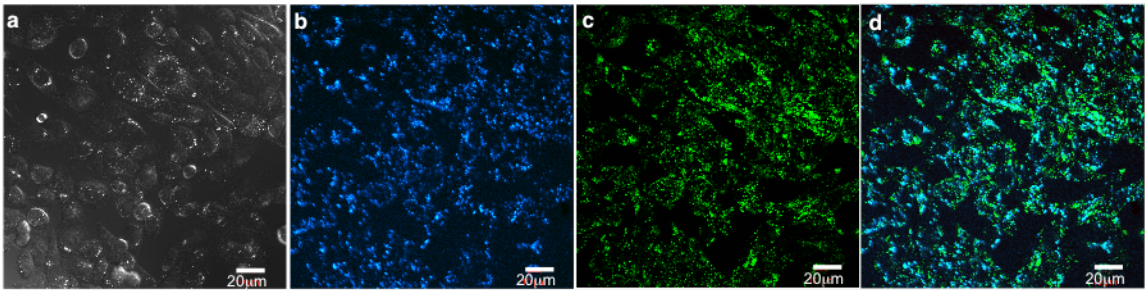

B. (**1**-avidin-FITC)

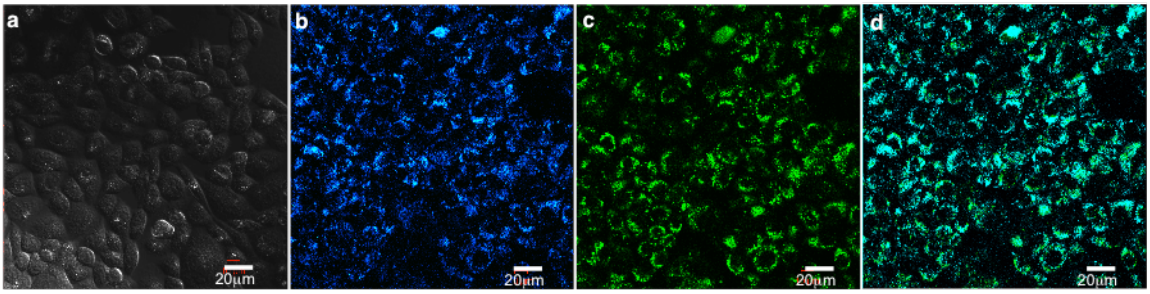

B. (**2**-avidin-FITC)

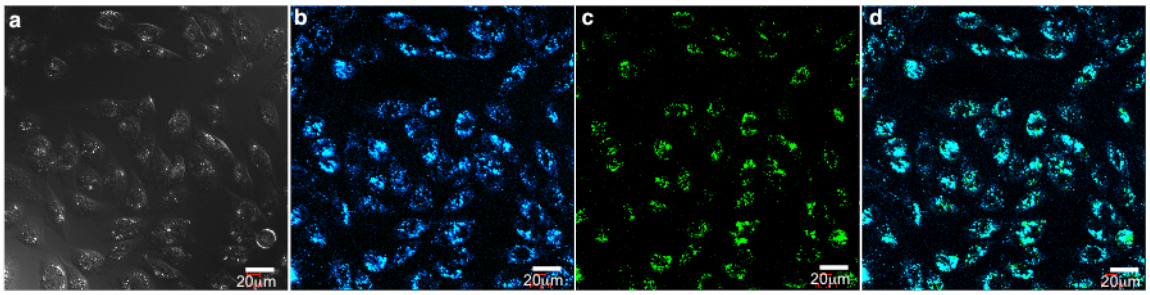

C. (**1**-*b*-galactosidase-Alexa Fluor® 488)

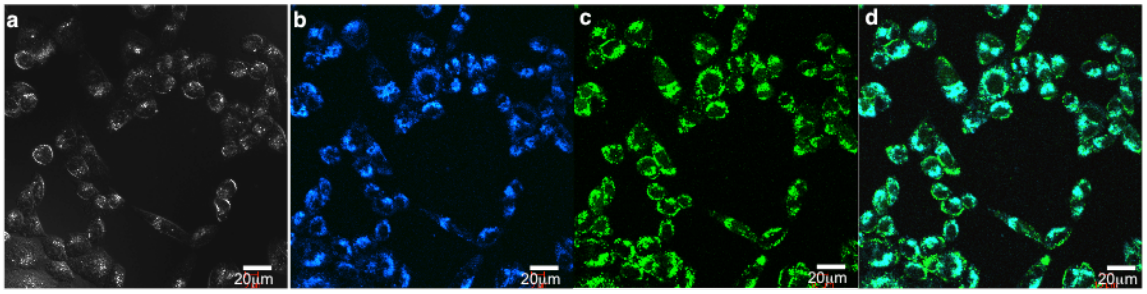

C. (**2**-*b*-galactosidase-Alexa Fluor® 488)

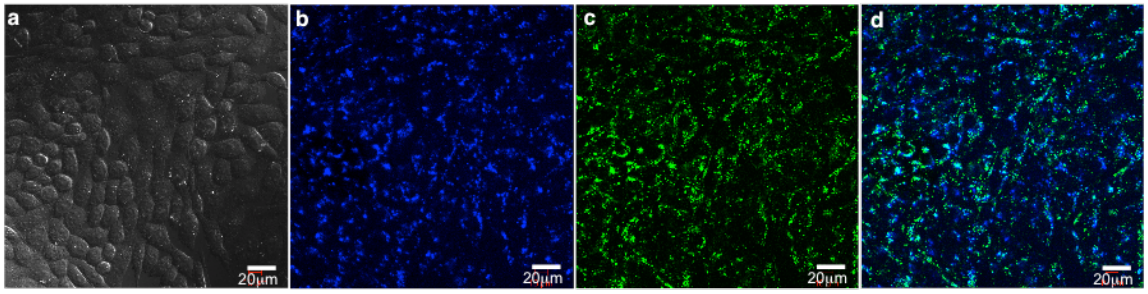

D. (**1**-GFP)

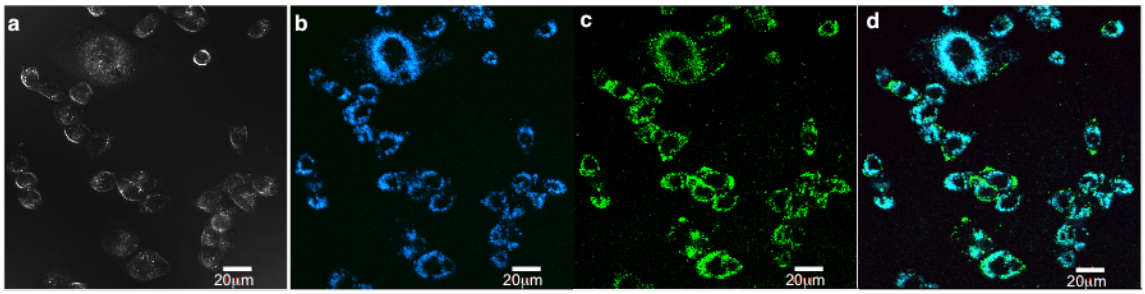

D. (**2**-GFP)

*Delivery Of BSA-Texas Red® at 4 °C Mediated By Polymer **1** in Clone 9 and CHO-K1 Cells*

Fluorescence Microscopy

Subcellular protein localization was measured on living Clone 9 and CHO K1 cells using a Zeiss Stallion Dual Detector Imaging System consisting of an Axiovert 200M inverted fluorescence microscope, CoolSnap HQ digital cameras and Intelligent Imaging Innovations (3I) software. Digital images of Texas Red-tagged BSA and **1** (blue polymer) were captured with a C-APO 63X/1.2 W CORR D=0.28M27 objective with the following filter sets: Exciter BP560/40, Dichroic FT 585, Emission BP 630/75 for Texas Red; and Exciter G 365, Dichroic FT 395, Emission BP 445/50 for **1**. Sequential optical sections (Z-stacks) from the basal-to-apical surfaces of the cell were acquired. Digital image acquisition was initiated approximately 1 μm below the basal surface of the cells and optical slices were collected at 0.5 μm steps through the apical surface of the cells with a high numerical objective lens (C-APO 63X/1.2 W CORR D=0.28M27). These wide-field images were subjected to deconvolution using 3I software.

The protein:carrier complexes were pre-formed at room temperature for 1 h by mixing (in a mol:mol ratio) the protein and the carrier in Ham's Nutrient Mixture F-12 with 10% fetal bovine serum (FBS) and DMEM supplemented with 10% fetal bovine serum (FBS) for Clone 9 cells and CHO K1 cells respectively. A 1:2 mol:mol ratio of protein:carrier was used. To study the cellular uptake of the proteins, the culture medium was removed, the preformed protein:carrier complex was added, and the cells

were incubated for another hour at 4 or 37 ºC. After the incubation period, the cells were washed with phosphate-buffered saline (PBS, pH 7.4) and heparin solution several times before imaging. For experiments at 4 ºC, cells were pre-incubated at 4 ºC for 30 min before being incubated with the protein solution for 1.5 h.

A

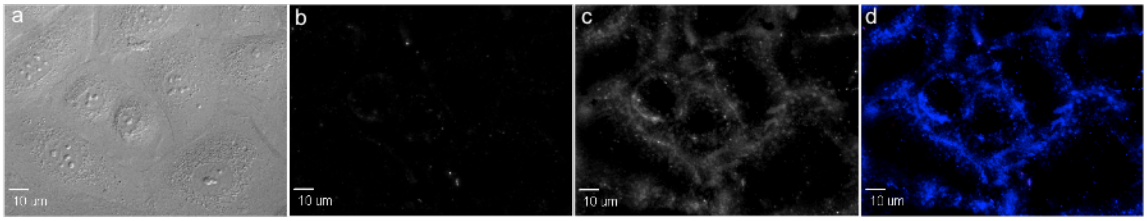

B

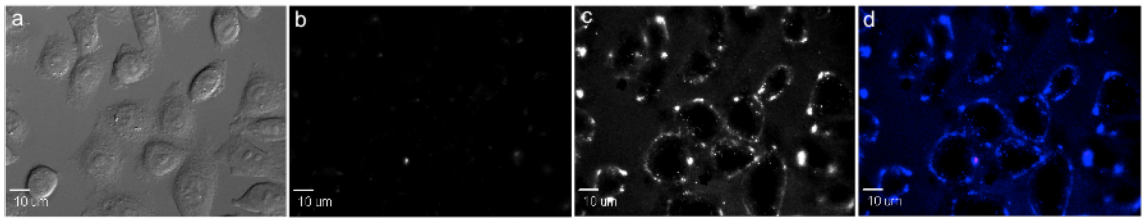

Figure A-S3. Delivery of BSA-Texas Red® into Clone 9 (**A**) and CHO-K1 (**B**) cells at 4 ºC mediated by polymers **1**; **a** channels represent differential interference contrast (DIC) images, **b** channels showing no BSA-Texas Red® is imported mediated by **1**; **c** channel showing polymer **1** fluorescence; **d** combined fluorescence for protein and polymer.

Effect Of Pyrenebutyrate

Clone 9 and CHO K1 cells were first incubated with pyrenebutyrate (1-pyrenebutyric acid) (50 μM) in serum-free Ham's medium for 2 min, and then the protein:polymer

complex in culture media was added to yield the final concentration of fetal bovine serum (FBS) 5%.

Kinetic Study

Clone 9 cells (1K cells, 1 mL, in Ham's medium) were suspended in a centrifuge tube. After centrifugation and removal of the medium, the protein:polymer complex in Ham's medium was added. The cells were incubated at 37 °C in 5% CO_2 and 95% air. After 5 min, 100 μL of the cell suspension was transferred to a new centrifuge tube, and the remained for the suspension was incubated for an additional minute (15, 30, and 60). The cells were washed thoroughly by centrifugation with PBS (2x) then heparin (3x). Thereafter, the cells were resuspended in 500 μL of serum-free Ham's media, and placed on a Lab-Tek chambered coverglass slides.

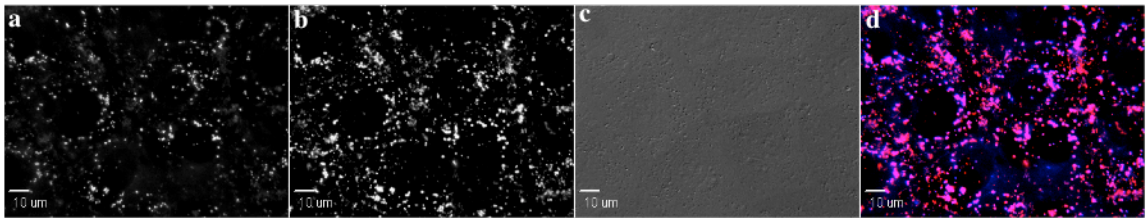

Figure A-S4. Delivery of BSA-Texas Red® in Clone 9 cells at 37 ºC mediated by **1** in the presence of pyrenebutyrate; **a** channel showing polymer **1** fluorescence; **b** channels showing BSA-Texas Red® import mediated by **1**; **c** represents differential interference contrast (DIC) images; **d** combined fluorescence for protein and polymer.

Kinetic Studies

A

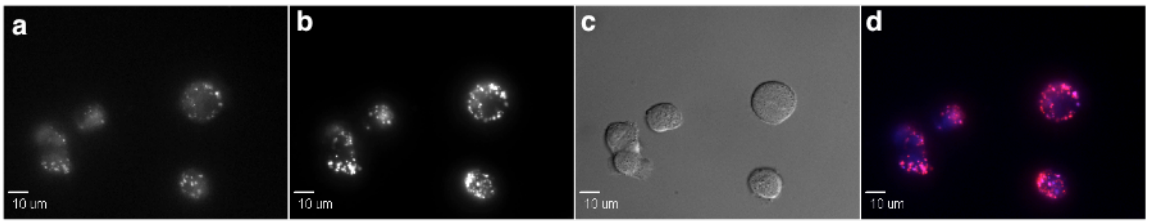

B

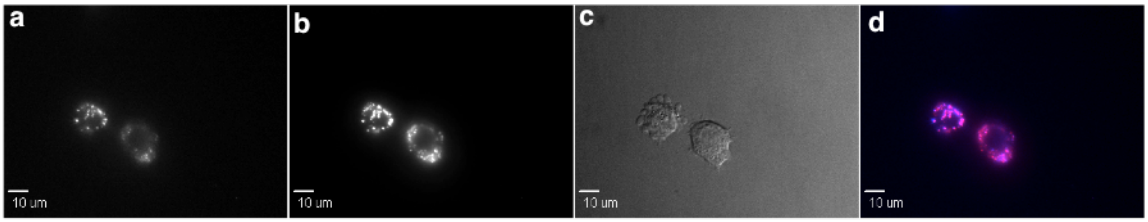

C

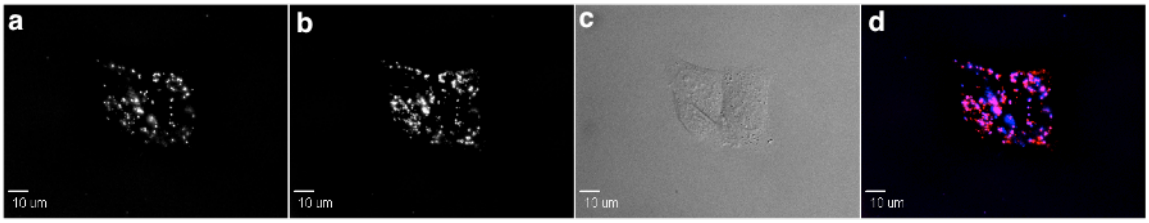

D

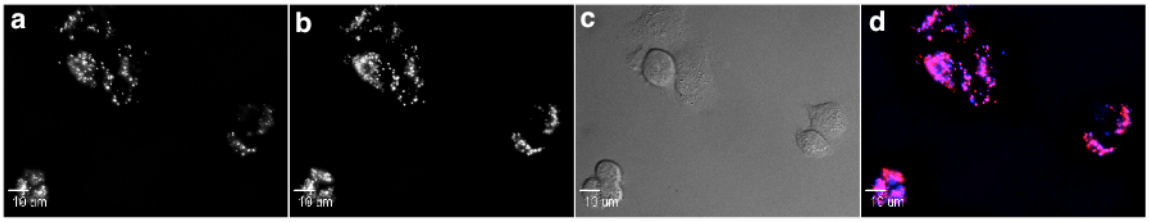

Figure A-S5. Delivery of BSA-Texas Red® in Clone 9 cells at 37 ºC mediated by **1** in the presence of pyrenebutyrate. The cells were incubated for different times, **A** 5 min, **B** 15 min, **C** 30 min and **D** 60 min; **a** channel showing polymer **1** fluorescence**; b** channels showing BSA-Texas Red® import mediated by **1**; **c** represent differential interference contrast (DIC) images; **d** combined fluorescence for protein and polymer. Throughout the carrier (1.0 μM), BSA-Texas Red® (0.5 μM) and the CHO K1 cell suspensions were incubated at 37 ºC with PBS; the cells were then washed 3x with PBS buffer and 3x heparin and analyzed by fluorescence microscopy. Images shown are after deconvolution using 3I software.

APPENDIX B

A NOVEL SMALL MOLECULE FOR ACTIVE TARGETING OF METASTATIC MELANOMA

B.1 Introduction

Molecular fragments that bind receptors selectively overexpressed on tumor cell-surfaces can be useful for *active targeting*.[1] Active targeting is distinct from strategies designed to perturb biochemical pathways upregulated in cancer, *eg* involving kinases or proteases. Small molecules that are commonly used for active targeting include some vitamins (*eg* folic acid,[20-21,23-24] biotin,[25] and cobalamin[26-27]), RGD peptidomimetics,[28-32] a few carbonic anhydrase ligands,[34-37] and mimics of the prostate specific antigen,[38-39] but little else. This is limiting because not all tumor types overexpress the corresponding receptors at usable cell surface copy-numbers, and some of these ligands have sub-optimal properties for targeting entities.[40] To facilitate discovery of novel ligands for targeting, we reported[259] the method shown in Figure 1 to identify small molecules that bind unknown receptors selectively expressed on the surface of cancer cells.

In the method described in Figure B-1, a set of monovalent dipeptide mimics were designed and prepared,[77,190,260-261] with a bias towards two side-chain pharmacophores that correspond to the most common amino acids found at protein-protein interfaces (Trp, Arg, Tyr, Lys, Glu, then Ser, Asn, Leu).[262]

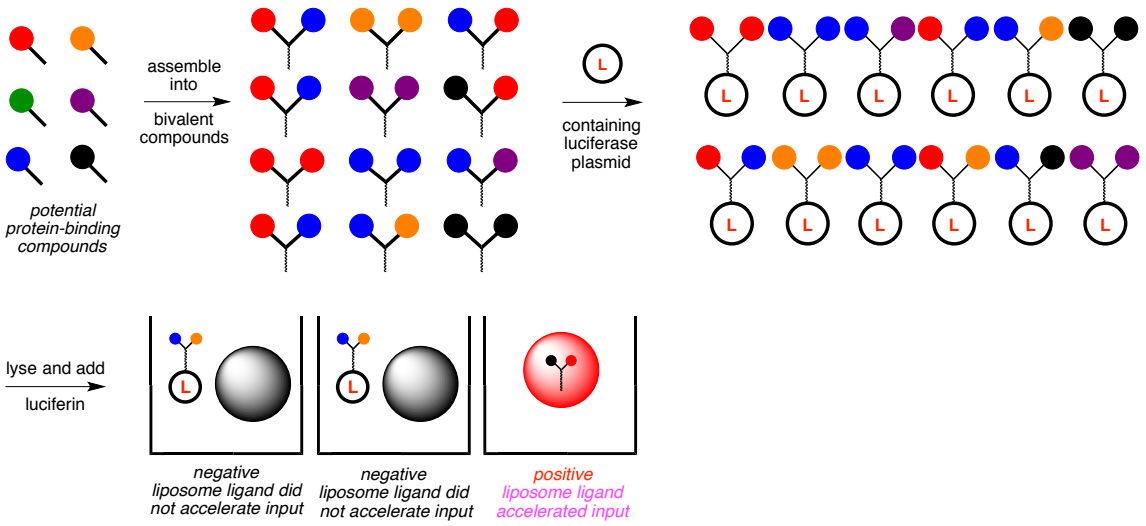

Figure B-1. A liposome assay to facilitate identification of small molecule ligands that promote preferential recognition of cancer cells over healthy tissue.

Our hypothesis is that these small molecules mimic side-chains orientations on various dipeptides that have a relatively high tendency to bind other proteins. Amino acid side-chains are important because they tend to dominate the thermodynamics of protein-protein interactions.[262] These monovalent molecules were assembled into bivalent one, each bearing a long hydrophobic chain substituent. Only n monovalent compounds are needed to make $2(n - 1)$ bivalent ones, so large libraries can be made from a small number of building blocks.[263] In a one-compound-per-well format, each bivalent molecule was allowed to associate with a liposome via capture of the hydrophobic side-chain into the surface bilayer. All the liposomes used in these experiments carried the plasmid encoding luciferase. Cells will fuse with liposomes at a certain rate, but this happens faster if the liposome-supported bivalent compounds bind a

cell-surface receptor, and mediate internalization. The degree of import after a set time can be determined by lysing the cells and adding agents to induce bioluminescence.[259]

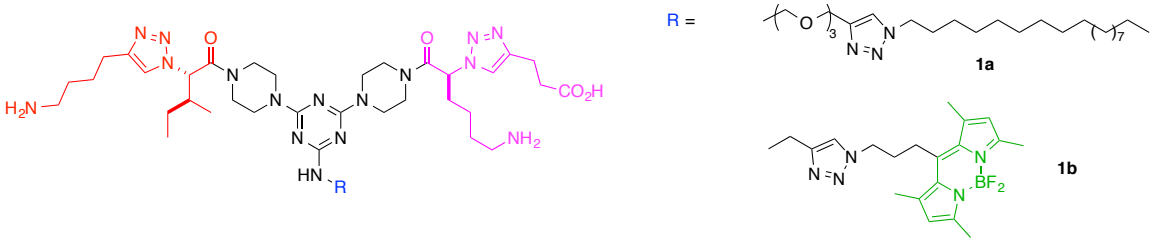

We now reveal one of the compounds found in this assay, **1a**, selectively bound to melanoma SK-MEL-28 cells and was internalized more than it was when interacting with HUVEC cells. The study reported here was designed to establish if: (i) the targeting fragments in **1** bind other live melanoma cells; (ii) they bind fixed tissue slices; (iii) modifications that replace the triazine core with a near-IR dye influence their binding.

A weakness of the liposome assay in Figure B-1 is that the HUVAC cells used as the "healthy control" are not closely related to skin. Fortunately, we have access to the Sinclair swine model[217,264] that allowed us to take biopsy material from pigs with naturally occurring metastatic melanoma. This was done to obtain samples of melanoma tumor and healthy skin tissue adjacent to the melanoma region. That the tissue was obtained *from the same animal* is significant because it relates directly to how a particular individual would respond to the featured active targeting method. The first step in treatment of an individual would be diagnosis. Figure B-2 shows healthy skin tissue from the pig was not stained by the fluorescent analog **1b**, whereas the melanoma

tissue stained strongly. This assay could be used for diagnosis of melanoma types that respond to ligands **1**.

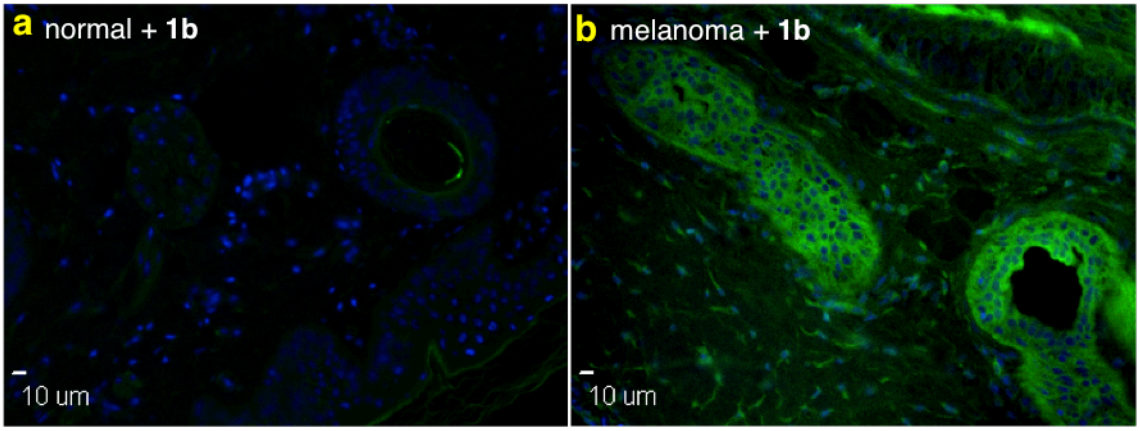

Figure B-2. Histochemistry with **1** does not stain healthy skin, but does stain melanoma tissue from the same Sinclair swine.

The *Georgetown method*[220,265] was used to obtain live cells from the melanoma. Thus, the pig tumor tissue was co-cultured with 3T3 Swiss fibroblast cells in the presence of the ROCK kinase inhibitor Y27632 and stem-like-melanoma cells were obtained after several passages. Figure B-3 shows that **1b** was internalized into the melanoma cells where it colocalized with a lysosome tracker. This observation implies conjugates of **1** may have a tendency to accumulate in melanoma cells *in vivo*.

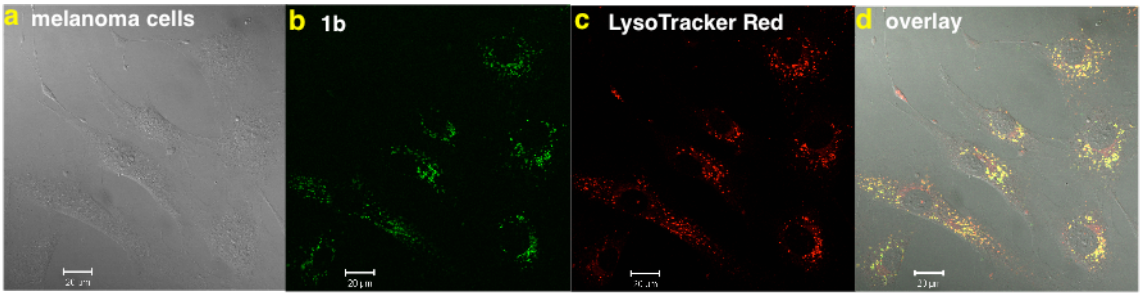

Figure B-3. **a** Melanoma cells from Sinclair swine; **b** compound **1** is internalized by these cells. **c** Internalization of a lysosome tracker into the melanoma cells, **d** overlays with the fluorescence from **1b**.

Experiments described above validate the melanoma targeting effects of the "warhead" fragments in **1**. This successful confirmation leads to a range possibility for subsequent research, and the one featured in this paper is formation of a theranostic that could be used for optical and PET imaging of melanoma.

It is possible to substitute ^{19}F in BODIPY dyes with ^{18}F hence reagents **1** might be suitable precursors for PET studies.[183-184] However, for *in vivo* optical imaging, the fluor in **1b**, which absorbs around 520 nm, is *unsuitable* because observation of non-superficial tissue requires agents that absorb at longer wavelengths (ideally, >700 nm).[97-98] One possibility would be to replace the BODIPY dye in **1** with a similar, but near-IR-absorbing, fluor. This is particularly important when intrinsically dark melanoma tissue is involved, though this too is permeable to light of λ_{max} >700 nm.[81-82] However, near-IR dyes tend to be large, and, in general, it is good practice to keep molecular size as small as possible to avoid adverse absorption, metabolism and excretion effects. For this reason we chose to investigate replacement of the triazine splitter in **1** with a near-IR dye

that could also act as a scaffold to present the melanoma-targeting groups. Thus Scheme B-1 describes a synthesis of our new target, the "aza-BODIPY"[221-222] system **2**. UV absorption maxima of aza-BODIPY fluors tend to be around 700 nm, and they are also amenable to $^{19}F/^{18}F$ metathesis (Gabbai, personal communication).

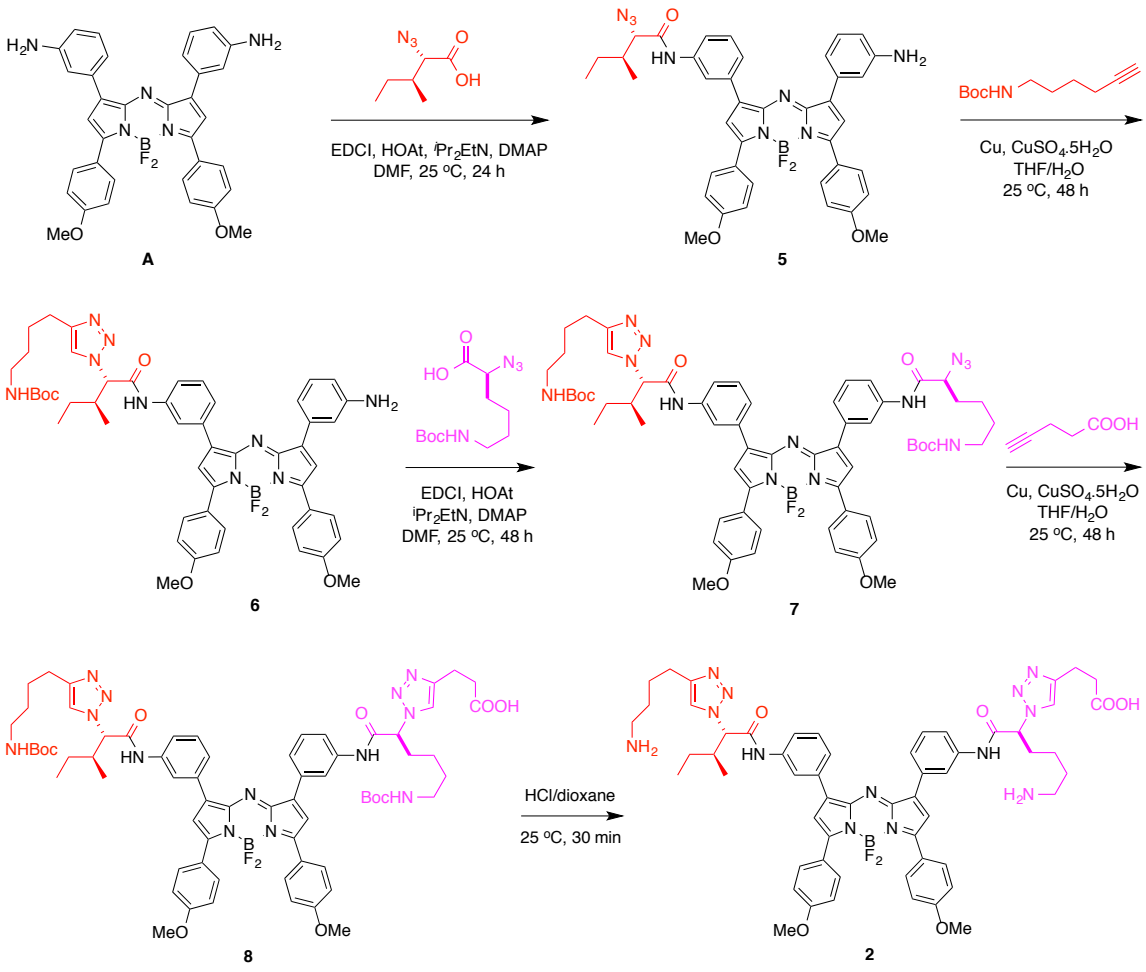

Scheme B-1. Functionalization of diamino aza-BODIPY **A** with the targeting groups in compounds **1**.

Scheme 1 begins with coupling one equivalent of an amino acid-derived azide[190,266] with the diamine **A**. Stereochemistry in the isoleucine side-chain is an intrinsic probe for epimerization in this coupling, and none was detectable by ^{1}H NMR. Copper-mediated Huisgen coupling gave **6** which has one dipeptide mimic supported on the aza-BODIPY scaffold. Construction of the other dipeptide in **8** was achieved in the same way, *ie* via **7**. Finally, acid-mediated deprotection afforded the target system **2**; this compound is not water-soluble, but can be dissolved in DMSO then diluted to 1 % DMSO in PBS buffer.

Predictably, since the first coupling involving **A** is only controlled by stoichiometry, by-products in the synthesis of **2** made it cost effective to prepare the symmetrical probes **3** and **4** as interesting controls. In the event, they were far more interesting than we had anticipated.

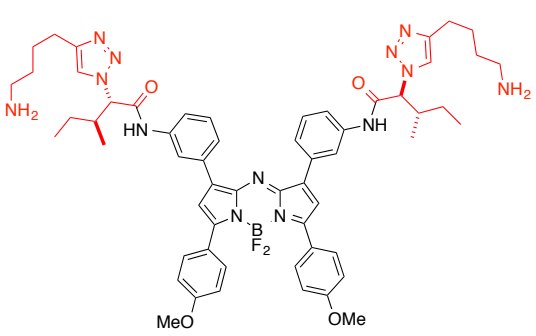

3

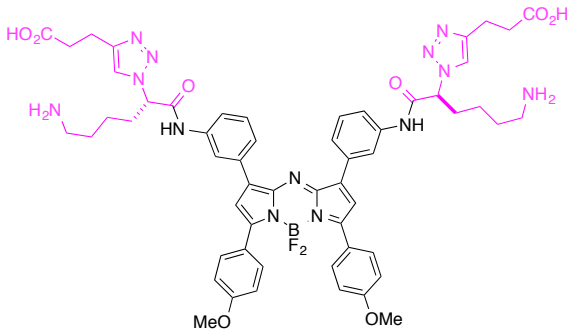

4

Disappointingly, treatment of pig melanoma tissue with dye **2** showed only very weak staining (Figure B-4a). However, to our surprise, the symmetrical control **3** gave a much stronger signal, whereas almost no staining was observed for the other

symmetrical control **4** (Figure B-4b and B-4c, respectively). Figures 4d and 4e compare normal skin and melanoma stained with agents **2** and **3**, respectively; these data confirm that **3** gives a far better contrast between tumor and healthy tissue than our original target **2**. From this point on, **3** became our lead probe, and no further studies were performed **2**. Overall, this is fortunate because **2**, which needs to be prepared via stepwise couplings, is significantly more time-consuming to make than the symmetrical analog **3** (see supporting for synthesis).

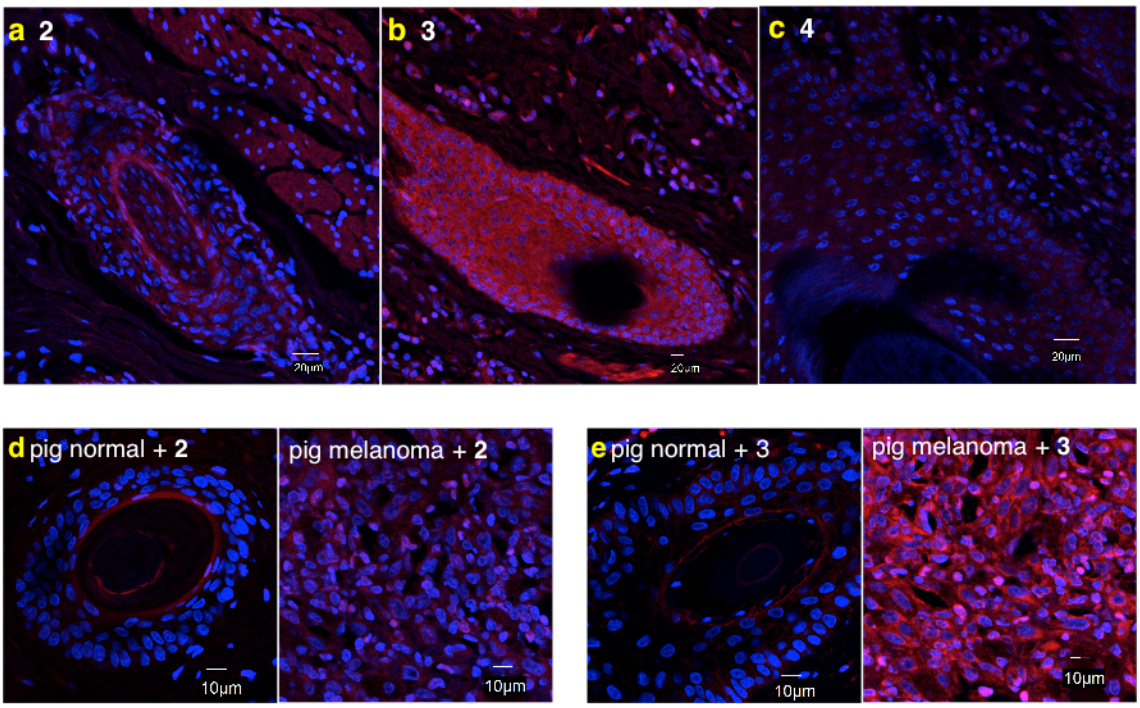

Figure B-4. Metastatic melanoma tissue stained with agents: the original lead probe **2** (**a**); and the symmetric probes **3** (**b**), and, **4** (**c**). **d** Probe **2** gives weak staining and almost no contrast between normal and melanoma tissue from the Sinclair swine, but **e** agent **3** gives a distinct contrast.

Data from one particular Sinclair swine is not reliably indicative of a trend in human melanoma. Thus a panel of commercially available human melanoma tissue samples was stained to estimate the fraction of cases that would bind agent **3** (Figure B-5). Duplicate tissue samples from 22 metastatic melanoma patients were tested, and *every one of them stained with agent **3***. Conversely, no significant staining was observed when the two duplicate samples of normal skin available were treated with the same probe.

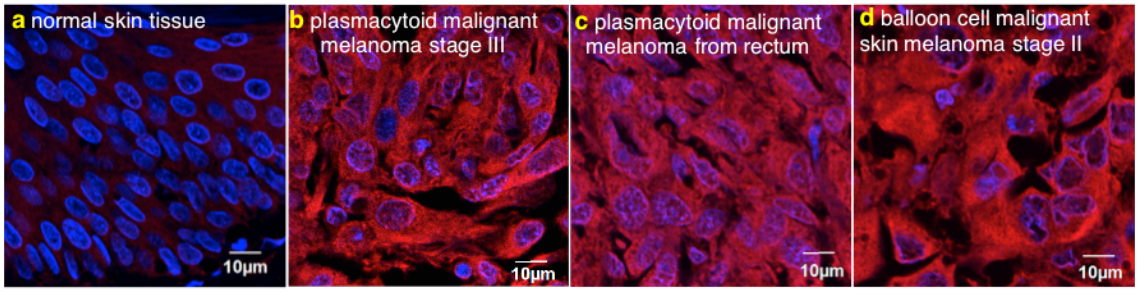

Figure B-5. **a** Human normal skin tissue did not stain with agent **3**; but, **b - d** human metastatic melanoma tissue did (illustrative data from tissue derived from three patients are shown).

B.3 ACKNOWLEDGMENT

We thank The National Institutes of Health (GM087981), The Robert A. Welch Foundation (A-1121), and High Impact Research (HIR (UM.C/625/1/HIR/MOHE/MED/17 & UM.C/625/1/HIR/MOHE/MED/33) from the Ministry of Higher Education, Malaysia, for financial support.

B.4 Materials and Methods

General Procedures

All reactions were carried out under an atmosphere of argon. Unless otherwise indicted, common reagents or materials were obtained from commercial source and used without further purification. All α-amino acids used were of the L-configuration. Dry DMF, (<50 ppm water) was purchased from Acros. Tetrahydrofuran (THF), Acetonitrile (MeCN), dichloromethane (CH_2Cl_2), and methanol (MeOH) were dried by Mbraun solvent drying system. Other solvents and reagents were used as received.

NMR spectra were recorded on a Bruker-400 MHz spectrometers (^1H at 400 MHz and ^{13}C at 100 MHz) at room temperature unless other mentioned. Chemical shifts of ^1H NMR spectra were recorded and chemical shifts are reported in ppm from the solvent resonance ($CDCl_3$ 7.26 ppm, CD_3OD 3.30 ppm, DMSO-d_6 2.50 ppm). Data are reported as follows: chemical shift, multiplicity (s = singlet, br = broad, d = doublet, t = triplet, q = quartet, m = multiplet), coupling constants, and number of protons. Proton decoupled ^{13}C NMR spectra were also recorded in ppm from tetramethylsilane (TMS) resonance ($CDCl_3$ 77.0, CD_3OD 49.1, DMSO-d_6 39.5 ppm). Analytical thin layer chromatography (TLC) was performed on EM Reagents 0.25 mm silica-gel 60-F plates, and visualized with UV light. Flash chromatography was performed using silica gel 60 (230–400 mesh). MS were measured under ESI or MALDI conditions.

Analytical HPLC analyses were carried out on 150 x 4.6 mm C-18 column using gradient conditions (10 – 90% B, flow rate = 0.75 mL/min). Preparative HPLC was carried out on 100 x 21.2 mm C-18 column using gradient conditions (10 – 70% B, flow

rate = 10.0 mL/min). The eluents used were: solvent A (H_2O with 0.1% AcOH) and solvent B (CH_3CN with 0.1% AcOH).

The purity of all biologically evaluated compounds is > 95% confirmed by analytical HPLC.

Syntheses Of aza-BODIPY Derivatives ***2-4***

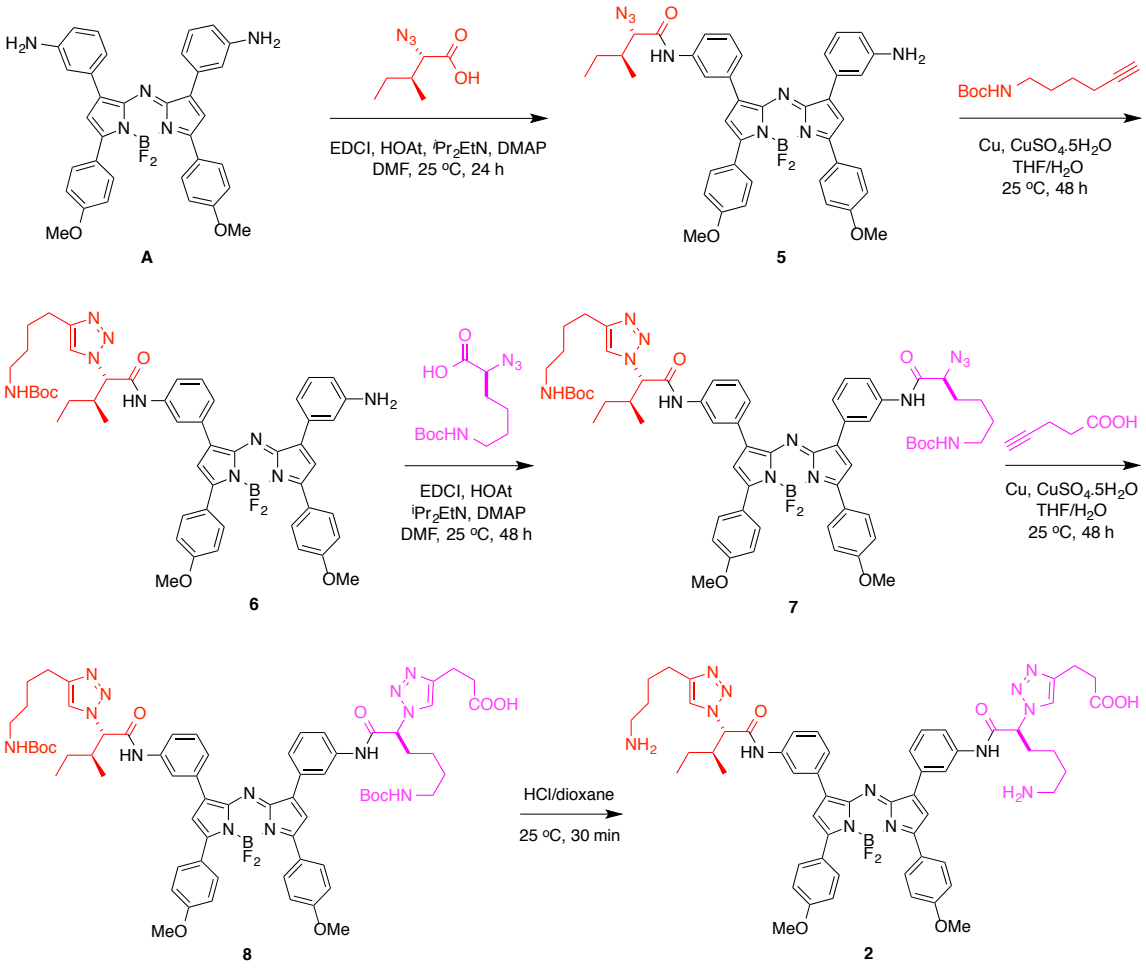

*Synthesis of compound **5***

EDCI (52.7 mg, 0.275 mmol) and HOAt (40.9 mg, 0.300 mmol) were added to a suspension of isoleucine azide[190] (39.3 mg, 0.250 mmol) in 1 mL DMF at 0 ^{o}C. After stirring at 0 ^{o}C for 30 min, **A** (146.9 mg, 0.250 mmol) was added to the above suspension followed by DIPEA (139 μL, 103.4 mg, 0.800 mmol) and catalytic amount of DMAP. The resulting solution was stirred at 0 °C for 1 h and then warmed to 25 ^{o}C and continue stirring for 12 h. Ethyl acetate (*ca.* 20 ml) was added to the reaction mixture, and the organic layer was washed with sat. $NaHCO_3$ and brine then dried with anhydrous Na_2SO_4. Solvents were removed to afford green solid. The crude product was purified by column chromatography on silica gel, and eluted with a mixture of hexanes and ethyl acetate (2:1 to 1:2, v/v) afforded the desired **5** (93.9 mg, 34%) as a greenish solid. ^{1}H NMR (400 MHz, $CDCl_3$) δ 8.37 (s, 1H), 812 (s, 1H), 8.11 (dd, *J* = 9.0, 4.1 Hz, 4H), 7.86 (t, *J* = 8.9 Hz, 2H), 7.62 – 7.55 (m, 1H), 7.48 (t, *J* = 7.9 Hz, 1H), 7.39 (d, *J* = 7.8 Hz, 1H), 7.10 (s, 2H), 7.04 (dd, *J* = 9.1 Hz, 1.2 Hz, 4H), 6.80 (dd, *J* = 7.9 Hz, 1.6 Hz, 1H), 3.97 (d, *J* = 4.9 Hz, 1H), 3.92 (s, 6H), 3.78 (s, 2H), 2.30 – 2.12 (m, 1H), 1.67 – 1.56 (m, 1H), 1.42 – 1.32 (m, 1H), 1.11 (d, *J* = 6.9 Hz, 3H), 0.97 (t, *J* = 7.4 Hz, 3H). ^{13}C NMR (100 MHz, $CDCl_3$) δ 167.7, 162.1, 161.9, 158.5, 157.6, 146.3, 145.5, 145.0, 143.3, 141.3, 137.2, 133.4, 131.7, 131.7, 131.6, 129.4, 129.1, 125.7, 124.1, 124.0, 121.9, 121.3, 119.6, 118.7, 116.7, 116.2, 114.3, 114.2, 69.8, 55.4 (2C), 29.7, 24.6, 16.1, 11.4. ^{11}B NMR (128 MHz, $CDCl_3$) δ 0.96 (t, *J* = 31.9 Hz).

*Synthesis of compound **6***

Copper powder (9.7 mg, 0.152 mmol) and $CuSO_4$ (0.1 equiv, from 0.05 M aqueous solution) were added to a solution of **5** (110.3 mg, 0.152 mmol) and alkyne (29.9 mg, 0.152 mmol) in 7 mL dry THF at 25 °C. The mixture was stirred at 25 °C for 2 days (monitored by TLC). Then, solvents were removed under reduced pressure and the residue was acidified with 0.2 *N* HCl. After extracting with ethyl acetate three times, the combined organic phase was washed with 0.05M EDTA and brine. The organic layer was separated and dried over Na_2SO_4. Finally, the solvents were removed to afford green solid, which was purified by column chromatography on silica gel, and eluted with a mixture of CH_2Cl_2, and methanol (99:1 to 97:3, v/v) to afford the desired **6** (117.2 mg, 84 %) as a green solid. ^{1}H NMR (400 MHz, $CDCl_3$) δ 9.29 (s, 1H), 8.32 (s, 1H), 8.10 (dd, *J* = 12.2, 9.0 Hz, 4H), 8.03 – 7.95 (m, 1H), 7.76 (s, 1H), 7.70 (d, *J* = 8.3 Hz, 2H), 7.42 (t, *J* = 8.0 Hz, 1H), 7.34 (t, *J* = 7.7 Hz, 1H), 7.12 (s, 1H), 7.09 – 6.99 (m, 6H), 5.09 (d, *J* = 10.7 Hz, 1H), 4.57 (s, 1H), 4.23 (s, 2H), 3.91 (s, 6H), 3.18 (d, *J* = 6.1 Hz, 2H), 2.79 (t, *J* = 7.6 Hz, 2H), 2.38 (dd, *J* = 9.3, 5.7 Hz, 1H), 1.77 (dt, *J* = 15.4, 7.7 Hz, 2H), 1.61 (s, 2H), 1.46 (s, 9H), 1.28 (s, 2H), 1.24 – 1.09 (m, 1H), 0.99 (d, *J* = 6.7 Hz, 3H), 0.89 (t, *J* = 7.3 Hz, 3H). ^{13}C NMR (100 MHz, $CDCl_3$) δ 166.8, 162.1, 161.9, 158.5, 157.6, 156.0, 148.3, 145.5, 145.3, 145.1, 143.3, 140.5, 137.3, 133.5, 133.1, 131.7, 131.6, 129.6, 129.1, 125.2, 124.0, 123.9, 122.5, 121.7, 120.1, 119.8, 118.6, 118.4, 118.1, 116.7, 114.3, 114.2, 79.1, 69.3, 55.4, 55.4, 40.3, 38.2, 29.7, 28.4, 26.5, 25.5, 24.8, 15.4, 10.3. ^{11}B NMR (128 MHz, $CDCl_3$) δ 0.91 (t, *J* = 32.0 Hz). MS-ESI: *m/z* 924.4684 $[M+H]^+$

Synthesis of compound 7

EDCI (133.9 mg, 0.70 mmol) and HOAt (96.8 mg, 0.71 mmol) were added to a suspension of Boc protected lysine azide[190] (172.7 mg, 0.63 mmol) in 2 mL DMF at 0 ^{o}C. After stirring at 0 ^{o}C for 30 min, **6** (117.2 mg, 0.13 mmol) was added to the above suspension followed by DIPEA (354 μL, 262.6 mg, 2.03 mmol) and catalytic amount of DMAP. The resulting solution was stirred at 0 °C for 1 h and warmed to 25 ^{o}C and stirred for 12 h. Ethyl acetate (*ca*. 50 ml) was added to the reaction mixture, and the resulting suspension was washed with 5 % HCl, water, sat. $NaHCO_3$ and brine. The organic layer was separated, dried with Na_2SO_4, and solvent was removed to afford green solid. The crude product was purified by column chromatography on silica gel, and eluted with a mixture of CH_2Cl_2 and methanol (99:1 to 97:3, v/v) to obtained **7** (123.5 mg, 83%) as a green solid. ^{1}H NMR (400 MHz, $CDCl_3$) δ 9.30 (s, 1H), 8.37 (s, 1H), 8.14 (d, *J* = 9.4 Hz, 2H), 8.05 (ddd, *J* = 7.3, 4.7, 2.0 Hz, 4H), 7.81 (d, *J* = 7.7 Hz, 1H), 7.75 (s, 2H), 7.64 (s, 2H), 7.36 (t, *J* = 7.9 Hz, 1H), 7.31 – 7.21 (m, 1H), 7.00 (s, 2H), 6.98 (d, *J* = 2.6 Hz, 4H), 5.11 (d, *J* = 9.6 Hz, 1H), 4.83 (s, 1H), 4.68 (t, *J* = 5.6 Hz, 1H), 4.08 – 3.92 (m, 1H), 3.88 (s, 6H), 3.14 (d, *J* = 5.2 Hz, 4H), 2.76 (t, *J* = 7.6 Hz, 2H), 2.40 (dd, *J* = 13.8, 7.4 Hz, 1H), 2.12 – 1.82 (m, 4H), 1.73 (dt, *J* = 15.3, 7.7 Hz, 2H), 1.63 – 1.49 (m, 6H), 1.45 (d, *J* = 7.1 Hz, 18H), 1.27 (d, *J* = 7.6 Hz, 1H), 1.24 – 1.14 (m, 1H), 1.09 (d, *J* = 6.7 Hz, 3H), 0.86 (t, *J* = 7.3 Hz, 3H). ^{13}C NMR (100 MHz, $CDCl_3$) δ 168.0, 167.9, 166.6, 162.1, 158.2, 158.1, 156.3, 156.1, 148.2, 145.3, 145.2, 142.3, 137.7, 137.3, 133.4, 133.2, 133.1, 131.8, 131.7, 131.7, 129.1, 129.0, 126.1, 125.8, 123.9, 123.9, 121.1, 121.0, 120.8, 120.6, 119.1, 114.3, 79.3, 79.1, 69.8, 64.0, 55.4 (2C), 40.2, 38.4, 31.7,

29.7, 29.6, 28.5, 28.4, 26.5, 25.4, 24.9, 22.7, 15.5, 10.4. ^{11}B NMR (128 MHz, $CDCl_3$) δ 0.92 (t, J = 31.9 Hz) ESI-MS: *m/z* 1178.7063 $[M+H]^+$

*Synthesis of compound **8***

Copper powder (6.7 mg, 0.11 mmol) and $CuSO_4$ (0.1 equiv, from 0.05 M aqueous solution) were added to a solution of **7** (123.5 mg, 0.11 mmol) and alkyne (10.3 mg, 0.11 mmol) in 7 mL dry THF at 25 °C. The mixture was stirred at 25 °C for 2 days. Then, solvents were removed under reduced pressure and the residue was acidified with 0.2 *N* HCl. After extracting with ethyl acetate three times, the combined organic phase was washed with 0.05 M EDTA and brine. The organic layer was separated and dried over Na_2SO_4. Finally, the solvents were removed to afford green solid, which was purified by column chromatography on silica gel, and eluted with a mixture of CH_2Cl_2, and methanol (99:1 to 97:3, v/v) to afford the desired **8** (86.0 mg, 64 %) as a green solid. No good ^{1}H NMR was recorded in CDCl3 or CD3OD. ^{13}C NMR (100 MHz, MeOD) δ 167.0, 162.0, 157.7, 157.1, 144.8, 141.6, 137.6, 137.5, 132.9, 131.6, 128.7, 126.2, 123.5, 120.7, 120.2, 118.7, 113.7, 78.6, 78.5, 68.9, 64.3, 54.6, 47.0, 46.5, 39.6, 37.8, 33.5, 32.3, 29.1, 28.9, 27.5, 26.3, 24.5, 22.7, 20.9, 14.6, 9.1, 7.8. ^{11}B NMR (128 MHz, $CDCl_3$) δ 0.86 (t, J = 32.3 Hz) ESI-MS: *m/z* 1276.7981 $[M+H]^+$.

tBu protected acid

^{1}H NMR (400 MHz, $CDCl_3$) δ 9.55 (s, 1H), 9.15 (s, 1H), 8.20 (d, J = 21.8 Hz, 2H), 8.13 – 7.97 (m, 4H), 7.89 – 7.65 (m, 4H), 7.52 (s, 2H), 7.30 (s, 1H), 7.25 – 7.11 (m, 1H), 6.98

(d, J = 8.1 Hz, 6H), 5.54 – 5.35 (m, 1H), 5.24 (d, J = 9.4 Hz, 1H), 4.94 (s, 1H), 4.72 (s, 1H), 3.88 (s, 6H), 3.12 (d, J = 4.5 Hz, 4H), 3.04 (t, J = 7.3 Hz, 2H), 2.75 (t, J = 7.4 Hz, 2H), 2.65 (t, J = 7.4 Hz, 2H), 2.40 (s, 1H), 2.34 – 2.07 (m, 4H), 1.84 – 1.64 (m, 2H), 1.54 (s, 6H), 1.49 – 1.37 (m, 27H), 1.27 (d, J = 8.0 Hz, 2H), 1.09 (d, J = 6.6 Hz, 3H), 0.84 (t, J = 7.3 Hz, 3H). ^{13}C NMR (100 MHz, $CDCl_3$) δ 172.0, 171.9, 166.9, 166.7, 162.0, 158.1, 156.4, 156.1, 148.2, 147.1, 145.3, 145.2, 142.6, 142.3, 137.7, 137.5, 133.4, 133.3, 133.2, 131.7, 129.0, 128.9, 126.3, 126.1, 125.9, 123.9, 121.2, 120.9, 120.8, 119.2, 119.1, 114.3, 80.6, 79.4, 79.0, 69.5, 64.4, 55.4, 40.3, 40.0, 38.4, 34.8, 32.7, 29.7, 29.1, 28.5, 28.4, 28.1, 26.5, 25.4, 24.8, 22.8, 21.3, 15.5, 15.4, 10.3, 10.3. ^{11}B NMR (128 MHz, $CDCl_3$) δ 0.90 (t, J = 31.8 Hz).

*Synthesis of compound **2***

8 (12.7 mg, 0.01 mmol) was dissolved in 100 µL HCl in 1,4-dioxane (4 M), and the reaction mixture was stirred at 25 °C for 30 min. After the reaction was done, the solvent was removed under reduced pressure to give desired product **2** as a green solid quantitatively. The purity was confirmed by analytical HPLC (C18 column, CH_3CN-H_2O 10-90 % with 0.1 % acetic acid).

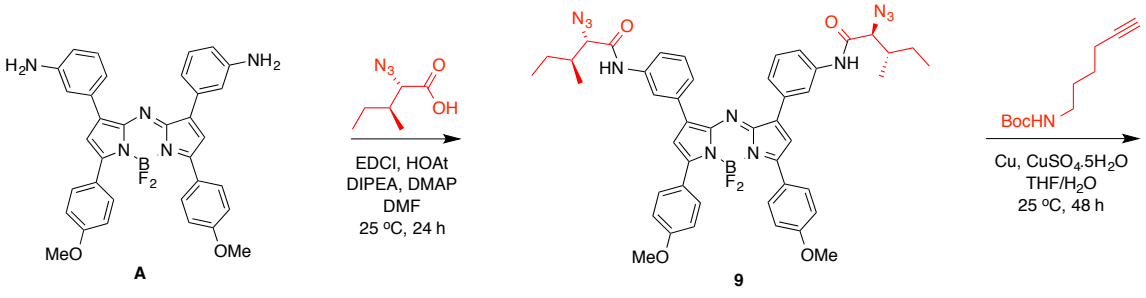

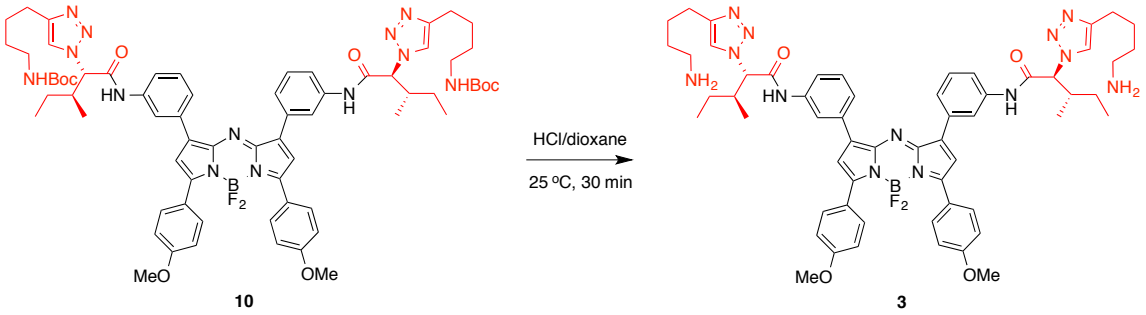

10 3

*Synthesis of compound **10***

To a solution of **9** (284.9 mg, 0.329 mmol) and alkyne (129.8 mg, 0.658 mmol) in 24 mL dry THF were added Cupper powder (41.8 mg, 0.658 mmol) and $CuSO_4$ (0.1 equiv, from 0.05 M aqueous solution) at 25 °C. The mixture was stirred at 25 °C for 2 days. The reactions were monitored by TLC. After the reaction was done, the solvent was removed under reduced pressure and 0.2 N HCl was added to the residue. After extracted with ethyl acetate three times, the combined organic phase was washed with 0.05M EDTA and brine. The organic layer was separated and dried over Na_2SO_4, and concentrated to afford green solid. The crude product was purified by column chromatography on silica gel, and eluted with a mixture of CH_2Cl_2 and methanol (100:2 to 100:4, v/v) afforded the desired **10** (197.1 mg, 48%) as green solid. ^{1}H NMR (400 MHz, $CDCl_3$) δ 9.45 (s, br, 2H), 8.14 (s, 2H), 8.06 (d, J = 8.4 Hz, 4H), 7.80 (s, 2H), 7.59 (dd, J = 29.3, 8.5 Hz, 4H), 7.26 (m, 2H), 7.00 (q, J = 9.3 Hz, 6H), 5.25 (d, J = 8.3 Hz, 2H), 4.65 (s, 2H), 3.88 (s, 6H), 3.13 (s, 4H), 2.76 (t, J = 6.9 Hz, 4H), 2.42 (s, 2H), 1.93 (s, 2H), 1.71 (s, 4H), 1.63-1.47 (m, 4H), 1.44 (s, 18H), 1.33-1.25 (m, 4H), 1.21 (d, J = 6.8 Hz, 6H), 0.88 (t, J = 7.3 Hz, 6H). ^{13}C NMR (100 MHz, $CDCl_3$) δ 166.70, 162.06,

158.13, 156.04, 148.27, 145.27, 142.85, 137.20, 133.37, 131.70, 129.01, 126.02, 123.94, 121.69, 121.16, 119.40, 114.26, 79.07, 69.82, 55.40, 40.26, 38.26, 29.65, 28.42, 26.48, 25.38, 24.88, 15.43, 10.34. ^{11}B NMR (128 MHz, $CDCl_3$) δ 0.84 (t, *J* = 31.8 Hz). ^{19}F NMR (376 MHz, $CDCl_3$) quartet at δ -132.16 HRMS-ESI+: cald 1282.6527, found 1282.6589 $[M+Na]^+$.

*Synthesis of compound **3***

6 (12.6 mg, 0.01 mmol) was dissolved in 100 μL HCl in 1,4-dioxane (4 M), and the reaction mixture was stirred at 25 °C for 30 min. After the reaction was done, the solvent was removed under reduced pressure to give desired product **1** as green solid quantitatively. The purity was confirmed by analytical HPLC (C18 column, CH_3CN-H_2O 10-90% with 0.1% acetic acid). ^{1}H NMR (400 MHz, MeOD) δ 8.32 (s, 2H), 8.16 (s, 2H), 8.08 (d, *J* = 8.9 Hz, 4H), 7.89 (d, *J* = 7.8 Hz, 2H), 7.58 (d, *J* = 8.0 Hz, 2H), 7.23 (t, *J* = 8.0 Hz, 2H), 7.16 (s, 2H), 6.99 (d, *J* = 9.0 Hz, 4H), 5.37 (d, *J* = 10.5 Hz, 2H), 3.87 (s, 6H), 2.98 (t, *J* = 7.1 Hz, 4H), 2.86 (t, *J* = 7.2 Hz, 4H), 2.49 (dd, *J* = 9.5, 5.8 Hz, 2H), 1.92 – 1.67 (m, 8H), 1.22 (dd, *J* = 7.3, 3.2 Hz, 2H), 1.14 (d, *J* = 6.7 Hz, 3H), 0.92 (t, *J* = 7.4 Hz, 3H). ^{13}C NMR (100 MHz, MeOD) δ 166.43, 162.36, 157.90, 146.37, 144.90, 142.09, 137.68, 133.04, 131.64, 128.76, 126.09, 123.51, 122.57, 120.78, 120.28, 118.98, 113.83, 69.49, 54.67, 38.98, 37.70, 26.54, 25.47, 24.51, 23.86, 14.33, 9.04. ^{11}B NMR (128 MHz, MeOD) δ 0.87 (t, *J* = 31.8 Hz)

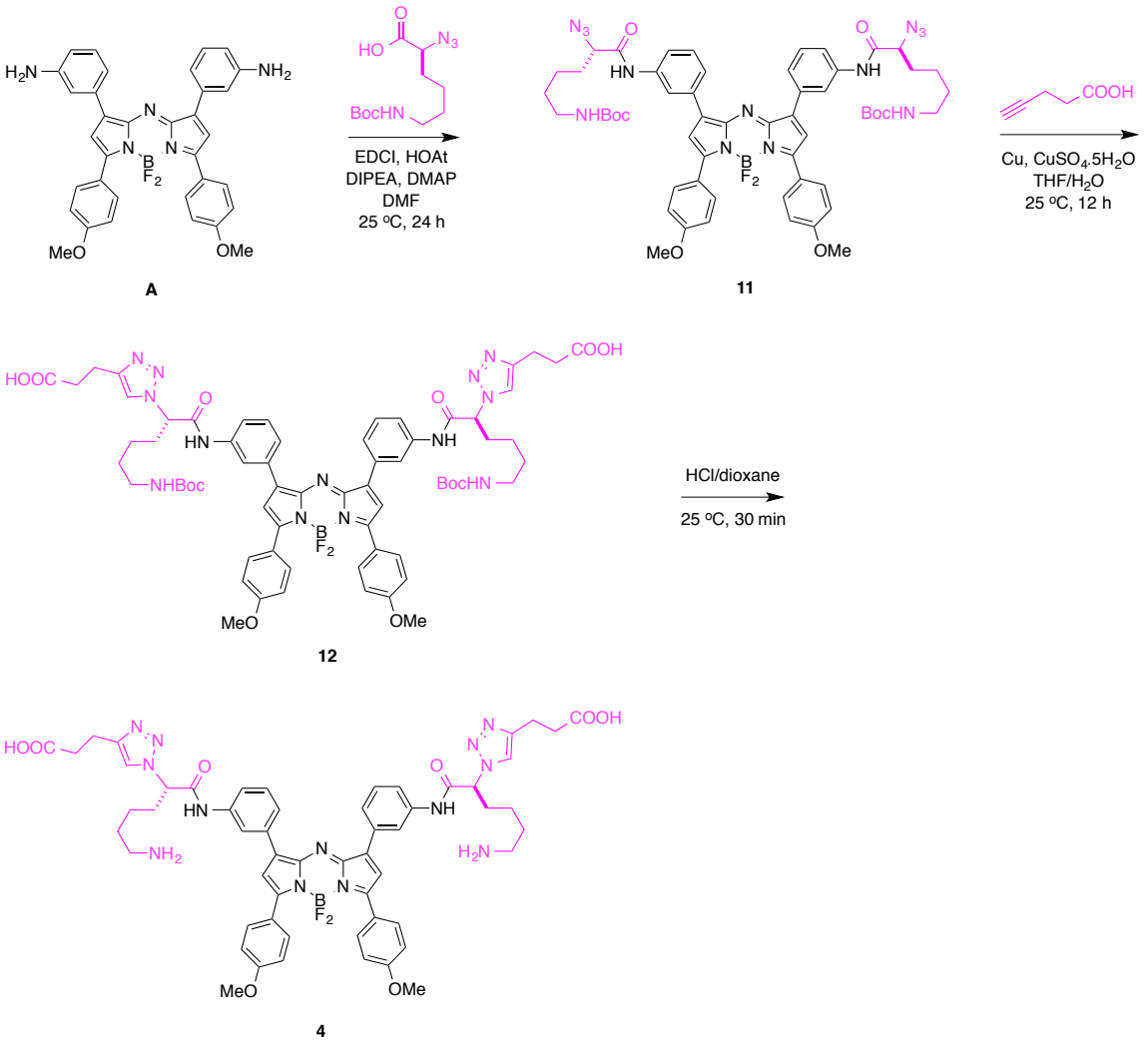

*Synthesis of compound **11***

EDCI (210.9 mg, 1.10 mmol) and HOAt (152.4 mg, 1.12 mmol) were added to a suspension of Boc protected lysine azide (272.3 mg, 1.00 mmol) in 4 mL DMF at 0 °C. After stirring at 0 °C for 30 min, **A** (117.2 mg, 0.127 mmol) was added to the above suspension followed by DIPEA (557 µL, 413.6 mg, 3.20 mmol) and trace amount of DMAP. The resulting solution was stirred at 0 °C for 1 h and warmed to 25 °C and

stirred for overnight. Ethyl acetate (ca. 100 ml) was added to the reaction mixture, and the resulting suspension was washed with 5%HCl, H_2O, sat. $NaHCO_3$ and brine. The organic layer was separated, dried with Na_2SO_4, and concentrated to afford green solid. The crude product was purified by column chromatography on silica gel, and eluted with a mixture of CH_2Cl_2 and methanol (100:4, v/v) afforded the desired **11** (299.1 mg, 91%) as green solid. ^{1}H NMR (400 MHz, $CDCl_3$) δ 8.27 (s, 2H), 8.06 (d, *J* = 6.8 Hz, 6H), 7.80 (d, *J* = 7.4 Hz, 4H), 7.39 (td, *J* = 7.8, 3.7 Hz, 2H), 7.03 (d, *J* = 3.0 Hz, 2H), 7.01 – 6.93 (m, 4H), 4.70 (s, 2H), 4.05 (s, 2H), 3.89 (s, 6H), 3.14 (s, 4H), 2.06 – 1.90 (m, 4H), 1.64 – 1.48 (m, 8H), 1.45 (s, 18H). ^{13}C NMR (101 MHz, $CDCl_3$) δ 167.68, 162.07, 158.13, 156.09, 145.20, 142.03, 137.53, 133.25, 131.73, 129.12, 125.69, 123.89, 120.61, 120.55, 118.96, 114.26, 79.22, 64.13, 55.42, 40.18, 31.84, 29.70, 28.41, 22.62. ^{11}B NMR (128 MHz, $CDCl_3$) δ 0.98 (t, *J* = 31.7 Hz).

*Synthesis of compound **12***

To a solution of **11** (110.2 mg, 0.100 mmol) and alkyne (19.6 mg, 0.200 mmol) in 24 mL dry THF were added Cupper powder (12.7 mg, 0.200 mmol) and $CuSO_4$ (0.1 equiv, from 0.05 M aqueous solution) at 25 °C. The mixture was stirred at 25 °C for 2 days. The reactions were monitored by TLC. After the reaction was done, the solvent was removed under reduced pressure and 0.2 N HCl was added to the residue. After extracted with ethyl acetate three times, the combined organic phase was washed with 0.05M EDTA and brine. The organic layer was separated and dried over Na_2SO_4, and concentrated to afford desired **12** (108.7 mg, 84%) as green solid.

*Synthesis of compound **4***

12 (12.9 mg, 0.01 mmol) was dissolved in 100 µL HCl in 1,4-dioxane (4 M), and the reaction mixture was stirred at 25 °C for 30 min. After the reaction was done, the solvent was removed under reduced pressure to give desired product **4** as green solid quantitatively. The purity was confirmed by analytical HPLC (C18 column, CH_3CN-H_2O 10-90% with 0.1% acetic acid). ^{1}H NMR (400 MHz, $CDCl_3$) δ 9.38 (s, 2H), 8.13 (s, 2H), 8.02 (d, *J* = 8.0 Hz, 4H), 7.77 (d, *J* = 29.8 Hz, 4H), 7.52 (s, 2H), 7.37 – 7.12 (m, 2H), 6.96 (d, *J* = 8.5 Hz, 6H), 5.49 (s, 2H), 4.92 (s, 2H), 3.86 (s, 6H), 3.29 – 2.86 (m, 4H), 2.62 (d, *J* = 5.0 Hz, 4H), 2.22 (d, *J* = 27.6 Hz, 4H), 1.98 (dt, *J* = 12.7, 6.3 Hz, 2H), 1.53 (dd, *J* = 21.1, 15.0 Hz, 2H), 1.43 (s, 18H), 1.36 – 1.09 (m, 6H), 0.93 (d, *J* = 6.0 Hz, 12H). ^{13}C NMR (101 MHz, $CDCl_3$) δ 166.89, 162.01, 158.02, 156.27, 147.60, 145.19, 142.20, 137.65, 133.21, 131.71, 128.94, 126.07, 123.87, 121.07, 120.79, 119.04, 114.22, 79.24, 64.37, 55.39, 40.03, 34.79, 32.84, 29.24, 28.60, 28.43, 22.84, 22.32, 22.29. ^{11}B NMR (128 MHz, $CDCl_3$) δ 0.87 (t, *J* = 31.9 Hz). ^{19}F NMR (376 MHz, $CDCl_3$) quartet at δ -131.76. MALDI-HRMS: theor 1258.6553 found 1258.6613 $[M-H]^-$

APPENDIX C

AZA-BODIPY DYES WITH ENHANCED HYDROPHILICITY

B.1 Introduction

Attempts to make a diamino disulfonic acid derivative of an aza-BODIPY showed it was difficult to add BF_2 to a disulfonated aza-dipyrromethene, and sulfonation of an aza-BODIPY resulted in loss of the BF_2 fragment. We conclude the electron-deficient character of aza-BODIPY dyes destabilizes them relative to BODIPY dyes. Consequently, sulfonation of the aza-BODIPY core is not a viable strategy to increase water solubility. This assertion was indirectly supported via stability studies of a BODIPY and an aza-BODIPY in aqueous media. To afford the desired compound type, an aza-BODIPY with two amino and two sulfonic acid groups was prepared via modification of the aryl substituents with cysteic acid.

Relative to most BODIPY dyes, fluors in the aza-BODIPY series[221-222,267] tend to have longer wavelength absorption and fluorescence emission maxima (Figure C-1).[94,188-189] This characteristic is advantageous for many potential applications of these materials as probes in biological systems, but it comes at a cost. Red-shifted absorption and emission in aza-BODIPY dyes seems to depend on the presence of aryl substituents in the 1,3,5,7-positions making the heterocycles highly hydrophobic and inclined to aggregation in aqueous media.

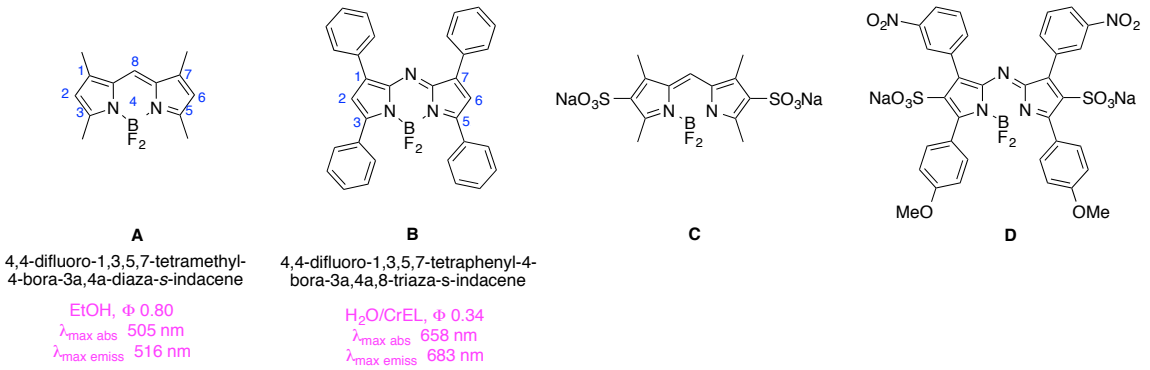

Figure C-1. Structures of BODIPYs and aza-BODIPYs.

The literature describes some efforts to increase the hydrophilicity of aza-BODIPY dyes based on functionalization of the aryl substituents.[268] Modified aza-BODIPYs resulting from those efforts feature ammonium salts,[269] oligoethylene glycol fragments,[270] sulfonic and carboxylic acids,[269] and carbohydrate derivatives.[271] We required a hydrophilic aza-BODIPYs with amino functionality on the aryl group that could be coupled with activated carboxylic acids to produce derivatized optical imaging agents. Negatively charged dyes were also attractive to us because they are intrinsically repelled by negative polar head-groups on cell surfaces.

Sometime ago we refined[272] a procedure[273-274] for adding sulfonic acid groups into the BODIPY 2- and 6-positions, that gave the water-soluble BODIPY dye **C**. Consequently, it seemed logical to apply the same approach to obtain the aza-BODIPY disulfonic acid **D**. This *Appendix* describes why that approach does *not* work, and an alternative that enables sulfonic acid and amino functionalities to be introduced into the aza-BODIPY system, via functionalization of the aryl groups.

C.2 Results and discussions

Treatment of the dinitro-aza-dipyrromethene (aza-DIPY; see SI) **1** under the sulfonation conditions for BODIPY dyes,[272] gave predominantly the mono- or di-sulfonated DIPY systems **2a** and **2b**, according to the equivalents of chlorosulfonic acid used (Scheme C-1). Sulfonate **2a** was isolated by chromatography on silica gel, whereas 2b was obtained more straightforwardly by precipitation from dichloromethane. Unfortunately, treatment of the DIPY systems 2 under a variety of conditions (Table C-S1) gave no trace of the corresponding aza-BODIPY dyes as monitored via fluorescence spectroscopy in water (with and without Triton X-100 to increase water solubility) or via ^{11}B NMR of the crude material.

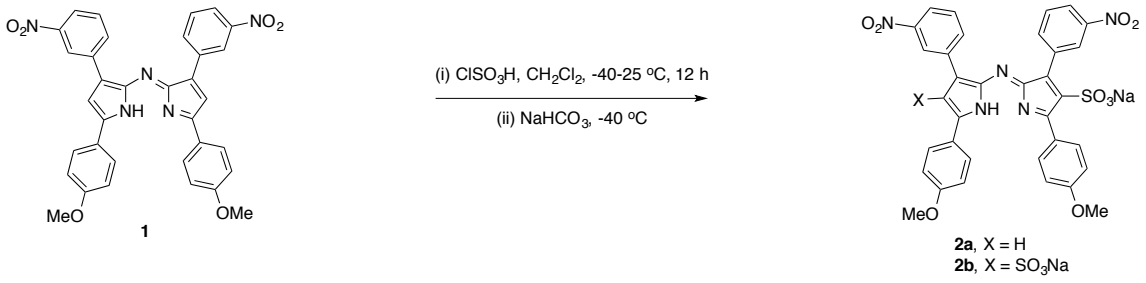

Scheme C-1. Synthesis of disulfonated aza-DIPY.

Scheme C-2 describes an alternative approach to compound **D** that was also unsuccessful. Treatment of the aza-BODIPY **3** with excess chlorosulfonic acid led to the aza-DIPY **2b** *corresponding to loss of the BF_2 fragment.* ^{11}B NMR, fluorescence and absorption spectroscopy (and ESI-MS), of the *crude* product from this reaction

showed no evidence that an aza-BODIPY was present, indicating loss of the BF_2 fragment was *not* caused by the work-up procedure (Fig. C-S1). Several variations of the conditions for sulfonation of **3** also gave the same results, *ie* formation of the aza-DIPY **2** and not the anticipated aza-BODIPY **D**.

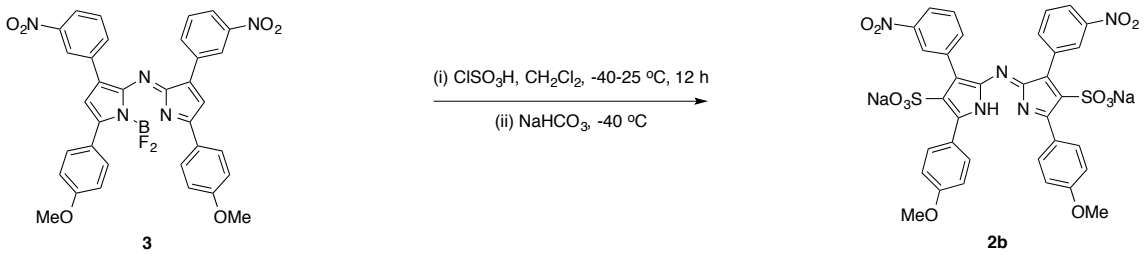

Scheme C-2. Attempt to sulfonate aza-BODIPY.

Based on the observations above, we decided to re-focus on obtaining the cysteic acid derivative **4** via the procedure outlined in Scheme 3. Thus hydrogenation of **1** then reaction with BF_3 gave the diamine **5** which was conveniently coupled with BOC-protected cysteic acid to give the disulfonic acid **6** (isolated by MPLC on a reverse phase column) then the diamino-disulfonic acid **4** after a deprotection step (in which no further purification procedure was necessary).

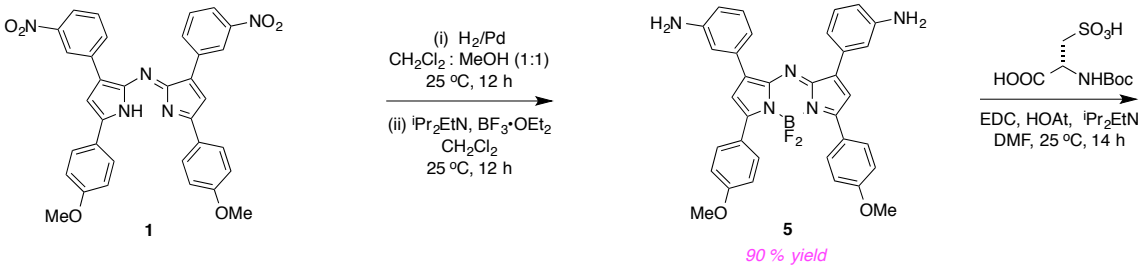

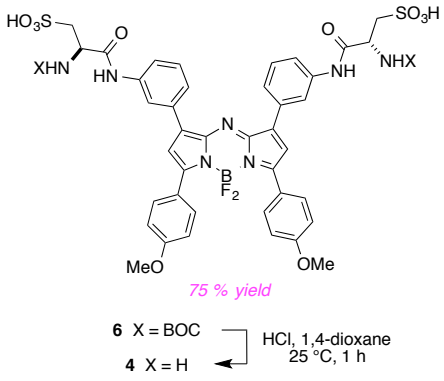

Scheme C-3. Synthesis of aza-BODIPY containing cysteic acid.

Disulfonic acid **4** appears to give a homogeneous bright green solution in water or 1 mM PBS buffer. The UV absorbance of the dye is broad and there is no significant fluorescence (Fig. C-2a). However, the UV absorbance of this dye sharpens considerably, and it becomes significantly more fluorescent, when 0.1 % Cremophor (CrEL) is added (F 0.34 ± 0.010, Fig C-2b); CrEL is a non-ionic surfactant that is commonly used as an excipient in pharmaceutical formulations. Near-IR concentration dependence of **4** in PBS buffer (without additives) was used to probe for further evidence of aggregation, but no significant dependence on the fluor concentration was observed (Fig. C-S3).

A UV-based method from the literature[275] was used to compare the aqueous thermodynamic equilibrium solubilities of dyes **3** - **5**. Thus 0.1 M stock solutions of the test compounds in DMSO were diluted with PBS to 0 – 100 mM in a 96-well plate, so that the highest concentration contained only 1 % DMSO. The plate was shaken horizontally for 6 h at 25 ^{o}C and kept overnight for equilibration. Thereafter, the plate

was centrifuged at 1000 rpm for 20 min, the supernatant was pipetted into a 96-well UV-transparent plate and analyzed using a microplate reader, l = 680 nm, *vs* a blank (Fig C-2c).

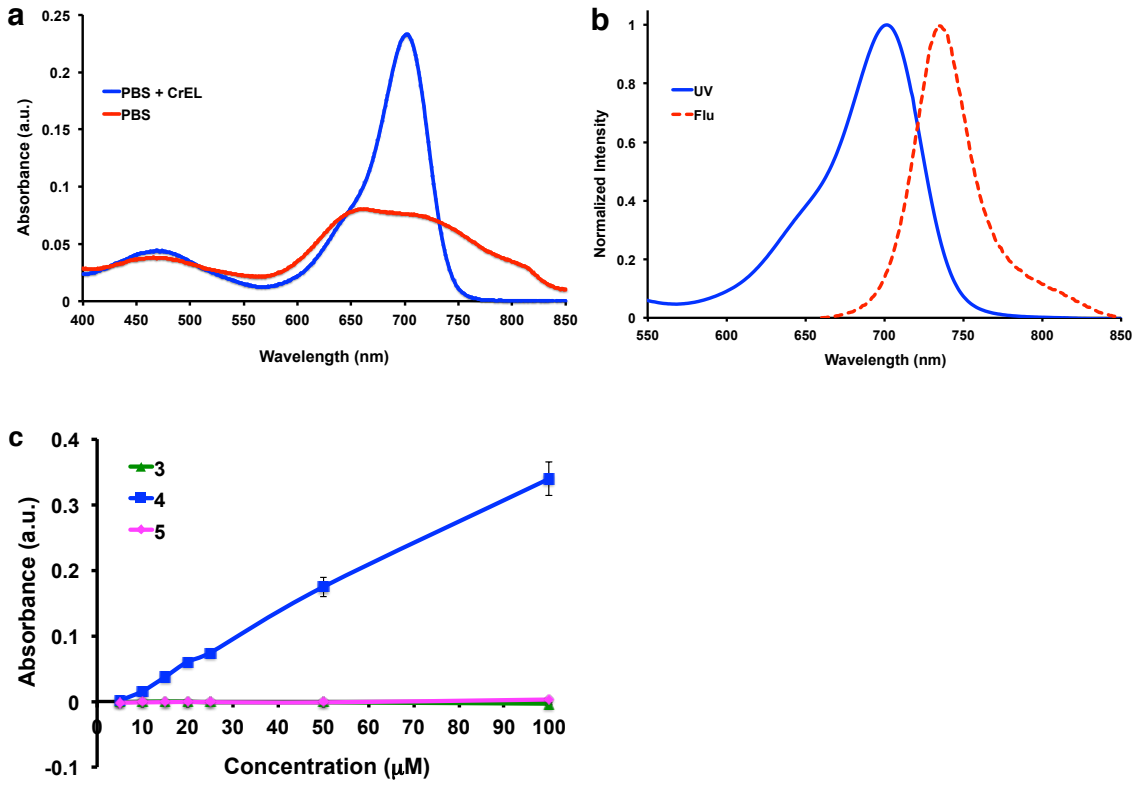

Figure C-2. **a** UV and **b** fluorescence (excitation l 650 nm) spectra of compound **4** in pH 7.4 PBS + 0.1 % CrEL. **c** Solubility profile of **3**, **4** and **5** in PBS at pH 7.4 (analyses performed in triplicate for each compound).

Data from the experiments described above show the featured sulfonic acid **4** is significantly more hydrophilic than the dinitro- and diamino-compound **3** and **5** (Fig. C-2c). In fact, the disulfonic acid **4** is soluble in PBS pH 7.4 up to 200 μM and even more

soluble (more than 1 mM) in carbonate buffer pH 9 (Fig. C-S4a). At pH 4, the solubility of **4** decreases (<20 μM) whereas **5** is more soluble (<50 μM, Fig. C-S4b).

Compound **5** is only very weakly fluorescent, and no staining was observed via confocal microscopy when this solution was incubated with 4T1 murine breast cancer cells. After acylation to obtain disulfonic acid BODIPY **4**, bright fluorescent was observed in 0.1 % CrEL/PBS, and the fluor was clearly internalized into lysosomes of the same cells (Figure C-3).

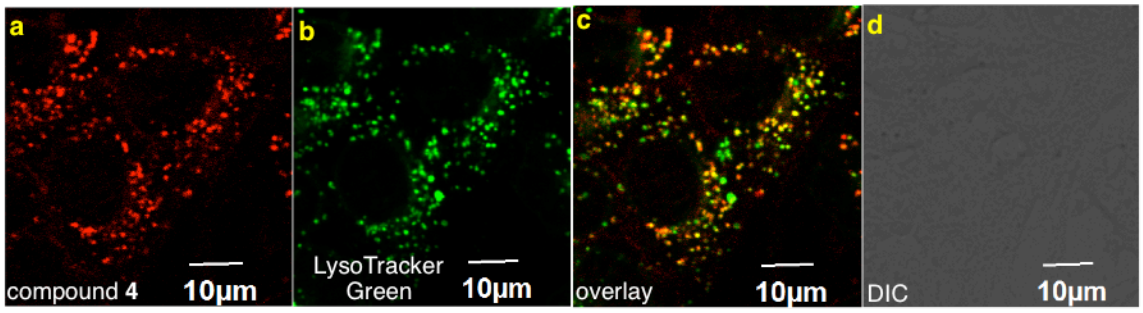

Figure C-3. **a** Compound 4 is readily internalized by murine 4T1 breast cancer cells. A LysoTracker dye (**b**) colocalized with the intracellular fluorescence (**c**). **d** Bright field image for reference.

Failure to obtain the sulfonic acid system **D** led us to hypothesize the aza-BODIPY framework with 2- and 6-sulfonic acids is too electron deficient to hold the BF_2 fragment. This would explain why the BODIPY disulfonic acid **C** is isolable whereas we were not able to obtain **D**. Extrapolating this logic, we also hypothesized that aza-BODIPY dyes generally would be less stable than BODIPY systems *even if*

there were no 2-, 6-substituents. Consequently, the stabilities of representative compounds were compared (Fig. C-4).

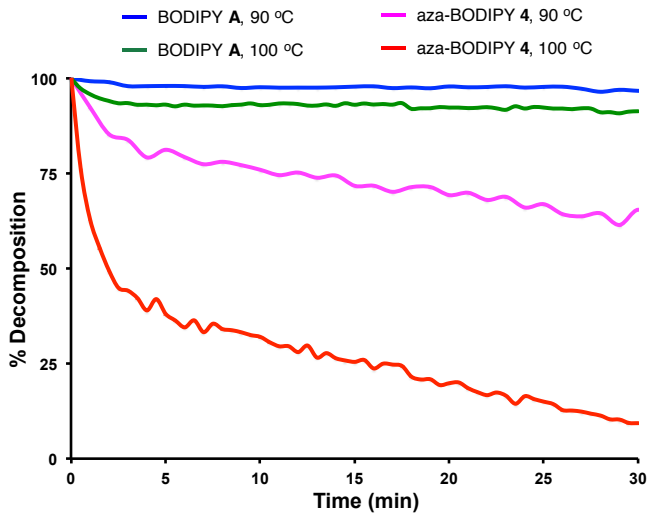

Figure C-4. Fluorescence studies to monitor stabilities of the fluors. The $t_{1/2}$ of aza-BODIPY **4** is 50 min at 90 ^{o}C and 2 min at 100 ^{o}C, whereas BODIPY **A** gave less than 10 % decomposition under the same conditions.

Heating the tetramethyl BODIPY **A** and our hydrophilic aza-BODIPY **4** in non-deoxygenated 1:1 dioxane:water (Fig. C-4) proved BODIPY **A** persisted at 90 and 100 °C, but the aza-BODIPY system showed significant decomposition after 30 min at 90 °C, and was mostly decomposed under the same conditions but at 100 °C.

C.3 Conclusions

Our failure to obtain the disulfonic acid **D** illustrates a difference between the chemistry of BODIPY and aza-BODIPY dyes; BODIPY systems are more electron-rich and can support strong electron withdrawing groups attached directly to the core,

whereas similar electron withdrawing groups may destabilize aza-BODIPY systems with respect to bonding to the BF_2 fragment. Consistent with this, the diformyl BODIPY **E** and the formyl aza-BODIPY **F** are known, but same authors have reported being unable to form the diformyl aza-BODIPY **G**.[276] Our interpretation of these observation is that the diformyl aza-BODIPY **G** may be unstable, even though the corresponding BODIPY is known. The fact that the monoformylated aza-BODIPY **F** was isolated was possible even though monosulfonation was not, because formyl groups are less electron withdrawing.[277]

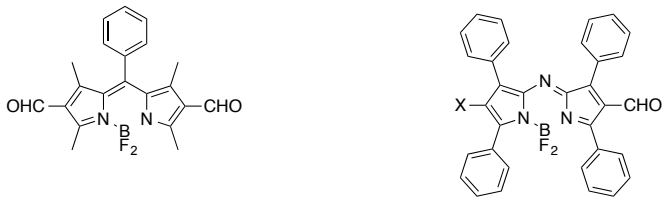

E

F, X = H
G, X = CHO

Figure C-5 The diformyl BODIPY **E** and the mono-formyl aza-BODIPY **F** are known, but the diformyl aza-BODIPY has been proven difficult to prepare.

Parenthetically, we note that, consistent with the observations above, attempts to derivatives of **3** with *para*- rather than *meta*-nitro groups failed because the BF_2 fragment could not be inserted.

The negatively charged cysteic acid derivative **4** is significantly more hydrophilic than its parent diamine **5**, and it has amino groups for functionalization with carboxylic acid derivatives. Use of neutral carboxylic acid derivatives for such functionalization

will give products with two negative charges overall. This is desirable because such negatively charged fluorescent derivatives tend to have an intrinsic repulsion for negative head groups on the cell membrane. Intrinsic repulsion reduces non-specific binding of conjugates and facilitates studies of aza-BODIPYs designed to selectively bind certain cell surface receptors.

C.4 Acknowledgement

We thank The National Institutes of Health (GM087981), The Robert A. Welch Foundation (A-1121), and High Impact Research (HIR (UM.C/625/1/HIR/MOHE/MED/17 & UM.C/625/1/HIR/MOHE/MED/33) from the Ministry of Higher Education, Malaysia, for financial support. The NMR instrumentation at Texas A&M University was supported by a grant from the National Science Foundation (DBI-9970232) and the Texas A&M University System. The Olympus FV1000 confocal microscope acquisition was supported by the Office of the Vice President for Research at Texas A&M University.

C.5 Supporting materials

General Procedures

All reactions were carried out under an atmosphere of dry argon. Glassware was oven-dried prior to use. Unless otherwise indicated, common reagents or materials were obtained from commercial source and used without further purification. Dry DMF, (<50 ppm water) was purchased from EMD. Tetrahydrofuran (THF), acetonitrile (MeCN),

dichloromethane (CH_2Cl_2), and methanol (MeOH) were dried by MBRAUN solvent drying system. Other solvents and reagents were used as received.

NMR spectra were recorded on a Bruker-400 MHz spectrometer (^1H at 400 MHz and ^{13}C at 100 MHz) at room temperature unless otherwise mentioned. Chemical shifts of ^1H NMR spectra were recorded and reported in ppm from the solvent resonance ($CDCl_3$ 7.26 ppm, CD_3OD 3.30 ppm, DMSO-d_6 2.50 ppm). Data are reported as follows: chemical shift, multiplicity (s = singlet, br = broad, d = doublet, t = triplet, q = quartet, m = multiplet), coupling constants, and number of protons. Proton decoupled ^{13}C NMR spectra were also recorded in ppm from tetramethylsilane (TMS) resonance ($CDCl_3$ 77.0, CD_3OD 49.1, DMSO-d_6 39.5 ppm). Analytical thin layer chromatography (TLC) was performed on EM Reagents 0.25 mm silica-gel 60-F plates, and visualized with UV light. Flash chromatography was performed using silica gel 60 (230–400 mesh). MS were measured under ESI or MALDI conditions.

Syntheses Of Sulfonated aza-BODIPY Derivatives

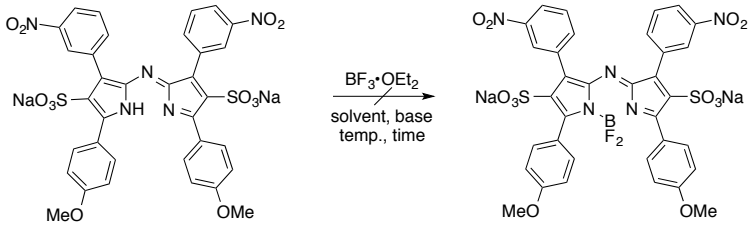

Table C-S1. Conditions to form BF_2 complex.

Solvent	Base	Temperature (^{o}C)	Time (h)
Toluene	$^{i}Pr_2EtN$	80	12
CH_2Cl_2	$^{i}Pr_2EtN$	25	12
CH_2Cl_2	Et_3N	25	12
CH_2Cl_2	NaH	25	12
$CH_2CH_2Cl_2$	$^{i}Pr_2EtN$	60	12

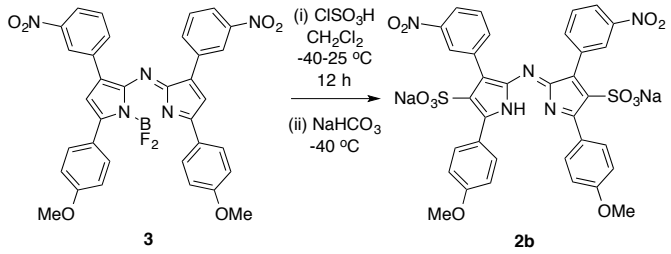

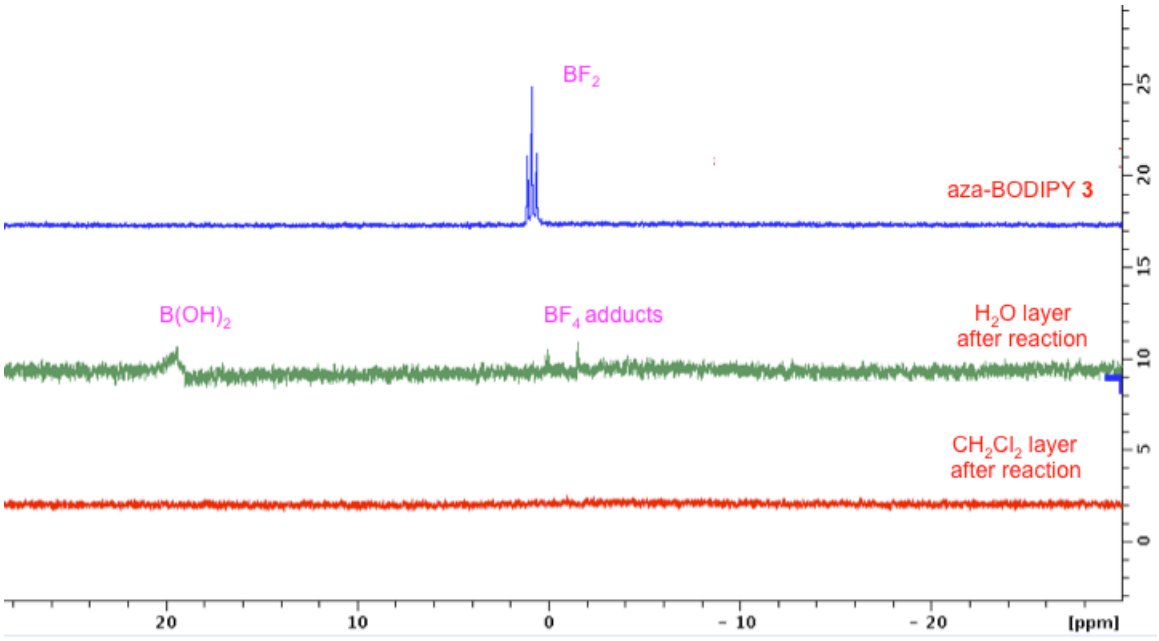

Figure C-S1. ^{11}B NMR of the crude product showed the loss of the BF_2 fragment.

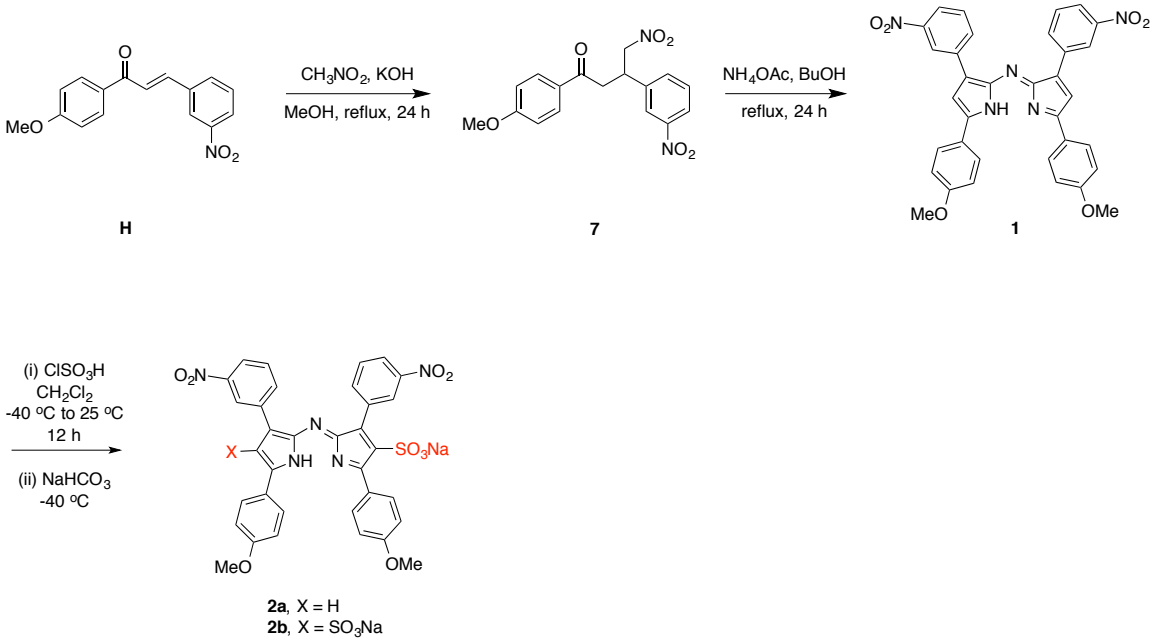

Scheme C-S1.

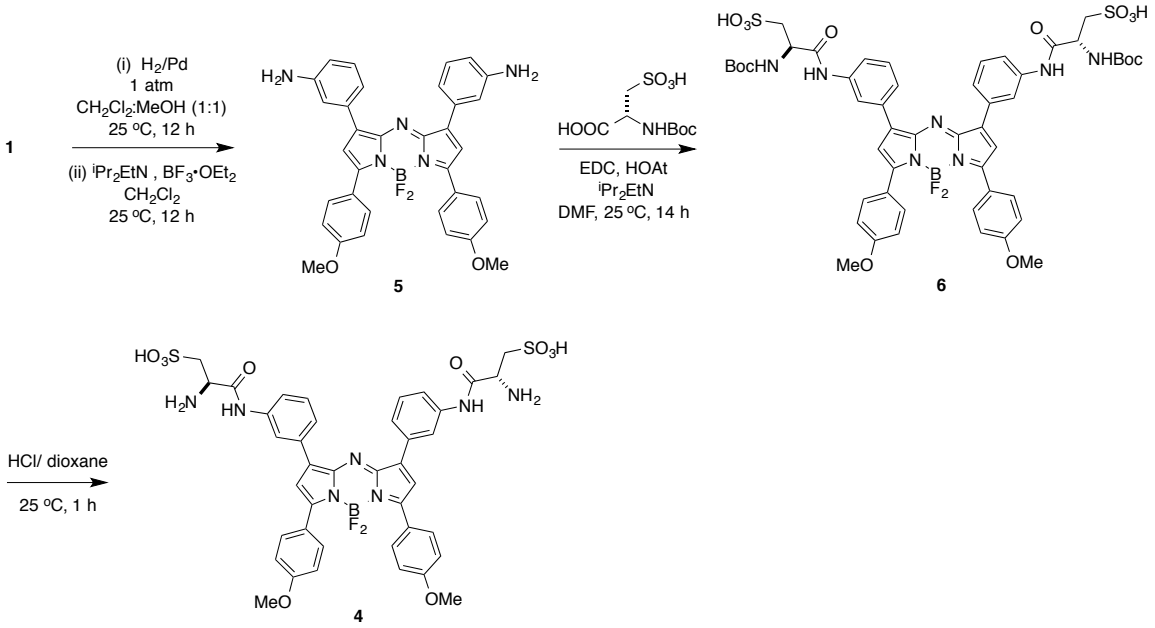

Scheme C-S2.

1-(4-methoxyphenyl)-4-nitro-3-(3-nitrophenyl)butan-1-one (7).

Potassium hydroxide (33.6 g, 60 mmol) was added to a solution of chalcone **H** (17 g, 60 mmol) in MeOH (250 mL) at 25 ^{o}C. Nitromethane (64 mL, 1.2 mol) was added to the reaction mixture, and then the reaction was heated to reflux at 78 ^{o}C for 24 h. After the reaction was cooled to 25 ^{o}C, HCl (0.2 N) was added to neutralize. Precipitate was filtered out and washed with cold MeOH. The product was obtained as slightly brown solid (14.5 g, 70 % yield) and used without further purification. ^{1}H NMR (400 MHz, $CDCl_3$) δ 8.21 (s, 1H), 8.19 (d, J = 7.7 Hz, 1H), 7.92 (d, J = 8.9 Hz, 2H), 7.69 (d, J = 7.7 Hz 1H), 7.54 (dd, J = 7.9, 7.9 Hz, 1H), 6.95 (d, J = 8.9 Hz, 2H), 4.89 (m, 1H), 4.75 (m, 1H), 4.38 (m, 1 H), 3.90 (S, 3 H), 3.47 (d, J = 6.9 Hz, 2H). ^{13}C (100 MHz, $CDCl_3$) δ 194.3, 164.1, 141.5, 134.3, 130.3, 130.2, 130.0, 129.1, 122.9, 122.2, 114.0, 79.0, 55.5, 40.7, 39.0. MS (ESI+) calcd for $C_{17}H_{17}N_2O_6$ $\{M+H\}^+$ 345.1087, found 345.1096.

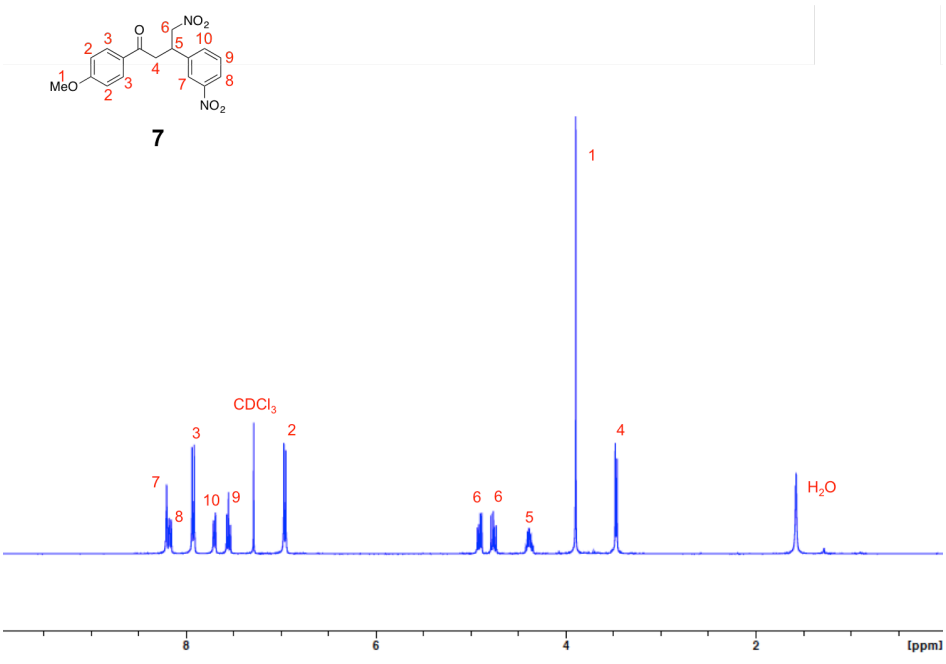

^{1}H-NMR of compound 7

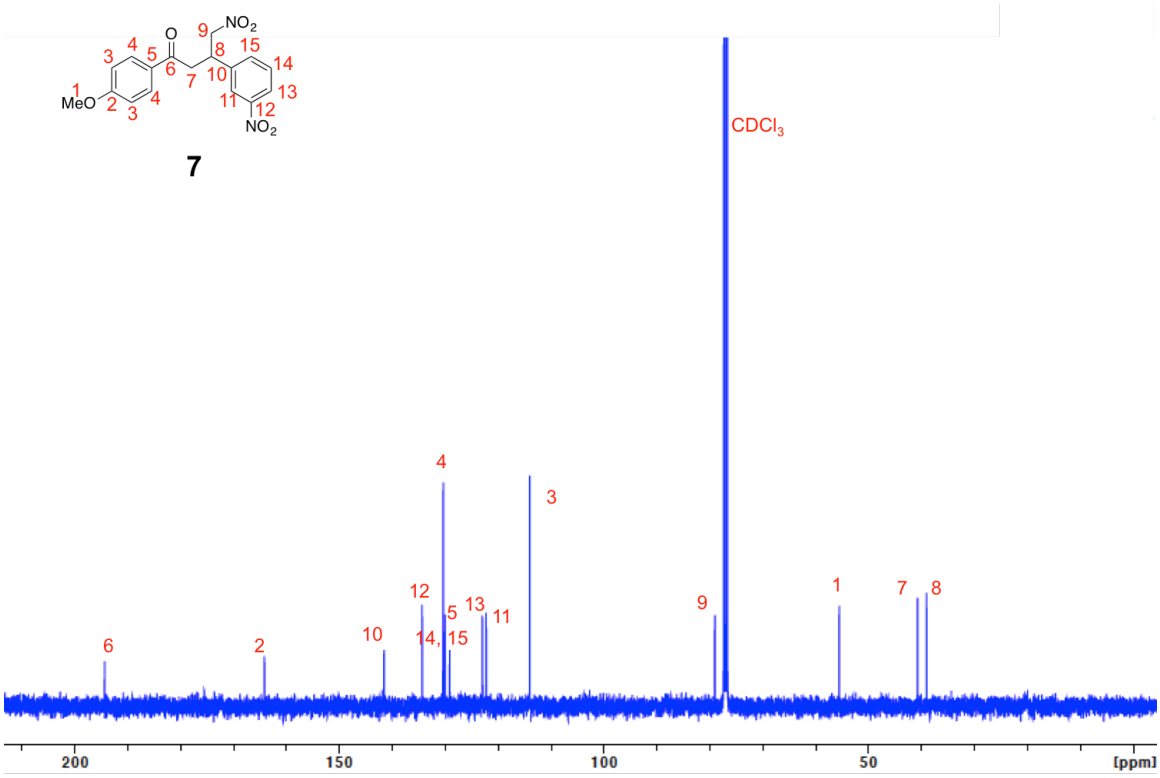

^{13}C-NMR of compound 7

(*Z*)-5-(4-methoxyphenyl)-*N*-(5-(4-methoxyphenyl)-3-(3-nitrophenyl)-1*H*-pyrrol-2-yl)-3-(3-nitrophenyl)-2*H*-pyrrol-2-imine (1).

7 (10 g, 29 mmol) was dissolved in ^{n}BuOH (300 mL). Ammonium acetate (78 g, 1 mol) was added to the solution. The reaction was heated up to reflux at 120 ºC and stirred for 24 h. The mixture was cooled to 40 ºC, then the solvent was removed. The residue was precipitated in cold EtOH, the solid was filtered to give dark solid **1** (9 g, 52 % yield). The product was used without further purification. NMR spectra cannot be obtained from compound **1** due to solubility. However, after complexation with BF_2 to yield compound **3**, the NMR was obtained nicely. ^{1}H NMR (400 MHz, $CDCl_3$) δ 8.92 (s, 2H),

8.37 (d, J = 7.2 Hz, 2H), 8.28 (d, J = 8.0 Hz, 2H), 8.14 (d, J = 8.6 Hz, 4H), 7.70 (t, J = 7.8 Hz, 2H), 7.20 (s, 2H), 7.06 (d, J = 8.6 Hz, 4H), 3.91 (s, 6H). ^{13}C (100 MHz, CD_2Cl_2) δ 161.6, 158.3, 155.5, 149.4, 148.7, 141.3, 140.8, 135.0, 133.7, 133.3, 132.4, 131.5, 130.7, 130.3, 130.2, 128.9, 124.2, 124.1, 124.0, 122.5, 122.3, 117.6, 116.7, 114.8, 114.6, 55.8. HRMS(ESI-) calcd for $C_{34}H_{24}BClF_2N_5O_6$ {M+Cl}$^-$ 682.1476, found 682.1464.

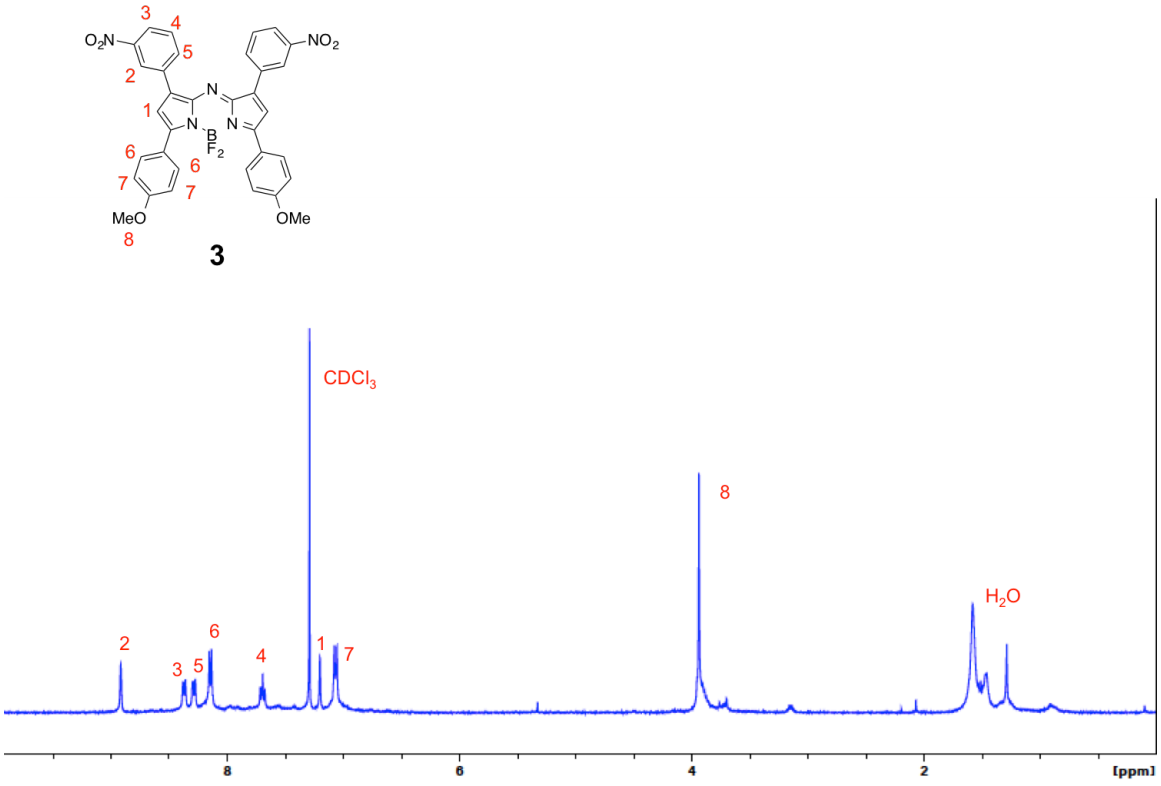

^{1}H-NMR of compound 3

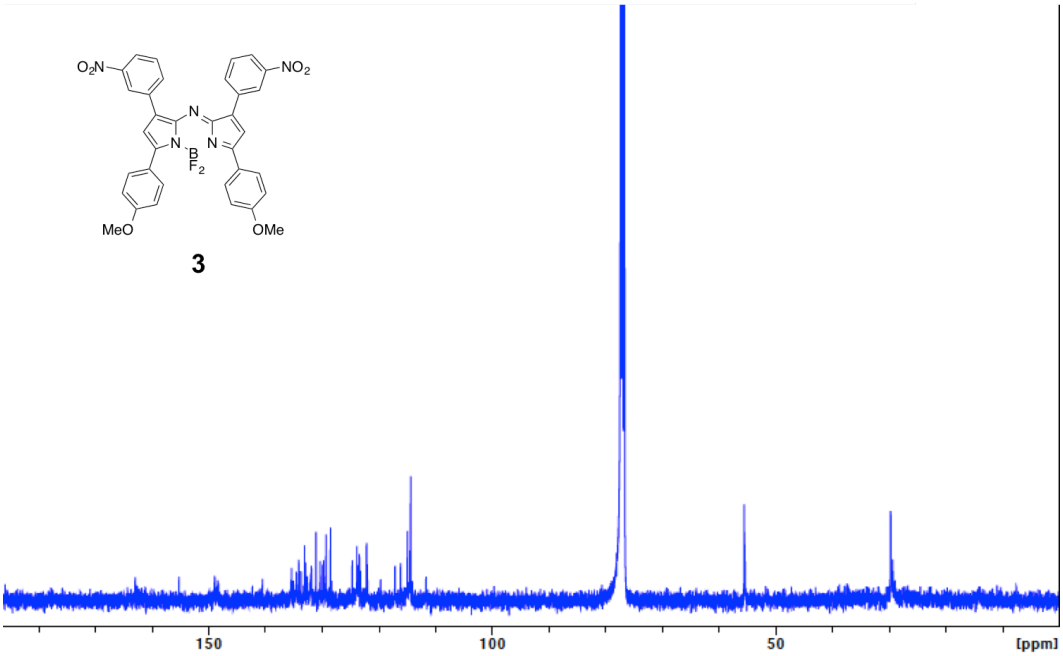

^{13}C-NMR of compound 3

Synthesis of disulfonic acid (2a, 2b)

1 (30 mg, 0.05 mmol) was dissolved in CH_2Cl_2 (5.5 mL) and the solution was cooled to -40 ^oC. Solution of chlorosulfonic acid (1 eq. for **2a** and 4 eq. for **2b**) in CH_2Cl_2 (0.5 mL) was slowly added to the solution over 5 min at -40 ^oC. The mixture was slowly warmed to 25 ^oC and stirred for 5-12 h. The reaction was quenched with sat. $NaHCO_3$ at -40 ^oC. Organic layer was separated and the crude product was purified by flash silica chromatography eluting with CH_2Cl_2:MeOH (85:15) to yield 20 mg (60 %) of **2a** as a purple powder. ^{1}H NMR (400 MHz, $CDCl_3$) δ 8.54 (s, 2H), 8.18 (d, J = 7.2 Hz, 1H), 8.18 (d, J = 7.6 Hz, 1H), 8.13 (d, J = 7.6 Hz, 1H), 8.06 (d, J = 7.2 Hz, 1H), 7.95 (d, J = 7.8 Hz, 2H), 7.91 (d, J = 8.1 Hz, 2H), 7.48 (t, J = 7.6 Hz, 1H), 7.37 (s, 1H), 7.34-7.8 (m, 1H, overlap with $CDCl_3$) 7.01-6.97 (m, 4H), 3.86 (s, 6H). HRMS (ESI-) calcd for

$C_{34}H_{24}N_5O_9S^-$ {M-Na}$^-$ 678.1300, found 678.1321. For **2b**, the product was precipitated from the reaction. The precipitate was filtered to give a purple powder 60 mg, 79 % yield. NMR cannot be obtained due to solubility. HRMS (ESI-) calcd for $C_{34}H_{23}N_5NaO_{12}S_2^-$ {M-Na}$^-$ 780.0676, found 780.0640.

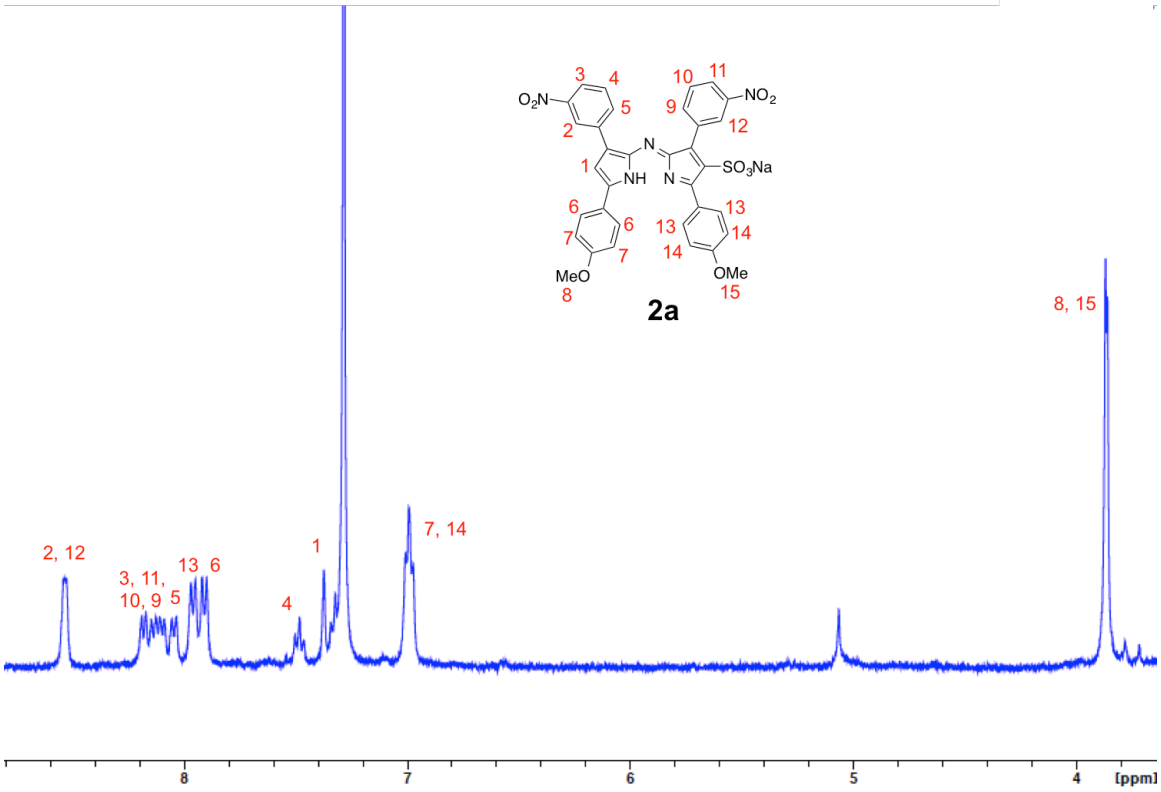

2a

^{1}H-NMR of compound 2a

3,3'-(5,5-difluoro-3,7-bis(4-methoxyphenyl)-5*H*-4λ^4,5λ^4-dipyrrolo[1,2-*c*:2',1'-*f*][1,3,5,2]triazaborinine-1,9-diyl)dianiline (5).

1 (1 g, 1.67 mmol) was dissolved in CH_2Cl_2 : MeOH (1:1, 30 mL). Pd/C (180 mg, 0.17 mmol) was added to the solution. The mixture was stirred under H_2 (1 atm) at 25 ^{o}C for

20 h, the reaction was followed by TLC. The product was filtered through Celite® to give dark blue solid after the solvent was removed. The solid was then dissolved in CH_2Cl_2 (200 mL), *N,N*-diisopropylethylamine (2.9 mL, 16.7 mmol) was added to the solution. The mixture was stirred at 25 °C for 20 min, BF_3•OEt_2 (3.1 mL, 25 mmol) was then added in portions and the mixture was stirred at 25 ºC for 12 h. The reaction was quenched with careful addition of H_2O (20 mL) and the system was stirred vigorously for 15 min. The organic layer was separated and washed with HCl (0.2 *N*, 1 × 10 mL), NaOH (2 *N*, 2 × 10 mL) and brine (10 mL). The organic layer was dried over $MgSO_4$, filtered, and the solvent was removed under reduced pressure. The residue was purified by flash silica chromatography eluting with EtOAc:Hexanes (3:1 to 2:1) to yield 883 mg (90 %) of **4** as a dark green solid. ^{1}H NMR (400 MHz, $CDCl_3$) δ 8.09 (d, *J* = 8.9 Hz, 4H), 7.71 (s, 2H), 7.33 (d, *J* = 7.8 Hz, 2H), 7.24 (d, *J* = 7.8 Hz, 2H), 7.03 (d, *J* = 9.8 Hz, 4H). 6.77-6.74 (m, 2H), 3.91 (s, 6H). ^{13}C (100 MHz, $CDCl_3$) δ 161.9, 158.0, 146.6, 145.3, 143.0, 133.5, 131.6, 129.4, 124.3, 119.3, 118.6, 116.4, 116.2, 114.2, 55.4. ^{11}B NMR (128 MHz, $CDCl_3$) δ 0.94 (t, *J* = 31.9 Hz, *B*F2) ppm. ^{19}F NMR (376 MHz, $CDCl_3$) δ -131.89 (q, *J* = 31.9 Hz, B*F*2). HRMS (ESI+) calcd for $C_{34}H_{29}BF_2N_5O_2$ $\{M+H\}^+$ 588.2382, found 588.2359.

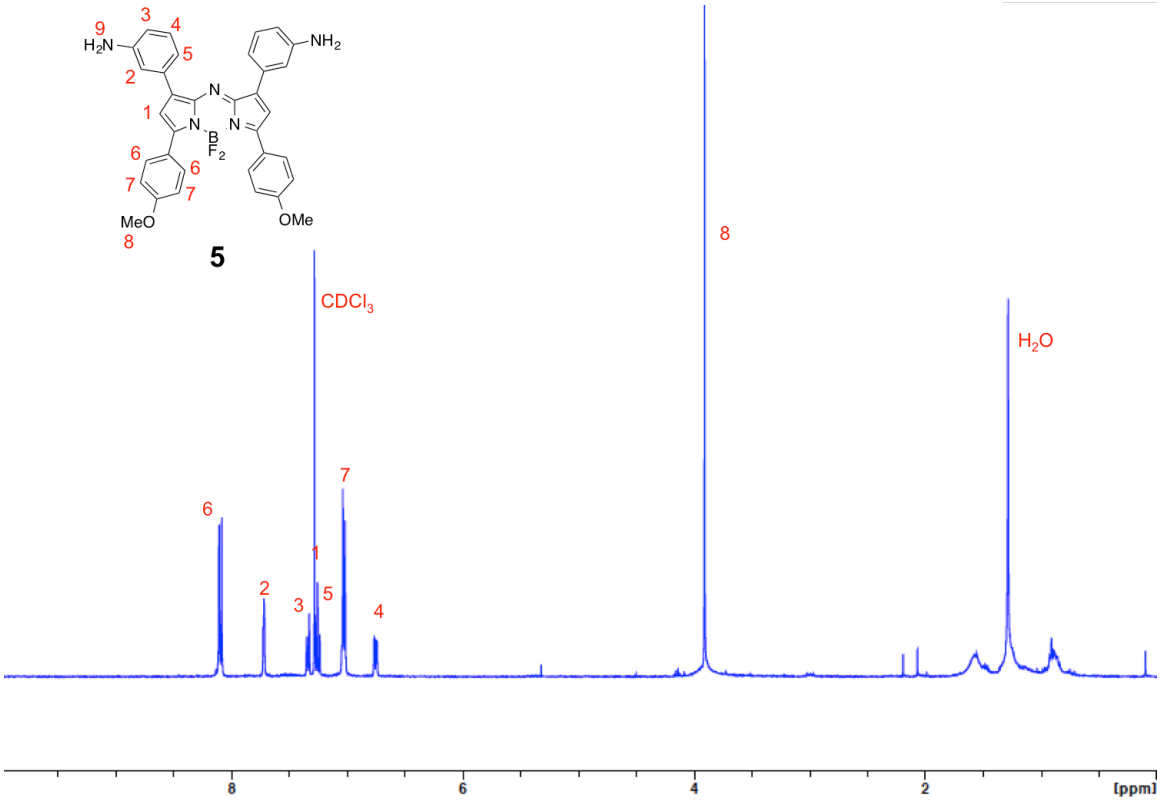

^{1}H-NMR of compound 5

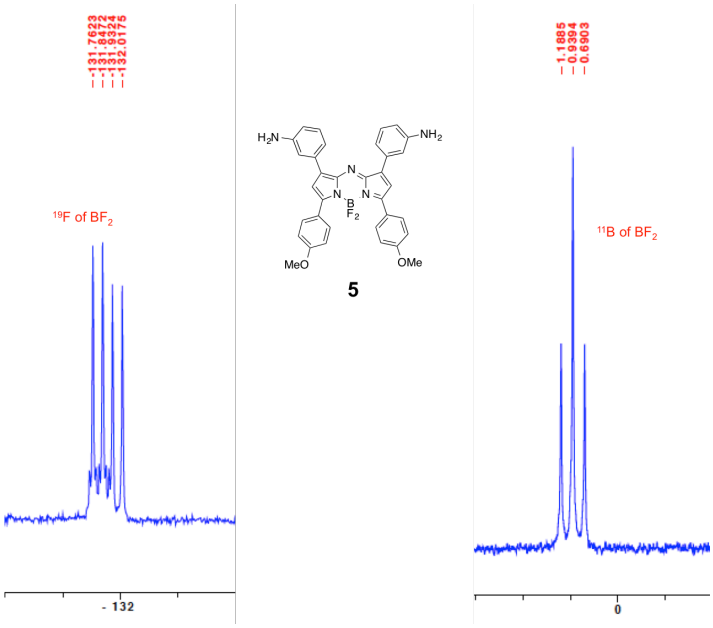

^{11}B, ^{19}F-NMR of compound 5

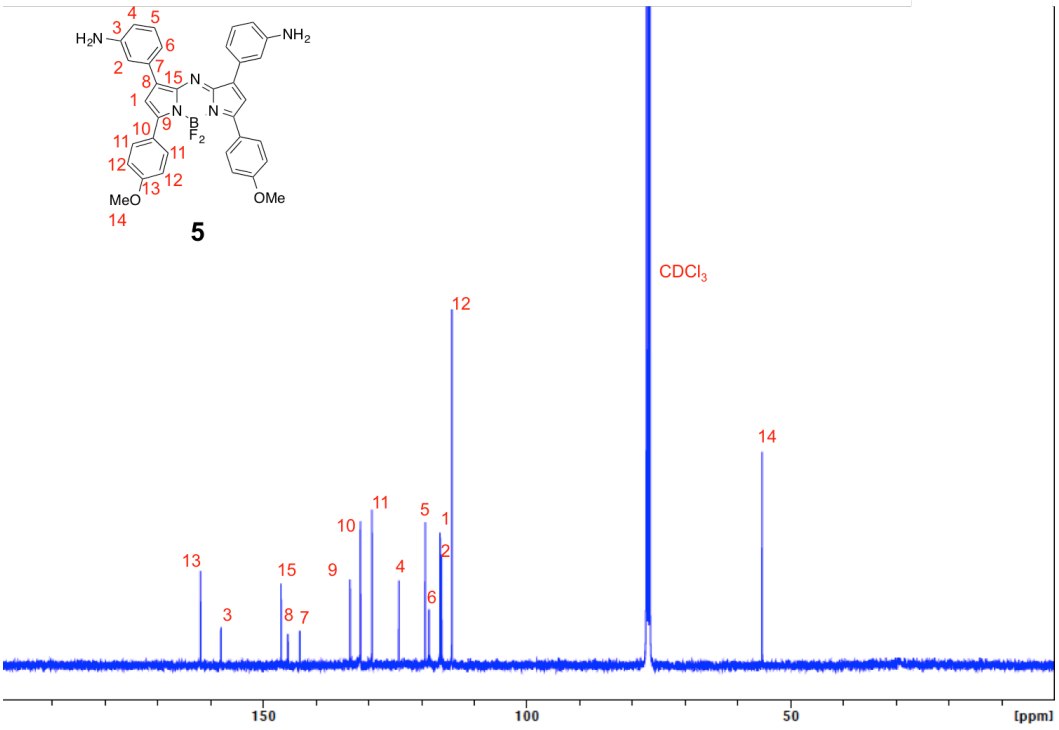

^{13}C-NMR of compound 5

(2*R*,2'*R*)-3,3'-(((5,5-difluoro-3,7-bis(4-methoxyphenyl)-5*H*-4λ^4,5λ^4-dipyrrolo[1,2-*c*:2',1'-*f*][1,3,5,2]triazaborinine-1,9-diyl)bis(3,1-phenylene))bis(azanediyl))bis(2-((*tert*-butoxycarbonyl)amino)-3-oxopropane-1-sulfonic acid) (6).

Boc-protected Cysteic acid (367 mg, 1.28 mmol) was dissolved in DMF and cooled to 0 ^{o}C. 1-Ethyl-3-(3-dimethylaminopropyl)carbodiimide, EDC (274 mg, 1.43 mmol) and 1-hydroxy-7-azabenzotriazole, HOAt (198 mg, 1.46 mmol) were added to the solution. After stirring for 30 min, compound **5** (150 mg, 0.26 mmol) was added to the reaction mixture. *N*,*N*-Diisopropylethylamine (0.45 mL, 2.6 mmol) was then added in one portion. The reaction was stirred at 25 ^{o}C for 14 h. The solvent was removed and the product was purified by reverse phase MPLC eluting with water and acetonitrile to yield

212 mg (75 %) as a greenish powder. ^{1}H NMR (400 MHz, $CDCl_3$) δ 8.14 (s, 2H), 8.08 (d, *J* = 8.6 Hz, 4H), 7.90 (d, *J* = 6.0 Hz, 2H), 7.53 (m, 2H), 7.33 (m, 2H), 7.15 (s, 2H), 6.98 (d, *J* = 8.6 Hz, 4H), 3.86 (s, 6H), 3.62-3.59 (m, 2H), 3.17-3.11 (m, 4H), 1.47 (s, 18H). ^{13}C (100 MHz, $CDCl_3$) δ 170.3, 162.2, 160.1, 157.7, 156.2, 144.9, 142.2, 138.4, 132.7, 131.7, 128.7, 125.7, 123.6, 120.4, 118.9, 79.7, 55.2, 54.8, 42.1, 27.4. HRMS (MALDI-) calcd for $C_{50}H_{53}BF_2N_7O_{14}S_2$ $\{M-H\}^-$ 1088.3156, found 1088.3108.

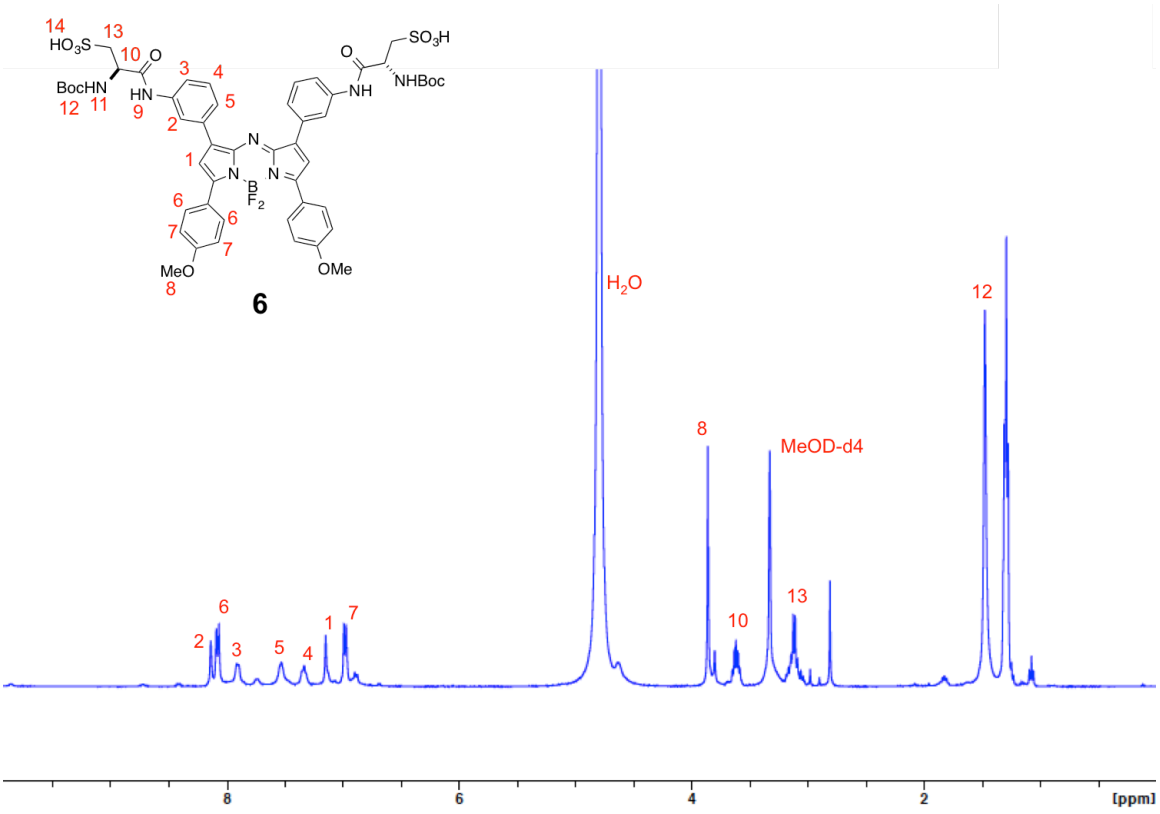

^{1}H-NMR of compound 6

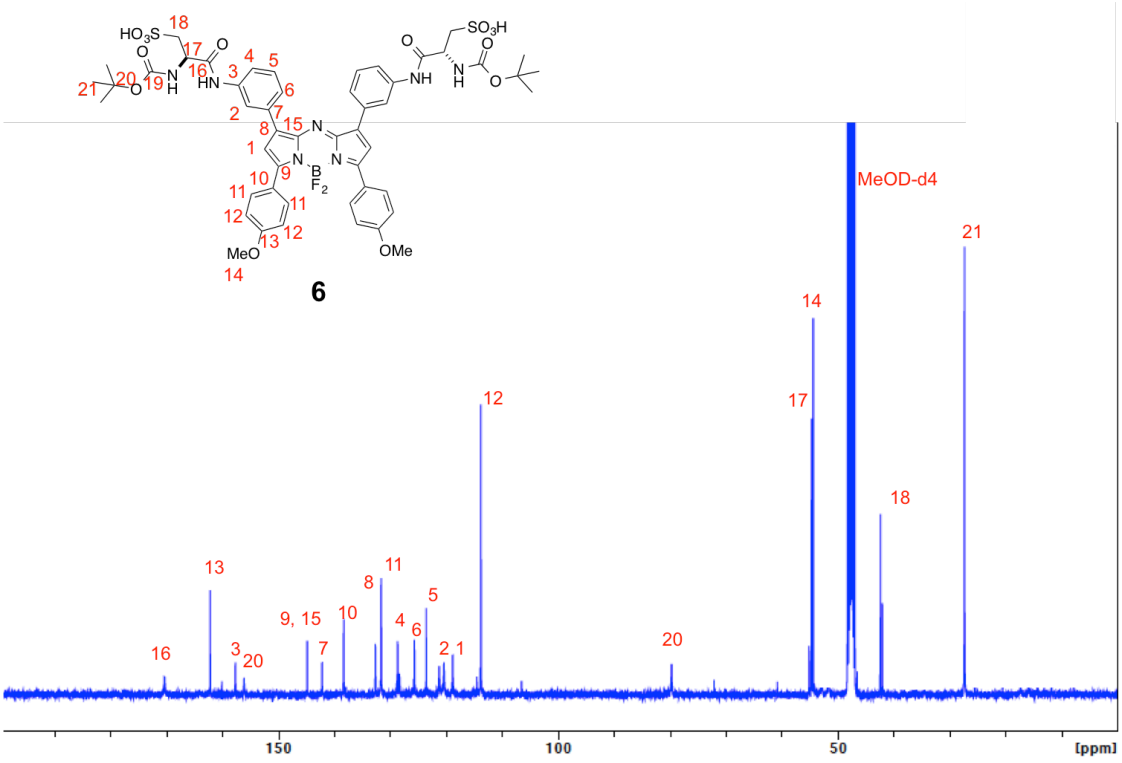

^{13}C-NMR of compound 6

(*R*)-2-amino-3-((3-(9-(3-((*R*)-2-amino-3-sulfopropanamido)phenyl)-5,5-difluoro-3,7-bis(4-methoxyphenyl)-5*H*-4λ^4,5λ^4-dipyrrolo[1,2-*c*:2',1'-*f*][1,3,5,2]triazaborinin-1-yl)phenyl)amino)-3-oxopropane-1-sulfonic acid (4).

Compound **5** (40 mg, 0.37 mmol) was dissolved in dioxane (5 mL). Solution of HCl in dioxane (2 M, 5 mL) was added into the solution. The reaction was stirred at 25 ^{o}C for 1 h. The solvent was removed to yield **4** 33 mg, quantitative yield as a green solid. ^{1}H NMR (400 MHz, $CDCl_3$) δ 10.81 (s, 2H), 8.25 (s, 2H), 8.17 (d, J = 8.9 Hz, 4H), 7.95 (d, J = 7.7 Hz, 2H), 7.74 (d, J = 7.2 Hz, 2H), 7.51 (t, J = 8.0 Hz, 2H), 7.44 (s, 2H), 7.16 (d, J = 8.9 Hz, 4H), 4.19 (br, 2H), 3.90 (s, 6H), 3.21-3.18 (m, 2H), 2.94 (dd, J = 9.8 Hz, 4H).

^{13}C (100 MHz, $CDCl_3$) δ 166.5, 162.6, 158.0, 145.0, 142.7, 139.0, 132.8, 132.3, 129.8 125.9, 123.6, 121.6, 120.5, 120.3, 115.0, 56.1, 51.5, 50.7. ^{11}B NMR (128 MHz, DMSO-*d6*) *δ*: 0.88 (t, *J* = 32.0 Hz, *B*F2) ppm. ^{19}F NMR (376 MHz, DMSO-*d6*) *δ*: -130.52 (q, *J* = 32.0 Hz, B*F*2). HRMS (MALDI-) calcd for $C_{40}H_{36}BF_2N_7NaO_{10}S_2$ {M-Na}$^-$ 910.1925, found 910.1968.

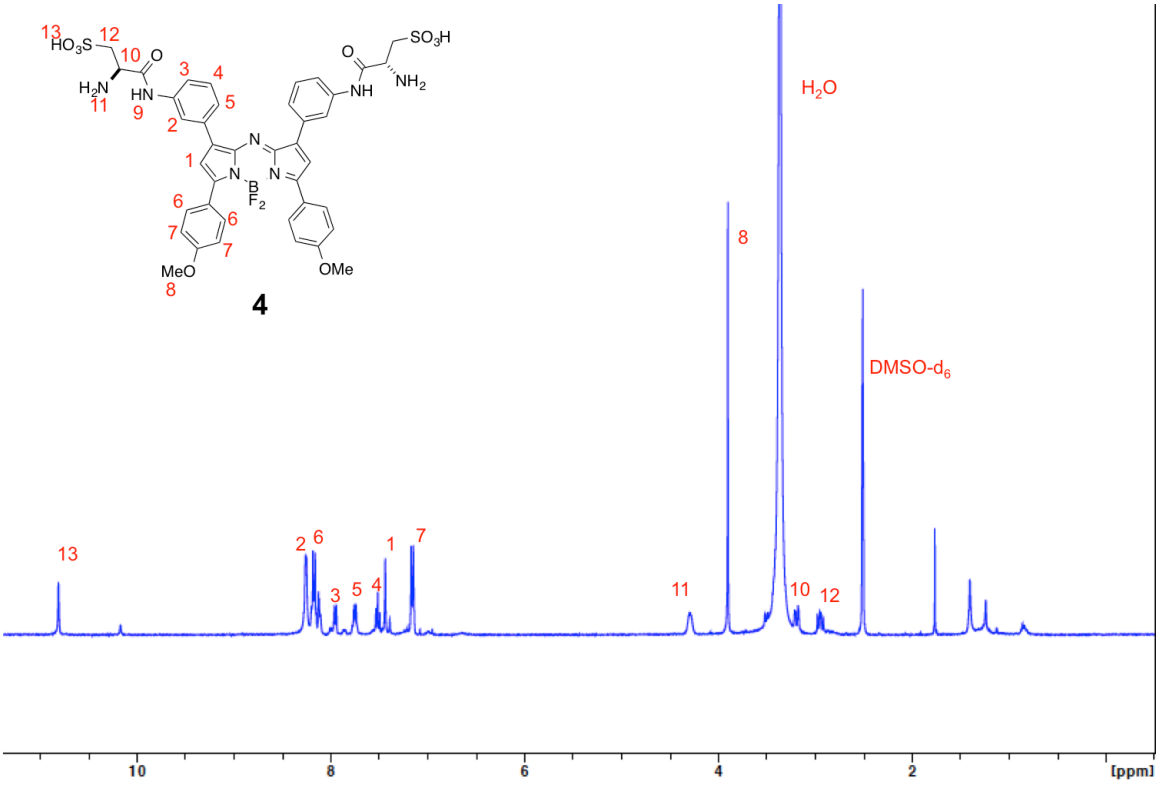

^{1}H-NMR of compound 4

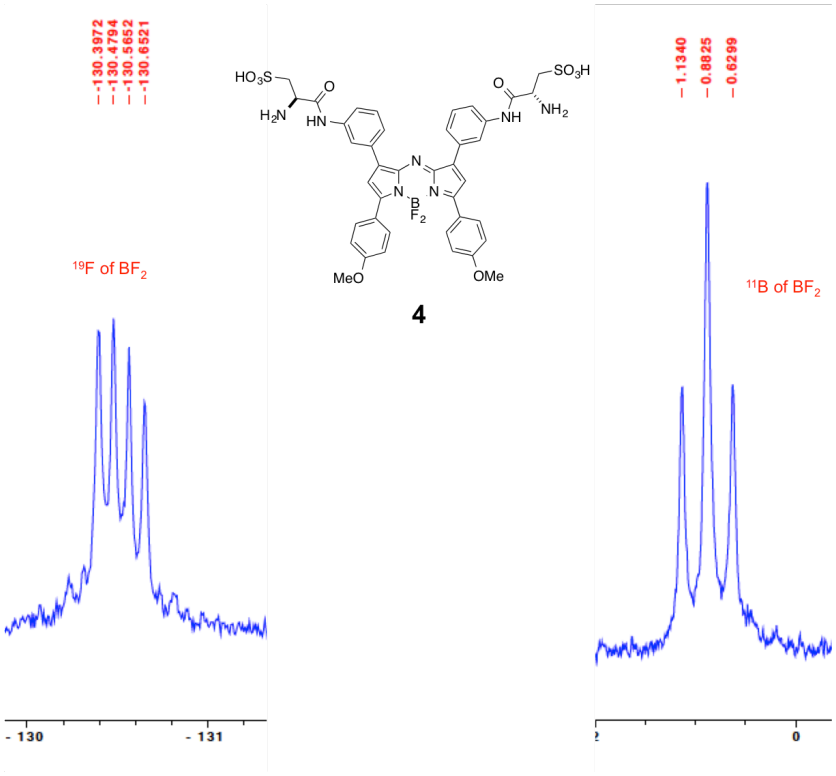

^{11}B, ^{19}F-NMR of compound 4

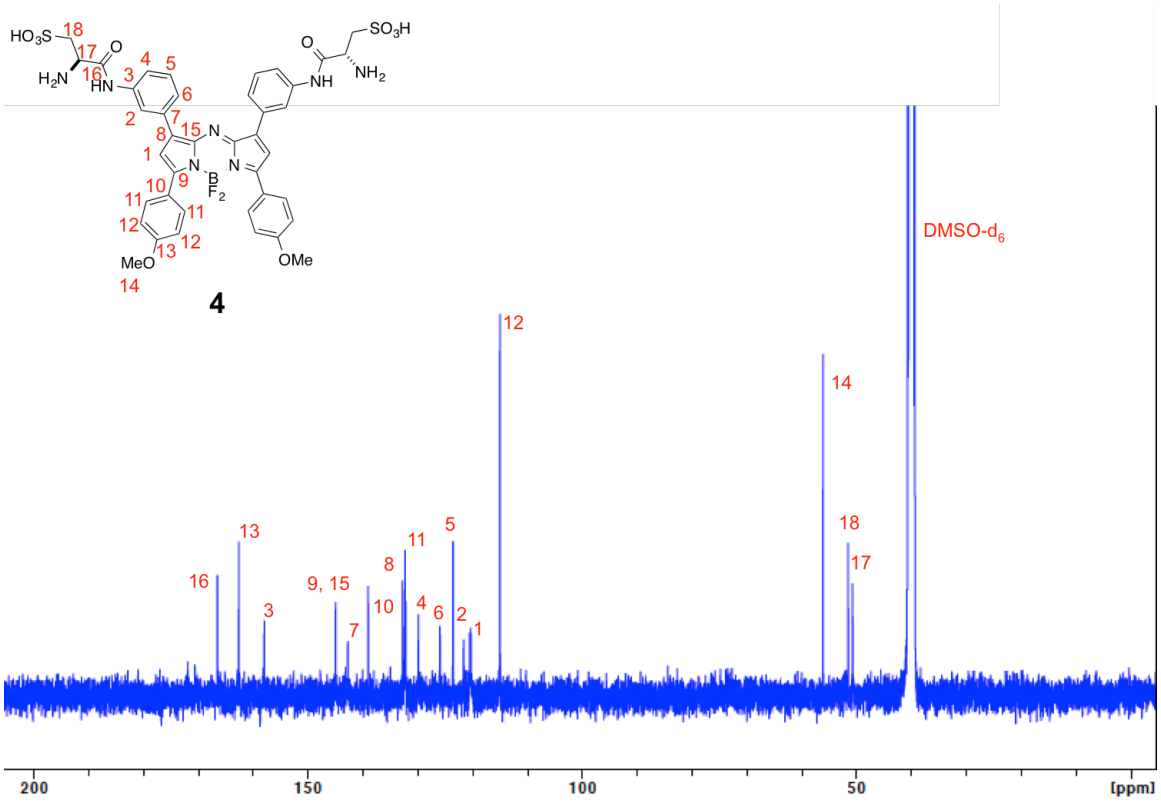

^{13}C-NMR of compound 4

Spectroscopic Data Of Compound 4.

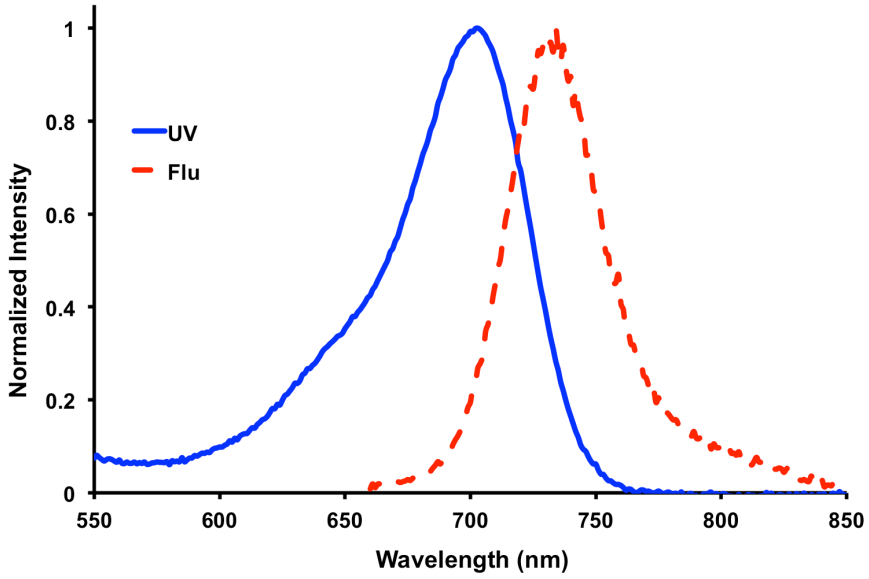

Fig. C-S2 UV and fluorescent spectra of **4** in DMSO.

Table C-S2. Spectroscopic Data of Compound **4**.

Solvent	$\lambda_{abs\ max}$ (nm)	ε ($M^{-1}\ cm^{-1}$) × 10^4	$\lambda_{emis\ max}$ (nm)[a]	Φ_F[b]
DMSO	703	6.12	730	0.17 ± 0.003
PBS[c]	701	4.72	729	0.34 ± 0.010

[a]Excited at 650 nm. [b]Relative to Zn-pthalocyanine in 1% pyridine/toluene (Φ_F = 0.30). [c]Contained 0.1% CrEL

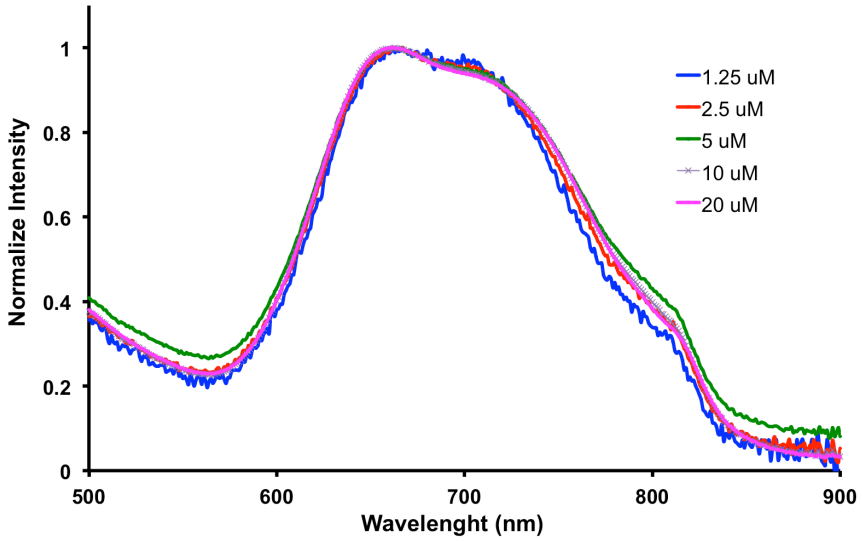

Fig. C-S3 UV absorptions of **4** at different concentrations. No evidence of aggregation was observed when concentration dependence of **4** in PBS buffer (without additives) was used.

Thermodynamic Equilibrium Solubility Measurement

Stock solutions (0.1 M) of test compounds were prepared in DMSO then diluted with aqueous media (PBS pH 7.4 or carbonate buffer pH 9 or acetate buffer pH 4) to desired concentrations (0 – 1000 μM, the highest concentration contained 1 % DMSO). Then, the plate covered with aluminium foil was shaken horizontally for 6 h at 25 ^{o}C and kept overnight for equilibration. Thereafter, the plate was centrifuged at 100 rpm for 20 min. Supernatant was pipetted into 96-well UV transparent plate (Corning® 96 Well Clear Flat Bottom UV-Transparent Microplate) and analyzed at λ = 680 nm of compounds against blank using microplate reader (Biotek Synergy H4).

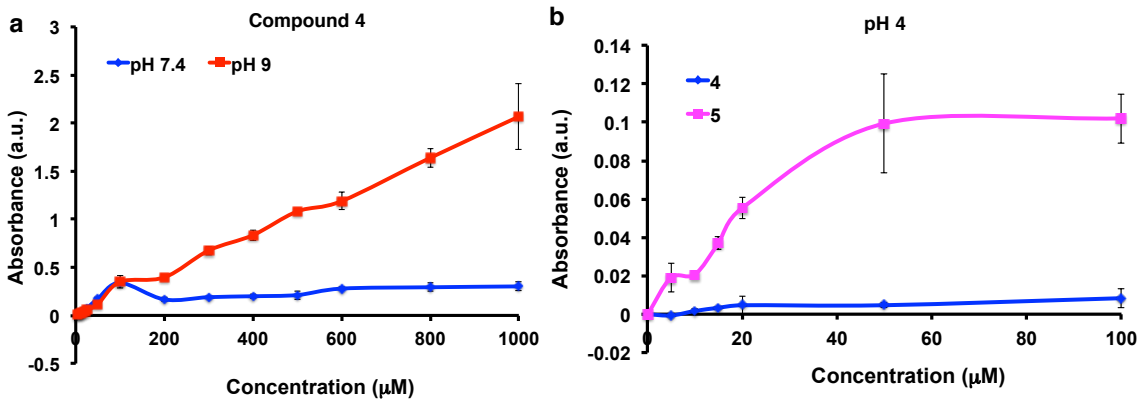

Fig. C-S4 Solubility Profile. **a** Compound **4** is soluble in PBS pH 7.4 up to 100 μM and more than 1 mM can be dissolved in carbonate buffer pH 9. **b** In acetate buffer, compound **4** is only soluble up to 20 μM, where as **5** can be soluble up to 50 μM. The analysis was performed in triplicate for each compound.

Cell Culture And Imaging Studies

4T1 cells were cultured on 75 cm^2 culture flasks in Dulbecco's Modified Eagle Medium/nutrient mixture F-12 (DMEM/F12, Sigma Chemical, St. Louis, MO) supplemented with 10 % FBS. Cells were cultures in a humidified incubator at 37 °C with 5 % CO_2 and 95 % air.

Subcellular localization was measured on living 4T1 cells using an Olympus FV1000 Confocal Microscope. Throughout, digital images were captured with a 100x / 1.4 oil objective with the following filter sets: for LysoTracker Green: excitation 488 nm; for aza-BODIPY **4**: excitation 633 nm. Sequential optical sections (Z-stacks) from the basal-to-apical surfaces of the cell were also acquired.

Lysosomal Co-localization

Cells were incubated with fluors for 3 h at 37 ^{o}C. After the cells were washed with PBS (2X), LysoTracker Green (0.5 μM) was added and the cells were incubated for 30 min at 37 ^{o}C. The cells were washed again with PBS before imaging.

APPENDIX D

SUPPORTING INFORMATION FOR CHAPTER II

General Methods

All reactions were carried out under an atmosphere of dry nitrogen. Glassware was oven-dried prior to use. Unless otherwise indicted, common reagents or materials were obtained from commercial source and used without further purification. All a-amino acids used were of the L-configuration. Triethylamine (TEA) was obtained anhydrous by distillation over calcium hydride. Acetonitrile (MeCN), dichloromethane (CH_2Cl_2), and methanol (MeOH) were dried by a Mbraun solvent drying system.

Flash column chromatography was performed using silica gel 60 (230-400 mesh). Analytical thin layer chromatography (TLC) was carried out on Merck silica gel plates with QF-254 indicator and visualized by UV. ^1H and ^{13}C NMR spectra were recorded on a Varian 300 (300 MHz ^1H; 75 MHz ^{13}C) or Varian 500 (500 MHz ^1H; 125 MHz ^{13}C) spectrometer at room temperature. Chemical shifts were reported in ppm relative to the residual $CDCl_3$ (δ 7.27 ppm ^1H; δ 77.0 ppm ^{13}C), or d^6-DMSO (δ 2.49 ppm ^1H; δ 39.5 ppm ^{13}C). NMR chemical shifts were expressed in ppm relative to internal solvent peaks, and coupling constants were measured in Hz. (br = broad).

Analytical HPLC analyses were carried out on 150 x 4.6 mm C-18 column using gradient conditions (10 – 90% B, flow rate = 0.75 mL/min). Preparative HPLC was carried out on 100 x 21.2 mm C-18 column using gradient conditions (10 – 70% B, flow

rate = 10.0 mL/min). The eluents used were: solvent A (H_2O with 0.1% TFA) and solvent B (CH_3CN with 0.1% TFA)

Syntheses For 6-Mercaptopurine Derivatives

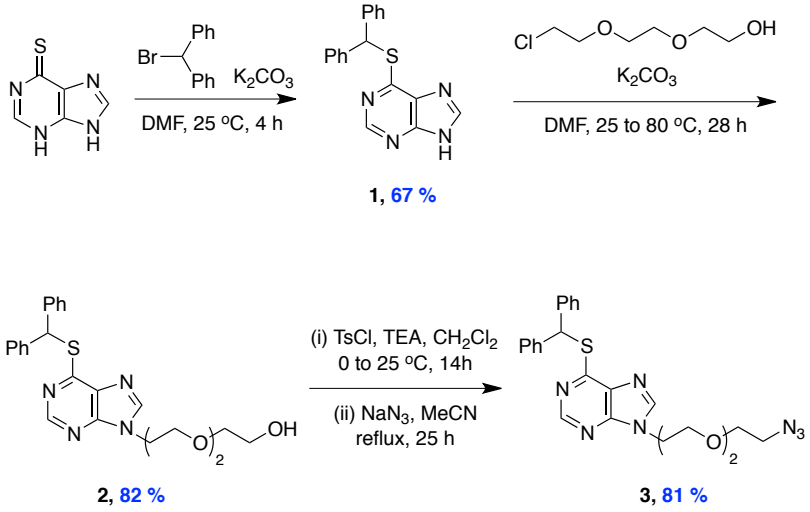

General Procedure For Compound 1

Preparation of compound **1** followed the procedure reported by F. I. Carroll and A. Philip.[278] To a solution of mercaptopurine (9.9 mmol, 1.0 equiv) in DMF (1.0 M) was added K_2CO_3 (9.9 mmol, 1.0 equiv) under N_2. The solution was stirred at 25 °C for 15 min. To the mixture was added bromodiphenylmethane (9.9 mmol, 1.0 equiv), and the mixture was stirred at 25 °C for 4 h. The mixture was diluted with water (90 mL), and then acidified with acetic acid. The mixture was stirred vigorously for 30 min, filtered, and then dried to give an amorphous solid. Recrystallization from MeOH gave 2.1 g (67 %) of compound **1** as white powder.

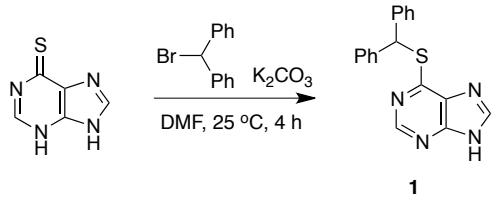

1

^{1}H NMR (500 MHz, DMSO) δ 8.63 (s, 1H), 8.45 (s, 1H), 7.51 (d, 4H, J = 7.5 Hz), 7.33 (t, 4H, J = 7.5 Hz), 7.24 (7, 2H, J = 7.5 Hz), 6.72 (s, 1H)

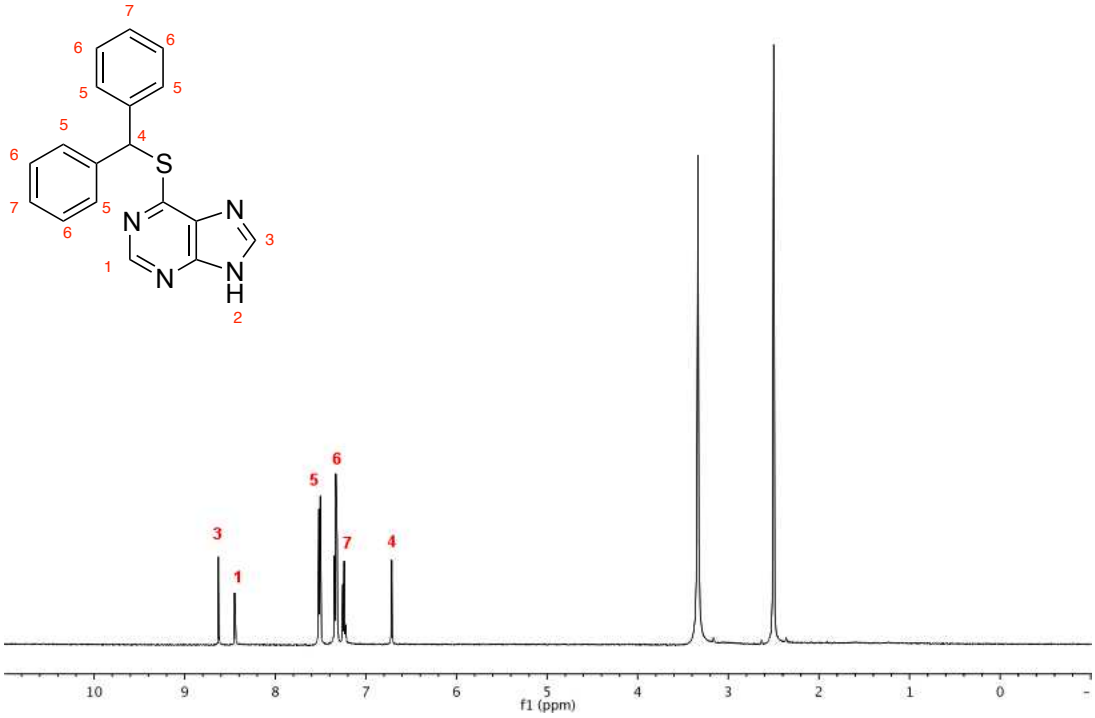

^{1}H NMR of **1**

General Procedure for Compound 2

To a solution of compound **1** (3.1 mmol, 1.0 equiv) in DMF (0.5 M) was added K_2CO_3 (3.1 mmol, 1.0 equiv) and 2-[2-9chloroethoxyl)-ethoxy]ethanol (3.1 mmol, 1.0 equiv)

under N_2 at 25 °C. The solution was warmed to 80 °C and then stirred at the temperature for 2 h. DMF was removed by lyophilizer, and then the mixture was purified by flash chromatography (1:19 MeOH/CH_2Cl_2). 1.2 g (82 %) of compound **2** was obtained as colorless oil.

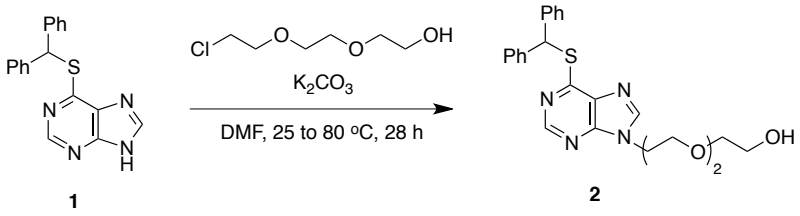

1 **2**

^{1}H NMR (500 MHz, $CDCl_3$) δ 8.67 (s, 1H), 8.38 (s, 1H), 7.51 (d, 4H, J = 7.5 Hz), 7.30 (dd, 4H, J = 7.0, 13.5 Hz), 7.22 (t, 2H, 7.5 Hz), 6.82 (s, 1H), 4.42 (t, 2H, J = 4.5 Hz), 3.80 (t, 2H, J = 5.0 Hz), 3.73 (t, 2H, J = 4.5 Hz), 3.57 (m, 4H), 3.54 (t, 2H, J = 4.0 Hz)

^{13}C NMR (125 MHz, $CDCl_3$) δ 159.2, 151.5, 148.2, 144.3, 140.9, 130.1, 128.4, 128.2, 127.0, 72.5, 70.3, 69.9, 68.6, 61.3, 50.5, 43.4

MS (ESI, m/z) calcd for $C_{24}H_{27}N_4O_3S$ $(M+H)^+$ 451.1, found 451.2

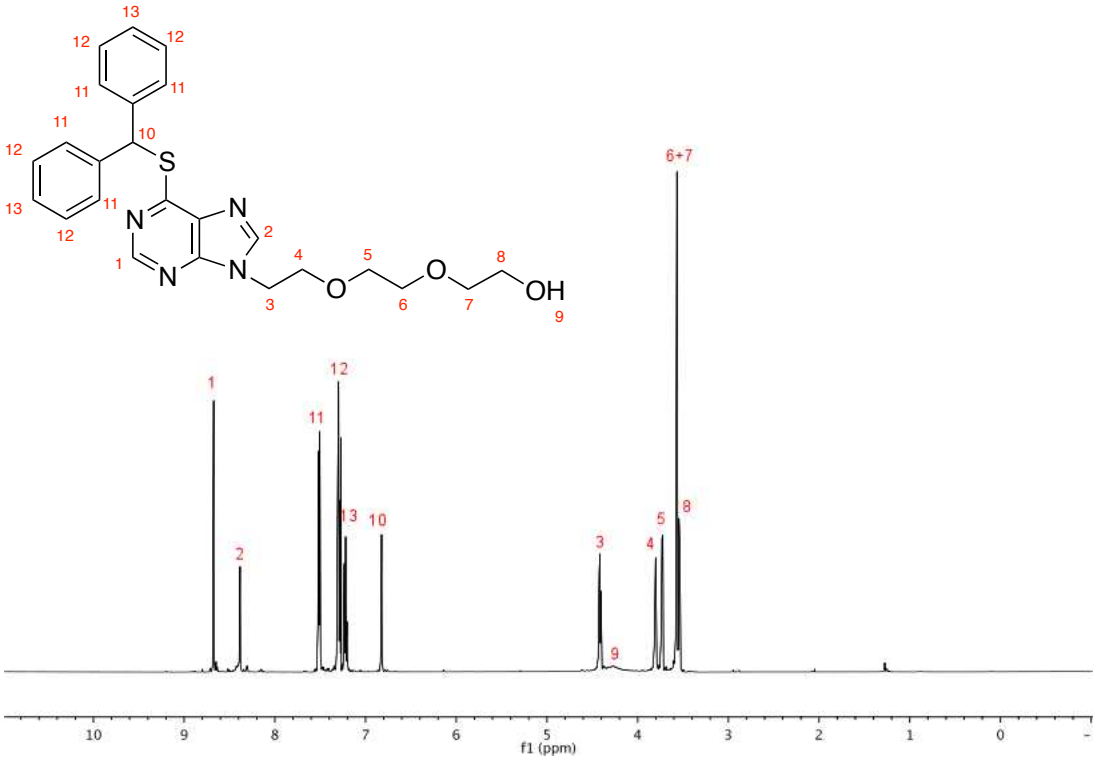

^{1}H NMR of **2**

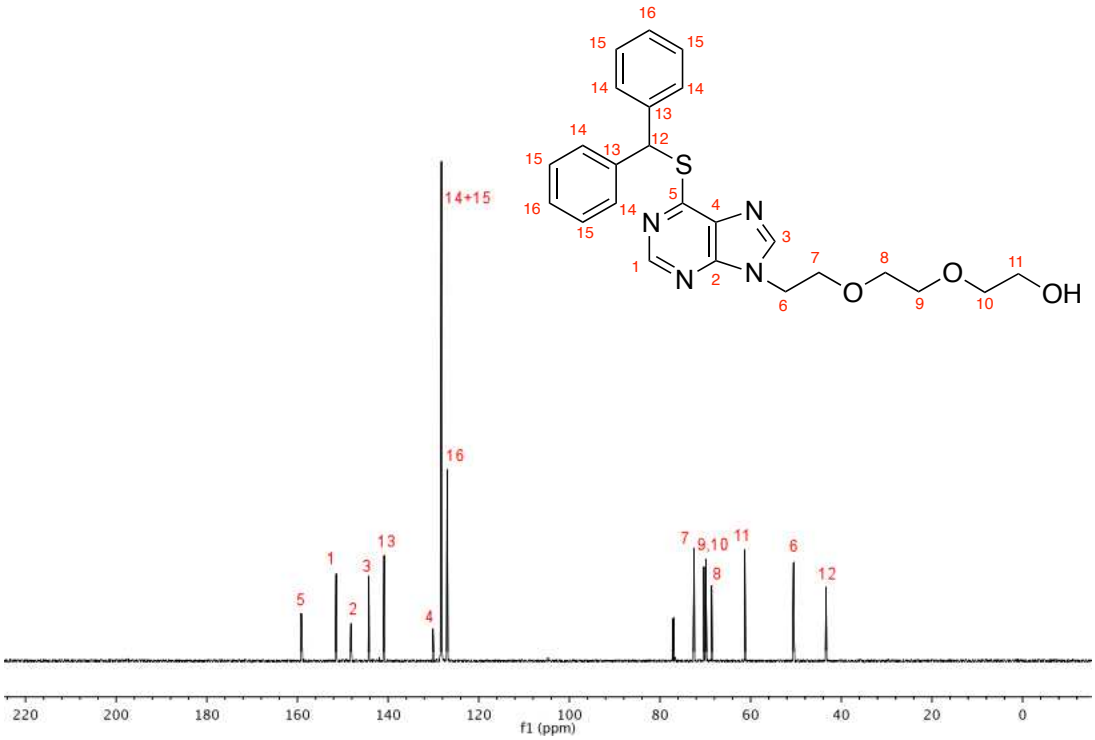

^{13}C NMR of **2**

General Procedure For Compound 3

To a solution of compound **2** (2.6 mmol, 1.0 equiv) in CH_2Cl_2 (0.15 M) was added DMAP (0.026 mmol, 0.01 equiv) and TEA (6.4 mmol, 2.5 equiv) under N_2 at 0 °C. 4-Toluenesulfonyl chloride (5.13 mmol, 2.0 equiv) was portioned over 10 min at 0 °C. The solution was stirred at 0 °C for 10 min, and then the solution was warmed to 25 °C. After 2 h, DMAP (0.26 mmol, 0.1 equiv) was added more to the mixture, and then stirred at 25 °C for 14 h. The mixture was diluted with water and then extracted with CH_2Cl_2. The combined organic phases were dried over $MgSO_4$. After completely removing the solvent, tosyl-protected compound **2'** was purified by flash chromatography (1:49 MeOH/CH_2Cl_2). 1.3 g (84%) of compound tosyl-protected compound was obtained as colorless oil.

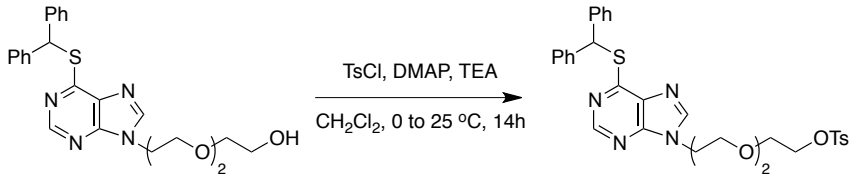

2 **2'**

^{1}H NMR (500 MHz, $CDCl_3$) δ 8.65 (s, 1H), 8.10 (s, 1H), 7.76 (d, 2H, J = 8.5 Hz), 7.52 (d, 4H, J = 8.0 Hz), 7.27 (m, 6H), 7.18 (t, 2H, J = 7.0 Hz), 6.85 (s, 1H), 4.32 (t, 2H, J = 5.0 Hz), 4.08 (t, 2H, J = 3.0 Hz), 3.72 (t, 2H, J = 4.5 Hz), 3.55 (t, 2H, J = 4.5 Hz), 3.46 (m, 4H), 2.34 (s, 3H)

^{13}C NMR (125 MHz, $CDCl_3$) δ 158.8, 151.2, 148.3, 144.5, 143.7, 140.9, 132.4, 130.3, 129.5, 128.2, 128.1, 127.5, 126.8, 70.2, 69.9, 68.9, 68,6, 68.2, 50.3, 43.2, 21.2

MS (ESI, m/z) calcd for $C_{31}H_{33}N_4O_5S_2$ $(M+H)^+$ 605.2, found 605.8

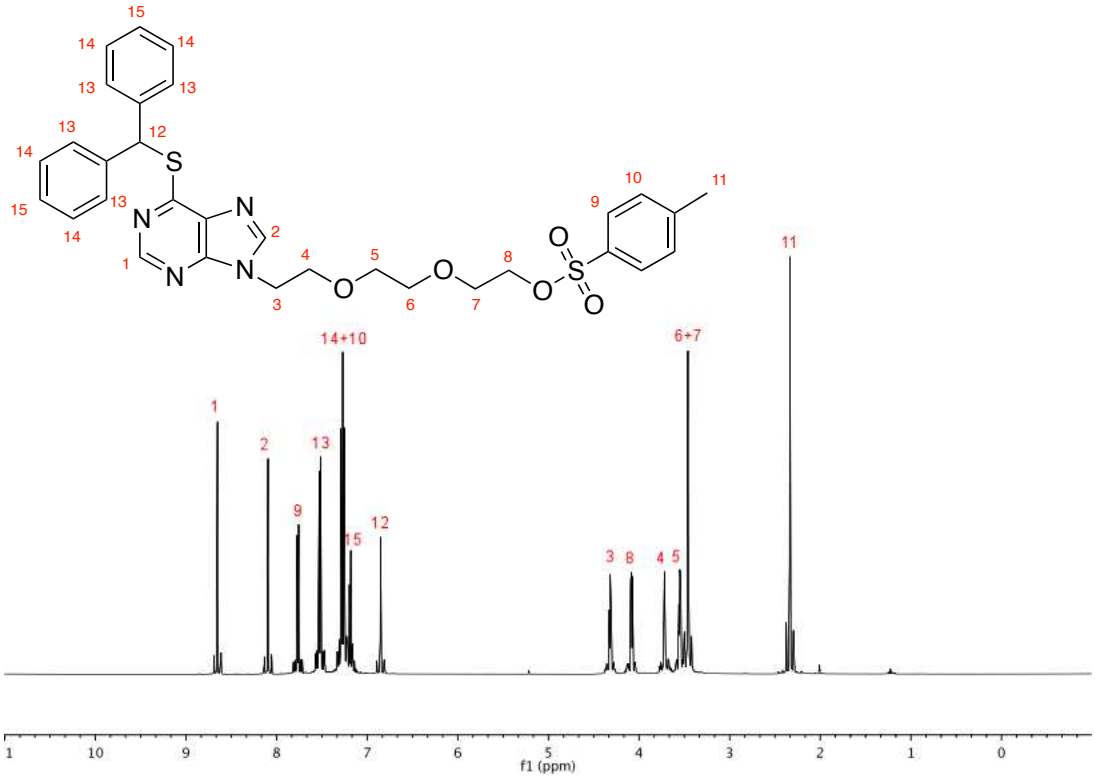

^{1}H NMR of **2'**

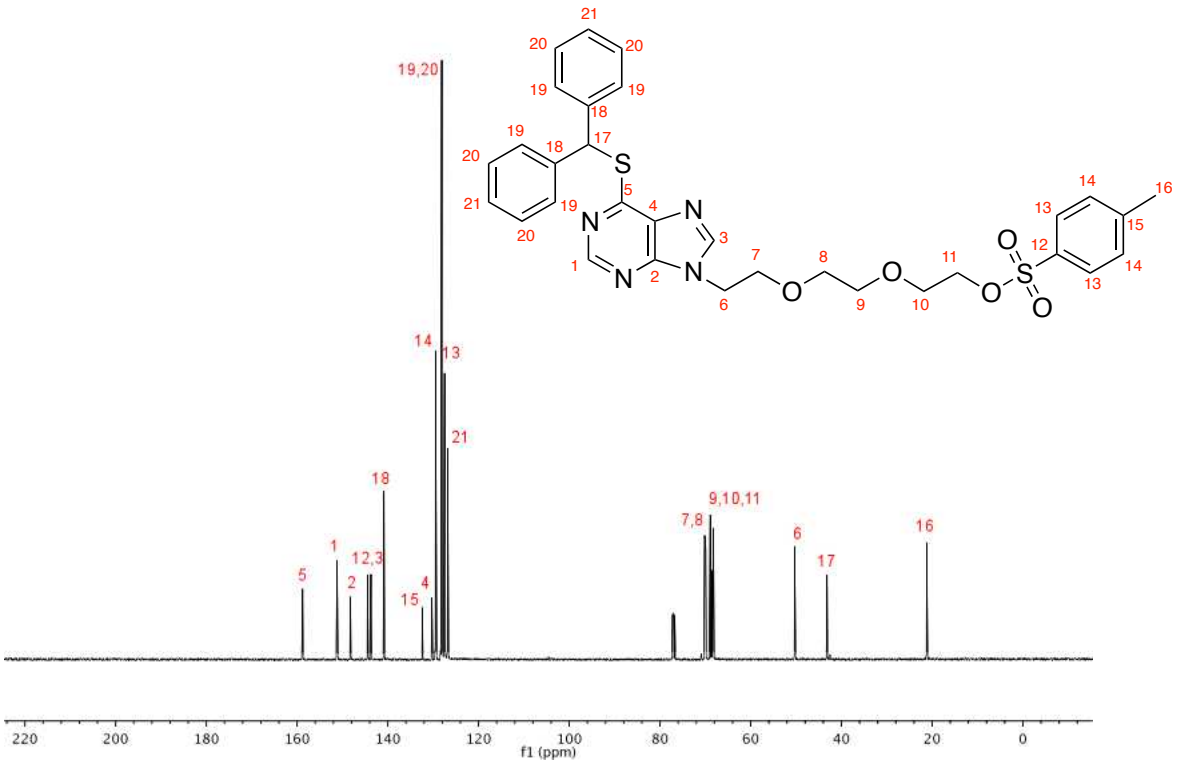

^{13}C NMR of **2'**

To a solution of compound **2'** (2.1 mmol, 1.0 equiv) in MeCN (0.1 M) was added NaN_3 (3.1 mmol, 1.5 equiv) under N_2. The mixture was refluxed for 25 h. After 25 h, the mixture was cooled down to room temperature, and diluted with water, and then extracted with CH_2Cl_2. The combined organic phases were dried over $MgSO_4$. After completely removing the solvent, compound **3** was purified by flash chromatography (3:97 MeOH/CH_2Cl_2). 1.0 g (97%) of compound **3** was obtained as yellowish oil.

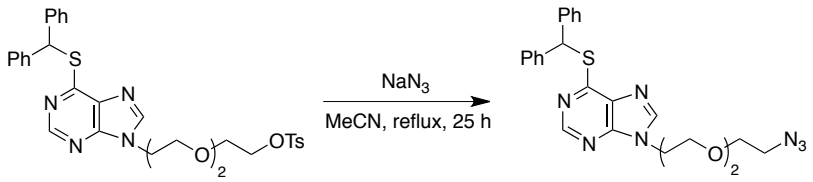

2' **3**

^{1}H NMR (500 MHz, $CDCl_3$) δ 8.70 (s, 1H), 8.28 (s, 1H), 7.53 (d, 4H, J = 8.0 Hz), 7.31 (t, 4H, J = 7.0 Hz), 7.23 (t, 2H, J = 80 Hz), 6.92 (s, 1H), 4.44 (t, 2H, J = 5.0 Hz), 3.82 (t, 2H, J = 5.0 Hz), 3.59 (m, 6H), 3.33 (t, 2H, J = 5.0 Hz)

^{13}C NMR (125 MHz, $CDCl_3$) δ 159.3, 151.5, 148.4, 143.9, 141.0, 130.5, 128.5, 128.3, 127.1, 70.4, 69.9, 68.9, 50.6, 50.4, 43.6

MS (ESI, m/z) calcd for $C_{24}H_{26}N_7O_2S$ $(M+H)^+$ 476.2, found 476.7

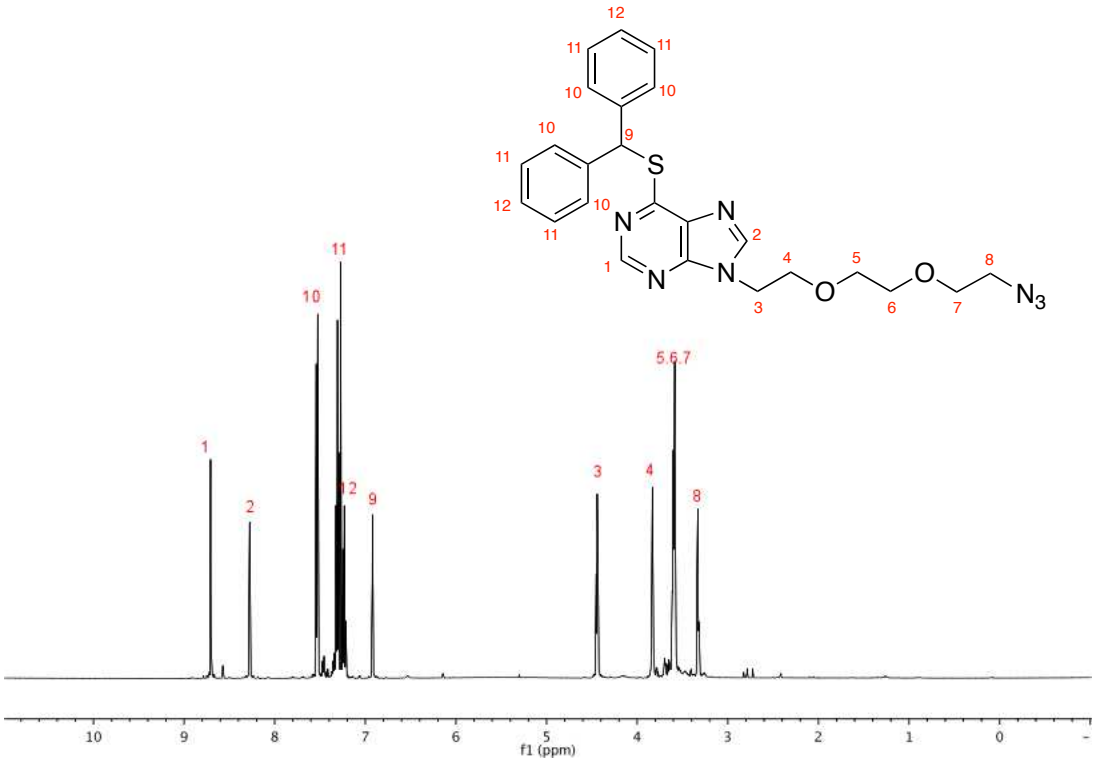

^{1}H NMR of **3**

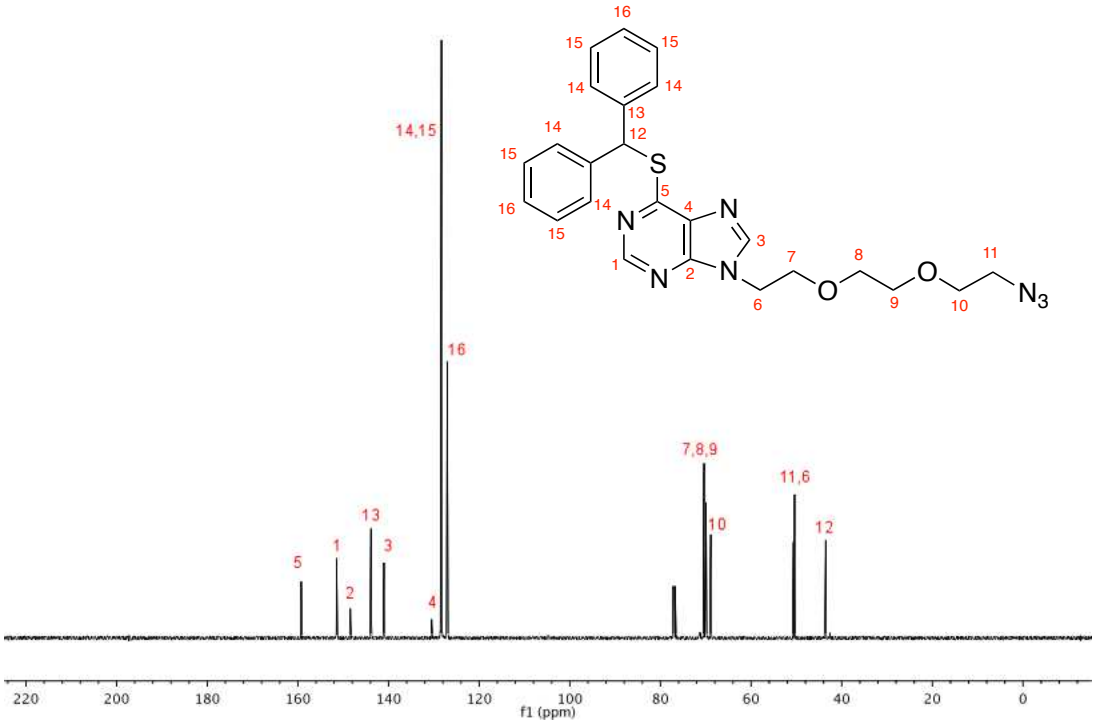

^{13}C NMR of **3**

Syntheses For IY-IY-6MP and 2mor-6MP

Compounds **IY-IY-TEG**, and **2mor-TEG** were prepared via the previously published methodology in our group.[77,190] To a solution of compound **3** (1.0 equiv) and **IY-IY-TEG** or **2mor-TEG** (1.0 equiv) in DMSO:H_2O (5:1, 0.01 M) were added TBTA (0.01 equiv) at 25 °C. $CuSO_4$ (0.1 equiv, from 0.05 M aqueous solution) and fresh Na ascorbate (0.4 equiv, from 0.05 M aqueous solution) were added to the mixture at 25 °C. The mixture was stirred at 25 °C for 24 h. The reactions were monitored by analytical HPLC. The crude compounds were lyophilized to remove DMSO, and then purified with RP-reparative HPLC to obtain the bivalent mimics **IY-IY-6MP'** or **2mor-6MP'**.

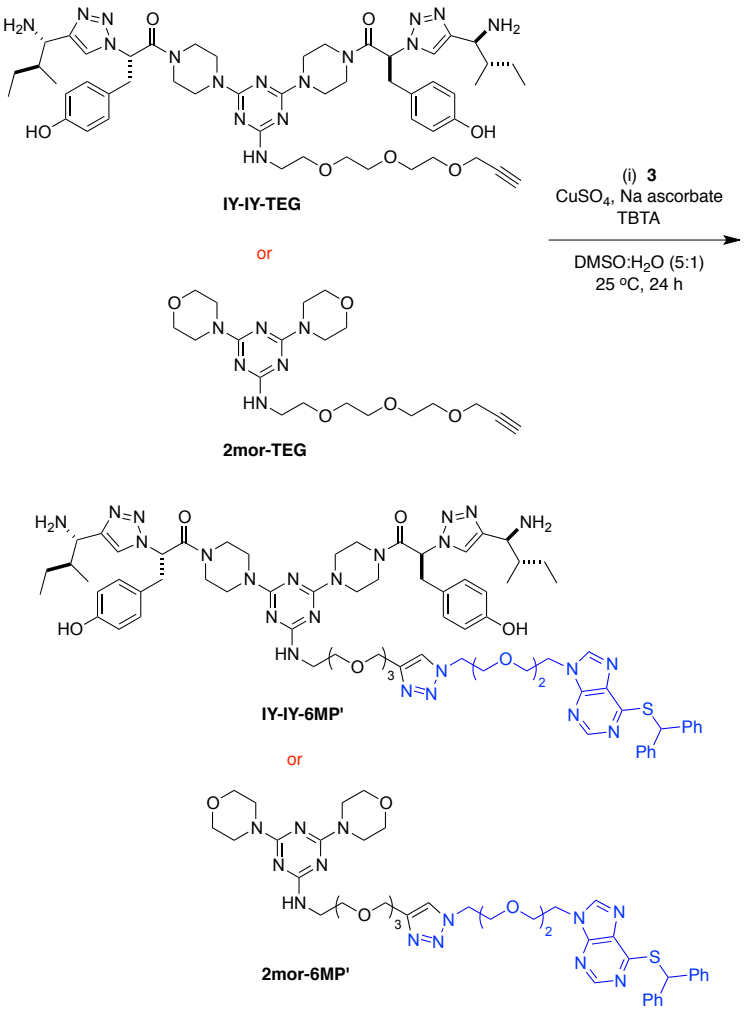

Table D-S1. Characterization of Compounds **IY-IY-6MP'** and **2mor-6MP'**.

compounds	retention time (min)	chemical formula	$[M+H]^+$ calculated	$[M+H]^+$ found[a]
IY-IY-6MP'	14.4	$C_{76}H_{100}N_{23}O_9S$	1510.8	1510.6
2mor-6MP'	17.2	$C_{44}H_{59}N_{13}O_7S$	913.4	913.9

[a]MALDI-MS

Deprotection of diphenylmethyl group from thione **IY-IY-6MP'** or **2mor-6MP'** was performed with 50 % TFA/CH_2Cl_2 and phenol (3.0 equiv) at 25 °C. The mixture was stirred at 25 °C for 16 h. The reactions were monitored by analytical HPLC. The crude compounds were purified with RP-reparative HPLC to obtain the bivalent mimics **IY-IY-6MP** or **2mor-6M**. The final products were lyophilized three times in 1.0 % acetic acid to remove TFA.

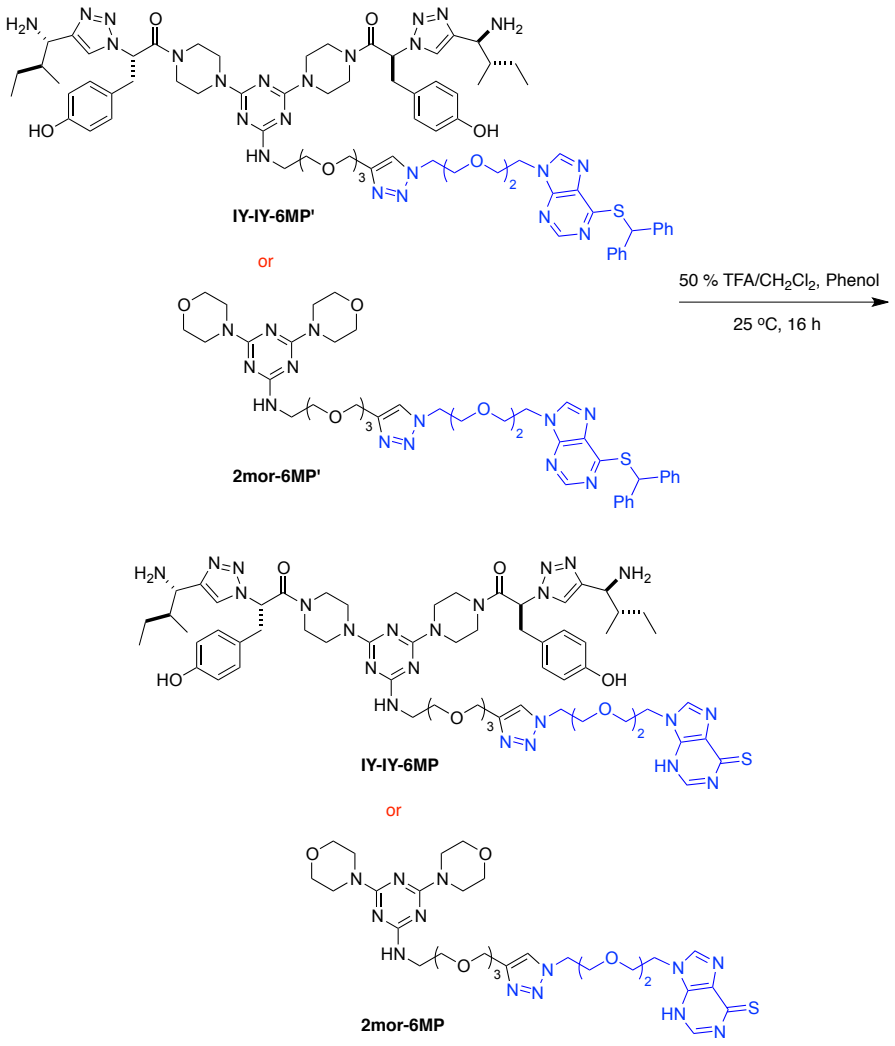

Table D-S2. Characterization of Compounds **IY-IY-6MP** and **2mor-6MP**.

compounds	retention time (min)	chemical formula	$[M+H]^+$ calculated	$[M+H]^+$ found[a]
IY-IY-6MP	10.6	$C_{63}H_{90}N_{23}O_9S$	1344.7	1345.1
2mor-6MP	10.5	$C_{31}H_{49}N_{13}O_7S$	747.4	746.7

[a]MALDI-MS

Syntheses For Rosamine Derivatives

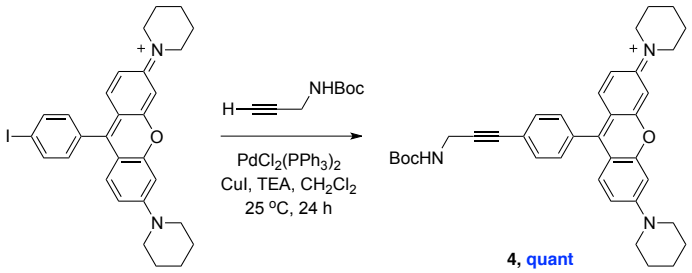

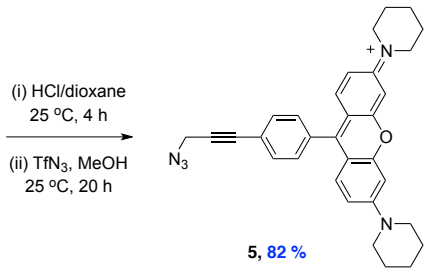

General Procedure For Compound 4

Iodo-rosamine[279] (0.36 mmol, 200 mg), $PdCl_2(PPh_3)_2$ (0.036 mmol, 25.2 mg) and CuI (0.036 mmol, 6.86 mg) were added to a dried round bottom flask. The flask was placed under vacuum for 15 min, and then dried CH_2Cl_2 (24 mL) was added under N_2; red solution was observed. To the mixture were added *tert*-butyl prop-2-yn-1-ylcarbamate (3.6 mmol, 562 mg) and TEA (0.36 mmol, 0.50 mL). The reaction mixture was stirred at 25 ^oC for 24 h.[280] The solvents were removed under reduced pressure and the residue was purified by flash chromatography (5 % $MeOH/CH_2Cl_2$) to afford the pure product **4** (240 mg, quantitative) as a purple solid.

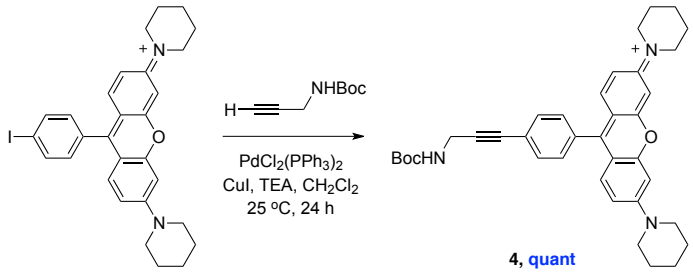

^1H NMR (300 MHz, $CDCl_3$) δ 7.64 (d, 2H, J = 8.4 Hz), 7.33 (d, 2H, J = 9.5 Hz), 7.29 (d, 2H, J = 8.4 Hz), 7.07 (dd, 2H, J = 9.5, 2.7 Hz), 7.00 (d, 2H, J = 2.7 Hz), 4.87 (br, 1H), 4.20 (d, 2H, J = 5.4 Hz), 3.75 (br, 8H), 1.78 (br, 12H), 1.47 (s, 9H)

^{13}C NMR (75 MHz, $CDCl_3$) δ 165.0, 158.3, 156.4, 155.8, 132.2, 131.8, 131.5, 129.6, 125.3, 115.0, 113.4, 97.7, 88.4, 81.9, 49.3, 28.4, 26.0, 24.1

MS (ESI) m/z calcd for $C_{37}H_{42}N_3O_3^+$ 576.3221; found 576.2374.

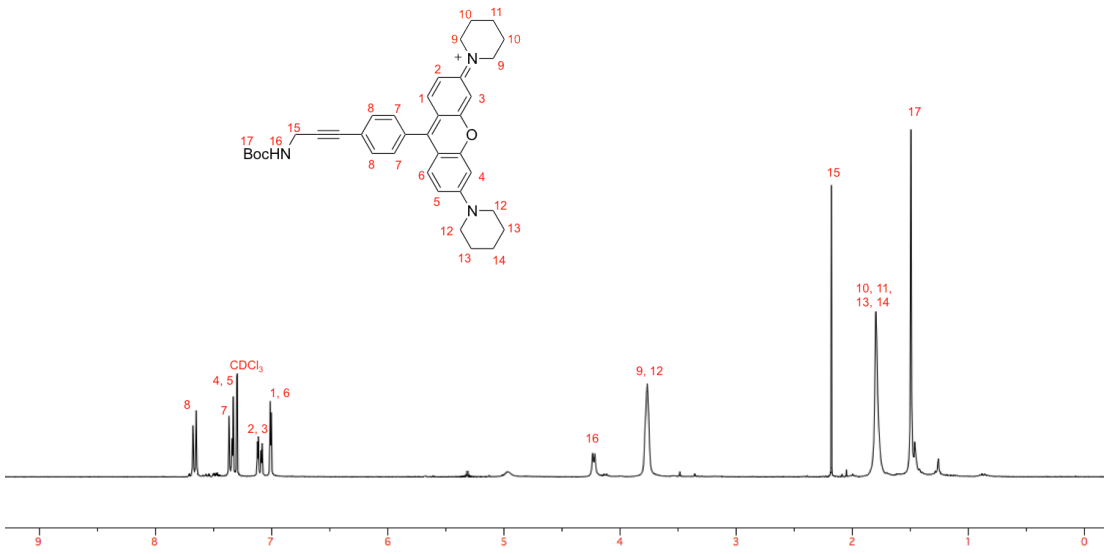

^{1}H NMR of **4**

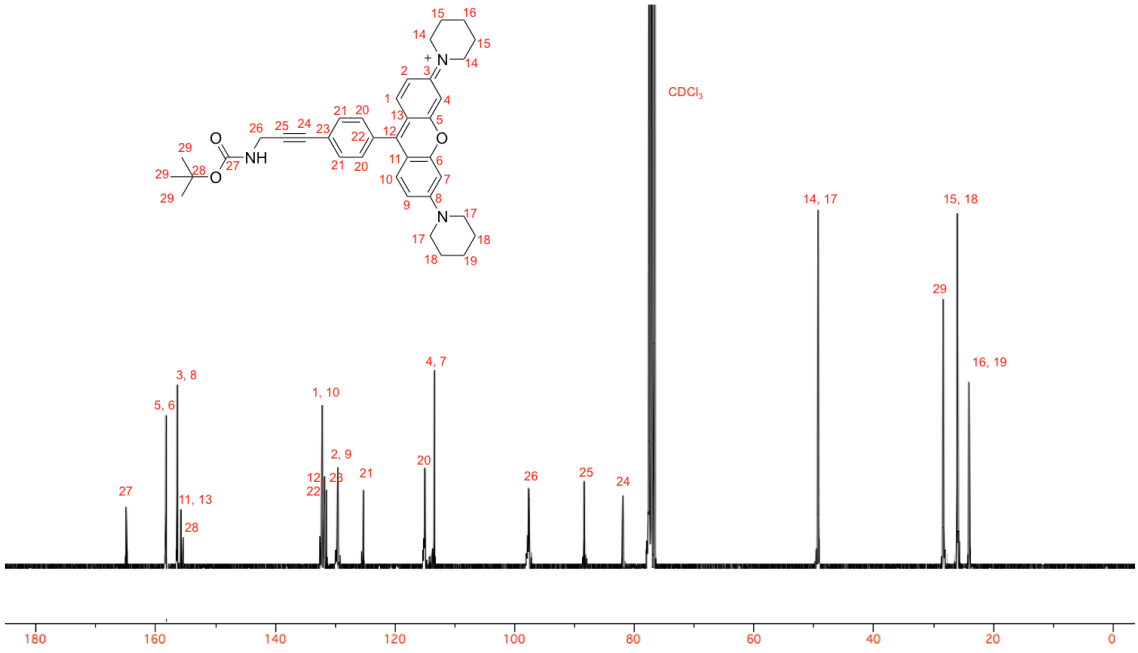

^{13}C NMR of **4**

General Procedure For Compound 5

Boc-protected amino rosamine **4** (0.42 mmol, 240 mg) was dissolved in dioxane (5 mL). Hydrogenchloride (4 M in dioxane, 2 mL) was added at once and the solution was stirred at 25 ^{o}C for 4 h. The solvent was removed under reduced pressure and the product was used without further purification.

A solution of sodium azide (10 mmol, 650 mg) in a 2:1 mixture of H_2O (4 mL) and CH_2Cl_2 (2 mL) was cooled using an ice bath. Triflic anhydride (2.0 mmol, 0.34 mL) was added over 5 min and the solution was then stirred at 0 °C for further 2 h. The CH_2Cl_2 phase was separated, and the aqueous portion was extracted with CH_2Cl_2 (3 x 5 mL). The organic fractions were combined, washed once with saturated Na_2CO_3, and the solution was used without further purification.[190]

Amino rosamine (after Boc deprotection) (0.20 mmol, 100 mg) was combined with K_2CO_3 (0.30 mmol, 40 mg), $CuSO_4$ (0.002 mmol, 0.32 mg), H_2O (1 mL) and CH_3OH (4 mL). The CH_2Cl_2 solution of triflyl azide prepared above was added in one portion, and the mixture was stirred at 25 ^{o}C for 20 h. The organic phase was separated, then washed with a 1:3 mixture of NH_4OH (3 mL) and H_2O (9 mL), brine, and dried over Na_2SO_4. The solvents were removed under reduced pressure and the residue was purified by flash chromatography (5 % MeOH/CH_2Cl_2) to afford rosamine azide **5** (82 mg, 82 %) as a purple solid.

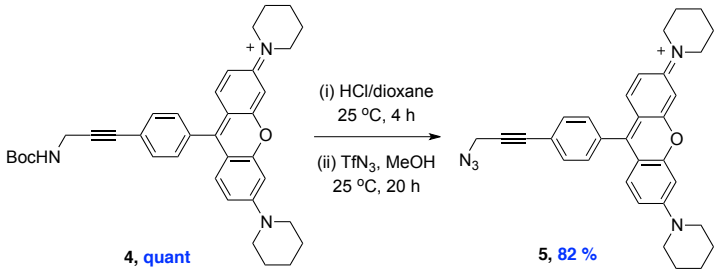

^{1}H NMR (500 MHz, DMSO-d_6) δ 7.78 (d, 2H, J = 8.5 Hz), 7.55 (d, 2H, J = 8.5 Hz), 7.30 (dd, 2H, J = 2.5, 9.5 Hz), 7.21 (d, 2H, J = 9.5 Hz), 7.15 (d, 2H, J = 2.5 Hz) 4.48 (s, 2H), 3.77 (m, 8H), 1.71 (m, 4H), 1.63 (m, 8H)

^{13}C NMR (125 MHz, DMSO-d_6) δ 158.2, 156.4, 155.3, 132.9, 132.4, 131.9, 130.5, 123.6, 115.5, 113.3, 97.4, 86.1, 85.4, 49.0, 26.2, 24.2

MS (ESI) m/z calcd for $C_{32}H_{32}N_5O^+$ 502.2601; found 502.2859

FT-IR (NaCl): N_3 band at 2109.24 cm^{-1} and sp-C band at 2363.25 cm^{-1}.

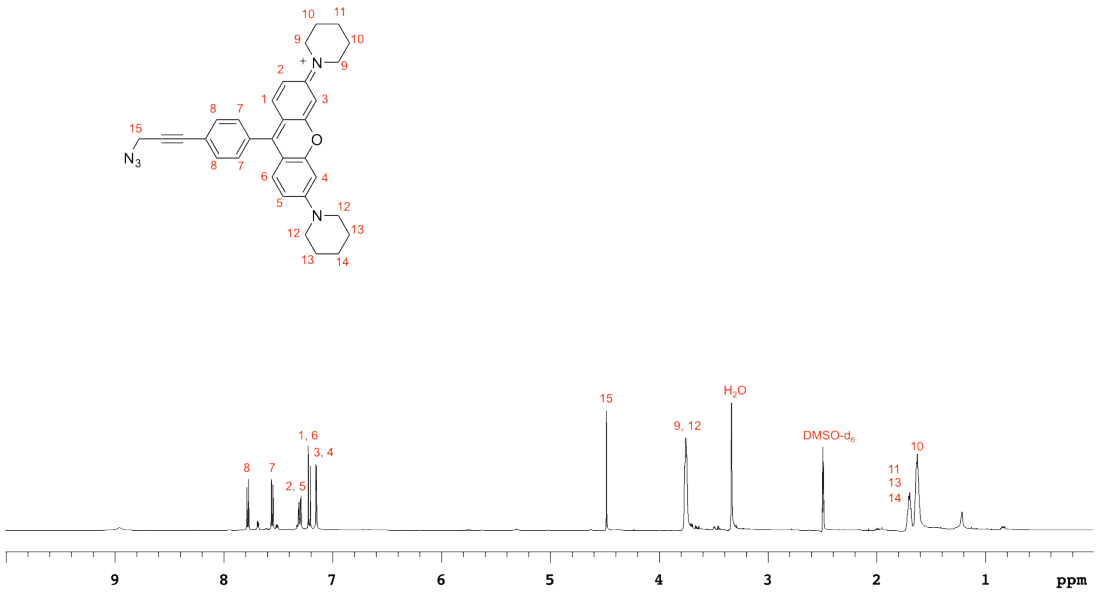

^{1}H NMR of **5**

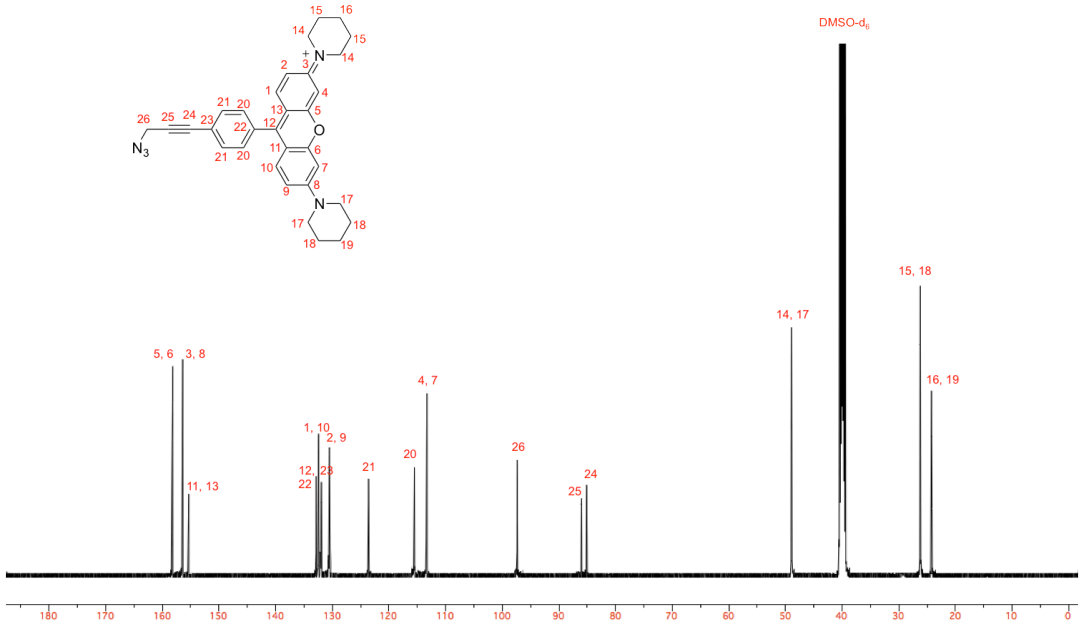

^{13}C NMR of **5**

Syntheses For IY-IY-Ros, YI-YI-Ros and 2mor-Ros

Compounds **IY-IY-TEG**, **YI-YI-TEG**, and **2mor-TEG** were prepared via the previously published methodology in our group. To a solution of compound **5** (1.0 equiv) and **IY-IY-TEG, YI-YI-TEG** or **2mor-TEG** (1.0 equiv) in DMSO:H_2O (5:1, 0.01 M) were added TBTA (0.01 equiv) at 25 °C. $CuSO_4$ (0.1 equiv, from 0.05 M aqueous solution) and fresh Na ascorbate (0.4 equiv, from 0.05 M aqueous solution) were added to the mixture at 25 °C. The mixture was stirred at 25 °C for 24 h. The reactions were monitored by analytical HPLC. The crude compounds were lyophilized to remove DMSO, and then purified with RP-reparative HPLC to obtain the bivalent

mimics **IY-IY-Ros, YI-YI-Ros** or **2mor-Ros**. The final products were lyophilized three times in 1.0 % acetic acid to remove TFA.

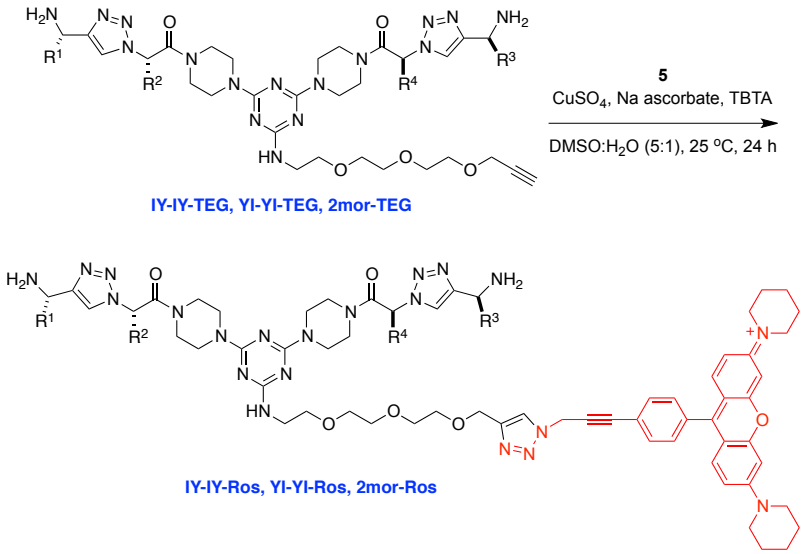

IY-IY-Ros

^{1}H NMR (500 MHz, DMSO-d$_6$) δ 9.27 (br, 1H), 8.33 (br-s, 1H), 8.23 (br, 7H), 7.71 (d, 2H, *J* = 8.5 Hz), 7.48 (d, 2H, *J* = 8.5 Hz), 7.24 (m, 2H), 7.11 (m, 4H), 6.92 (d, 2H, *J* = 8.5 Hz), 6.74 (br, 1H), 6.53 (d, 2H, *J* = 8.5 Hz), 5.61 (s, 2H), 4.50 (s, 2H), 4.32 (m, 2H), 3.68 (m, 8H), 3.44 (m, 28H), 3.18 (s, 2H), 1.84 (m, 2H), 1.63 (m, 4H), 1.56 (m, 8H), 1.26 (m, 2H), 0.92 (m, 2H), 0.80 (t, 6H, *J* = 7.0 Hz), 0.67 (d, 6H, *J* = 6.5 Hz)

^{13}C NMR (125 MHz, DMSO-d$_6$) δ 166.3, 165.0, 164.9, 158.4, 158.2, 156.8, 156.4, 156.1, 155.3, 144.8, 142.0, 133.0, 132.7, 132.5, 131.8, 130.8, 130.4, 125.9, 124.6, 124.0, 123.5, 115.5, 113.4, 97.4, 85.4, 84.9, 70.2, 70.1, 70.0, 69.5, 69.5, 63.8, 52.7, 51.1, 49.0, 45.0, 45.4, 37.6, 26.2, 25.6, 24.3, 14.1, 11.6

Hi-Res MALDI-MS: m/z calcd for $C_{84}H_{107}N_{21}O_8^+$ 1536.8528; found 1536.8582

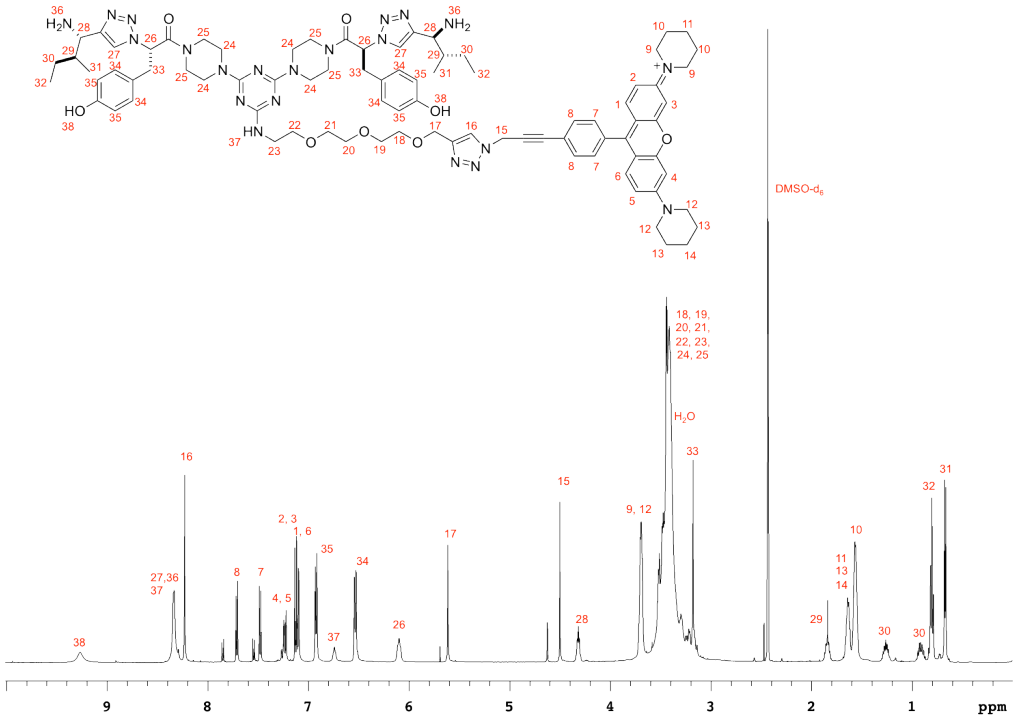

^{1}H NMR of **IY-IY-Ros**

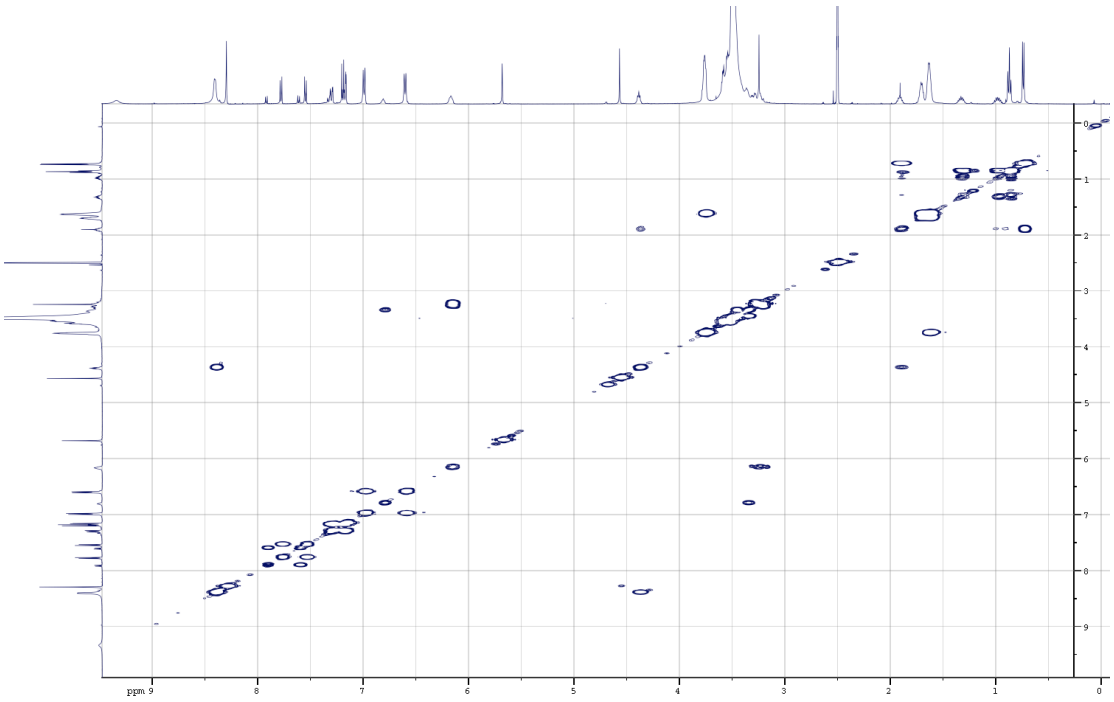

COSY NMR of **IY-IY-Ros**

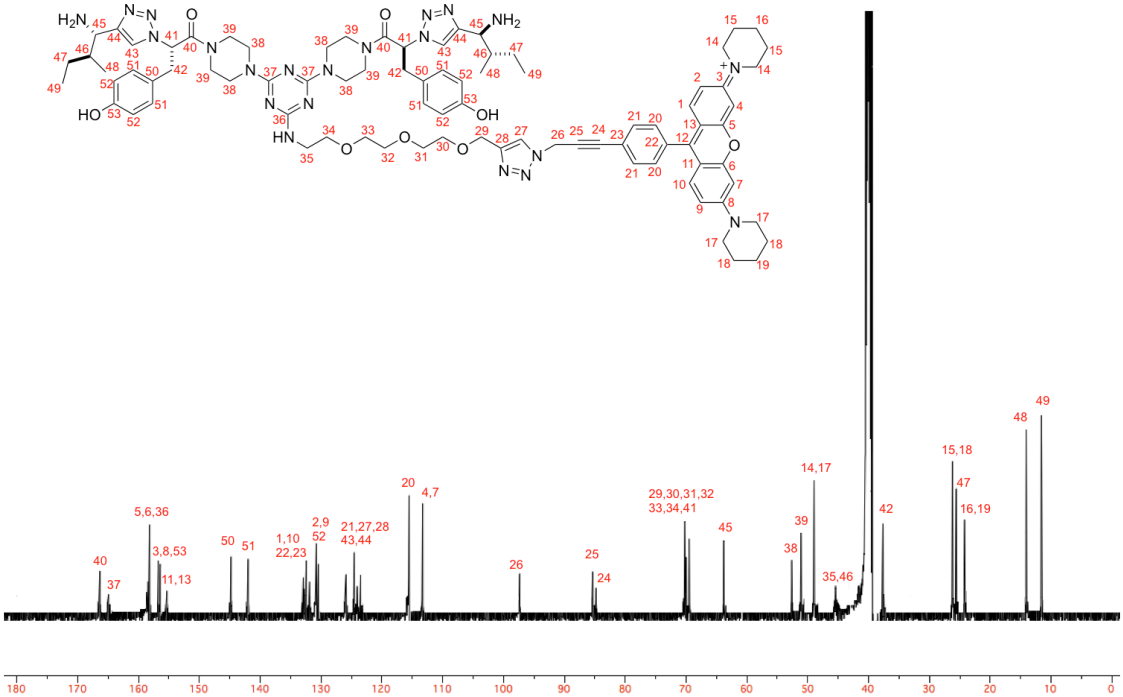

^{13}C NMR of **IY-IY-Ros**

Table S3. Characterization of Compounds **IY-IY-Ros**, **YI-YI-Ros** and **2mor-Ros**.

compounds	retention time (min)	chemical formula	M calculated	M found
IY-IY-Ros	15.6	$C_{84}H_{107}N_{21}O_8^+$	1536.8528	1536.8582[a]
YI-YI-Ros	15.8	$C_{84}H_{107}N_{21}O_8^+$	1536.8528	1536.8571[a]
2mor-Ros	18.0	$C_{52}H_{65}N_{11}O_6^+$	938.5036	938.5072[b]

[a] Hi-resolution MALDI-M; [b] Hi-resolution ESI-MS

Cytotoxicity Comparison

MTT Cell Viability Assays with IY-IY-6MP and 2mor-6MP

TrkC NIH3T3 cells (TrkC) (10,000-12,000 cells/well, 50 mL in Dulbecco's Modified Eagle Medium/nutrient mixture F-12 (DMEM/F12, Sigma Chemical, St. Louis, MO) including G418 (200 mg/mL, GIBCO) were plated on 96-well plates and allowed to adhere at 37 °C in 5 % CO_2 and 95 % air for 3 h. Thereafter, the cells were treated with 50 mL aliquot of each test compounds in PFHM-II and 10 % NBCS (newborn calf serum, GIBCO) at different concentrations, ranging from 0.1 mM to 200 mM. The final concentration of NBCS was 5 %. The cells were then incubated for 56 ~ 60 h. For wild-type NIH3T3 cells, 50 mL in Dulbecco's Modified Eagle

Medium/nutrient mixture F-12 (DMEM/F12) that does not include G418 was used, but other process are the same to TrkC Cells' one. The cell's viability was assessed through an MTT conversion assay.[254] Briefly, 20 mL of MTT (5mg/mL, in Hank's balanced salt solution, HBSS) were added and the cells were incubated for an additional 2 – 3 h. Thereafter, the cells were lysed and the dark blue crystals solubilized with 100 mL of an aqueous solution containing 35 % (v/v) DMF, 15 % (v/v) glacial acetic acid, 15 % (w/v) SDS with an adjusted pH of 3.8. The optical density (OD) of each well (at 570 mm) was measured with a BioTek Synergy 4 Microplate Reader. The viability of each cell line in response to the treatment with tested compounds was calculated as: % dead cells = 100 – (OD treated/OD control) ×100.

Calcein AM Cell Viability Assays with IY-IY-Ros, and YI-YI-Ros

4T1 cells were maintained in monolayer cultures in DMEM supplemented with 10% FBS. Cells (10,000-12,000 cells/well for NIH3T3-TrkC and WT; 5,000-7,000 cells/well for 4T1, 50 µL, in Ham's medium) were plated on 96-well plates and allowed to adhere at 37 °C in 5% CO_2 and 95 % air for 12 h. The cells were then treated with 50 µL of each test compounds in PHFM-II (protein free medium) at 0 to 30 µM concentrations. The cells were incubated for 30 h at 37 °C, then, 100 µL of a 2 µM calcein AM solution (life technologies) were added to each well and incubated for 45 min at 37 °C. Finally, fluorescence was measured in constant intervals (5-10 min) at an excitation wavelength of 485 nm and an emission wavelength of 530 nm using a BioTek Synergy 4 Microplate

Reader. The viability of each cell line in response to the treatment with tested compounds was calculated as: % dead cells = 100 - (F treated/F control) x 100.

Table D-S4. Summary of Cytotoxicities in Different Cells.

compounds	IC_{50} (μM)	
	TrkC[a]	**WT**[b]
IY-IY-Ros	15.80 ± 0.18	27.58 ± 1.38
YI-YI-Ros	25.80 ± 2.24	25.79 ± 1.79
	4T1[c]	
IY-IY-Ros	19.88 ± 2.53	

[a]**TrkC**: TrkC-overexpressed NIH3T3 cells. [b]**WT**: wild-type NIH3T3 cells. [c]**4T1**: murine beast cancer cell line

Competition Assay

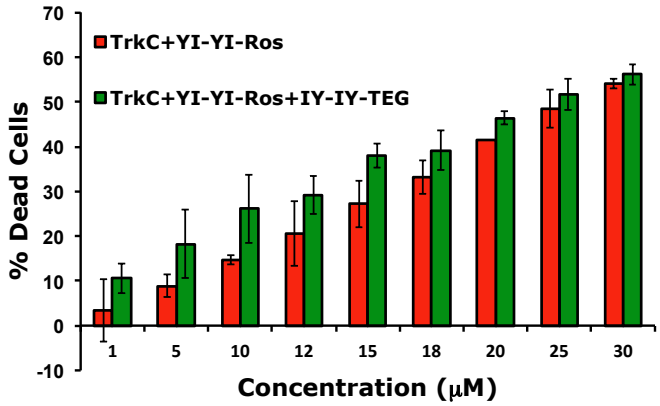

Figure D-S1. Competition assay. Dose-dependent reduction of **YI-YI-Ros** cytotoxicity (red) in competition with the TrkC ligand **IY-IY-TEG** (green) does not occur for **TrkC** cells.

IY-IY-Ros with MitoTracker

Fluorescence Microscopy

Subcellular protein localization was measured on living NIH-TrkC and 4T1 cells using a Zeiss 510 META NLO Multiphoton Microscope System consisting of an Axiovert 200 MOT microscope. Throughout, digital images were captured with a 40x / 1.3 oil objective with the following filter sets:

- for LysoTracker® Green DND-26 (abbreviated to "LysoTracker Green" above): excitation 488 nm; emission BP 500-530
- for rosamine conjugates: excitation 543 nm; emission BP 565-615

Sequential optical sections (Z-stacks) from the basal-to-apical surfaces of the cell were acquired. Digital image acquisition was initiated approximately 1 μm below the basal surface of the cells and optical slices were collected at 0.5 μm steps through their apical surface. These wide-field images were subjected to deconvolution using Intelligent Imaging Innovations (3I) software.

Lysosomal Colocalization

Cells were incubated with IY-IY-Ros for 30 min at 37 ^{o}C. After the cells were washed with PBS, LysoTracker Green was added and the cells were incubated for 30 min at 37 ^{o}C. The cells were washed again with PBS before imaging.

Mitochondrial Colocalization

Cells were incubated with 2mor-Ros for 30 min at 37 ^{o}C. After the cells were washed with PBS, MitoTracker Green was added and the cells were incubated for 20 min at 37 ^{o}C. The cells were washed again with PBS before imaging.

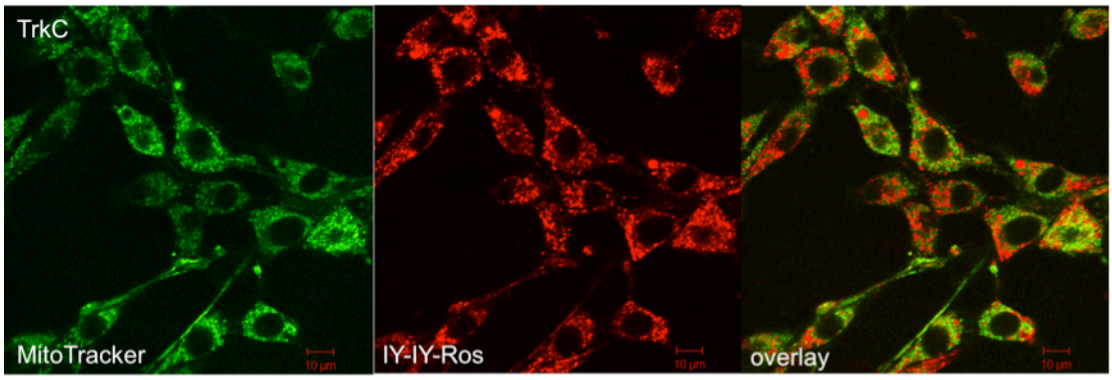

Figure D-S2. IY-IY-Ros and MitoTracker do not colocalize in **TrkC** cells.

APPENDIX E

SUPPORTING INFORMATION FOR CHAPTER III

General Procedures

All reactions were carried out under an atmosphere of dry nitrogen. Glassware was oven-dried prior to use. Unless otherwise indicted, common reagents or materials were obtained from commercial source and used without further purification. All α-amino acids used were of the L-configuration. Dry DMF, (<50 ppm water) was purchased from Acros. Triethylamine (Et_3N) was distilled from CaH_2. Tetrahydrofuran (THF), Acetonitrile (MeCN), dichloromethane (CH_2Cl_2), and methanol (MeOH) were dried by Mbraun solvent drying system. Other solvents and reagents were used as received.

NMR spectra were recorded on a Bruker-400 MHz and Inova-500 MHz spectrometers (^1H at 400 MHz or 500 MHz, and ^{13}C at 100 or 125 MHz) at room temperature unless other mentioned. Chemical shifts of ^1H NMR spectra were recorded and chemical shifts are reported in ppm from the solvent resonance ($CDCl_3$ 7.26 ppm, CD_3OD 3.30 ppm, DMSO-d_6 2.50 ppm). Data are reported as follows: chemical shift, multiplicity (s = singlet, br = broad, d = doublet, t = triplet, q = quartet, m = multiplet), coupling constants, and number of protons. Proton decoupled ^{13}C NMR spectra were also recorded in ppm from tetramethylsilane (TMS) resonance ($CDCl_3$ 77.0, CD_3OD 49.1, DMSO-d_6 39.5 ppm). Analytical thin layer chromatography (TLC) was performed on EM Reagents 0.25 mm silica-gel 60-F plates, and visualized with UV light. Flash

chromatography was performed using silica gel 60 (230–400 mesh). MS were measured under ESI or MALDI conditions.

Analytical HPLC analyses were carried out on 150 x 4.6 mm C-18 column using gradient conditions (10 – 90% B, flow rate = 0.75 mL/min). Preparative HPLC was carried out on 100 x 21.2 mm C-18 column using gradient conditions (10 – 70% B, flow rate = 10.0 mL/min). The eluents used were: solvent A (H_2O with 0.1% TFA) and solvent B (CH_3CN with 0.1% TFA).

The purity of all biologically evaluated compounds is > 95% confirmed by analytical HPLC.

Syntheses Of DiiodoBODIPY Derivatives

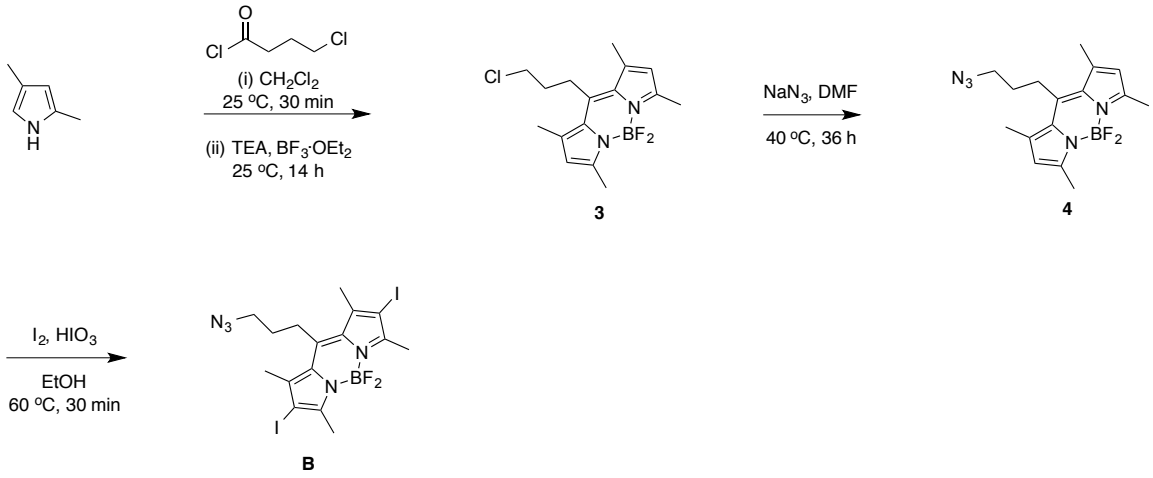

10-(3-Chloropropyl)-5,5-difluoro-1,3,7,9-tetramethyl-5*H*-4λ^4,5λ^4-dipyrrolo[1,2-*c*:2',1'-*f*][1,3,2]diazaborinine (3). 2,4-Dimethylpyrrole (2.0 mL, 19 mmol) was added to a solution of 4-chlorobutanoyl chloride (0.99 mL, 8.8 mmol) in CH_2Cl_2 (20 mL) over

10 min at 0 ºC. The reaction was stirred at 0 ºC for 30 min, then warmed up to 25 ºC and stirred for an additional 30 min. Triethylamine (3.7 mL, 26 mmol) was then added in small portions at 0 ºC and the mixture was stirred at 25 ºC for 10 min. BF_3•OEt_2 (5.5 mL, 44 mmol) was then added in portions and the mixture was stirred at 25 ºC for 14 h. The reaction was quenched with careful addition of H_2O (20 mL) and the system was stirred vigorously for 15 min. The aqueous layer was extracted with CH_2Cl_2 (3 × 10 mL). The organic layers were combined and washed with H_2O (2 × 10 mL) and brine (10 mL). The organic layer was dried over $MgSO_4$, filtered, and the solvent was removed under reduced pressure. The brown powder was dissolved in small amount of CH_2Cl_2 and filtered through a short plug of silica. The solvent was removed under reduced pressure and the remaining powder was recrystallized from ethyl acetate to yield 0.90 g (32 %) of **4** as a red needles. ^{1}H NMR (300 MHz, $CDCl_3$) δ 6.06 (s, 2H), 3.70 (t, J = 6.0 Hz, 2H), 3.13 (t, J = 8.4 Hz, 2H), 2.52 (s, 6H), 2.43 (s, 6H), 2.08-2.16 (m, 2H). ^{13}C (100 MHz, $CDCl_3$) δ 154.4, 144.4, 140.3, 131.4, 121.8, 44.7, 34.0, 25.9, 16.5, 14.4. HRMS (ESI) calcd for $C_{16}H_{19}BClF_2N_2$ $\{M-H\}^-$ 323.1298, found 323.1287.

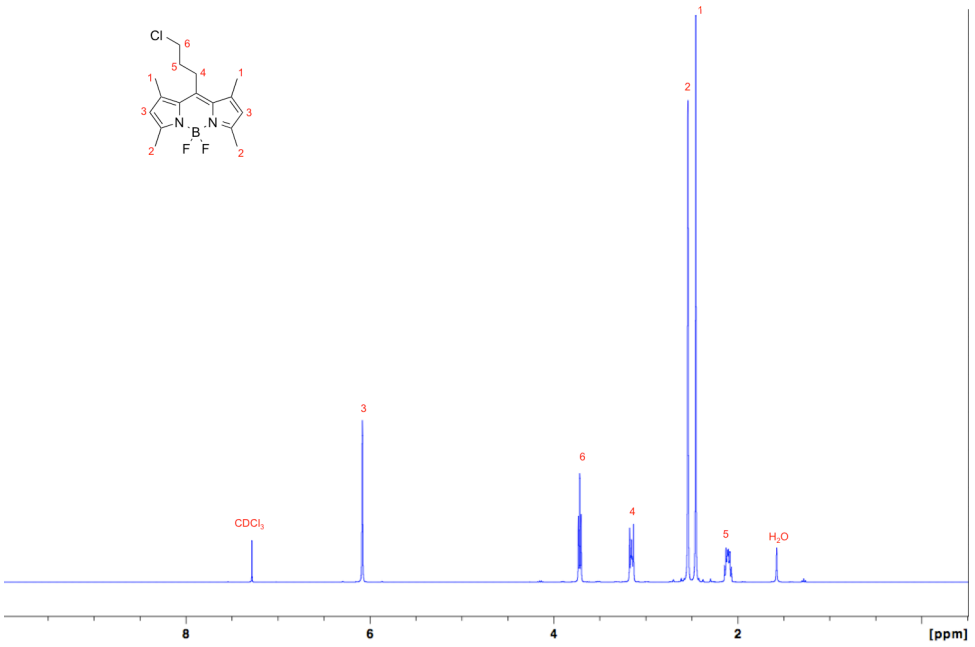

^{1}H-NMR of compound 3

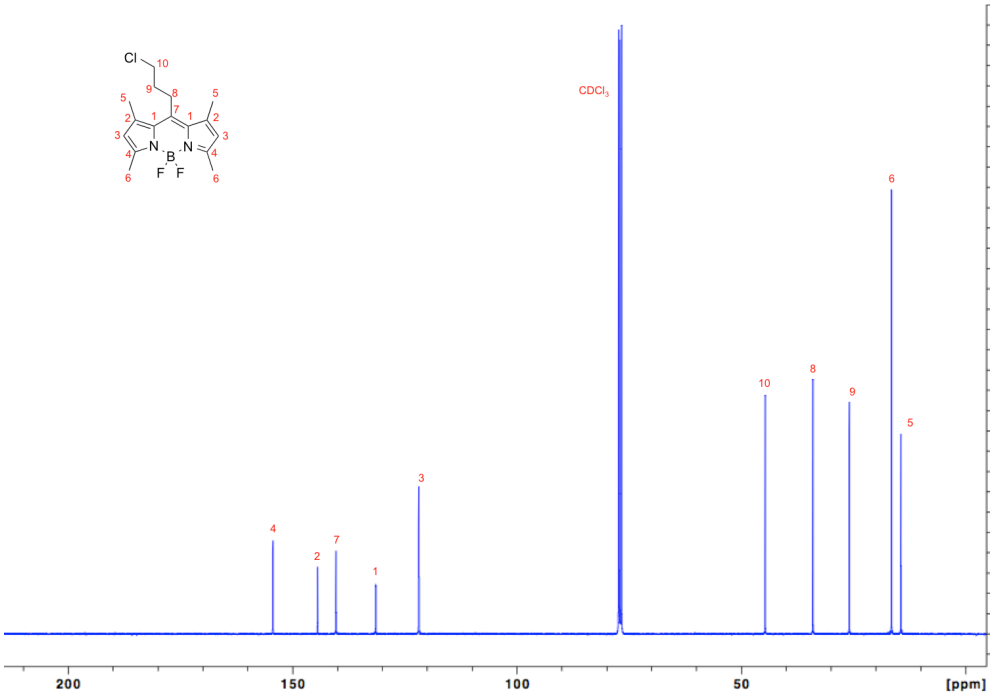

^{13}C-NMR of compound 3

10-(3-Azidopropyl)-5,5-difluoro-1,3,7,9-tetramethyl-5*H*-4λ^4,5λ^4-dipyrrolo[1,2-*c*:2',1'-*f*][1,3,2]diazaborinine (4). Sodium azide (240 mg, 3.6 mmol) was added to a solution of **4** (600 mg, 1.9 mmol) in DMF (36 mL). The mixture was stirred at 40 ºC for 36 h. Water (20 mL) was then added and the suspension was extracted with ethyl acetate (3 × 20 mL). The combined organic layers were washed with H_2O (2 × 20 mL) and brine (20 mL). The organic layer was dried over $MgSO_4$, filtered and the solvent was removed under reduced pressure to afford 600 mg (99 %) of **5** as an orange powder. ^{1}H NMR (500 MHz, $CDCl_3$) δ 6.06 (s, 2H), 3.49 (t, J = 6.0 Hz, 2H), 3.03 (t, J = 8.4 Hz, 2H), 2.51 (s, 6H), 2.46 (s, 6H), 1.86-1.93 (m, 2H). ^{13}C (100 MHz, $CDCl_3$) δ 154.3, 144.6, 140.3, 131.4, 121.9, 51.5, 31.4, 25.6, 16.5, 14.4. HRMS (ESI) calcd for $C_{16}H_{19}BF_2N_5$ {M-H}$^-$ 330.1702, found 330.1712. FT-IR (NaCl): N_3 band at 2098 cm^{-1}.

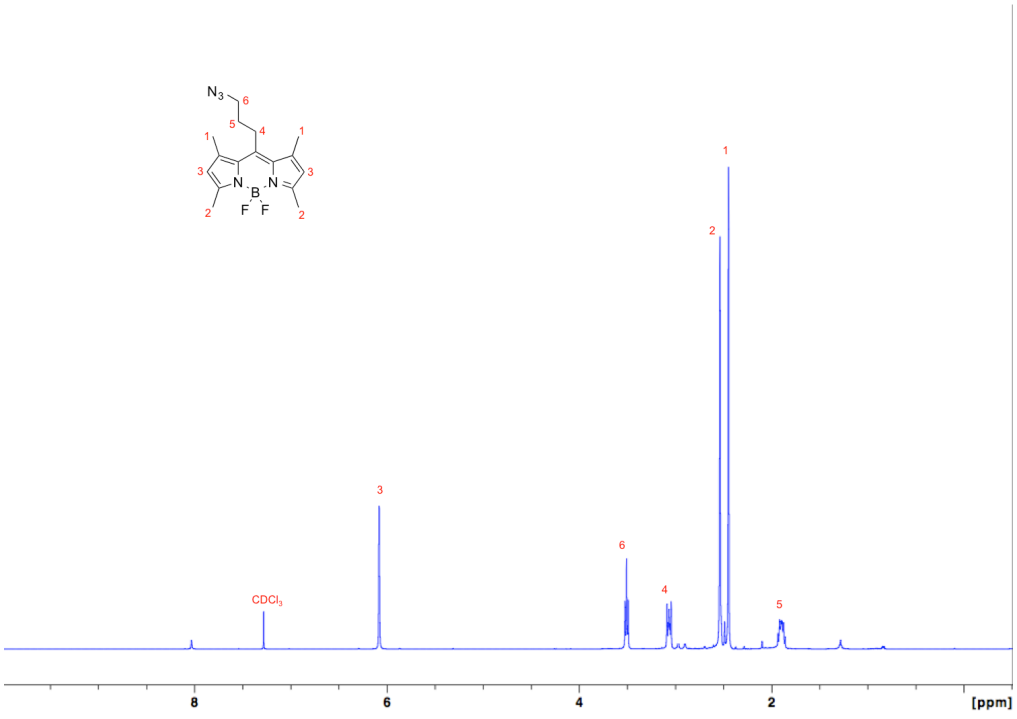

^{1}H-NMR of compound 4

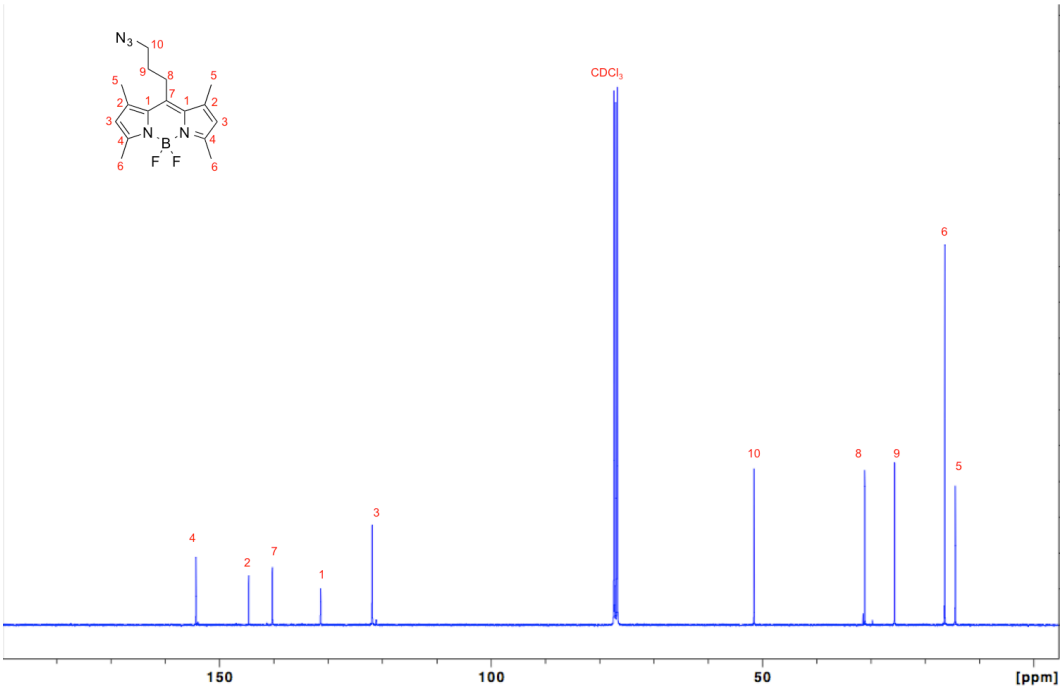

^{13}C-NMR of compound 4

10-(3-Azidopropyl)-5,5-difluoro-2,8-diiodo-1,3,7,9-tetramethyl-5*H*-4λ^4,5λ^4-dipyrrolo[1,2-*c*:2',1'-*f*][1,3,2]diazaborinine (B). Iodine (585 mg, 2.31 mmol) and iodic acid (342 mg, 1.94 mmol) were added to a suspension of **5** (351 mg, 0.92 mmol) in ethanol (20 mL). The mixture was stirred at 60 ºC for 30 min. The mixture was cooled to 25 ºC and water (30 mL) was added. The product was extracted with CH_2Cl_2 (3 × 20 mL). The combined organic layers were dried over $MgSO_4$, filtered, and the solvent was removed under reduced pressure. The residue was purified by flash silica chromatography eluting with hexanes:CH_2Cl_2 (3:1 to 2:1) to yield 351 mg (65 %) of **B** as a red powder. ^{1}H NMR (400 MHz, $CDCl_3$) δ 3.53 (t, J = 6.5 Hz, 2H), 3.13 (t, J = 8.5 Hz, 2H), 2.61 (s, 6H), 2.48 (s, 6H), 1.85-1.92 (m, 2H). ^{13}C (100 MHz, $CDCl_3$) δ 155.8, 144.3, 142.2, 131.3, 86.8, 51.4, 31.0, 26.5, 19.1, 16.2. HRMS (ESI) calcd for

$C_{16}H_{17}BF_2I_2N_5$ {M-H}$^-$ 581.9635, found 581.9609. FT-IR (NaCl): N_3 band at 2106 cm^{-1}.

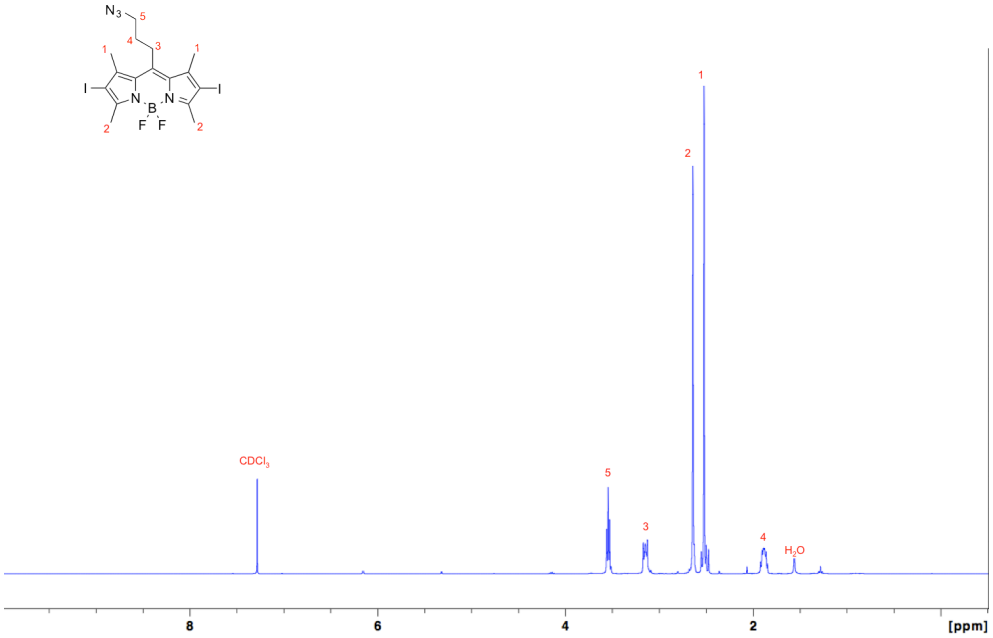

^{1}H-NMR of compound B

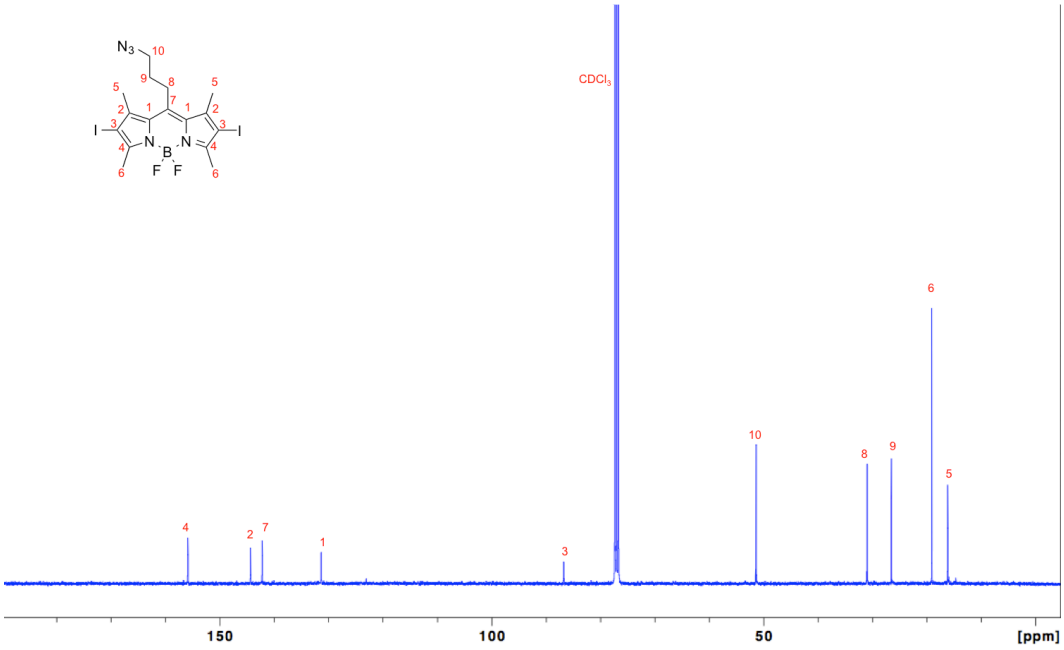

^{13}C-NMR of compound B

Experimental Procedures And Characterization Of IY-IY-PDT And YI-YI-PDT

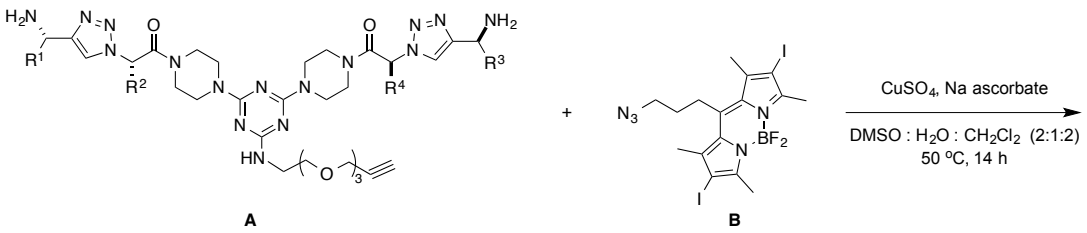

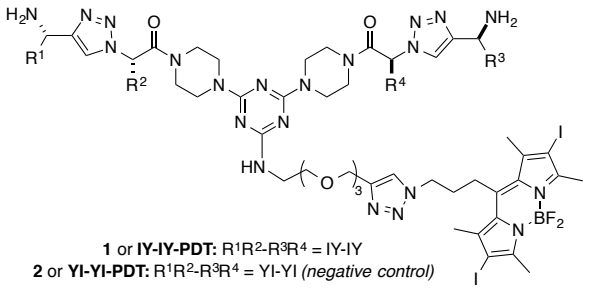

1 or **IY-IY-PDT:** R^1R^2-R^3R^4 = IY-IY
2 or **YI-YI-PDT:** R^1R^2-R^3R^4 = YI-YI *(negative control)*

IY-IY-TEG, and **YI-YI-TEG (structure A)** were prepared via the previously published methodology from our group.[77,190] To a solution of **B** (1.5 equiv) and **IY-IY-TEG** or **YI-YI-TEG** (1.0 equiv) in DMSO:H_2O:CH_2Cl_2 (2:1:2, 0.01 M) were added $CuSO_4$ (0.1 equiv, from 0.05 M aqueous solution) and fresh Na ascorbate (0.4 equiv, from 0.05 M aqueous solution) at 25 °C. The mixture was stirred at 25 °C for 24 h. The reactions were monitored by analytical HPLC. The crude compounds were lyophilized to remove DMSO, and then purified by RP-preparative HPLC to obtain the bivalent mimics **IY-IY-PDT** or **YI-YI-PDT**. The final products were lyophilized three times in 1.0 % acetic acid to remove TFA.

IY-IY-PDT

After purification and lyophilization, the product was obtained as a red powder (27-35 % yield). The purity was found to be *ca.* >99% by HPLC analysis, retention time 16.083.

^{1}H NMR (400 MHz, DMSO-d_6) δ 8.38 (br, 4H), 8.29 (s, 2H), 8.23 (s, 1H), 7.00 (d, 4H, *J* = 8.5 Hz), 6.78 (br, 2H), 6.61 (d, 4H, *J* = 8.4 Hz), 6.17 (t, 2H, *J* = 7.3 Hz), 4.63-4.54 (m, 2H), 4.38 (t, 2H, *J* = 5.6 Hz), 3.64-3.42 (m, 30H), 3.34-3.19 (m, 4H), 3.06-2.98 (m, 2H), 2.53 (s, 6H), 2.25 (s, 6H), 2.14-2.07 (m, 2H), 1.98-1.87 (m, 2H), 1.40-1.30 (m, 2H), 1.08-0.94 (m, 2H), 0.93-0.86 (m, 6H), 0.79-0.70 (m, 6H)

^{13}C NMR (100 MHz, DMSO-d_6) δ 166.4, 158.6, 158.3, 156.8, 155.2, 145.7, 144.6, 143.3, 142.0, 131.3, 130.7, 125.9, 125.0, 115.5, 115.5, 88.1, 70.3, 70.3, 70.2, 70.1, 70.0, 69.5, 69.4, 63.9, 51.2, 49.6, 45.4, 42.7, 42.2, 37.7, 31.8, 25.6, 19.0, 16.3, 15.2, 14.1, 11.3

Hi-Res MALDI-MS: m/z calcd for $C_{68}H_{93}BF_2I_2N_{21}O_7^+$ $\{M+H\}^+$ 1618.5723 found 1618.5836.

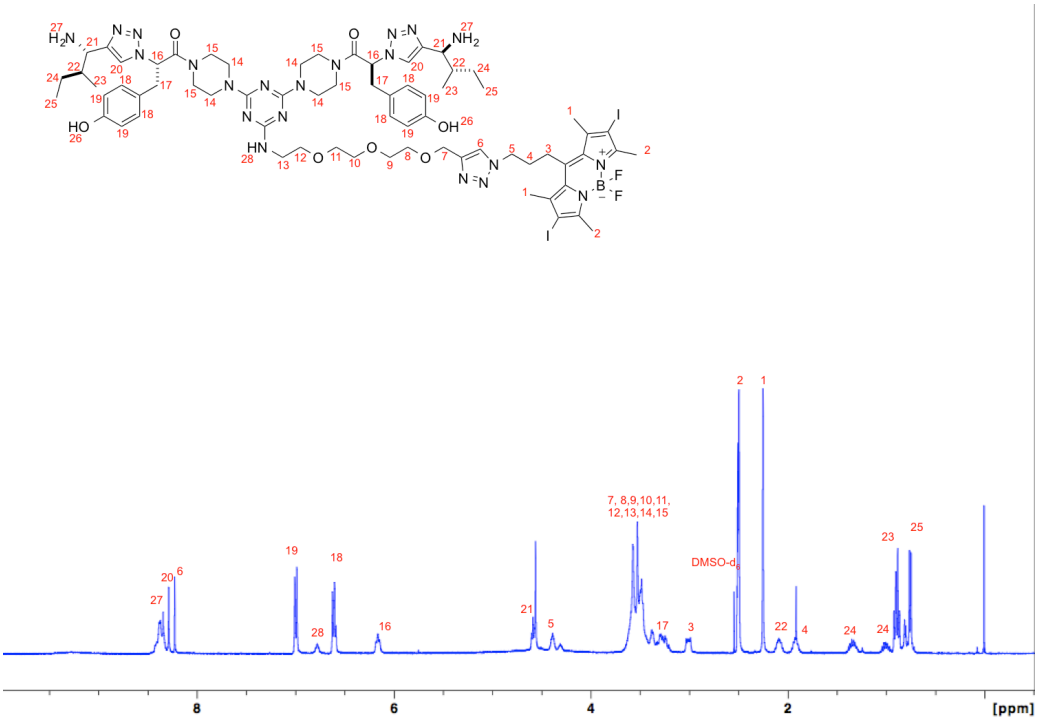

^{1}H-NMR of compound 1 or IY-IY-PDT

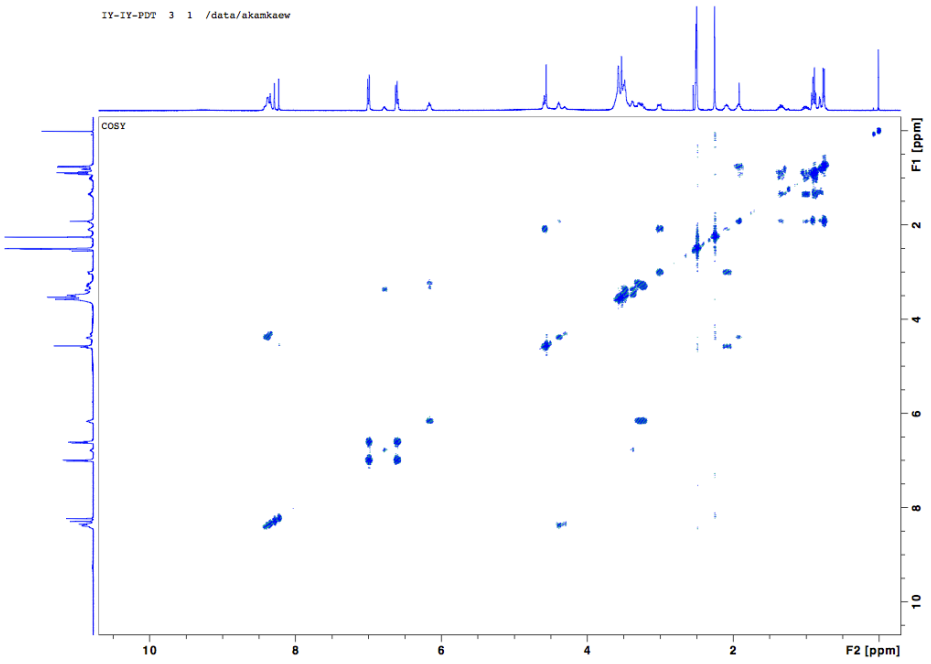

COSY-NMR of compound 1 or IY-IY-PDT

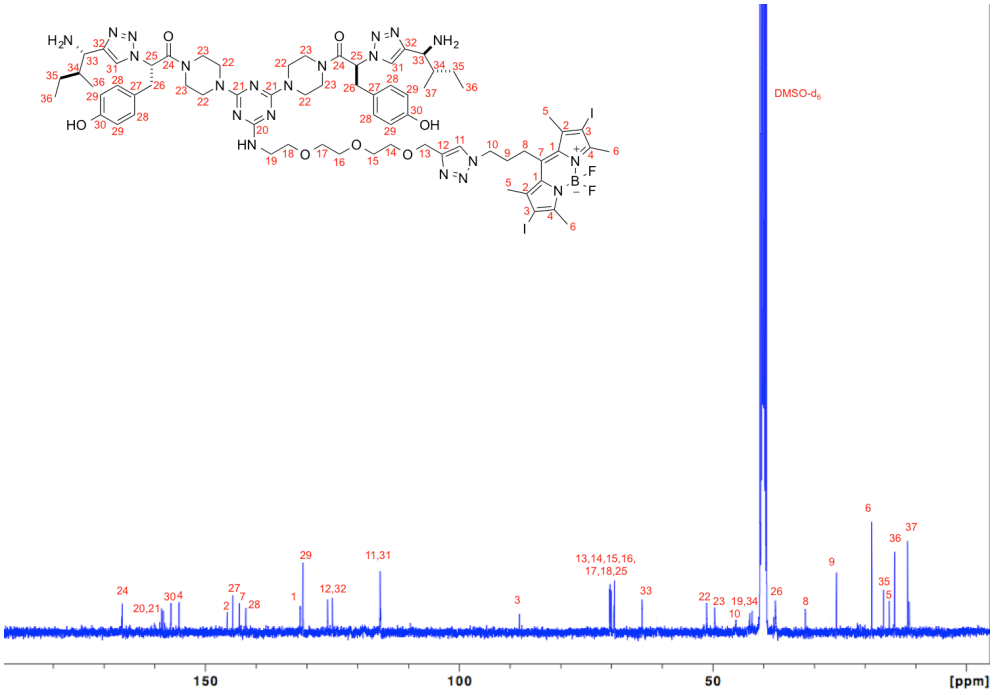

^{13}C-NMR of compound 1 or IY-IY-PDT

YI-YI-PDT

After purification and lyophilization, the product was obtained as a red powder (34-42 % yield). The purity was found to be *ca.* >99% by HPLC analysis, retention time 16.283. ^{1}H NMR (400 MHz, DMSO-d_6) δ 8.46 (br, 4H), 8.23 (s, 2H), 8.16 (s, 1H), 7.01 (br, 1H), 6.88 (d, 4H, J = 8.4 Hz), 6.83 (br, 2H), 6.61 (d, 4H, J = 8.4 Hz), 5.70 (d, 2H, J = 9.7 Hz), 4.70-4.63 (m, 2H), 4.60 (t, 2H, J = 5.4 Hz), 3.79-3.43 (m, 30H), 3.46-3.38 (m, 4H), 3.23-3.07 (m, 2H), 3.06-2.98 (m, 2H), 2.50 (s, 6H), 2.25 (s, 6H), 2.15-2.04 (m, 2H), 0.98-0.90 (m, 6H), 0.89-0.84 (m, 2H), 0.84-0.78 (m, 6H), 0.77-0.72 (m, 2H). ^{13}C NMR (100 MHz, DMSO-d_6) δ 166.4, 158.9, 158.4, 156.7, 155.2, 145.7, 144.6, 143.9, 143.3, 131.3, 130.7, 126.0, 125.0, 123.6, 115.5, 115.5, 88.0, 70.3, 70.3, 70.2, 70.1, 70.0, 69.4, 69.4, 63.9,

49.6, 48.8, 45.6, 43.6, 42.1, 38.0, 31.8, 26.5, 24.2, 18.7, 16.3, 15.4, 11.0. Hi-Res MALDI-MS: m/z calcd for $C_{68}H_{93}BF_2I_2N_{21}O_7^+$ $\{M+H\}^+$ 1618.5723 found 1618.5946.

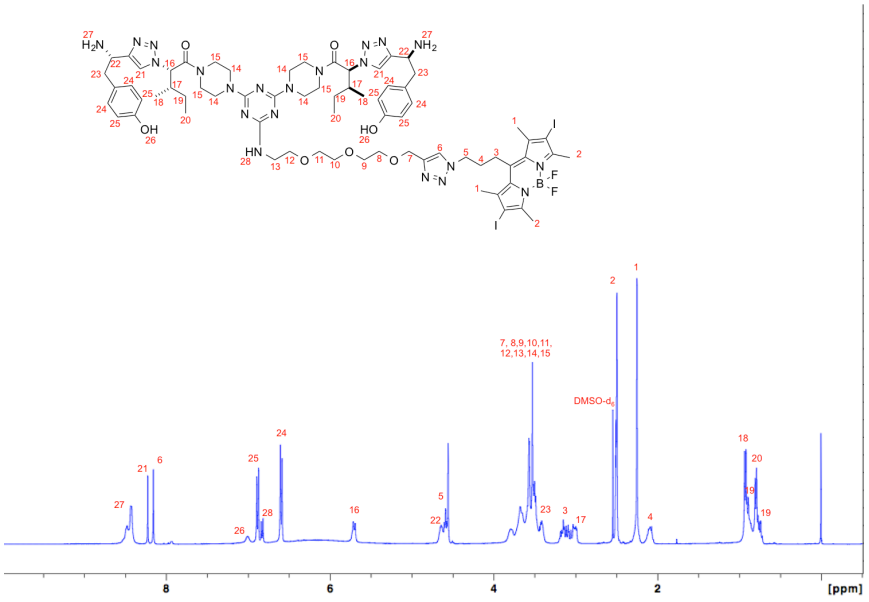

^{1}H-NMR of compound 2 or YI-YI-PDT

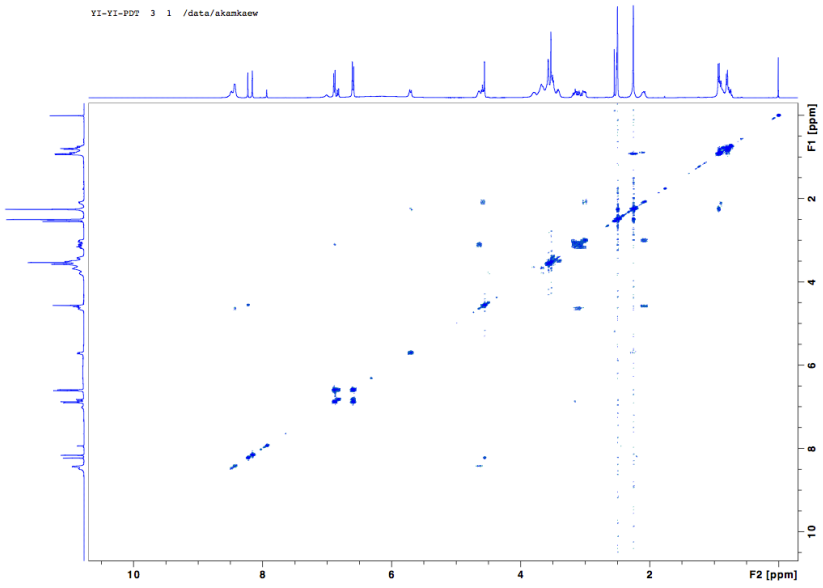

COSY-NMR of compound 2 or YI-YI-PDT

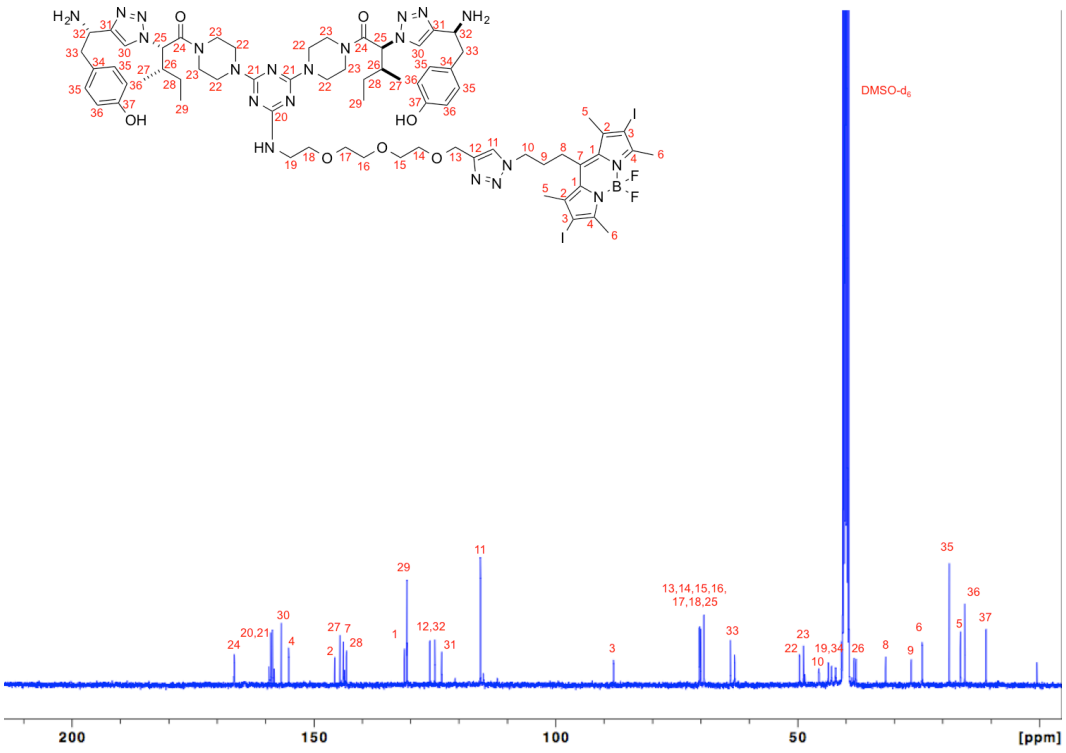

^{13}C-NMR of compound 2 or YI-YI-PDT

Photophysical Properties For IY-IY-PDT And YI-YI-PDT

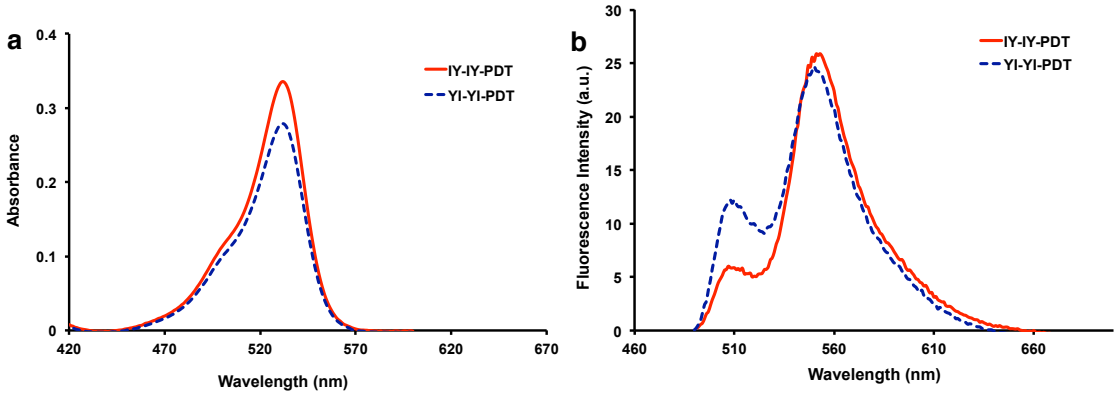

Figure E-S1. **a** UV-Vis and **b** fluorescence spectra (excited at 480 nm) of **1** and **2** (both at 5.5 mM) in DMSO.

Table E-S1. Absorption and Fluorescence Data for compound 1 and 2 in DMSO

Compound	λ_{abs} (nm)	ε (M^{-1} cm^{-1})	λ_{emiss} (nm)[a]	Φ_F[b] (in DMEM)
1 or **IY-IY-PDT**	532	61430	550	0.02 (0.01)
2 or **YI-YI-PDT**	532	50221	550	0.03 (0.01)

[a]Excited at 480 nm. [b]Relative to Rhodamine G6 in EtOH (Φ_F = 0.94).

Cellular Studies For IY-IY-PDT And YI-YI-PDT

Table E-S2. Summary Of Photocytotoxicities In Different Cells.

compounds	IC_{50} (μM)		
	NIH3T3-TrkC[a]	**NIH3T3-WT**[b]	**SY5Y**[c]
IY-IY-PDT	0.35 ± 0.06	> 2	0.15 ± 0.02
IY-IY-PDT	> 2	> 2	0.54 ± 0.04

[a]**TrkC**: TrkC-overexpressed NIH3T3 cells. [b]**WT**: wild-type NIH3T3 cells. [c]**SY5Y**: human neuroblastoma cells.

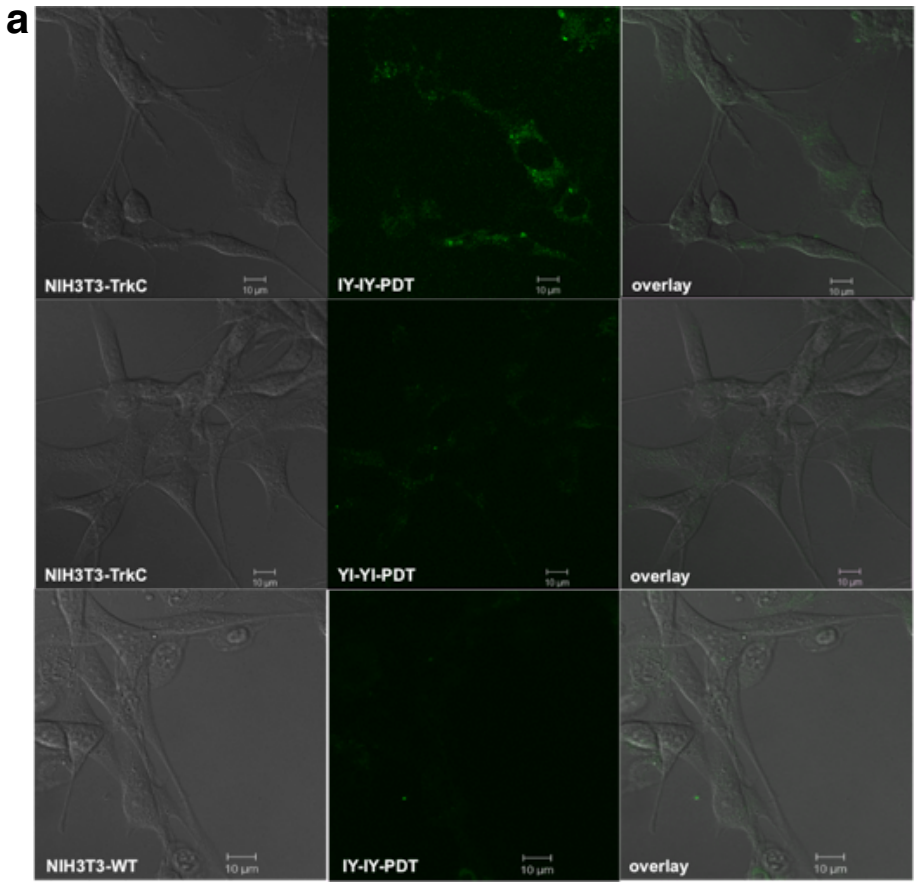

Figure E-S2. **a** Confocal imaging of: *first row*, the featured targeting ligand on $TrkC^{+}$ cells showing the compound is internalized; *second row*, the negative control YI-YI-PDT is not localized under the same conditions; *third row*, the featured agent is not observed in $TrkC^{-}$ cells under the same conditions. **b** Quantitative indications of the fluorescence intensity in each of the three experiments described above (error bars from 100 cells).

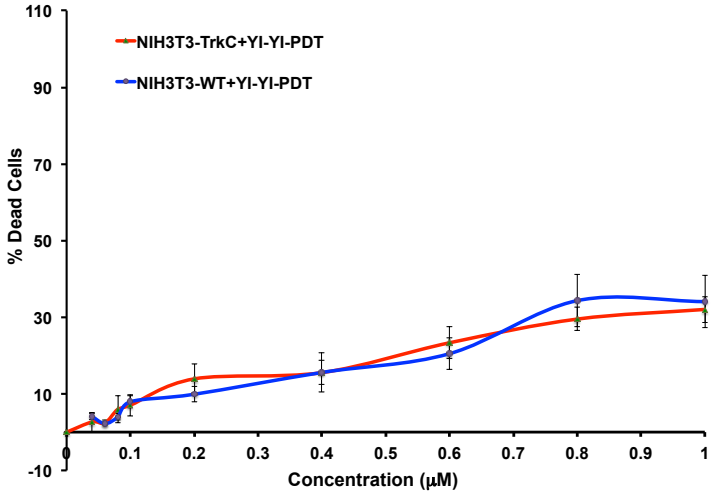

Figure E-S3. Photoinduced cytotoxicity assays. YI-YI-PDT (a negative control) show similar cytotoxicity for the TrkC expressing cells, NIH3T3-TrkC (red) and non-TrkC cells, NIH3T3-WT (blue). In the experiments the cells were illuminated with a broad spectrum source, filtered to only deliver photons of >480 nm wavelength, at a flux of approximately 12.2 mW/cm^2 for 10 mins. Error bars were based on 3 runs.

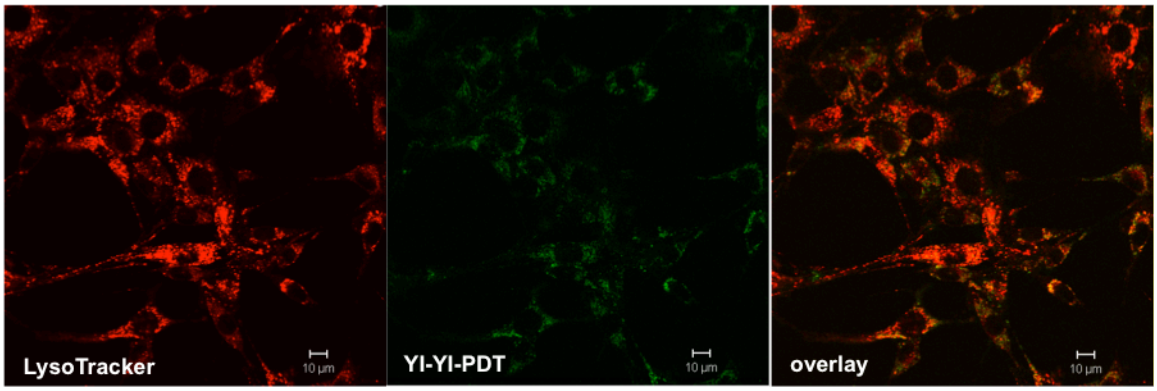

Figure E-S4. YI-YI-PDT *partially* colocalizes with *LysoTracker Red* in TrkC$^+$ cells.

APPENDIX F

SUPPORTING INFORMATION FOR CHAPTER IV

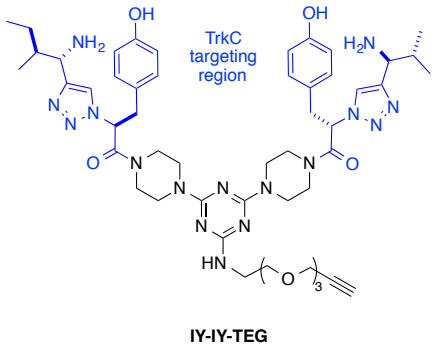

Figure F-S1. Structure of IY-IY-TEG.

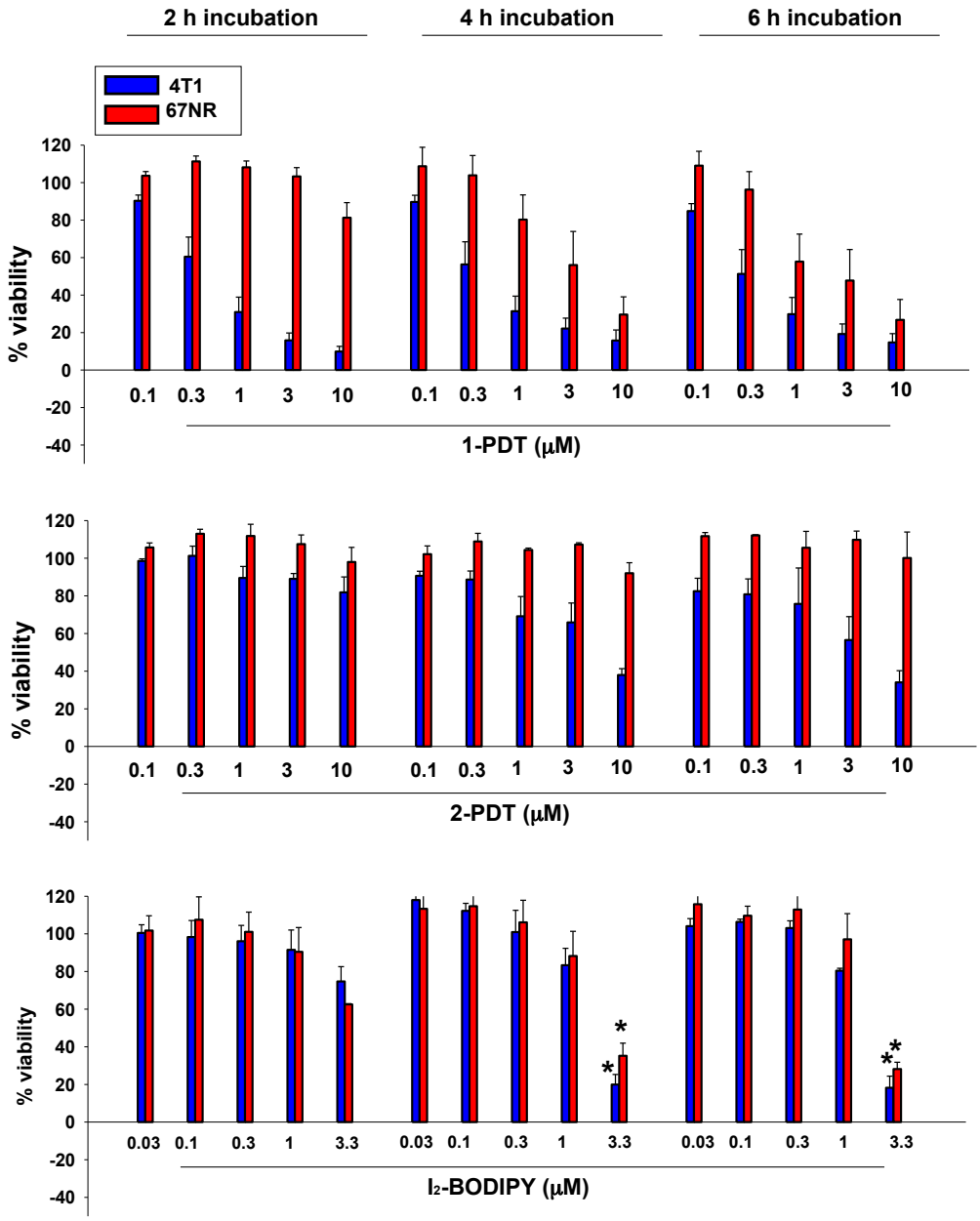

Figure F-S2. Compounds induced non-selective photocytotoxicity in TrkC$^+$ and TrkC$^-$ cells when treated for prolonged periods. 4T1 and 67NR cells were cultured in 96-well plates. After 24 h, **1-PDT**, **2-PDT** and **I_2-BODIPY** with indicated concentrations were added to cells and incubated for 2 h, 4 h and 6 h. Media was removed and the cells were washed with PBS before new media was added. Cells were then irradiated with 7.3 J/cm^2 of light at a fluence rate of 12.2 mW/cm^2. MTT was carried out 24 h after irradiation. Data represent mean ± SEM of three independent experiments. * $p < 0.05$, ** $p < 0.005$ *vs* 2 hours treatment, Student's t-test.

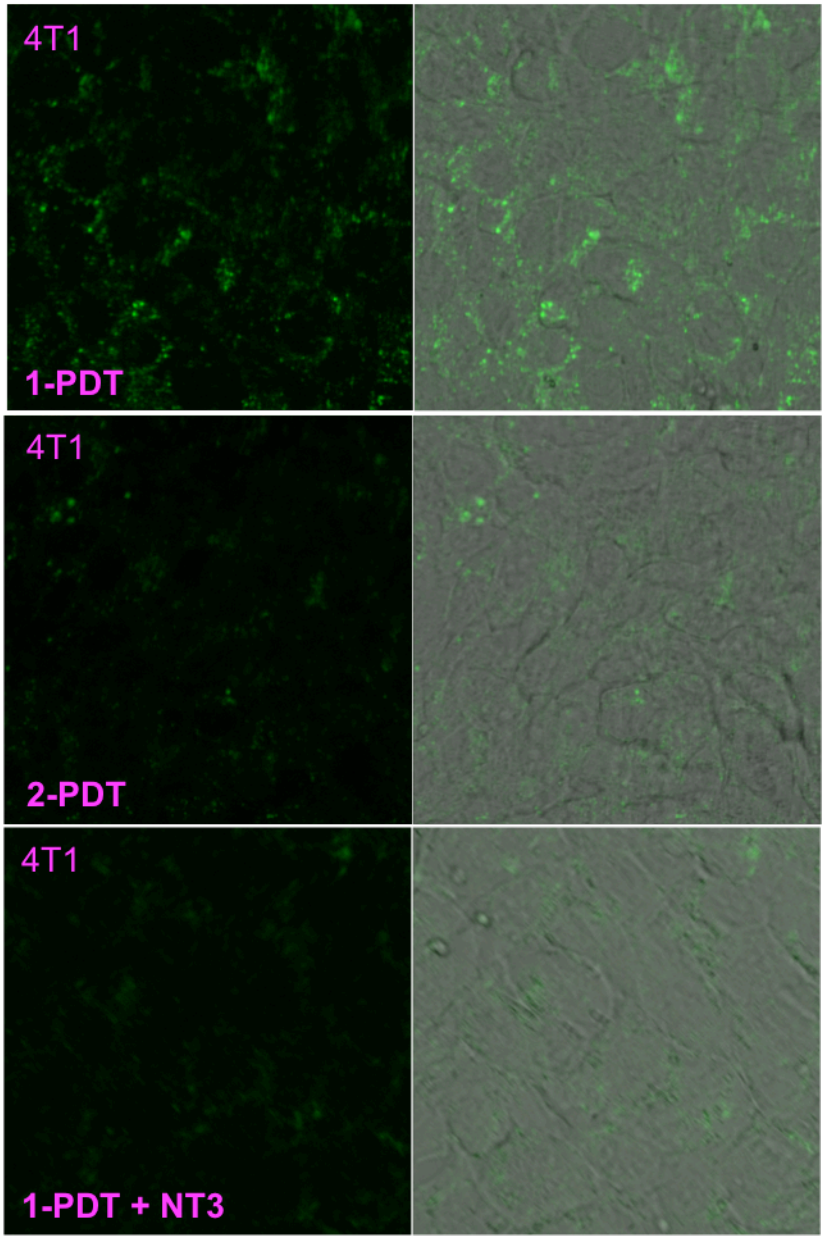

Figure F-S3. Uptake of compounds in TrkC$^+$ cells. 4T1 cells were cultured in 2-well chambers. After 48 h, **1-PDT** and **2-PDT** were added to cells (final concentration is 0.5 μM) and incubated for 2 h. Media was removed and the cells were washed with PBS before new media was added. Images were captured using confocal microscope (20X).

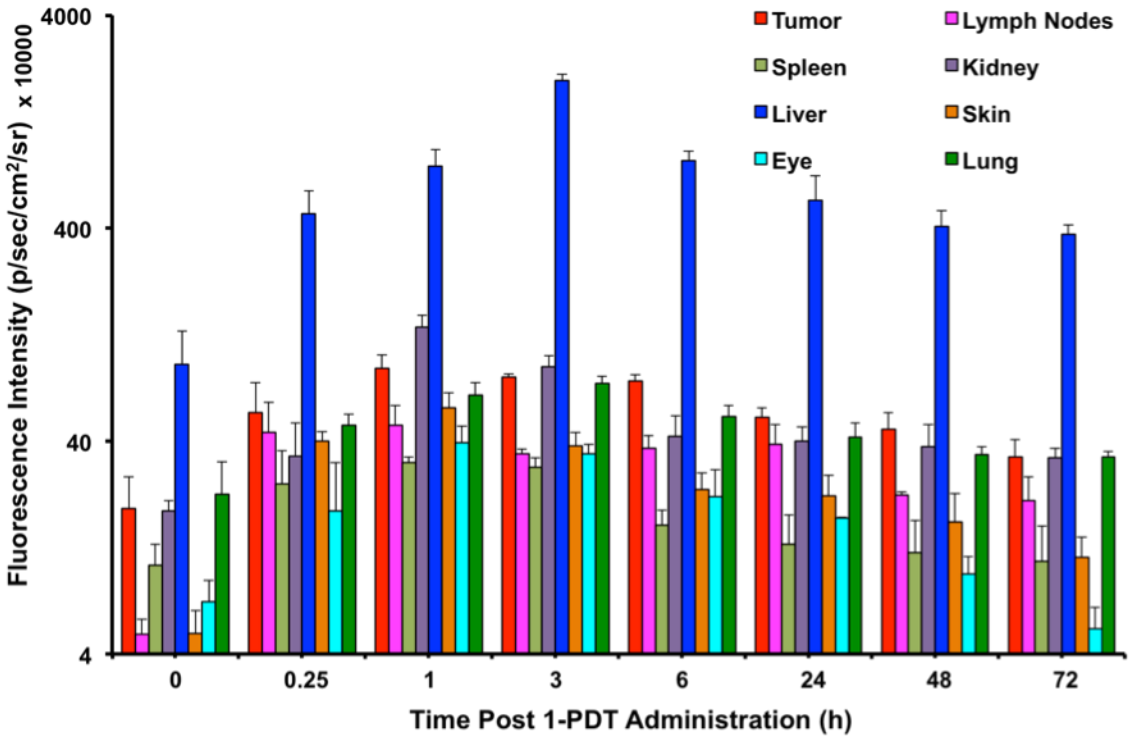

Figure F-S4. Biodistribution of 1-PDT in 4T1 tumor bearing mice. Biodistribution of **1-PDT** was monitored in 4T1 tumor bearing mice (n=3) up to 72 h. Significant fluorescent signals were detected the liver (20 folds more than that of the tumor), kidney and lung within the first 3 h post administration. Although the amount of **1-PDT** in tumor was significantly lower ($p<0.05$ for all monitoring time points, One way ANOVA-Tukey post-hoc test) than that of the liver, the tumor accumulation level of **1-PDT** was found to resemble to that of the heavily vascularized kidney and lung in the first 3 hours post **1-PDT** administration, and persistently higher than that of these organs in the following 69 hours of monitoring period. Taking into consideration of the relatively lower vascularization in tumor compare to the kidney and lung, and the consistency of the **1-PDT** level within the tumor throughout the monitoring period, it would be fair to suggest that the accumulation of **1-PDT** in tumor is somehow not random but associated to the targeting of 1-PDT by the associated IY ligands to the tumor tissue.

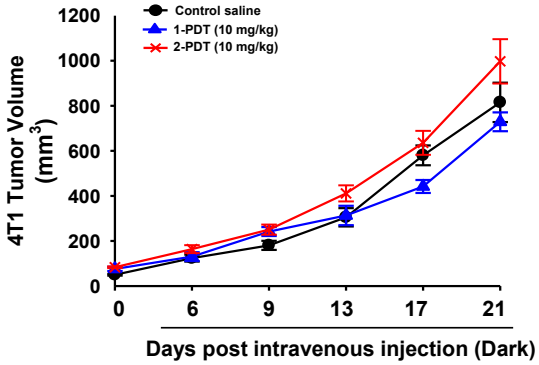

Figure F-S5. 1-PDT in the dark did not promote 4T1 tumor growth. 4T1 tumor cells were inoculated subcutaneously to female balb/c mice. Both 1-PDT and 2-PDT were intravenously injected via tail vein when the tumor size reached 70-100 mm^3. Tumor size was monitored for 30 days. Graph represents mean ± SEM of seven 4T1 tumor bearing mice.

In the graph of % of initial tumor volume, **1-PDT** has slower tumor growth compared to **2-PDT** in dark. We hypothesize that **1-PDT** might indirectly regulates certain cytokines profile and immune response; we are currently working on exploring this idea.

APPENDIX G

SUPPORTING INFORMATION FOR CHAPTER V

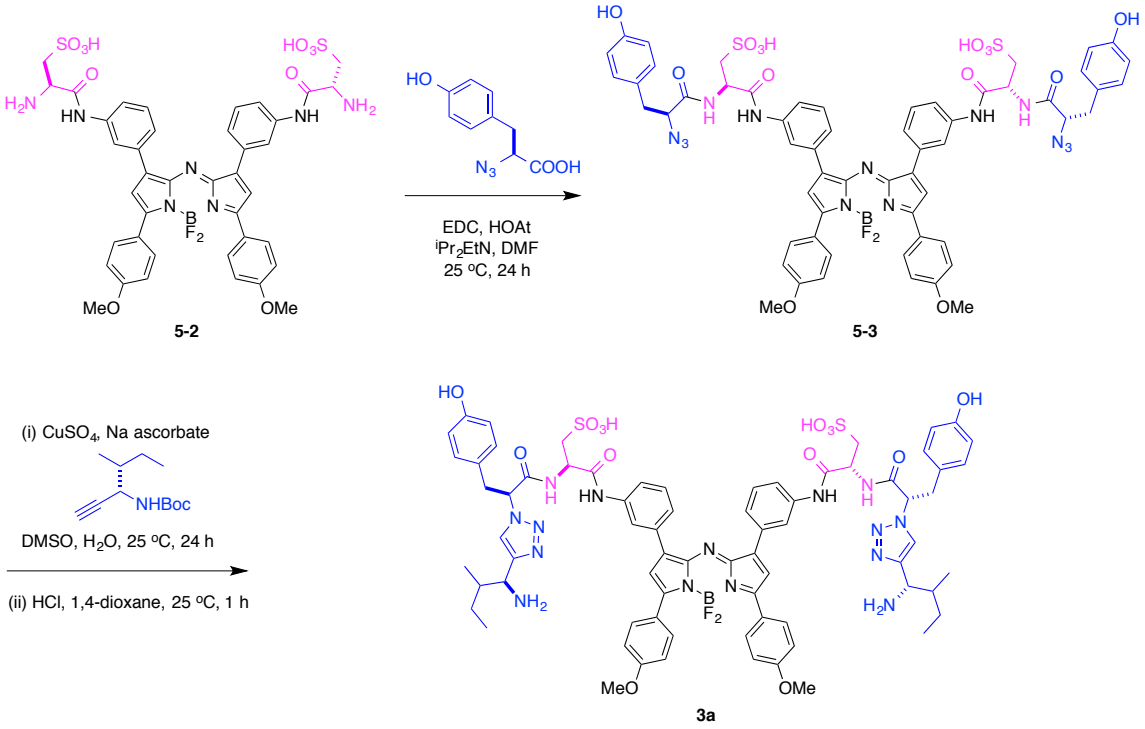

Scheme S1. Synthesis of **3a**.

Synthesis of **5-3**.

Tyrosine azide (41 mg, 0.2 mmol) was dissolved in DMF (0.4 mL), then cooled to 0 °C. EDCI (41 mg, 0.22 mmol) and HOAt (20 mg, 0.21 mmol) were added to the solution. After stirring at 0 °C for 30 min, **5-2** (35 mg, 0.04 mmol) was added to the above suspension followed by DIPEA (70 µL, 0.4 mmol). Then, the resulting solution was warmed to 25 °C and stirred for 24 h. Solvent was removed under reduced pressure. After that, the residue was purified by reverse phase MPLC using H_2O:CH_3CN

(gradient) to afford **5-3** as a green powder (30 mg, 60 %). ^{1}H-NMR (400 MHz, DMSO-d_6) δ 10.28 (s, 2H), 9.23 (s, 2H), 8.61 (d, *J* = 8.9 Hz, 2H), 8.61-8.60 (m, 6H), 8.17 (d, *J* = 8.8 Hz, 2H), 7.94 (d, *J* = 7.6 Hz, 2H), 7.68 (t, *J* = 8.0 Hz, 2H), 7.51 (s, 2H), 7.16-7.09 (m, 6H), 6.69 (d, *J* = 8.8 Hz, 2H), 4.66-4.61 (m, 2H), 4.09-4.05 (m, 2H), 3.59 (s, 6H), 3.13-3.11 (m, 2H), 3.04-2.99 (m, 6H). ^{13}C (100 MHz, DMSO-d_6) δ 169.4, 162.5, 157.9, 156.6, 143.1, 140.0, 132.5, 132.3, 130.5, 129.6, 128.9, 127.5, 123.7, 120.0, 63.8, 56.1, 54.0, 52.4, 49.0, 42.3.

Synthesis of **3a**.

5-3 (50 mg, 0.04 mmol) and Boc-Isoleucine alkyne (20 mg, 0.09 mmol) were dissolved in DMSO (1 mL). Then, aqueous solution of $CuSO_4$ (0.1 M, 78 μL, 0.008 mmol) and sodium ascorbate (0.2 M, 156 μL, 0.032 mmol) were added to the mixture at 25 °C. The reaction was stirred at 25 °C for 24 h (monitored by C18-TLC). Solvent was removed under reduced pressure. After that, the residue was purified by reverse phase MPLC using H_2O:CH_3CN (gradient) to afford **Boc-3a** as a green powder (39 mg, 58 %). Subsequently, **Boc-3a** (39 mg, 0.023 mmol) was dissolved in 1,4-dioxane (0.5 mL). Then HCl in 1,4-dioxane (2 M, 0.5 mL) was added into the solution. Reaction mixture was stirred at 25 °C for 1h, then solvent was removed under reduced pressure to give desired product **3a** as green solid quantitatively.

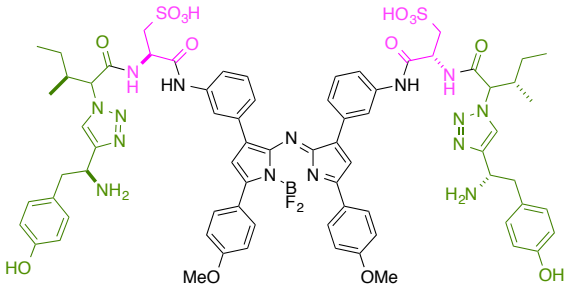

Figure G-S1. Structure of control compound (isomer of **3a**).

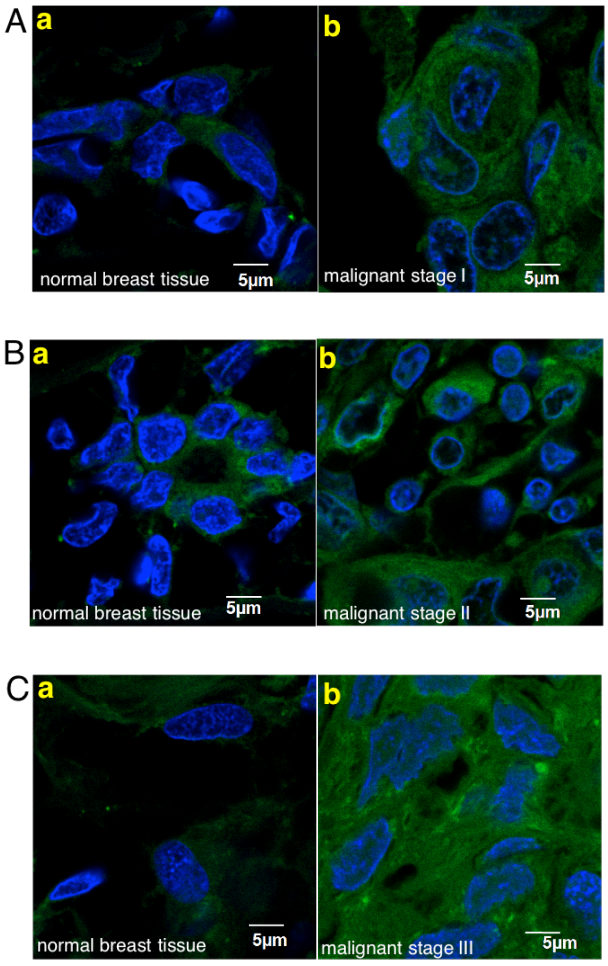

Figure G-S2. Histochemistry on human breast tissue array. Fluorescently labeled TrkC mAb also stained the normal tissue (**a**); but much brighter staining was observed on malignant breast cancer tissue (**b**) (example from 3 cases).

APPENDIX H

ATTEMPTED REACTIONS

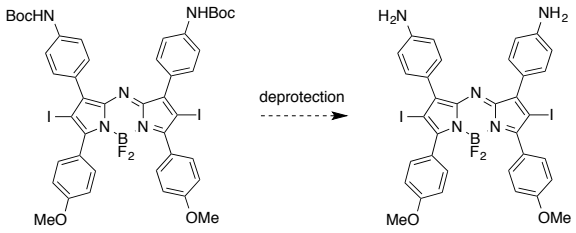

Conditions:

TFA removed BF_2 and Boc

HCl removed Boc and Iodine

BF_3 remove Boc and Iodine

Successful Condition:

10 eq. iPr_2EtN, 15 eq. $BF_3 \bullet OEt_2$ in CH_2Cl_2 at 25 ^oC

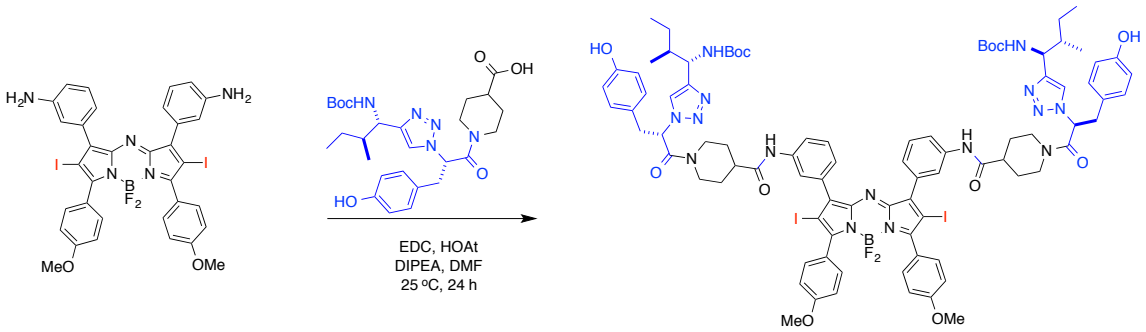

Iodine fell off by using this condition.

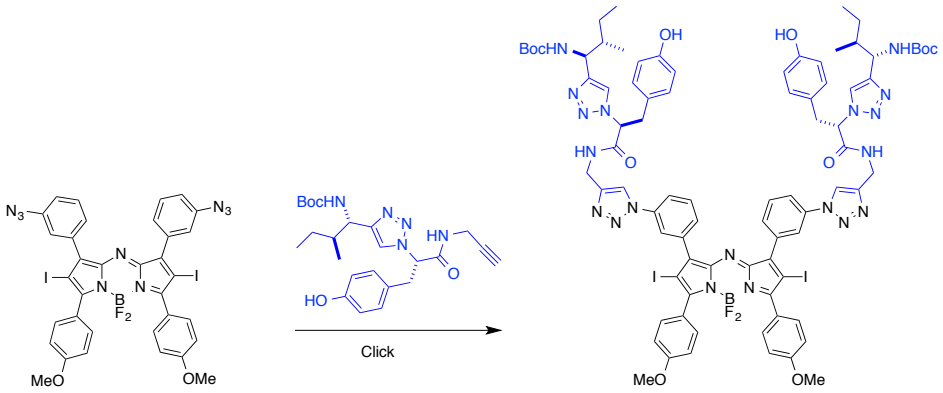

or

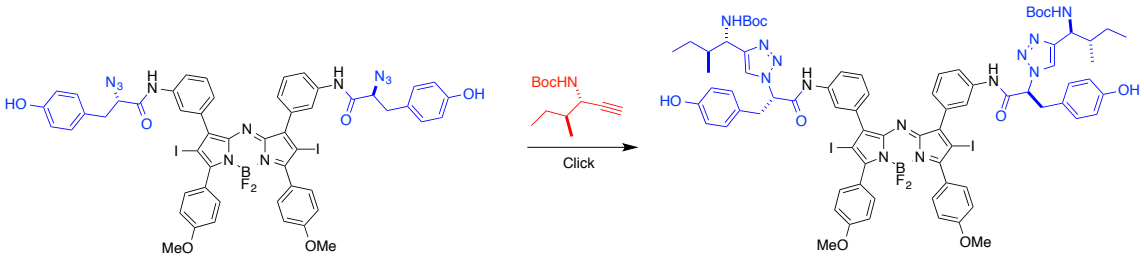

Iodine was reduced when using Cu catalyst reaction.

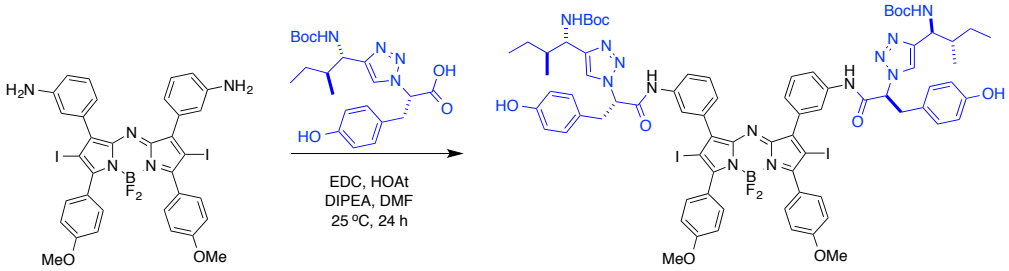

problem with epimerization

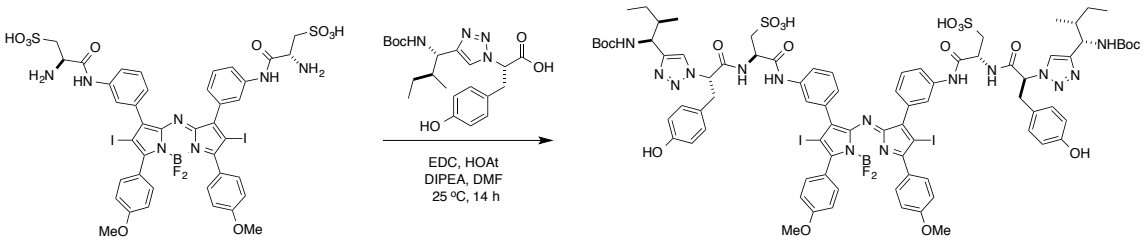

Product contained free IY ligand, difficult to separate.

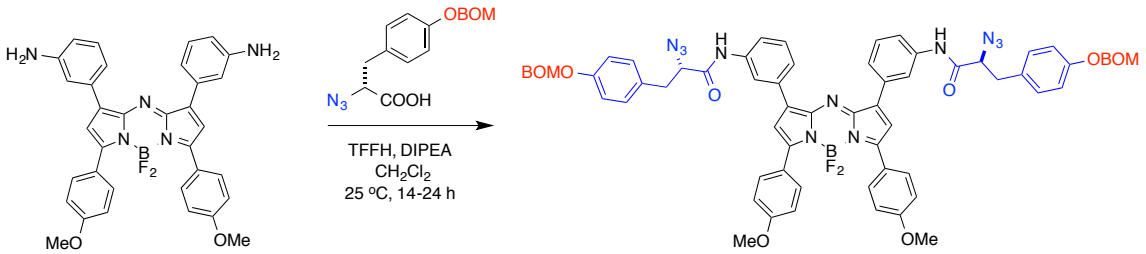

This reaction gave low yield (10 %).

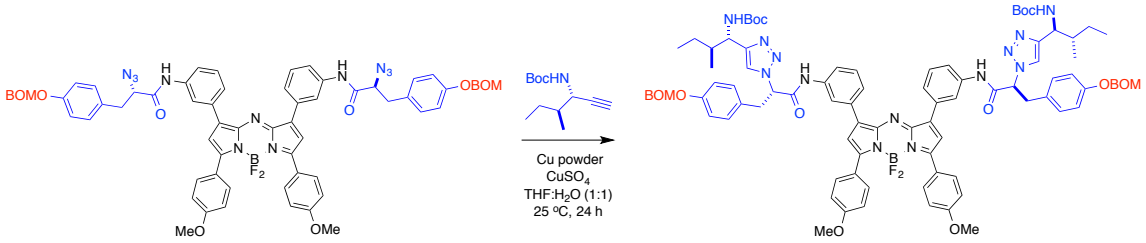

No new spot was obsereved on TLC after 24 h.

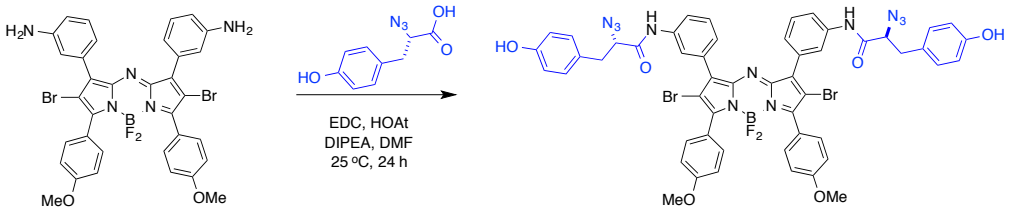

BF_2 fell off under this condition.

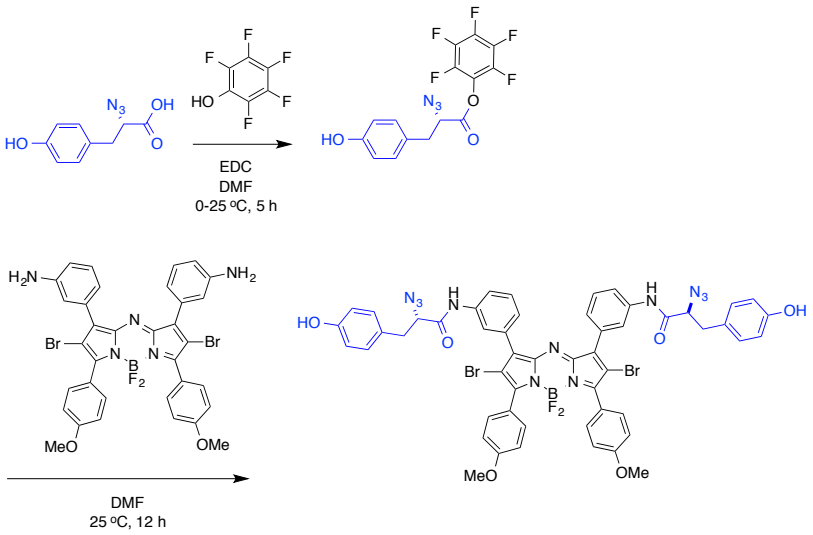

Trace amount of product was obtained.

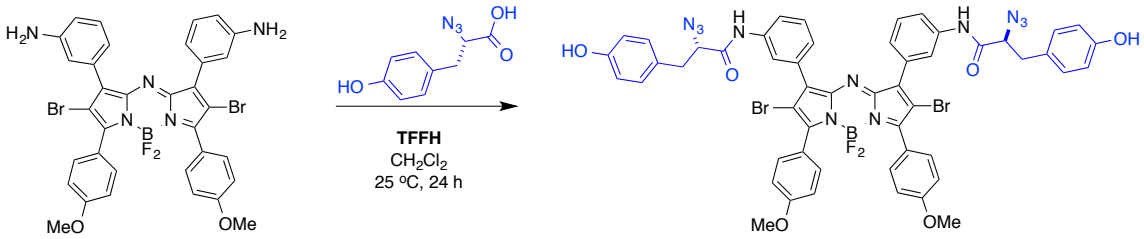

This reaction gave low yield (10 %).

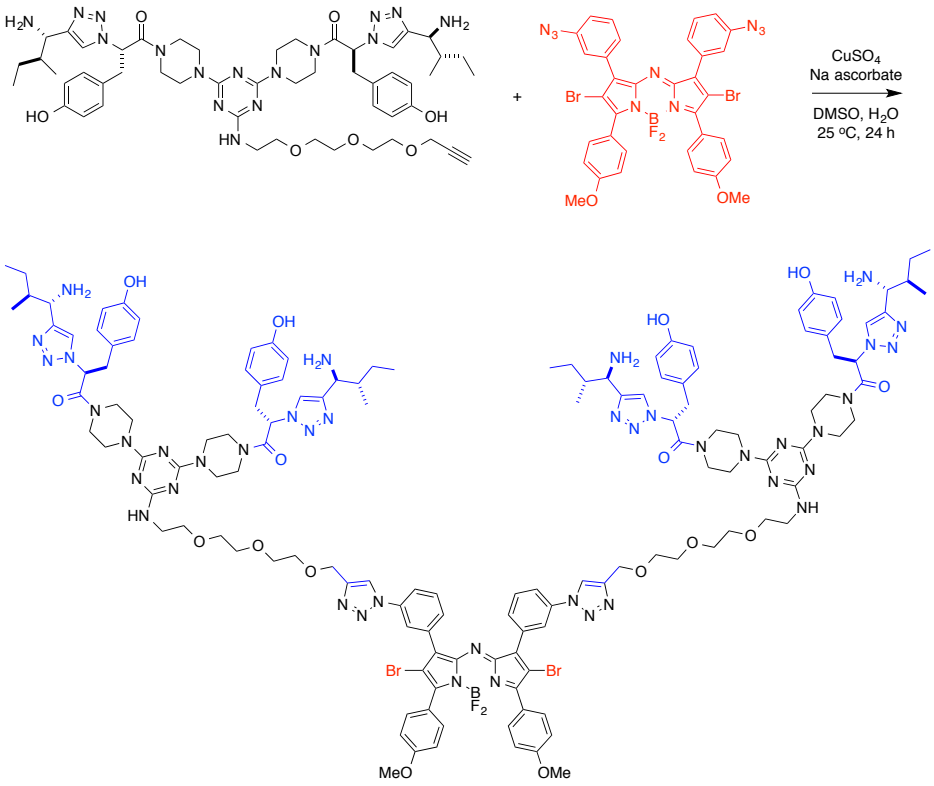

Reaction was extremely slow, could not identify product peak in HPLC.